



Mathematical Statistics
Stockholm University

**Aspects of non-linearities in Kalman
filtering with application to a simplistic
model of the atmosphere**

Jelena Bojarova

**Research Report 2004:3
Licentiate Thesis**

ISSN 1650-0377

Postal address:

Mathematical Statistics
Dept. of Mathematics
Stockholm University
SE-106 91 Stockholm
Sweden

Internet:

<http://www.math.su.se/matstat>



ASPECTS OF NON-LINEARITIES IN KALMAN FILTERING WITH APPLICATION TO A SIMPLISTIC MODEL OF THE ATMOSPHERE

JELENA BOJAROVA*

May 2004

ABSTRACT. Different extensions of the Kalman filter idea for improved treatment of non-linearities with application to meteorological data assimilation are investigated in this thesis. Five different approaches have been applied for meteorological data assimilation within the framework of a simplistic model, a one-dimensional shallow water model, under the perfect model assumption. The observations were simulated by linear as well as non-linear observation operators.

The forecast provided by the bias corrected Kalman filter turned out to be closer to the "true" state with respect to spatial average squared error compared with the forecast provided by the standard extended Kalman filter due to a reduced bias of the innovation vector, in the case of a non-linear observation operator. Among the methods considered in the report, the time-window smoother provides the best filtering of observation errors, if the amount of assimilated observations is large. Under the perfect model assumption, if the amount of assimilated data is large, the time development of the posterior mode of the model state estimated by the time-window smoother is the best estimate of the "true" model state with respect to the spatial average squared error. The dynamical updating of the initial forecast error covariance matrix at the beginning of each assimilation window improves the characteristics of the analysed state. The ensemble Kalman filter is a very attractive method because it is very cheap from a computational point of view, and it still provides a comparably good estimate of the "true" state. However, the data assimilation must be performed with a relatively large ensemble size. The ensemble Kalman filter constructs the analysed state with use of an implicit linearisation of the observation operator, while it preserves the non-linear dynamics. The importance sampling uses the results provided by the time-window smoother (the posterior mode and the curvature around it) and gives wide possibilities for probabilistic inference about smaller dimensional non-linear transforms of the model state variable. The estimate of the posterior predictive mean of the model state variable by the importance sampling appears to be a less efficient estimate of the "true" model state than the posterior mode propagated in time.

* Postal address: Mathematical Statistics, Stockholm University, SE-106 91, Sweden. E-mail: jelena@math.su.se.

CONTENTS

1. Introduction	4
2. The one-dimensional shallow water model	6
2.1. Analytical model formulation	6
2.2. The semi-implicit Eulerian time stepping scheme	9
2.3. The time filter	10
2.4. The complete discrete one time-step model state propagator	11
2.5. The state space model	12
2.6. The design of the initial forecast error covariance matrix	13
2.7. Approximation of physical balances	17
2.8. The process of the geostrophic adjustment	23
2.9. Normal mode decomposition and the non-linear normal mode initialisation	26
3. The Kalman filter and the fixed interval smoother techniques	29
3.1. The second-order regression	29
3.2. The standard Kalman filter	30
3.3. The classical fixed interval smoother	36
4. The application of the Kalman filter and the classical fixed interval smoother in the case of non-linear dynamics	40
4.1. The extended Kalman filter	44
4.2. The bias corrected Kalman filter	49
4.3. The time-window smoother	58
4.4. The ensemble Kalman filter	67
4.5. The estimate of the posterior predictive mean evolution based on importance sampling	76
5. Validation of data assimilation provided by the different Kalman filter extensions	88
5.1. Posterior mean as a point estimate	90
5.2. Posterior mode as a point estimate	91
5.3. The estimate of the posterior predictive mode versus the estimate of the posterior predictive mean of $\hat{X}(t)$	93
5.4. The estimate of the posterior predictive mode of $\hat{X}(t)$ provided by different methods as estimators of $\bar{X}(t)$	100
5.5. Validation of the future forecasts of the "true" model state obtained by means of the different data assimilation approaches	104
6. Conclusions	108
Acknowledgements	111

1. INTRODUCTION

The aim of the meteorological data assimilation procedure is to determine initial data fields for numerical weather prediction. In general, this task coincides with the problem of a model state observer (model state estimator through feedback control) for the non-linear system, governing the development of the atmosphere. However, several specific problems make the task quite challenging.

First of all, the number of observations is several orders smaller than the dimension of the state variable. Prior information about the model state variable must be involved in the construction of a state observer and a merging of this prior information and observed data must be performed, taking observation errors into account. This prior information is usually introduced in the form of a short-range forecast (a model state prediction), often called the first-guess, statistical knowledge about the errors (the deviations from the true atmospheric state) and physical balances between different components of the model state variable, which help to overcome the strong lack of statistical knowledge.

Secondly, the model state variable is just a discrete approximation of the continuous atmospheric fields and its evolution is governed by discrete approximations of continuous physical laws. The discrete approximations of the balances as well as the variances of short range forecast errors strongly depend on the spatial and temporal scales of motion. So, the observed information must be assimilated taking into account the scale of the phenomena of interest avoiding misinterpretation of unresolved small scale variations. Besides that, observed quantities are often related to the model variable through complicated non-linear dependencies, and the observations are irregularly distributed both in space and time.

The method to merge a first-guess field and observed quantities in a way consistent with the estimated accuracy of each type of information was introduced by Eliassen (1954) and Gandin (1963) and within the meteorological community this is called the optimum interpolation method. The main idea of this method is that the deviations of an analysed state (an estimator of the initial model state) from a first-guess can be given by a weighted sum of the innovations (the deviations of the observed data from the first-guess). The weights are determined to achieve the minimum of the estimated mean square error of the analysed state. In other words, the analysed state (the "best" estimate of the initial state) is constructed like an optimal (minimal variance) linear combination of a first-guess field and observed data. The solution to this problem is the well known linear regression. The first-guess and the observed data compete by their accuracy and the distance to the analysed point (in the sense of a spatial auto-correlation of the model state variable). The method was extended to three-dimensional multivariate analysis (Lorenc, 1981) and for a long time it was successfully used for the operational numerical weather prediction by many weather services. Like all linear regression techniques, the method does not require any strong assumptions on the distribution of the random variables, besides existence of second moments. The method has the disadvantage of being able to treat in a proper way only observed data that are linearly related to the model state variable.

An important step forward in numerical weather prediction was the development of three-dimensional variational data assimilation (Parrish and Derber, 1992) and its extension to four dimensions (Le Demit and Talagrand, 1987, Courtier et al., 1994). The analysed state is determined through the posterior mode. It provides the optimal analysis for linear (Gaussian) dynamical systems, but allows for non-linear observation operators, which transform the model state variable into observed quantities. The core of the variational data assimilation is an iterative searching of the model state, closest to the first-guess field

which fits the observations in the best way. In the four-dimensional variational data assimilation, the forecast model enters as a strong constraint over an assimilation time window. The valid physical balance relationships between different model state variable components explicitly enters into the data assimilation procedure through the estimated (or more precisely constructed) forecast error covariance matrix of the model state variable. The utilisation of the physical balances increases weights of data - observed quantities analysed together have more value than individually analysed quantities. The serious disadvantage of the three-dimensional scheme is the stationary forecast error covariance matrix. In the four-dimensional scheme the time evolution of the forecast error covariance is implicitly taken care of.

Theoretically, the time evolution of the probability distribution function describing the forecast error population development in time can be obtained using Kolmogorov's forward equation (more known the as Fokker-Plank equation). However, for practical implementation this is an unfeasible task due to the huge dimension of the model state variable. The large dimension does not allow estimation of the forecast error covariance matrix statistically, so in most operational assimilation schemes it is mainly deduced analytically. This deduction is based on very crude simplifications of the forecast error structure. Secondly, the stationary forecast error covariance matrix does not reflect information about the accuracy of already assimilated observations, which of course influence the accuracy of the first-guess.

The recently implemented four-dimensional variational data assimilation scheme partly solves these problems. The data assimilation procedure is applied over a time window. The observation operator includes a propagation of the model state in time, such that it provides an implicit time evolution of the forecast error covariance matrix during the period of the assimilation time window, and it retains all advantages of the three-dimensional variational data assimilation scheme in treating non-linear relations between the model state and observed quantities. The implicit time evolution of the covariance matrix by the model equations should ideally improve the assumed structure of the forecast errors. This means that sequential observations combined with the implicit knowledge about the time evolution of the error covariance will give much better information about model dynamical balances, and the sequential observations will be given more proper weights in accordance with this.

As it is well known, having linear dynamics and a linear observational operator for a Gaussian system, the optimal discrete sequential estimation is the Kalman (1960) filter. However, the numerical equations propagating the development of the atmosphere are non-linear, so the assimilation based on the Kalman filter does not give the optimal results. The possibility to use some generalisations and extensions of the Kalman filter idea for the purpose of meteorological data assimilation is the topic of the present report. Four different approaches, namely (1) the bias-corrected Kalman filter, (2) the time-window smoother, (3) the ensemble Kalman filter and (4) the importance sampling estimate of the posterior mean will be compared with the widely used so-called extended Kalman filter in the sense of both data assimilation and future forecasting performance. It is impossible to judge the results of the data assimilation procedure without taking into account the usefulness of the constructed initial state for the purposes of future prediction.

The data assimilation experiment will be carried out within the framework of a one-dimensional shallow water model on a β -plane. Such a simplified atmospheric model can simulate some important characteristics of large-scale atmospheric flow. The model is governed by a system of equations "very close" to linear ones, with non-linearity represented only in the form of advection with an ageostrophic wind component, having very

small amplitude. So this model can be supposed to be treated well enough by the Kalman filter. The different extensions of the Kalman filter will be validated by their abilities to handle both linear and non-linear observation operators.

The shallow water model and the numerical methods applied are described and discussed in section 2 of this report. Forecast error covariance matrices modelled from prior physical knowledge of the atmosphere are also introduced in section 2. The basic Kalman filter and the fixed interval smoother techniques are then introduced in section 3. Section 4, the core section of the report, provides descriptions and discussions about the different extensions of the Kalman filter idea. Section 5 presents results from a comparison between the different extensions, both with respect to validation of the estimation of the "true" model state and with respect to forecasting abilities. Section 6, finally, provides a summary and some concluding remarks.

2. THE ONE-DIMENSIONAL SHALLOW WATER MODEL

2.1. Analytical model formulation. A shallow water model is a simplified model of a rotating atmosphere. The model represents the flow of a rotating homogeneous incompressible fluid of depth h with a free upper surface. The dynamics of the particles are described in a three-dimensional co-ordinate system (x, y, z) . Here z is the height of the location of the particle above the zero level, the x direction is taken along the latitude and y is taken along the longitude. The Coriolis force, which appears when an inertial motion is viewed from a rotating system, acts perpendicular to the velocity vector, and has in general three orthogonal components, namely in the vertical direction (the z axis), in the north-south direction (the y axis) and in the east-west direction (the x axis), producing the corresponding accelerations

$$\begin{aligned} \left(\frac{dv}{dt}\right)_{Co} &= -2\Omega \sin(\psi)u, \\ \left(\frac{dw}{dt}\right)_{Co} &= 2\Omega \cos(\psi)u \end{aligned}$$

and

$$\left(\frac{du}{dt}\right)_{Co} = 2\Omega \sin(\psi)v - 2\Omega \cos(\psi)w \approx 2\Omega \sin(\psi)v,$$

(ψ - the latitude, Ω - the angular speed of the rotation of the Earth, (u, v, w) designates the eastward, northward and upward velocity components respectively, subscript Co indicates that this is the acceleration due to the Coriolis force only). The influence of the Coriolis force in the vertical direction is much smaller than the one from the gravity force, so for synoptic scale studies usually only the north-south and the east-west components of the Coriolis force are considered. The velocity component in the vertical direction w has usually a much smaller amplitude in comparison with the horizontal ones, u and v , and this allows simplification of the expression for the Coriolis acceleration in the east-west direction.

In our case, for simplicity, the Coriolis parameter $f(\psi) = 2\Omega \sin \psi$, where $\left(\frac{dv}{dt}\right)_{Co} = -f(\psi)u$, is assumed to follow a so-called β -plane approximation. This means that it can be well approximated by a linear function in y . Let the origin of the co-ordinate system $y_0 = 0$ be located at a point with the latitude ψ_0 . Then the displacement y in the north-south direction is approximately equal $y = a * (\psi - \psi_0)$, where a is the radius of

the Earth. The Coriolis parameter can then be approximated through a Taylor expansion around the origin

$$f(\psi) = f(\psi(y)) = f(\psi_0) + \frac{df}{d\psi} \Big|_{\psi=\psi_0} y + \dots = f_0 + \beta y + \dots$$

In fact, if $\Delta\psi = \psi - \psi_0$ is small enough, then

$$\begin{aligned} f(\psi) - f(\psi_0) &= 2\Omega(\sin \psi - \sin \psi_0) \\ &= 2\Omega(2 \sin(\frac{\Delta\psi}{2}) \cos(\psi_0 + \frac{\Delta\psi}{2})) \\ &\approx 2\Omega \cos \psi_0 \Delta\psi = \frac{2\Omega \cos \psi_0}{a} y \\ &= \beta y \end{aligned}$$

In order to simplify the calculation algorithm and to reduce the dimensionality of the model variables as much as possible we will assume homogeneity in the y -direction.

Before the elimination of the y direction, the model is governed by the following equations

$$(1) \quad \frac{du}{dt} - fv + \frac{\partial\phi}{\partial x} = 0$$

$$(2) \quad \frac{dv}{dt} + fu + \frac{\partial\phi}{\partial y} = 0$$

$$(3) \quad \frac{d\phi}{dt} + \phi\left(\frac{\partial u}{\partial x} + \frac{\partial v}{\partial y}\right) = 0$$

$$(4) \quad \phi = gh$$

$$(5) \quad f = f_0 + \beta y$$

where g is the gravitational acceleration, u and v are the motion speed components (wind) in x - and y -directions, respectively. The first two equations represent the motion and the third equation represents mass continuity.

The elimination of the y -direction is done by the perturbation method, which is widely applied for qualitative analysis of the nature of atmospheric motions. All meteorological field variables are divided into two parts, a basic state which is assumed to be independent of time and longitude, and a perturbation which represents the local deviation of the field from the basic state.

The one-dimensional shallow water model for mid-latitude synoptic systems is constructed from the following assumptions

$$\begin{aligned}
(6) \quad u &= \bar{u} + u'(x, t) \\
v &= v'(x, t) \\
\phi &= \bar{\phi}(y) + \phi'(x, t)
\end{aligned}$$

$$(7) \quad f_0 \bar{u} = -\frac{\partial \bar{\phi}}{\partial y}$$

For mid-latitude systems (far away from the equator) the Coriolis parameter f is different from zero. The mean zonal wind \bar{u} and the mean zonal geopotential gradient $\frac{\partial \bar{\phi}}{\partial y}$ are assumed to be in exact linear geostrophic balance (equation (7)).

The governing system of partial differential equations for the one-dimensional shallow water model, after reformulation through divergence $\delta = \frac{\partial u}{\partial x} + \frac{\partial v}{\partial y}$ and vorticity $\xi = \frac{\partial v}{\partial x} - \frac{\partial u}{\partial y}$, has the form

$$\begin{aligned}
(8) \quad \frac{\partial \delta}{\partial t} + \frac{\partial}{\partial x}(u\delta) - f_0 \xi + \beta u' + \frac{\partial^2 \phi}{\partial x^2} &= 0 \\
\frac{\partial \xi}{\partial t} + \frac{\partial}{\partial x}(u\xi) + f_0 \delta + \beta v' &= 0 \\
\frac{\partial \phi}{\partial t} + \frac{\partial}{\partial x}(u\phi') - f_0 \bar{u} v' + \bar{\phi} \delta &= 0
\end{aligned}$$

We will use a spectral representation with cyclic boundary conditions in the x -direction at $x = 0$ and $x = L$. Non-linear terms will be calculated by the Fourier transform method. Let k denote the wave number in the x -direction, and the non-linear model for the spectral coefficients is given by

$$\begin{aligned}
(9) \quad \frac{d\hat{u}_k}{dt} &= (-i\bar{k}\bar{u} + i\frac{\beta}{k})\hat{u}_k + f_0 \hat{v}_k - i\bar{k}\hat{\phi}_k - \mathcal{F}_k(\mathcal{F}^{-1}(\hat{u})\mathcal{F}^{-1}(i\bar{l}\hat{u})) \\
\frac{d\hat{v}_k}{dt} &= -f_0 \hat{u}_k + (-i\bar{k}\bar{u} + i\frac{\beta}{k})\hat{v}_k - \mathcal{F}_k(\mathcal{F}^{-1}(\hat{u})\mathcal{F}^{-1}(i\bar{l}\hat{v})) \\
\frac{d\hat{\phi}_k}{dt} &= -\bar{\phi} k i \hat{u}_k + f_0 \bar{u} \hat{v}_k - i\bar{k}\bar{u}\hat{\phi}_k - i\bar{k}\mathcal{F}_k(\mathcal{F}^{-1}(\hat{u})\mathcal{F}^{-1}(\hat{\phi}))
\end{aligned}$$

for $-M \leq k \leq M$, $k \neq 0$, $\bar{k} = \frac{2*\pi*k}{L}$ and

$$\begin{aligned}
\frac{d\hat{u}_0}{dt} &= f_0 \hat{v}_0 - \mathcal{F}_0(\mathcal{F}^{-1}(\hat{u})\mathcal{F}^{-1}(i\bar{l}\hat{u})) \\
\frac{d\hat{v}_0}{dt} &= -f_0 \hat{u}_0 - \mathcal{F}_0(\mathcal{F}^{-1}(\hat{u})\mathcal{F}^{-1}(i\bar{l}\hat{v})) \\
\frac{d\hat{\phi}_0}{dt} &= +f_0 \bar{u} \hat{v}_0
\end{aligned}$$

Here $\hat{u} = \mathcal{F}(\vec{u}')$, $\hat{v} = \mathcal{F}(\vec{v}')$, $\hat{\phi} = \mathcal{F}(\vec{\phi}')$. The notations $(i\bar{l}\hat{u})$ and $(i\bar{l}\hat{v})$ are used for spectral representation of the partial derivatives (with respect to x) of the u' -, and v' -wind fields, respectively. \mathcal{F} and \mathcal{F}^{-1} are the Fourier and the inverse Fourier transforms, respectively.

Discrete Fourier and Inverse discrete Fourier transforms for a field $\vec{a} = (a(x_j), 1 \leq j \leq N)$ and a vector of spectral components $\hat{a} = (\hat{a}_k, -M \leq k \leq M)$ are defined in the following way

$$\hat{a}_k = \mathcal{F}_k(\vec{a}) = \frac{1}{N} \sum_{j=1}^N a(x_j) \exp(-i\bar{k}x_j)$$

$$a(x_j) = \mathcal{F}^{-1}(\hat{a}) = \sum_{k=-M}^M \hat{a}_k \exp(i\bar{k}x_j)$$

where $N \geq 3M + 1$, $0 = x_0 < x_1 < \dots < x_N = L$, N is the dimension in grid-point space, M is the dimension in spectral space. The assumed cyclic boundary conditions mean $a(x_0) = a(x_N)$. Since all fields in grid-point space are real-valued, we will have $\hat{a}_{-k} = \hat{a}_k^*$ (complex conjugate).

The relationship $N \geq 3M + 1$ is used instead of the usual $N \geq 2M + 1$ to permit aliasing-free computations of quadratic terms (Eliassen et al., 1970, Orszag, 1971). The non-linear wave interaction instantaneously creates high-frequency waves. In a finite spectral representation unrealistic energy will concentrate on small scale waves, which will propagate and corrupt the solution. The neglecting of small scale waves preserves the solution with little loss of total field energy.

The calculation of spectral components \hat{c} for a non-linear term in the form of a product of two fields $\vec{c} = \vec{a} * \vec{b}$ by the transform method means that instead of a direct derivation of \hat{c} from \hat{a}, \hat{b} we first obtain fields \vec{a}, \vec{b} by the discrete inverse Fourier transform, then we calculate $\vec{c} = \vec{a} * \vec{b}$ in grid point space and at the end we obtain \hat{c} from \vec{c} by the discrete Fourier transform. This procedure simplifies derivations of the algorithm for integration of the model.

2.2. The semi-implicit Eulerian time stepping scheme. Let $\hat{X}_k(t)$, $0 < k < M$, denote the model state variable at time t .

$$\hat{X}_k(t) = \begin{pmatrix} \hat{u}_k(t) \\ \hat{v}_k(t) \\ \hat{\phi}_k(t) \end{pmatrix}$$

The dynamics of the one-dimensional shallow-water model can be written in vector notation

$$(10) \quad \frac{d\hat{X}_k(t)}{dt} = \vec{C}_k \hat{X}_k(t) + B_k(t)$$

where the matrix \vec{C}_k has the form

$$\begin{pmatrix} (-i\bar{k}\bar{u} + i\frac{\beta}{k}) & f_0 & -i\bar{k} \\ -f_0 & (-i\bar{k}\bar{u} + i\frac{\beta}{k}) & 0 \\ -\bar{\phi}i\bar{k} & +f_0\bar{u} & -i\bar{k}\bar{u} \end{pmatrix}$$

and the vector $B_k(t)$ represents the non-linear terms

$$\begin{pmatrix} -\mathcal{F}_k(\mathcal{F}^{-1}(\hat{u}(t))\mathcal{F}^{-1}(i\bar{l}\hat{u}(t))) \\ -\mathcal{F}_k(\mathcal{F}^{-1}(\hat{u}(t))\mathcal{F}^{-1}(i\bar{l}\hat{v}(t))) \\ -i\bar{k}\mathcal{F}_k(\mathcal{F}^{-1}(\hat{u}(t))\mathcal{F}^{-1}(\hat{\phi}(t))) \end{pmatrix}$$

Due to the non-linearity of the differential equations, it does not seem to be possible to obtain an analytic solution to the equations. A numerical semi-implicit Eulerian time stepping scheme (Kwizak and Robert, 1971) is used for the time integration. This scheme provides an implicit treatment of the pressure gradient and divergence-convergence terms of the governing equations (10), which will allow us to use a longer time-step for the discrete time integration of the model. The main effect of the implicit treatment is to retard the speed of the gravity waves (see next section).

The non-linear discrete propagator for the shallow water model has the following form

$$(11) \quad \begin{pmatrix} \hat{X}_k(t+1) \\ \hat{X}_k(t) \end{pmatrix} = \begin{pmatrix} \vec{C}_{1,k}^{si} & \vec{C}_{2,k}^{si} \\ I & 0 \end{pmatrix} \begin{pmatrix} \hat{X}_k(t) \\ \hat{X}_k(t-1) \end{pmatrix} + \begin{pmatrix} B_k^{si}(t) \\ 0 \end{pmatrix}$$

for $t \geq 2$. $X_k(0), X_k(1)$ are assumed to be known. Here and in the following we use index $t-1$ to denote time $t-\Delta t$ and index $t+1$ to denote time $t+\Delta t$.

Furthermore

$$\vec{C}_{1,k}^{si} = \vec{C}_{0,k}^{-1}\vec{C}_{1,k}, \quad \vec{C}_{2,k}^{si} = \vec{C}_{0,k}^{-1}\vec{C}_{2,k}, \quad B_k^{si} = \vec{C}_{0,k}^{-1}B_k(t)$$

where

$$\vec{C}_{1,k} = \begin{pmatrix} (-i\bar{k}\bar{u} + i\frac{\beta}{k}) & f_0 & 0 \\ -f_0 & (-i\bar{k}\bar{u} + i\frac{\beta}{k}) & 0 \\ 0 & +f_0\bar{u} & -i\bar{k}\bar{u} \end{pmatrix}, \quad \vec{C}_{1,0} = \begin{pmatrix} 0 & f_0 & 0 \\ -f_0 & 0 & 0 \\ 0 & +f_0\bar{u} & 0 \end{pmatrix}$$

$$\vec{C}_{2,k} = \begin{pmatrix} \frac{1}{2\Delta t} & 0 & \frac{-i\bar{k}}{2} \\ 0 & \frac{1}{2\Delta t} & 0 \\ \frac{-i\bar{k}\phi}{2} & 0 & \frac{1}{2\Delta t} \end{pmatrix}$$

$$\vec{C}_{0,k}^{-1} = \begin{pmatrix} \frac{2\Delta t}{1+2\phi k^2 \Delta t^2} & 0 & \frac{-i2\bar{k}\Delta t^2}{1+2\phi k^2 \Delta t^2} \\ 0 & 2\Delta t & 0 \\ \frac{-i2\phi k \Delta t^2}{1+2\phi k^2 \Delta t^2} & 0 & \frac{2\Delta t}{1+2\phi k^2 \Delta t^2} \end{pmatrix}$$

This system does not provide an accurate time evolution of the complete solution, but it provides the evolution of the main phenomena of interest, the Rossby waves, and it guarantees a much better computational stability. The time integration step Δt for the scheme is limited by the speed of the fastest Rossby wave, which is much slower than the speed of the fastest gravity waves.

2.3. The time filter. Being a three time level scheme, the semi-implicit Eulerian scheme provides a solution for every time integration as a combination of physical and computational modes. This problem is caused by the fact that a three time level scheme needs additional computational initial condition $X_k(1)$, besides a physical one $X_k(0)$. The effect of the computational mode can be noticed from a two time-step noisy solution. In our time integration scheme, an Eulerian forward time stepping is used to obtain the first computational initial condition $X_k^*(1)$.

$$(12) \quad \hat{X}^*_k(1) = (I + \Delta t_1 \vec{C}_k) \hat{X}_k(0) + \Delta t_1 B_k(0)$$

using a much smaller time step than the chosen one for the time integration, for example $\Delta t_1 = \frac{\Delta t}{4}$. To obtain the final computational condition $X_k(1)$, the semi-implicit Eulerian scheme is used repeatedly increasing Δt_1 up to the chosen time-step Δt . The existence of a computational mode depends on the skill in choosing the computational initial condition $X_k(1)$. For a simple linear oscillation equation, the analytical requirements for the careful choice of the computational initial condition can be derived, and the negative influence of the existence of the computational mode can almost be eliminated. For a complicated non-linear model it does not seem to be possible. During a long time of integration the existence of the computational mode completely corrupts the solution and it must be treated in some way. One possible way to handle the problem is to apply a time filter (Asselin, 1972). A time filter damps the high-frequency noise by a value proportional to the simplest approximation of the second derivative in time of $\hat{X}_k(t)$. The second derivative is negative at the maximum of a function and is positive at the minimum of a function. After the solution $\hat{X}_k(t+1)$ at time $(t+1)\Delta t$ has been obtained from $(\hat{X}_k(t), \hat{X}_k(t-1))$ by (11), the solution at time step t can be corrected

$$\hat{X}_k^f(t) = \hat{X}_k(t) + S(\hat{X}_k(t+1) + \hat{X}_k(t-1) - 2\hat{X}_k(t))$$

where S is the smoothing parameter ($S \approx 0.003$) of the time filter.

We will then have

$$(13) \quad \begin{aligned} \hat{X}_k^f(t) &= \vec{C}_{1,k}^f \hat{X}_k(t) + \vec{C}_{2,k}^f \hat{X}_k(t-1) + S B_k^{si}(t) \\ \vec{C}_{1,k}^f &= (1 - 2S)I + S \vec{C}_{1,k}^{si} \\ \vec{C}_{2,k}^f &= S(\vec{C}_{2,k}^{si} + I) \end{aligned}$$

2.4. The complete discrete one time-step model state propagator. Thus, the complete model state propagator F_k from time moment t to time moment $(t+1)$ will have form

$$(14) \quad \begin{pmatrix} \hat{X}_k(t+1) \\ \hat{X}_k(t) \end{pmatrix} = F_k \begin{pmatrix} \hat{X}_k(t) \\ \hat{X}_k(t-1) \end{pmatrix} = \begin{pmatrix} C_k^{11} & C_k^{12} \\ C_k^{21} & C_k^{22} \end{pmatrix} \begin{pmatrix} \hat{X}_k(t) \\ \hat{X}_k(t-1) \end{pmatrix} + \begin{pmatrix} B_k^1 \\ B_k^2 \end{pmatrix} (t)$$

$$\begin{pmatrix} C_k^{11} & C_k^{12} \\ C_k^{21} & C_k^{22} \end{pmatrix} = \begin{pmatrix} \vec{C}_{1,k}^{si} & \vec{C}_{2,k}^{si} \\ \vec{C}_{1,k}^f & \vec{C}_{2,k}^f \end{pmatrix}$$

$$\begin{pmatrix} B_k^1 \\ B_k^2 \end{pmatrix} (t) = \begin{pmatrix} B_k^{si}(t) \\ S B_k^{si}(t) \end{pmatrix}$$

for $t \geq 2$, with $\hat{X}_k(1)$ obtained as it is described in the previous section:

$$\begin{pmatrix} \hat{X}_k(1) \\ \hat{X}_k(0) \end{pmatrix} = F_k^*(\hat{X}_k(0))$$

2.5. The state space model. In the state space model approach it is assumed that the development of the system over time is determined by an unobserved series of $p \times 1$ -dimensional vectors $\hat{X}(t_0), \hat{X}(t_1), \dots, \hat{X}(t_{N_{ass}})$, the inference about which must be obtained from a series of observable $q \times 1$ dimensional quantities $y_1, \dots, y_{N_{ass}}$. The relationship between the unobservable vectors is determined through the composite model state propagator F^{i-1} , approximating the dynamical evolution of the system over the period (t_{i-1}, t_i) , $1 \leq i \leq N_{ass}$ of the observation time window.

$$(15) \quad \hat{X}(t_i) = F^{i-1}(\hat{X}(t_{i-1})) + R_{i-1}\eta_{i-1}, \quad 1 \leq i \leq N_{ass}$$

The relationship between $\hat{X}(t_i)$ and y_i is determined as well and is called the observation operator Z

$$(16) \quad y_i = Z(\hat{X}(t_i)) + \varepsilon_i, \quad 1 \leq i \leq N_{ass}.$$

The error terms ε_i and η_i are assumed to be serially independent, to be independent of each other at every time step and to obey some known probability distributions. They are assumed to be independent of the initial state vector $\hat{X}(0)$ as well. The $p \times p^*$ operators $R_i, 0 \leq i \leq N_{ass}$ allow us to reduce the dimension and to simplify the structure of the model errors. If the error terms in the dynamics (15) are omitted, namely $\eta_i \equiv 0, 0 \leq i \leq N_{ass} - 1$, the dynamical model is said to be perfect.

In the present study, the composite propagator F^{i-1} from time t_{i-1} to time t_i is determined through a sequence of the one time-step propagators (14).

Experiments are performed both with linear and non-linear observation operators. Non-linear observation operators are introduced to illustrate the effects of non-symmetric posterior distributions.

The linear observation operator denoted Z_l is defined in the following way. Every row of the $q \times p$ dimensional matrix Z consists of a discrete inverse Fourier transform from the spectral representation to the grid-point space of a certain meteorological field (u -wind component, v -wind component or geopotential) observed at a certain position.

The non-linear observation operators consist of triples. The observation operator denoted nlZ_1 gives values of

$$0.5 * \log((\bar{u} + u_j)^2 + v_j^2), \arctan \frac{v_j}{\bar{u} + u_j}, \log(1. + \frac{10 * \phi_j}{\bar{\phi}}),$$

the non-linear observational operator denoted nlZ_2 gives values of

$$0.5 * \log((\bar{u} + u_j)^2 + v_j^2), \arctan \frac{v_j}{\bar{u} + u_j}, \log(\frac{\bar{\phi}}{50} + \phi_j),$$

and the third one denoted nlZ_3 gives values of

$$0.5 * \log((\bar{u} + u_j)^2 + v_j^2), \arctan \frac{v_j}{\bar{u} + u_j}, \frac{\phi_j}{1. + \frac{20 * \phi_j}{\bar{\phi}}},$$

obtained at the grid-point position x_j .

The non-linear transformation of the geopotential field by the observation operator nlZ_2 yields after data assimilation a skewed distribution with one heavy tail for the geopotential

field, and the one by the observation operator nlZ_3 results after data assimilation in a lighter-tail distribution for the geopotential field.

In our study, the observation error terms $\varepsilon_i, 1 \leq i \leq N_{ass}$ are assumed to have a Gaussian distribution with zero mean and a known stationary diagonal covariance matrix H .

$$(17) \quad \varepsilon_i \sim \mathcal{N}(0, H)$$

The dynamical evolution model is deterministic, and we use a perfect model assumption. The initial state vector \hat{X}_{t_0} , often called the first-guess field and usually denoted \hat{X}_0^{fg} is assumed to have a Gaussian distribution as well, namely

$$(18) \quad \hat{X}_0^{fg} - \bar{X}_{t_0} \sim \mathcal{N}(0, B_0)$$

where \bar{X}_{t_0} is a projection of the true continuous meteorological field on the discrete model space valid at time moment t_0 . In our study we use only simulated observations. The discrete model state \bar{X}_{t_0} (including its dynamical forward propagation) is assumed to be "the truth" for our simulation studies. Observations are constructed by transforming \bar{X}_{t_0} including model forward propagation with the chosen observation operator and by adding normally distributed errors with the desired precision.

The initial model state forecast error covariance matrix B_0 is designed to represent the valid physical relationship between the different components of the model state variable. The atmosphere is a chaotic system. Some perturbations grow rapidly, a much larger amount of them are damped. Like it has been outlined (Leith, 1980), the atmospheric state is attracted toward a slow manifold, with a flow which can be approximated by a near geostrophic balance. This property of the atmosphere must be reflected in the data assimilation scheme, and usually it is imposed explicitly by designing the forecast error covariance matrix with the linear geostrophic balance as a starting point. Because the balance is close to linear, the forecast errors, like any small deviations from the true atmospheric state, must also approximately follow the geostrophic balance, and forecast errors of the ageostrophic wind need to have a much smaller variance than the geostrophic ones. The non-linear normal mode initialisation procedure is used later (see below) to improve the structure of the forecast error covariance matrix designed in this way.

2.6. The design of the initial forecast error covariance matrix. The design of the initial forecast error covariance matrix B_0 is done in two steps. First the covariance matrix B_0^* , based on the assumptions of linear geostrophic balance and spatial homogeneity of the meteorological fields (u -, v - wind components and geopotential), is constructed. Secondly, the tangent linear operator of the non-linear normal mode initialisation procedure is used to improve the oversimplified structure of B_0^* to obtain the initial forecast error covariance matrix B_0 .

As a starting point we assume spatial homogeneity of all three meteorological fields. This means, that the variance of the u -wind component, the variance of the v -wind component and the variance of the geopotential are all constant in grid-point space. The tangent-linear normal mode initialisation improves the covariance matrix. The non-homogeneous variance of all three fields obtained after the initialisation procedure is illustrated in Figure 1. The non-homogeneity in the variance appears due to the cross-correlation between spectral components corresponding to different wave numbers established by the initialisation procedure. The v -wind component remains almost homogeneous. Due to the small horizontal scales compared to the Rossby radius of deformation in our model, the tangent linear normal mode initialisation procedure provides to a large extent a geostrophic adjustment of the geopotential field to the v -wind component.

The assumed spatial homogeneity of the random field $a(x)$, namely

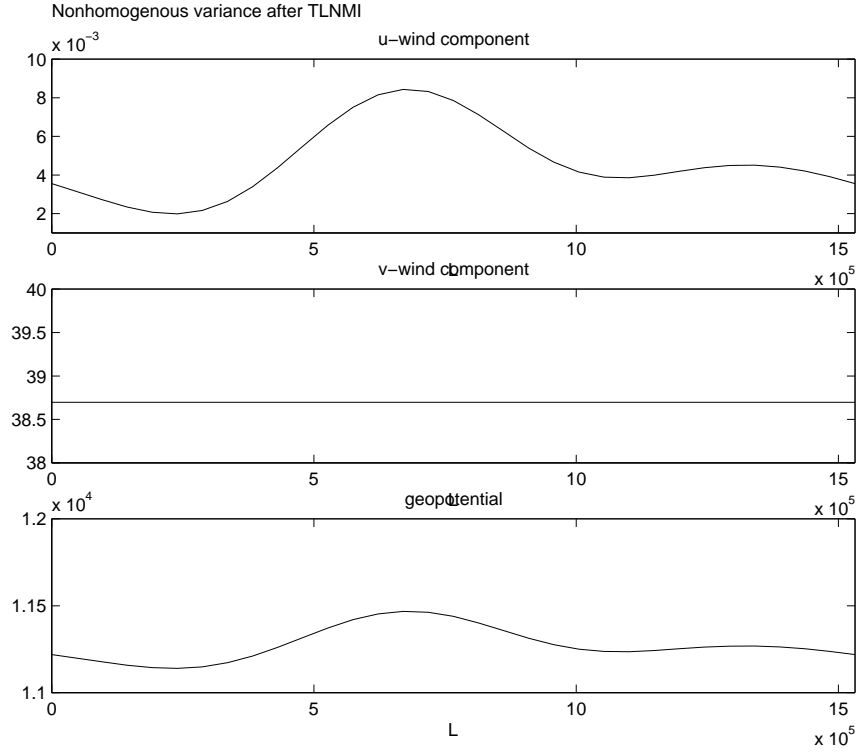


FIGURE 1. Non-homogeneous variance obtained after a tangent-linear normal mode initialisation procedure for the u - and v - wind components and geopotential starting from the initial homogeneity assumptions.

$$\begin{aligned}
 (19) \quad E(a(x)) &= \text{const} = a_0, \\
 \text{Var}(a(x)) &= \text{const} = \sigma_a^2, \\
 \text{Cov}(a(x_1), a(x_2)) &= \rho_a(x_1 - x_2)
 \end{aligned}$$

results in a diagonal covariance matrix for the spectral components \hat{a} . Indeed, with the assumptions above and a diagonal covariance matrix of the spectral components, for every grid-point x_j

$$\begin{aligned}
 (20) \quad E(a(x_j)) &= E\left(\sum_{k=-M}^{k=M} \hat{a}_k e^{\frac{2\pi}{L} ikx_j}\right) = \\
 &= \sum_{k=-M}^{k=M} E(\hat{a}_k) e^{\frac{2\pi}{L} ikx_j} = \\
 &= \text{const} = a_0
 \end{aligned}$$

Due to the uniqueness of the Fourier transform, this implies

$$\begin{aligned}
 (21) \quad E(\hat{a}_0) &= a_0, \\
 E(\hat{a}_k) &= 0, \quad 1 \leq k \leq M \\
 E(\hat{a}_{-k}) &= \text{conj}(E(\hat{a}_k)) = 0
 \end{aligned}$$

Without loss of generality we can assume $a_0 = 0$. Then, for every grid-point x_j

$$\begin{aligned}
 (22) \quad \text{Var}(a(x_j)) &= \text{Var}\left(\sum_{k=-M}^M \hat{a}_k e^{\frac{2\pi}{L} i k x_j}\right) = \\
 &= \sum_{k=-M}^M \sum_{l=-M}^M E(\hat{a}_k \hat{a}_l) e^{\frac{2\pi}{L} i(k+l)x_j} = \\
 &= \sum_{m=-2M}^{2M} v_m e^{\frac{2\pi}{L} i m x_j}
 \end{aligned}$$

where

$$(23) \quad v_m = \sum_{k=-M}^M E(\hat{a}_k \hat{a}_{m-k}) I_{\{-M \leq m-k \leq M\}}$$

If the spectral components are uncorrelated,

$$\begin{aligned}
 (24) \quad E(\hat{a}_k \hat{a}_l) &= 0, \quad k \neq -l \\
 E(\hat{a}_k \hat{a}_{-k}) &= \text{Var}(\hat{a}_k) = \sigma_k^2,
 \end{aligned}$$

the variance will be constant at every grid-point

$$\begin{aligned}
 (25) \quad v_0 &= \sum_{k=-M}^M E(\hat{a}_k \hat{a}_{-k}) = \sum_{k=-M}^M \sigma_k^2 = \sigma_a^2 \\
 v_m &= v_{-m} = 0, \quad 1 \leq m \leq M
 \end{aligned}$$

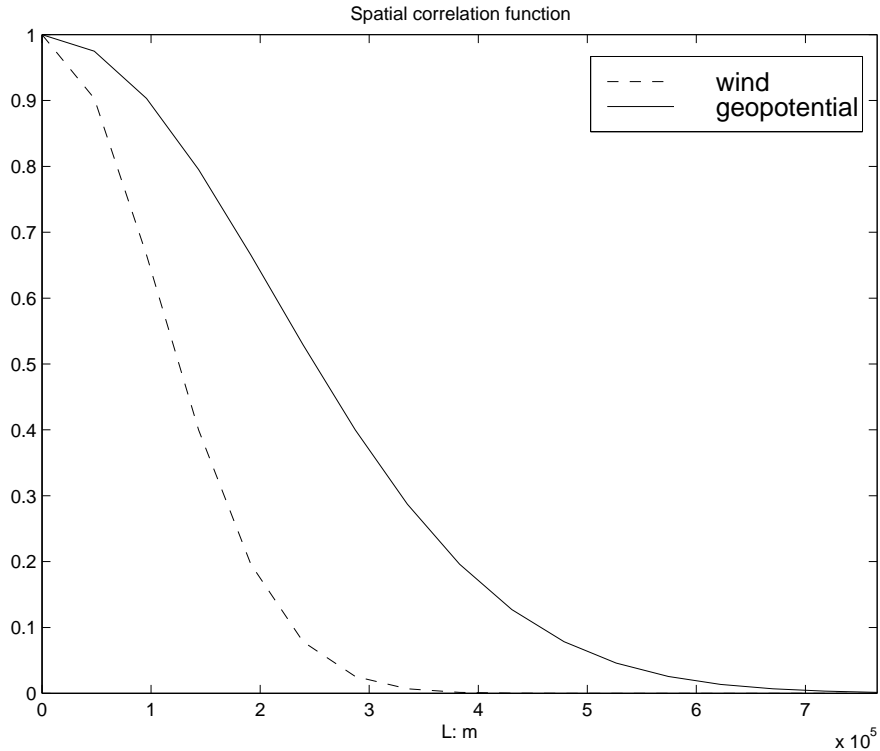


FIGURE 2. Spatial auto-correlation for wind and geopotential

In Figure 2 we have illustrated the spatial auto-correlation of the wind field and the geopotential field, as we initially have assumed it in our model. The auto-correlation is assumed Gaussian for both fields $\rho(r) = e^{-\frac{r^2}{\sigma}}$, with a coefficient for the geopotential $\sigma_\phi = 2500$ and with a coefficient for both wind field components $\sigma_u = \sigma_v = 25$. This is our initial ad-hoc assumption about how the auto-correlation for both fields should look like. We use this assumption for construction of the initial forecast error covariance matrix B_0^* . The auto-correlation based on this assumption is improved by the tangent-linear normal mode initialisation procedure and it will no longer remain homogeneous. The auto-correlation of the wind field is assumed to decrease faster with distance than the auto-correlation of the geopotential field because the wind field is in an approximate linear geostrophic balance with the gradient of the geopotential field, $v \approx \frac{1}{f_0} \frac{\partial \phi}{\partial x}$, and therefore has a larger amount of energy in short waves.

Besides that, in the case of homogeneity, the variances of the spectral components σ_k^2 are uniquely determined through the specification of the spatial auto-correlation $\rho(r)$ of the field $a(x)$.

This is given by the inverse cosine transform

$$\begin{aligned}
(26) \quad Cov(a(x_i), a(x_j)) &= E(a(x_i)a(x_j)) = \\
&= \sum_{k=-M}^M \sum_{l=-M}^M E(\hat{a}_k \hat{a}_l) e^{\frac{2\pi}{L} i(kx_i + lx_j)} = \\
&= \sum_{k=-M}^M E(\hat{a}_k \hat{a}_{-k}) e^{\frac{2\pi}{L} ik(x_i - x_j)} = \\
&= \sigma_0^2 + 2 \sum_{k=1}^M \sigma_k^2 \cos\left(\frac{2\pi}{L} k(x_i - x_j)\right) = \rho(x_i - x_j)
\end{aligned}$$

We can see in Figure 3 that the normal mode initialisation procedure (more precisely the tangent linear version of it) puts very small amount of energy in the ageostrophic wind component. The u -wind component in our model is purely ageostrophic. The spectral covariance of the u -wind component after tangent linear normal mode initialisation has been multiplied by a factor 100 in Figure 3. The covariance spectrum of the v -wind component attains a particular form with a maximum in the inner part of the spectrum (around $2/3$) after the tangent-linear normal mode initialisation. This is again due to fact that the initialisation procedure puts the v -wind component and the geopotential in an approximate linear geostrophic balance. In spectral space this balance has the following form $v_k \propto k\phi_k$, $k = 0, M$.

The v -wind spectral components are assumed to be sums of two uncorrelated random fields, the geostrophic and the ageostrophic ones. The geostrophic wind is almost a linear function of the geopotential, and for the one dimensional shallow water model the covariance between the spectral components of the geopotential ϕ_k and the north-south wind component v_k can be approximated by the following expression:

$$(27) \quad cov(v_k, \phi_k) \approx \frac{2\pi k i}{Lf} var(\phi_k)$$

The variances of the spectral components of the north-south wind v_k are taken to be given by

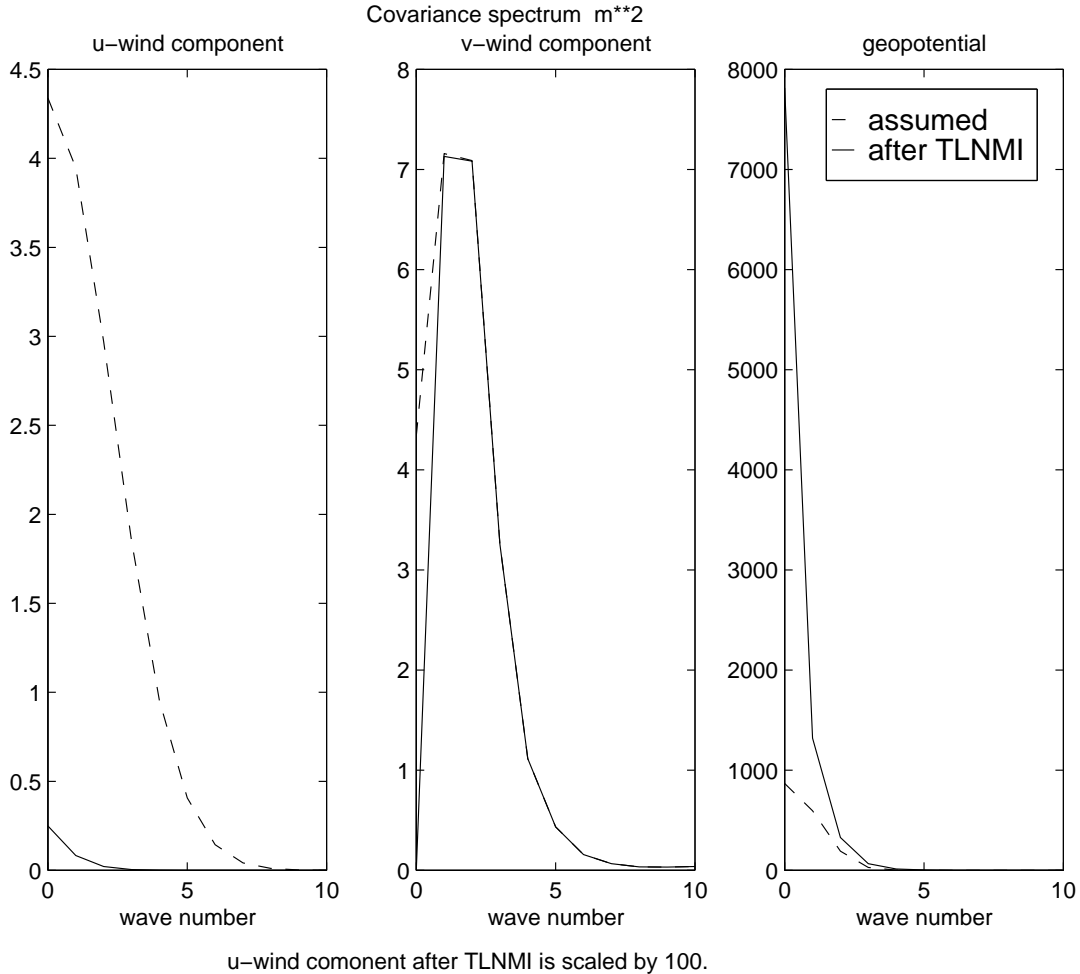


FIGURE 3. Covariance spectrum before (dashed lines) and after (full lines) the normal mode initialisation procedure for the three meteorological fields: u -wind component, v -wind component and geopotential.

$$(28) \quad \text{var}(v_k) \approx \frac{4\pi^2 k^2}{L^2 f^2} \text{var}(\phi_k) + \sigma_k^{ag}$$

where k is a wave number in the spectral representation, f is the Coriolis parameter and L is the length of the grid-point area in the east-west direction. The east-west wind components u_k are purely ageostrophic and assumed to be uncorrelated with the geopotential and the north-south wind component at the first step in the design of the forecast error covariance matrix.

$$(29) \quad \text{var}(u_k) \approx \sigma_k^{ag}$$

The basic theory of linear geostrophic balance, the necessity for improvement of this simplified balance as well as the normal mode initialisation procedure, as one of the possible methods to improve the balance, are the issues to be discussed in the rest of this section.

2.7. Approximation of physical balances. Outside the tropical areas, the geopotential and the wind fields are approximately related through the non-linear balance equation in the real atmosphere. Let $\vec{V} = (u, v)$ denote the wind velocity vector. Any velocity field

can be divided into two parts: the non-divergent \vec{V}_ψ , associated with rotational motion, and the irrotational \vec{V}_e , associated with divergent motion.

$$(30) \quad \vec{V} = \vec{V}_\psi + \vec{V}_e$$

The horizontal divergent motion can also be considered as horizontally propagating oscillations, also known as shallow water gravity waves. The restoring force for such waves is in the vertical direction, and it is transverse to the direction of propagation. One can notice from the dynamical equations describing the shallow water model (equations (1) and (2)), that as soon as an unbalanced horizontal geopotential gradient exists (in this case this is the same as a disturbance, for example depression, in the geopotential field), an acceleration toward the origin of the disturbance will appear. This means that the fluid will converge toward the origin of the disturbance. Since the fluid is incompressible, the convergence must be compensated by divergence on both sides of the original disturbance. So depressions will appear from both sides of the original disturbance. Again, the unbalanced horizontal geopotential gradient will cause accelerations into the depressions and, as a result, the outward propagation of the disturbance will continue in the form of wave motion. In the real atmosphere, the shallow water waves have very small amplitude, i.e. the divergent motion is small relative to the rotational motion. In other words, starting from a state close to a balanced one, the time tendencies of the divergent motion must remain close to zero. Let $\delta = \frac{\partial u}{\partial x} + \frac{\partial v}{\partial y}$ denote the divergence of the wind field. Then, the condition for the filtering out of the gravity waves can be expressed

$$(31) \quad \frac{\partial \delta}{\partial t} = 0$$

Taking into account the identity

$$u \frac{\partial u}{\partial x} = \frac{\partial}{\partial x} \left(\frac{u^2 + v^2}{2} \right) - v \frac{\partial v}{\partial x}$$

and noticing that for the one-dimensional shallow water model, vorticity $\xi = \frac{\partial v}{\partial x} - \frac{\partial u}{\partial y}$ simplifies to $\xi = \frac{\partial v}{\partial x}$, one can rewrite the dynamical equations (equations (1) and (2)) in the following way

$$\begin{aligned} \frac{\partial u}{\partial t} + \frac{\partial}{\partial x} \left(\frac{u^2 + v^2}{2} \right) - v(f + \xi) + \frac{\partial \phi}{\partial x} &= 0 \\ \frac{\partial v}{\partial t} + u(f + \xi) + \frac{\partial \phi}{\partial y} &= 0 \end{aligned}$$

Then

$$\begin{aligned} \frac{\partial \delta}{\partial t} &= \frac{\partial}{\partial x} \left(\frac{\partial u}{\partial t} \right) + \frac{\partial}{\partial y} \left(\frac{\partial v}{\partial t} \right) \\ &\quad - \frac{\partial^2}{\partial x^2} \left(\frac{u^2 + v^2}{2} + \phi \right) + \frac{\partial}{\partial x} (v(f + \xi)) + \\ &\quad - \frac{\partial^2 \phi}{\partial y^2} - \frac{\partial}{\partial y} (u(f + \xi)) \end{aligned}$$

Thus, to satisfy condition (31), the following differential equation must hold

$$(32) \quad \frac{\partial^2}{\partial x^2} \left(\frac{u^2 + v^2}{2} + \phi \right) + \frac{\partial^2 \phi}{\partial y^2} = \frac{\partial}{\partial x} (v(f + \xi)) - \frac{\partial}{\partial y} (u(f + \xi))$$

In fact, in the real atmosphere, condition (31) never holds precisely, because gravity waves exist and are important and essential for the dynamics (for example, physical processes like heating by the sun create imbalances, the balancing of which is handled by gravity waves). It is for the non-divergent wind component, that the relationship stated above between wind and geopotential (equation (32), also known as the non-linear balance equation) must hold. Usually, the non-divergent part of the wind field is expressed in the terms of the stream-function ψ . In a Cartesian coordinate system we will have

$$u_\psi = -\frac{\partial \psi}{\partial y}, \quad v_\psi = \frac{\partial \psi}{\partial x}.$$

For the one-dimensional shallow water model the u -wind component is completely associated with divergent motion and the stream-function is determined simply through the following differential equation

$$v_\psi = \frac{\partial \psi}{\partial x}.$$

Taking into account that

$$\xi_\psi = \frac{\partial v_\psi}{\partial x} = \frac{\partial^2 \psi}{\partial x^2}$$

the non-linear balance equation can be expressed in terms of the geopotential and the stream-function only

$$(33) \quad \frac{\partial^2}{\partial x^2} \left(\phi + \frac{1}{2} \left(\frac{\partial \psi}{\partial x} \right)^2 \right) = \frac{\partial}{\partial x} \left(\frac{\partial \psi}{\partial x} \left(f + \frac{\partial^2 \psi}{\partial x^2} \right) \right)$$

However, as a first order linear approximation (neglecting non-linear terms) for mid-latitude synoptic scale motion (the Coriolis parameter f does not approach 0), assuming a β plane, the geopotential field is approximately related to the stream-function through the linear balance equation

$$(34) \quad \frac{\partial^2}{\partial x^2} (\phi) = f_0 \frac{\partial^2}{\partial x^2} (\psi)$$

However, it must always be taken into account that the linear balance equation describes only a crude static dependence between the wind field and the geopotential, in comparison with the non-linear balance equation which represents the dynamical balance, valid for the model, imposing certain conditions on the tendencies.

The approximate linear relationship between the geopotential and the wind fields (i.e. the non-divergent part of the wind field) is known as the linear geostrophic balance and it takes the following form for the one-dimensional shallow water model on a β -plane

$$(35) \quad v_\psi = \frac{1}{f_0} \frac{\partial \phi}{\partial x}$$

and in general on the sphere

$$u_{\psi} = -\frac{1}{f} \frac{\partial \phi}{\partial y}, \quad v_{\psi} = \frac{1}{f} \frac{\partial \phi}{\partial x}$$

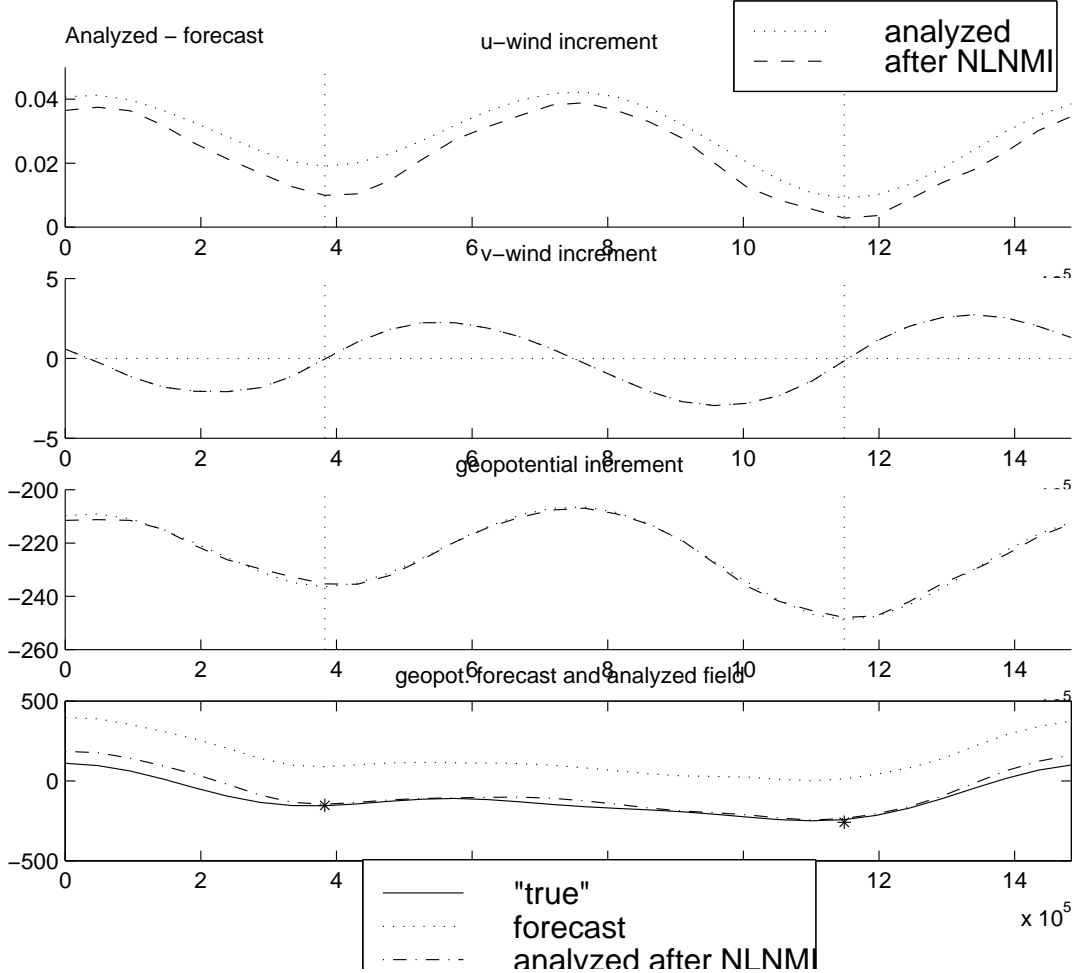


FIGURE 4. Analysis increments after assimilation by means of the extended Kalman filter of two geopotential observations in a "single" observation experiment (the first assimilation term). The observations were simulated by a linear observation operator. Two observations of geopotential of different precision were introduced. The locations of the observations were marked by *

To understand better the effect of an approximate linear geostrophic balance, we have carried out so called "single" observation experiments. For the first experiment, we have introduced two observations of the geopotential field, marked with * in Figure 4. The observations were assimilated after 6 hours of time integrations of the model was performed. The first observation to the left has a lower precision (larger error variance) than the second one, and therefore a weaker influence on the geopotential field. In Figure 4 we can see the analysis increments, namely the differences between the analysed and the forecast field, for the u -, v -wind components and the geopotential. Even if we have introduced observations of the geopotential only, all three analysed field are affected, due to the cross-correlation between spectral components of the different meteorological fields. As a starting point in the construction of the forecast error covariance matrix, we have assumed that the u -wind component field is uncorrelated with the geopotential

field, and with the v -wind component as well. The effect of these unrealistic assumptions is partly improved by the normal mode initialisation procedure, and partly a more realistic structure is developed during the dynamical model integration. The fields are in an approximate geostrophic balance. Because the balance is close to a linear one, the increments must be in an approximate linear geostrophic balance as well. The influence of each observation on the analysed geopotential field is strongest at the position where each observation was inserted, and the influence decreases symmetrically with distance according to the assumed spatial correlation of the field. The inserted observations of geopotential create changes to the analysed v -wind field, as geostrophic balance requires. In case of the linear geostrophic approximation, the v -wind component must be equal to the spatial derivative in the x -direction of the geopotential. At the positions where observations are inserted and the geopotential increment has extremes, the v -wind increment is approximately equal zero. The v -wind component decreases to the left of the positions where the observations were inserted and increases to the right of these positions, with the largest influence attained at a distance pre-supposed by the structure of the spatial cross-correlation between the v -wind and the geopotential. Further away, the influence of observations on v -wind analysis field decreases. The balance imposed by the forecast error covariance structure is closer to the linear geostrophic balance than a realistic dynamical balance should require. The normal mode initialisation procedure improves this crude approximation toward a more realistic one and forces the increment fields away from the exact linear geostrophic balance.

For the second single observation experiment, illustrated in Figure 5, we have introduced two v -wind observations. The observations were introduced after 6 hours of time integration of the model was performed. Again, the first observation has a lower precision and has therefore a weaker influence on the analysed fields. When the observations of the v -wind components were inserted and the v -wind field was adjusted to the observations, the corresponding changes of the geopotential were created as well. The observation to the right indicates that the "true" wind in the south-north direction has a lower speed than the forecast wind. The change of the geopotential field is zero at the the position of the v -wind observation, but the increment field here has its largest negative spatial derivative in the x -direction. In accordance with the form of the analysed v -wind field, the geopotential increases to the left of the observation point and decreases to the right of the observation point. The changes are largest at a certain distance from the observation point and reduces further away. This distance depends on the assumed geopotential correlation structure.

The figures above were prepared with data assimilation by means of the extended Kalman filter. Besides the adjustment to the observations, a secondary influence can be noticed. Noisy disturbances created by assimilating single erroneous observations may have nothing to do with the features of the "true" process that the analysed state should estimate. The adjustment to different erroneous observations at a certain time reduces the amplitude of the real disturbance. However, by assimilating several observations at a time, the analysed field may receive more energy in short scale motion or may receive larger amplitudes of higher frequency waves as compared to the "true" model state. We can notice this because, in order to demonstrate the effect of the assimilated observations, we have assumed the relative precision of the observations to be better than the one of the background state. Therefore, the influence of the observations on the analysed state becomes quite strong. We can see in Figure 6 how the analysed state looks like after assimilation of a group of 9 observations. We have marked the locations of the observations with the * symbol. The mutual adjustment of the fields after insertion of different erroneous observations at a time results in a quite noisy analysed v -wind component field, for example. The influence

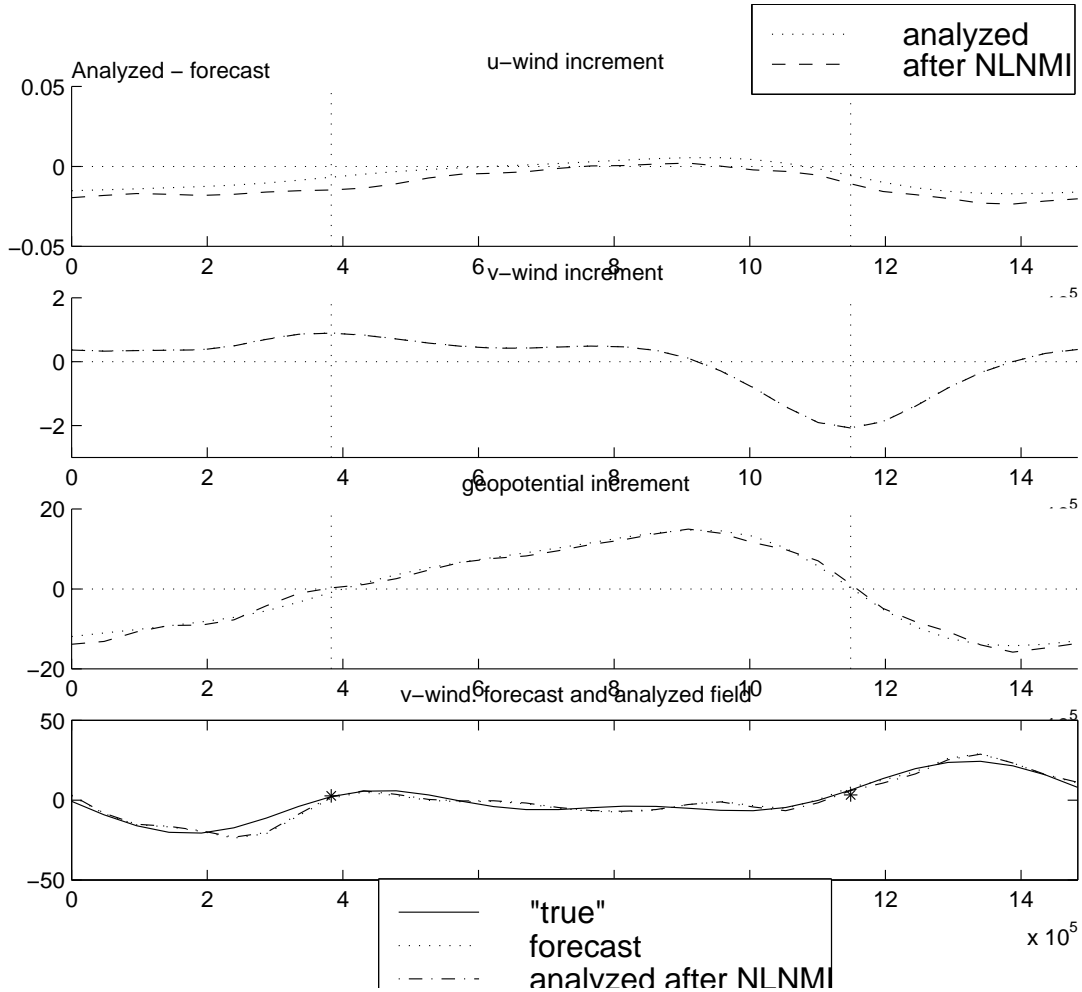


FIGURE 5. Analysis increments after assimilation by means of the extended Kalman filter of two v -wind component observations in a "single" observation experiment (the first assimilation term). The observations were simulated by a linear observation operator. Two observations of v -wind component of different precision were introduced. The locations of the observations are marked by *

of this mutual adjustment can be better seen in Figure 7 where the analysis increments for different fields are shown. The observations of the u -wind component and the geopotential are located at the same positions. These positions are marked with dotted lines. The observations of v -wind component are located at separate positions, marked with dashed lines.

The result of the assimilation of two observations of the u -wind component are illustrated in Figure 8. The covariance spectrum of the u -wind component decreases very quickly with the wave number. Consequently, the field has a very small amount of energy in short waves, and we can notice a large scale correlation pattern. The u -wind component in the one-dimensional shallow water model represents a purely ageostrophic wind and is in fact a deduced quantity. Even if the u -wind component has a very small amplitude, it is of very great importance. It represents the instantaneous speed of the wave propagation in east-west direction. As we can notice, the v -wind component and the geopotential are changed as well after insertion of the observations. These changes are (approximately) in accordance with the linear geostrophic balance. The correlation between the u -wind

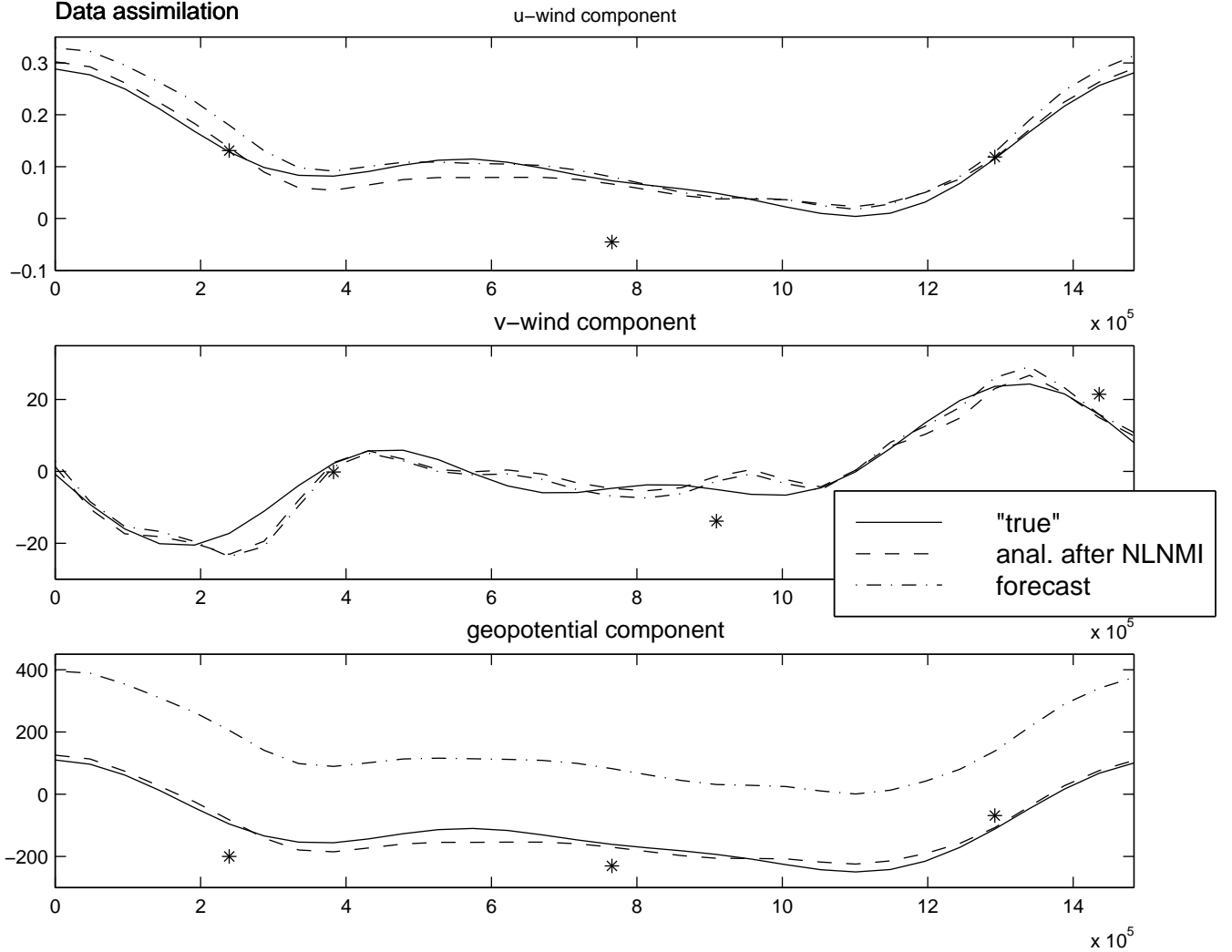


FIGURE 6. The analysed fields after assimilation by means of the extended Kalman filter of a group of 9 observations at a time (the first assimilation term). The observations were simulated by a linear observation operator. The location of observations are marked by *

component, the v -wind component and the geopotential are established by the mechanism of geostrophic adjustment, which we will describe and discuss below.

Like it was discussed above (with reference to Leith, 1980), the atmospheric state is attracted toward a slow manifold, with a flow which can be approximated by the linear geostrophic balance. This means, that perturbations disturbing the balance will be damped and the state will attain balance again by a process of mutual adjustment. However, if the unbalanced perturbations are unrealistically large, the governing system of the shallow water equations will not be able to describe a realistic time evolution of such a state and the numerical integration becomes meaningless.

2.8. The process of the geostrophic adjustment. The application of the linear geostrophic balance for the design of the initial forecast error covariance matrix has two serious limitations with regard to a representation of a realistic structure of the atmosphere. First of all, as it was already mentioned, the linear geostrophic balance mainly describes a static relationship between the geostrophic wind and the geopotential instead of a dynamical balance valid for the system. Secondly, the ageostrophic and the geostrophic winds

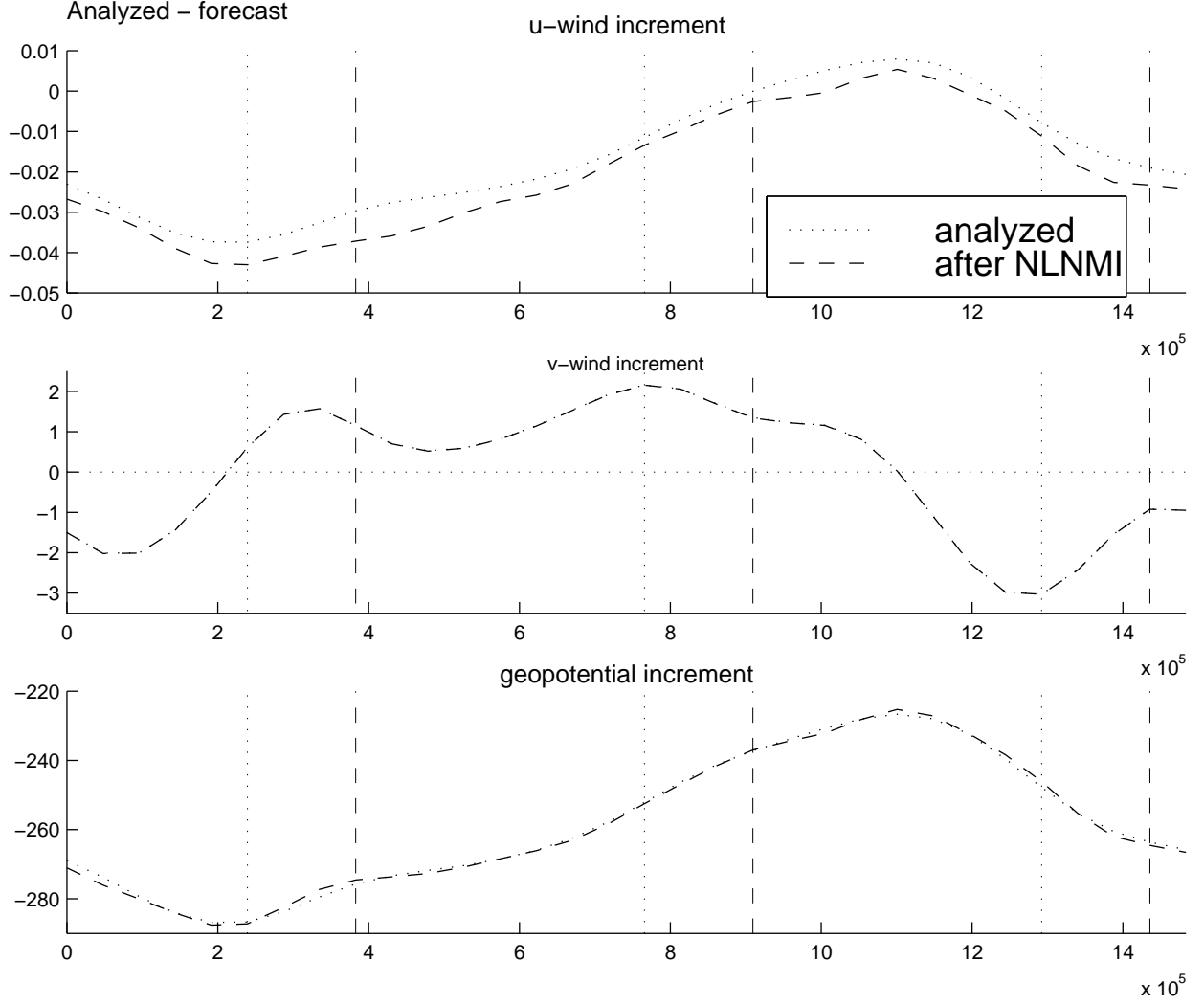


FIGURE 7. The analysis increments after assimilation by means of the extended Kalman filter of a group of 9 observations at a time (the first assimilation term). The observations were simulated by a linear observation operator. Vertical dotted lines mark positions of geopotential and u -wind component observations and dashed vertical lines mark positions of v -wind component observations. The location of observations are marked by * in Figure 6.

are strongly correlated as well, and this is completely not reflected by the linear balance equation.

The absolute motion of a particle in the x -direction, along the ψ latitude circle, is simply a rotational motion, with a total angular speed

$$\omega = \Omega + \frac{u}{R_\psi}$$

where Ω is the angular speed of the Earth, u is the speed of the particle in the x -direction relative to the ground and $R_\psi = a \cos \psi$ is the radius of the latitude circle. Here a is the radius of the Earth.

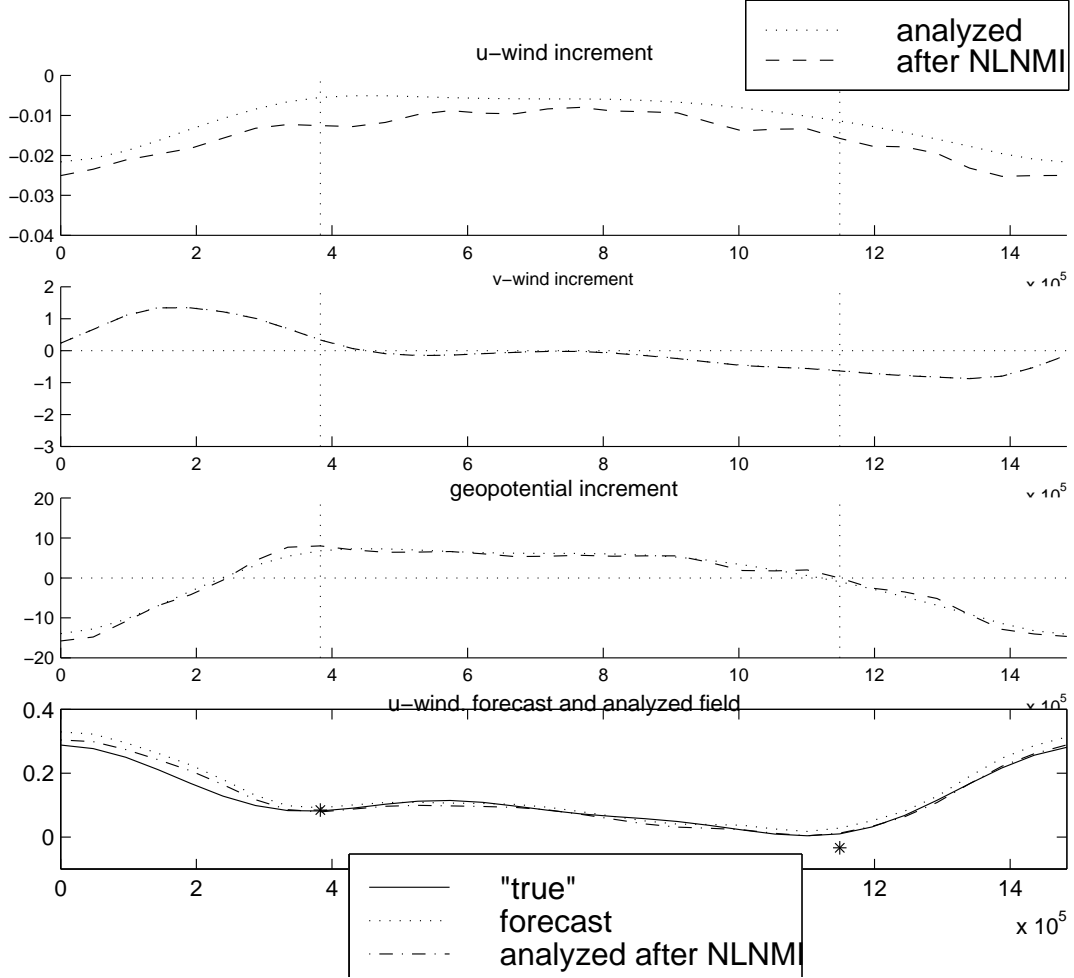


FIGURE 8. Analysis increments after assimilation by means of the extended Kalman filter of two u -wind components observations in a "single" observation experiment (the first assimilation term). The observations were simulated by a linear observation operator. Two observations of u -wind component of different precision were introduced. The locations of the observations are marked by *

The angular momentum of the particle is equal

$$(36) \quad \mathcal{M}_\omega = \omega R_\psi^2 = \left(\Omega + \frac{u}{R_\psi}\right) R_\psi^2$$

The spatial variations of geopotential in the x -direction create the geostrophic north-south wind component, forcing the particle to move across the latitude circles, and after a time period Δt the particle will be on the $\psi + \Delta\psi$ latitude circle with radius $R_{\psi+\Delta\psi} = R_\psi + \Delta R_\psi$. Obviously, the speed of the particle in the x -direction must change as well from u to $u + \Delta u$ in order to maintain conservation of angular momentum. So, the following non-linear relationship must be satisfied

$$(37) \quad \left(\Omega + \frac{u}{R_\psi}\right) R_\psi^2 = \left(\Omega + \frac{u + \Delta u}{R_\psi + \Delta R_\psi}\right) (R_\psi + \Delta R_\psi)^2$$

While the v -wind component is positive, the particle is moving to the north, and the radius of the particle rotation decreases $\Delta R_\psi < 0$. Then in order to maintain the relationship (37) the u -wind component must increase, i.e. $\Delta u > 0$.

This is the main mechanism that establishes the correlation between the ageostrophic and the geostrophic wind in general, and between the u - and v - wind components in our model. The geostrophic adjustment relates changes of u -wind component in this special dependence to changes of v -wind component and geopotential. We can see this pattern of dependency in the all figures we have discussed in the previous subsection. But we must remember, that this pattern of spatial dependence between the u - and the v -wind components (and the geopotential) connects the fields statically. The geostrophic adjustment establishes a dynamical dependence which forces the fields to propagate in time in such a way that this static dependence is always maintained.

The normal mode initialisation procedure is one possibility to improve the statistical structure of the forecast error, defined through the designed covariance matrix, and to make it more realistic.

2.9. Normal mode decomposition and the non-linear normal mode initialisation. The dynamics of the one-dimensional shallow water model can be written in vector notation

$$(38) \quad \frac{d\hat{X}_k(t)}{dt} = \vec{C}_k \hat{X}_k(t) + B_k(t)$$

where the vector $\hat{X}_k = (\hat{u}_k, \hat{v}_k, \hat{\phi}_k)'$, the matrix \vec{C}_k has form

$$\begin{pmatrix} (-i\bar{k}\bar{u} + i\frac{\beta}{k}) & f_0 & -i\bar{k} \\ -f_0 & (-i\bar{k}\bar{u} + i\frac{\beta}{k}) & 0 \\ -\bar{\phi}i\bar{k} & +f_0\bar{u} & -i\bar{k}\bar{u} \end{pmatrix}$$

and the vector $B_k(t)$ represent the non-linear part

$$\begin{pmatrix} -\mathcal{F}_k(\mathcal{F}^{-1}(u(\hat{t}))\mathcal{F}^{-1}(i\bar{l}u(\hat{t}))) \\ -\mathcal{F}_k(\mathcal{F}^{-1}(u(\hat{t}))\mathcal{F}^{-1}(i\bar{l}v(\hat{t}))) \\ -i\bar{k}\mathcal{F}_k(\mathcal{F}^{-1}(u(\hat{t}))\mathcal{F}^{-1}(\phi(\hat{t}))) \end{pmatrix}$$

For every spectral component ($k > 0$), \vec{C}_k has 3 distinct eigenvalues $i\omega_k^l$, $l = 1, 2, 3$, with $(\omega^1 > \omega^2 > \omega^3)$ and 3 almost orthogonal eigenvectors $\vec{\gamma}_k^l$, $l = 1, 2, 3$. Let the matrix $\vec{\Gamma}_k = (\vec{\gamma}_k^1, \vec{\gamma}_k^2, \vec{\gamma}_k^3)$. The model state variable \hat{X}_k can be projected onto these three almost orthogonal waves, also called normal modes.

$$(39) \quad \hat{X}_k = \sum_{l=1}^3 \beta_k^l \vec{\gamma}_k^l$$

where

$$\beta_k = \vec{\Gamma}_k^{-1} \hat{X}_k,$$

and

$$\beta_k = (\beta_k^1, \beta_k^2, \beta_k^3)'$$

In other words, the model state solution can be decomposed into three different waves

$$(40) \quad \hat{X}_k(t) = G1_k \bar{\gamma}_k^1 + G2_k \bar{\gamma}_k^2 + R_k \bar{\gamma}_k^3$$

The components $G1_k, G2_k$ correspond to a pair of fastly propagating gravity waves, moving in the opposite direction to one another and R_k corresponds to a slowly propagating Rossby wave. The gravity waves are associated with divergent motion and the Rossby wave is associated with rotational motion. As soon as unbalanced horizontal pressure gradients exist, fastly propagating gravity waves are created. Indeed, gravity waves will be created even from a linearly balanced initial state due to the non-linear interaction between wave components.

The speed c^g of the gravity wave propagation can be simplified by the following approximate expression

$$(41) \quad c^g = \bar{u} \pm \sqrt{\bar{\phi}}.$$

The quantity $\sqrt{\bar{\phi}}$ is called the shallow water wave speed. For synoptic scale motion, in the real atmosphere, the valid assumption of the fastest gravity wave speed is $\approx \sqrt{10 \text{ m/s}^2 * 9000 \text{ m}} \approx 300 \text{ m/s}$, so gravity waves propagate with a huge speed. We have chosen $\bar{\phi} = 10 \text{ m/s}^2 * 5000 \text{ m}$. Thus in our model the fastest gravity waves propagates with $\approx 224 \text{ m/s}$.

The Rossby waves R_k are of most importance for large scale meteorological processes. Rossby waves owe their existence to the variation of the Coriolis force with latitude. The Coriolis force is the main internal force of non-inertial rotational systems such as the Earth. This is the force, which maintains the preservation of the angular momentum on the Earth. Rossby waves propagate westerly relative to the mean zonal flow \bar{u} with an approximate speed $c_k^r = \bar{u} - \frac{\beta}{k^2}$, which depends on the wave number ($\bar{k} = \frac{2*\pi*k}{L}$, $-M \leq k \leq M$). For synoptic scale motion, Rossby waves are quite slow and have a speed comparable with the mean flow speed. In our case with $M = 10$ the wave number dependent part of the Rossby wave speed ranges from 0.2 m/s to 0.002 m/s while $\bar{u} = 40 \text{ m/s}$.

The non-linear normal-mode initialisation (Machenhauer, 1977) is a slightly intuitive but powerful technique to force a generated model state into an approximate non-linear balance, established by the physical constraints of the model. Even without any initialisation procedure, the model would reach a balanced state due to the mutual adjustment of the wind and the geopotential, provided that the generated model state represents a realistic meteorological state, having a small amount of energy in the ageostrophic part of the motion.

An introduction of new data certainly disturbs the relationship between the model state variables. This imbalance creates unrealistically large amplitudes for the gravity waves and moves the analysed state away from a realistic development. The intuitive idea of non-linear mode initialisation lies in the fact (as observed by Machenhauer (1977) from experimental simulation data) that the linear tendencies for the gravity waves are balanced by their non-linear counterparts.

The model equations in normal mode space take the form

$$(42) \quad \begin{aligned} \dot{G}1_k &= i\omega_k^1 G1_k + B_{G1} \\ \dot{G}2_k &= i\omega_k^2 G2_k + B_{G2} \\ \dot{R}_k &= i\omega_k^3 R_k + B_R \end{aligned}$$

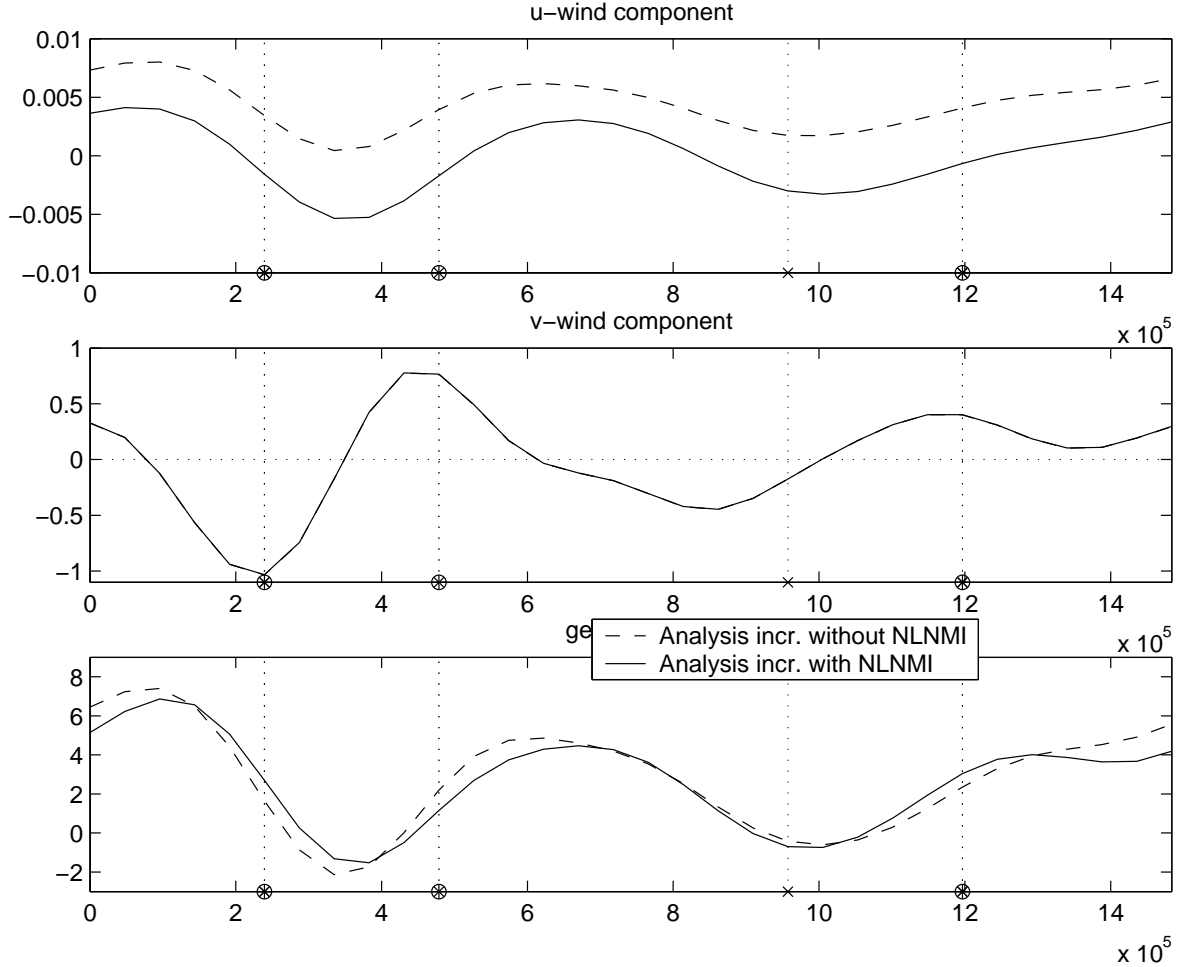


FIGURE 9. The analysis increment after 8 assimilation terms of the data assimilation by means of the bias corrected Kalman filter of 9 observations non-linearly related to the model state variable. The observations were simulated by the non-linear observation operator nlZ_1 .

A balanced state is obtained through an iterative procedure to obtain the balance conditions

$$(43) \quad \dot{G}1_k = \dot{G}2_k = 0$$

During the normal-mode initialisation procedure, the gravity wave tendencies are simply forced to approach 0. During each step of iteration, the correction to the model state is obtained by

$$\delta X_k = \vec{\Gamma}_k \begin{pmatrix} \frac{i}{\omega_k^1} \dot{G}1_k \\ \frac{i}{\omega_k^2} \dot{G}2_k \\ 0 \end{pmatrix}$$

where $\dot{G}1_k$ and $\dot{G}2_k$ are calculated by the dynamical model equations.

After the initialisation procedure the gravity waves have small amplitudes and they contain a small part of the total wave energy, which is a characteristic of a realistic flow.

In Figure 9 we can see the analysed increments obtained after 8 cycles of data assimilation of a set of 9 observations non-linearly related to the model state variable. For simulating the observations we have used the observational operator nlZ_1 , as we have defined it in

section 2.5. The observations of the same type the assumed to have the same observation error variance. The variance of the observation errors $H_i = \text{var}(\varepsilon_i)$ is 4 times smaller than the initial variance of the model state variable, projected on the observations space $tlZ_1 B_0 (tlZ_1)^T$ and averaged over all grid points. The tangent linear observation operator tlZ_1 is defined later in the introduction to section 4. The normal mode initialisation procedure, applied to the analysis increment, makes more essential corrections in the case of a non-linear observation operator. The reason is that the analysis increment has a non-linear relationship to the forecast of the model state variable. This non-linear transform of the balanced forecast state can result in an increment which is moved away from geostrophic balance. Due to this, the projection of the analysis increment on the "balanced" space is important in order to obtain an analysed state, which has properties of the real atmosphere.

3. THE KALMAN FILTER AND THE FIXED INTERVAL SMOOTHER TECHNIQUES

3.1. The second-order regression. We consider prediction of X on v , where X and the q -dimensional vector v have a known joint distribution. Without loss of generality, let $E(v) = 0$. The linear function $\hat{X} = \hat{\alpha} + \hat{\beta}^T v$, with

$$(44) \quad \hat{\alpha} = E(X)$$

$$(45) \quad \hat{\beta} = \text{var}(v)^{-1} \text{cov}(v, X)$$

will give the best linear prediction of X on v in the sense of the mean square error $E(X - \hat{X})^2$. \hat{X} is often called a second-order regression function of X on v . For this particular choice of parameters the residual term $\varepsilon = X - \hat{X}$ is uncorrelated with the explanatory variable v , has a zero mean and a variance equal

$$(46) \quad \begin{aligned} \text{var}(\varepsilon) &= \text{var}(X) - \hat{\beta}^T \text{var}(v) \hat{\beta} = \\ &= \text{var}(X) - \text{cov}(X, v) \text{var}(v)^{-1} \text{cov}(v, X) \end{aligned}$$

If the linear model for the X and v dependency works indeed, the best linear prediction \hat{X} will be the best prediction with respect to the mean squared error, and therefore equal to the conditional mean $E(X | v)$. Without any assumption on distribution, besides the existence of the second moment, the analytical expressions for the conditional mean $E(X | v)$ and the conditional variance $\text{var}(X | v)$ can be obtained by

$$(47) \quad \begin{aligned} E(X | v) &= \hat{X} = E(X) + \text{cov}(X, v) \text{var}(v)^{-1} v, \\ \text{var}(X | v) &= \text{var}(\varepsilon) = \text{var}(X) - \text{cov}(X, v) \text{var}(v)^{-1} \text{cov}(v, X) \end{aligned}$$

If the dependence of X on v is not linear, we have the more general formulas

$$(48) \quad \begin{aligned} E(X | v) &= \hat{X} + E(\varepsilon | v), \\ E(\text{var}(X | v)) &= E(\text{var}(\varepsilon | v)) = \text{var}(\varepsilon) - \text{var}(E(\varepsilon | v)) \end{aligned}$$

Hence, on the average, $\text{var}(\varepsilon) = \text{var}(X) - \text{cov}(X, v) \text{var}(v)^{-1} \text{cov}(v, X)$ will overestimate the conditional variance $\text{var}(X | v)$.

However, if the conditions

$$(49) \quad \begin{aligned} E(\varepsilon | v) &= 0 \\ \text{var}(\varepsilon | v) &= \text{const} \quad (\text{i.e.} = \text{var}(\varepsilon)) \end{aligned}$$

hold at least approximately, the conditional mean $E(X | v)$ and the conditional variance $\text{var}(X | v)$ can be approximated by (47).

The extension to the multivariate case is straightforward.

3.2. The standard Kalman filter. The standard Kalman filter (Kalman, 1960) was derived for a general Gaussian state space linear model, which can be written in the following form

$$(50) \quad y_t = Z_t X_t + \varepsilon_t,$$

$$(51) \quad X_t = T_{t-1} X_{t-1} + R_{t-1} \eta_{t-1}$$

which has some similarities with a formulation of linear regression of y_t on Z_t (50) with extra variability in the unobservable parameters X_t , $t \geq 1$ (51).

In the usual notations, y_t is a $q \times 1$ -dimensional vector of observations and X_t is an unobserved $p \times 1$ -dimensional state vector, the inference about which we want to obtain. Usually, the probability density of the initial state vector X_0 is assumed to be known, and the error terms ε_t and η_t are assumed to be serially independent, mutually independent at every time step and independent of the initial state vector.

The idea of filtering is to provide a sequential updating of our knowledge about the system X_t each time new observations are available. If we denote $\mathcal{Y}_t = \{y_1, \dots, y_t\}$, the whole set of history of observations available up to time moment t , the aim of filtering is to determine the density $p(X_t | \mathcal{Y}_t)$ recursively through the density $p(X_{t-1} | \mathcal{Y}_{t-1})$.

Applying the definition of conditional probability,

$$p(X_t | \mathcal{Y}_t) \propto p(X_t, \mathcal{Y}_t) \propto p(X_t, y_t | \mathcal{Y}_{t-1}),$$

the probability multiplication rule

$$p(X_t, y_t | \mathcal{Y}_{t-1}) = p(y_t | X_t, \mathcal{Y}_{t-1}) p(X_t | \mathcal{Y}_{t-1}),$$

and factorisation of the predictive posterior density $p(X_t | \mathcal{Y}_{t-1})$ over the parameter X_{t-1}

$$p(X_t | \mathcal{Y}_{t-1}) = \int p(X_t, X_{t-1} | \mathcal{Y}_{t-1}) dX_{t-1} = \int p(X_t | X_{t-1}, \mathcal{Y}_{t-1}) p(X_{t-1} | \mathcal{Y}_{t-1}) dX_{t-1}.$$

Finally, by taking into account the Markovian properties of the state space model,

$$\begin{aligned} p(y_t | X_t, \mathcal{Y}_{t-1}) &= p(y_t | X_t), \\ p(X_t | X_{t-1}, \mathcal{Y}_{t-1}) &= p(X_t | X_{t-1}), \end{aligned}$$

the recursive formula for conditional updating of the posterior distribution can be obtained

$$(52) \quad p(X_t | \mathcal{Y}_t) \propto p(y_t | X_t) \int p(X_t | X_{t-1})p(X_{t-1} | \mathcal{Y}_{t-1})dX_{t-1}$$

with $p(X_0 | Y_0) \equiv p(X_0)$.

Under the perfect model assumption, which means that the time evolution of the underlying system is deterministic, $X_t = T_{t-1}X_{t-1}$, the posterior distribution equation (52) is significantly simplified

$$(53) \quad p(X_t | \mathcal{Y}_t) \propto p(y_t | X_t)p(X_t | \mathcal{Y}_{t-1}).$$

All the unobservable variables X_t , $t \geq 1$ are just deterministic functions of the random variable X_0 , the posterior pdf of which is to be obtained from the prior assumption on X_0 and from the observations y_t , $t \geq 1$.

For a standard Kalman filter, the state space model is assumed linear and Gaussian,

$$(54) \quad \begin{aligned} X_0 &\sim \mathcal{N}(a_0, B_0), \\ \varepsilon_t &\sim \mathcal{N}(0, H_t), \quad t = 1, \dots, n \\ \eta_t &\sim \mathcal{N}(0, Q_t), \quad t = 0, \dots, n-1 \end{aligned}$$

All probability densities involved in the expression above will be Gaussian and hence are completely determined by their mean and variance. Let us denote $p(X_{t-1} | \mathcal{Y}_{t-1}) = \mathcal{N}(a_{t-1}, B_{t-1})$. Applying the model equations, it is straightforward to obtain the analytical expressions for both the likelihood and the updated prior for the t -th sequential analysis cycle

$$\begin{aligned} p(y_t | X_t) &= \mathcal{N}(Z_t X_t, H_t), \\ p(X_t | \mathcal{Y}_{t-1}) &= \mathcal{N}(a_t^f, B_t^f), \end{aligned}$$

with

$$(55) \quad \begin{aligned} a_t^f &= T_{t-1}a_{t-1}, \\ B_t^f &= T_{t-1}B_{t-1}T_{t-1}^T + R_{t-1}Q_{t-1}R_{t-1}^T. \end{aligned}$$

The posterior density $p(X_t | \mathcal{Y}_t)$ is proportional to the likelihood $p(y_t | X_t)$ multiplied by the prior density $p(X_t | \mathcal{Y}_{t-1})$

$$p(X_t | \mathcal{Y}_t) \propto \exp\{(y_t - Z_t X_t)^T H_t^{-1}(y_t - Z_t X_t) + (X_t - a_t^f)^T (B_t^f)^{-1}(X_t - a_t^f)\}$$

and it is Gaussian as well. Collecting all the terms and completing the square around X_t , we obtain the recursive update formulas for a_t and B_t

$$(56) \quad p(X_t | \mathcal{Y}_t) = \mathcal{N}(a_t, B_t),$$

with

$$(57) \quad \begin{aligned} B_t^{-1} &= Z_t^T H_t^{-1} Z_t + (B_t^f)^{-1}, \\ a_t &= B_t (Z_t^T H_t^{-1} y_t + (B_t^f)^{-1} a_t^f). \end{aligned}$$

These formulas can be simplified and rewritten in a form which is much easier to apply for practical calculations. First, applying the Binomial inverse theorem (Woodbury(1950)), namely

$$(58) \quad (A + UBV)^{-1} = A^{-1} - A^{-1}UB(B + BVA^{-1}UB)^{-1}BVA^{-1},$$

equations (57) can be rewritten into a more known form, which avoids the necessity for inversion of the large dimensional matrix B_t^f .

$$\begin{aligned} B_t &= B_t^f - B_t^f Z_t^T H_t^{-1} (H_t^{-1} + H_t^{-1} Z_t B_t^f Z_t^T H_t^{-1})^{-1} H_t^{-1} Z_t B_t^f, \\ a_t &= a_t^f - B_t^f Z_t^T (H_t + Z_t B_t^f Z_t^T)^{-1} Z_t a_t^f + B_t^f Z_t^T (I - (H_t + Z_t B_t^f Z_t^T)^{-1} Z_t B_t^f Z_t^T) H_t^{-1} y_t. \end{aligned}$$

Secondly, we take the following identity into account

$$I - (H_t + Z_t B_t^f Z_t^T)^{-1} Z_t B_t^f Z_t^T = (H_t + Z_t B_t^f Z_t^T)^{-1} H_t.$$

The Kalman filter recursive formulas can be summarised by following filtering equations.

$$(59) \quad \begin{aligned} a_t &= a_t^f + K_t (y_t - Z_t a_t^f) \\ B_t &= B_t^f - B_t^f Z_t^T (H_t + Z_t B_t^f Z_t^T)^{-1} Z_t B_t^f \\ F_t &= H_t + Z_t B_t^f Z_t^T \\ K_t &= B_t^f Z_t^T F_t^{-1} \\ a_t^f &= T_{t-1} a_{t-1} \\ B_t^f &= T_{t-1} B_{t-1} T_{t-1}^T + R_{t-1} Q_{t-1} R_{t-1}^T \end{aligned}$$

This system of equations together with the assumptions (54) defines the Kalman filter. The system of equations describes not only the time evolution of the mean and the variance of the unobservable model state variable X , it describes much more. At the end of the analysis sequence we obtain the posterior distribution $p(X_n | \mathcal{Y}_n)$, the most that we can say about the unobservable variable X_n based on the observations y_1, \dots, y_n and the prior information about the initial state and the model errors.

Some basic features of Kalman filtering are illustrated in Figure 10, where the symbols on the x -axes denote location of observations. The group of 9 observations relates, in fact, non-linearly to the unobservable model state variable and are assimilated by means of the extension of the standard Kalman filter, the bias corrected Kalman filter. However, the basic principles of data handling remain essentially the same and here we will illustrate one of the basic ones. In the case of a perfect model assumption, after several data assimilation cycles, the lower precision data create stronger influence on the analysed field and produce larger analysis increments. Indeed, in the Kalman filter framework the weights of the observations reflect the relative precision of the observations compared to the precision of the unobservable model state. The precision is expressed in the terms of variances. Every time observations with a lower precision are assimilated, the posterior

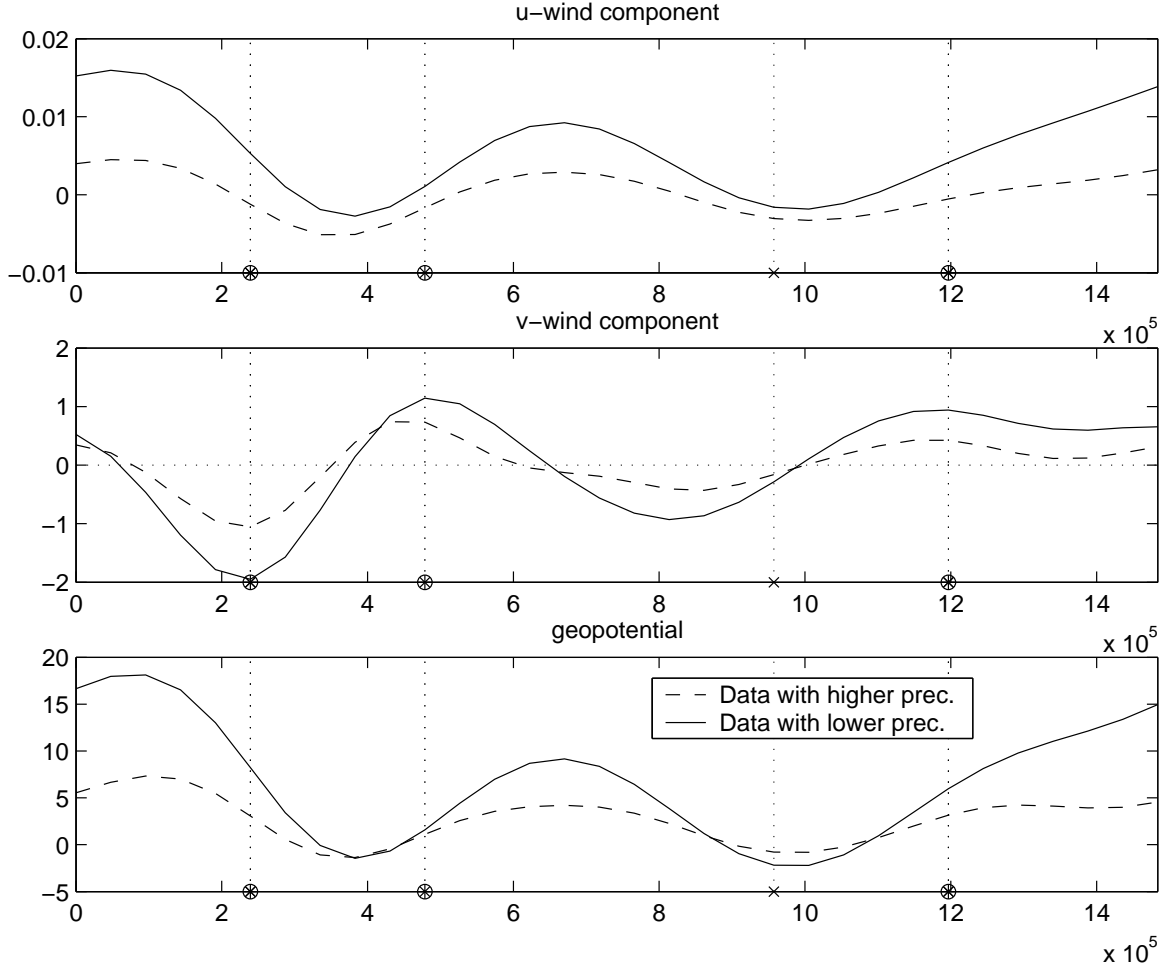


FIGURE 10. The analysis increments after 8 terms of assimilation by means of the bias corrected Kalman filter of two groups of 9 observations with different precision. The dashed line denotes the analysis increment corresponding to the "high" precision observations, the solid line denotes the analysis increments for the "low" precision data. The observations were simulated by the non-linear observation operator nlZ_3 . The position of the observations are marked on the x -axes by o for geopotential observations, by $*$ for u -wind component observations and by x for v -wind component observations.

variance of the unobservable model state variable $var(\hat{X}_t | \mathcal{Y}_t)$ remains larger than the one obtained by assimilating observations with higher precision, what can be seen from (57). Thus, the relative precision of observations with a larger variance of observation errors becomes higher than the relative precision of observations with a small variance of observational errors. Therefore, the impact of data with lower precision seems to be larger after several assimilation terms. Even if the observations are the main sources of information from the "true" model state, the high weights of the observations can make harm by letting the observation errors themselves influence the construction of the analysed state too much, and in such a way they can move the analysed state away from the "true" state.

When high precision observations were assimilated, the analysed state comes closer to observations from the start of the data assimilation. At the same time the analysed state comes closer to the "true" model state, as it is reflected in smaller analysis error variance.

A little impact of the later introduced observations is needed in order to improve the analysed state which is already close to the "true" state.

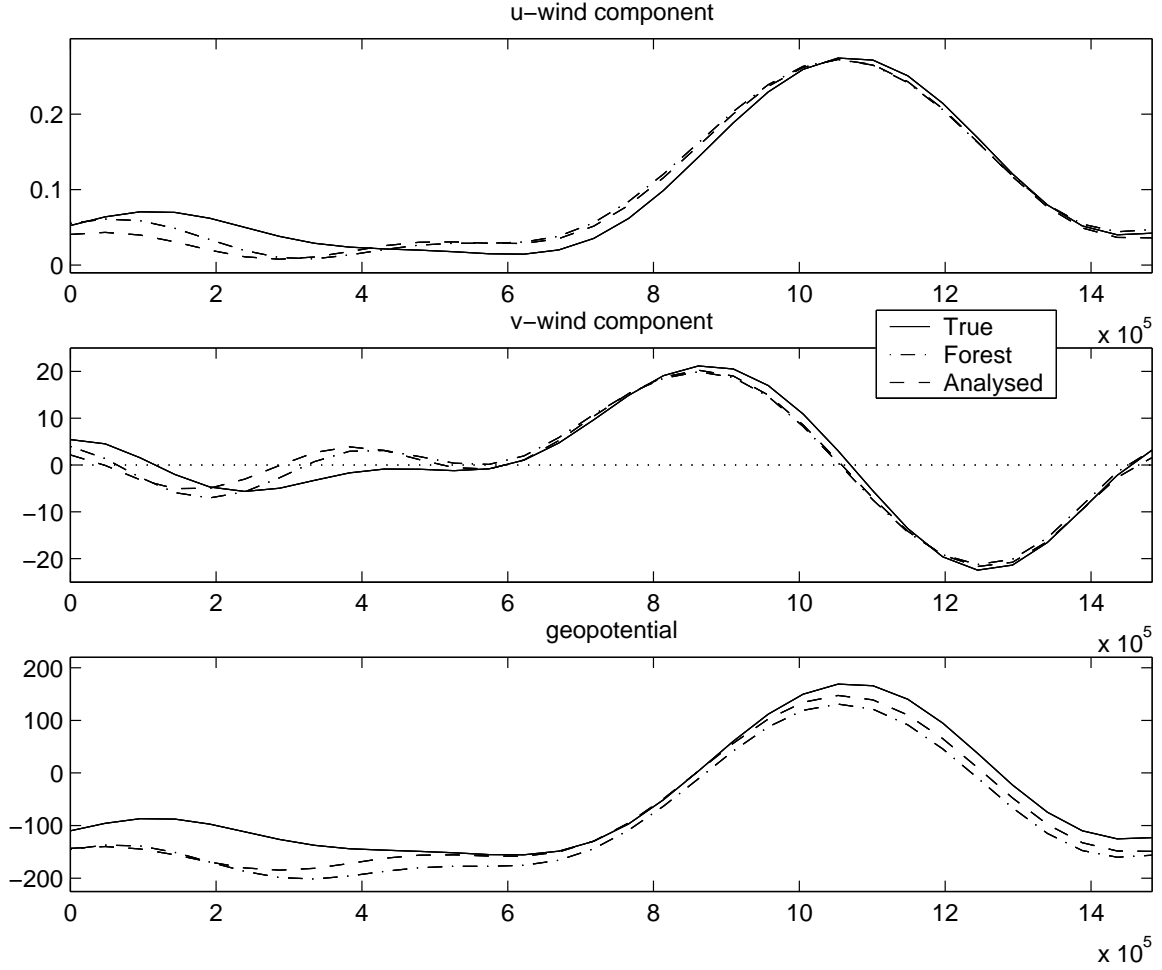


FIGURE 11. The analysed fields after assimilation of a group of 9 observations non-linearly related to the model state variable. Assimilation was performed by the bias corrected Kalman filter. Results shown here are after 4 assimilation terms. The observations were simulated by the non-linear observation operator nlZ_3 and they are of "high" precision. The positions of the observations are marked on Figure 12.

In Figures 11 and Figure 12 we present the result of 4 cycles of the application of the bias corrected Kalman filter for the assimilation of a group of 9 observations non-linearly related to the model state variable. For simulation of the observations we have chosen the observation operator tlZ_3 (see section 2.5). The variance of the observation error H_i is the same for the same type of observation located at different position and is 4 times smaller than the initial forecast error variance of the model state, projected to the space of observations $(tlZ_3B_0(tlZ_3)^T)_i$ and averaged over all grid-points. The symbols on the "x"-axes denote the locations of observations. Like in the case with a linear observation operator, the analysis increment of the meteorological fields, as well as the meteorological fields themselves, are in good accordance with the geostrophic adjustment process. Again, while the v -wind component is negative, i.e. an air mass particle is displaced southward, the radius of the particle rotation is increasing. The u -wind component is then decreasing in order to maintain the conservation of angular momentum. The v -wind component is approximately equal to the spatial derivative of the geopotential, thus the analyses state is

in a balance well approximated by the geostrophic one. It is interesting to notice that the geopotential adjusts to the v -wind component field in the case of non-linear observations as well. Like we already have mentioned, the model has smaller spatial scales compared to the Rossby radius of deformation, and according to theory the geopotential field is adjusted to the v -wind component. The two observations located closely to one another produce a more noisy analysis field but help to filter out the observation errors.

The time evolution of the posterior mean and the posterior variance of the variable holds under much weaker assumptions than the usual ones assumed for a linear Gaussian state space model. As we will show below, it can be derived from the approach based on the best linear prediction (section 3.1) which is free from any assumptions about the form of the distributions. The only requirement for the validity of the formulas is the linearity of the state space model, that is, both the model propagator T and the observation operator Z must be linear. The state variable X_t is regressed on the innovation vector $v_t = y_t - E(y_t | \mathcal{Y}_{t-1})$, a linear function of the newly obtained observations, given the whole previous history of observations \mathcal{Y}_{t-1} . The innovation vector has zero mean, $E(v_t) =$

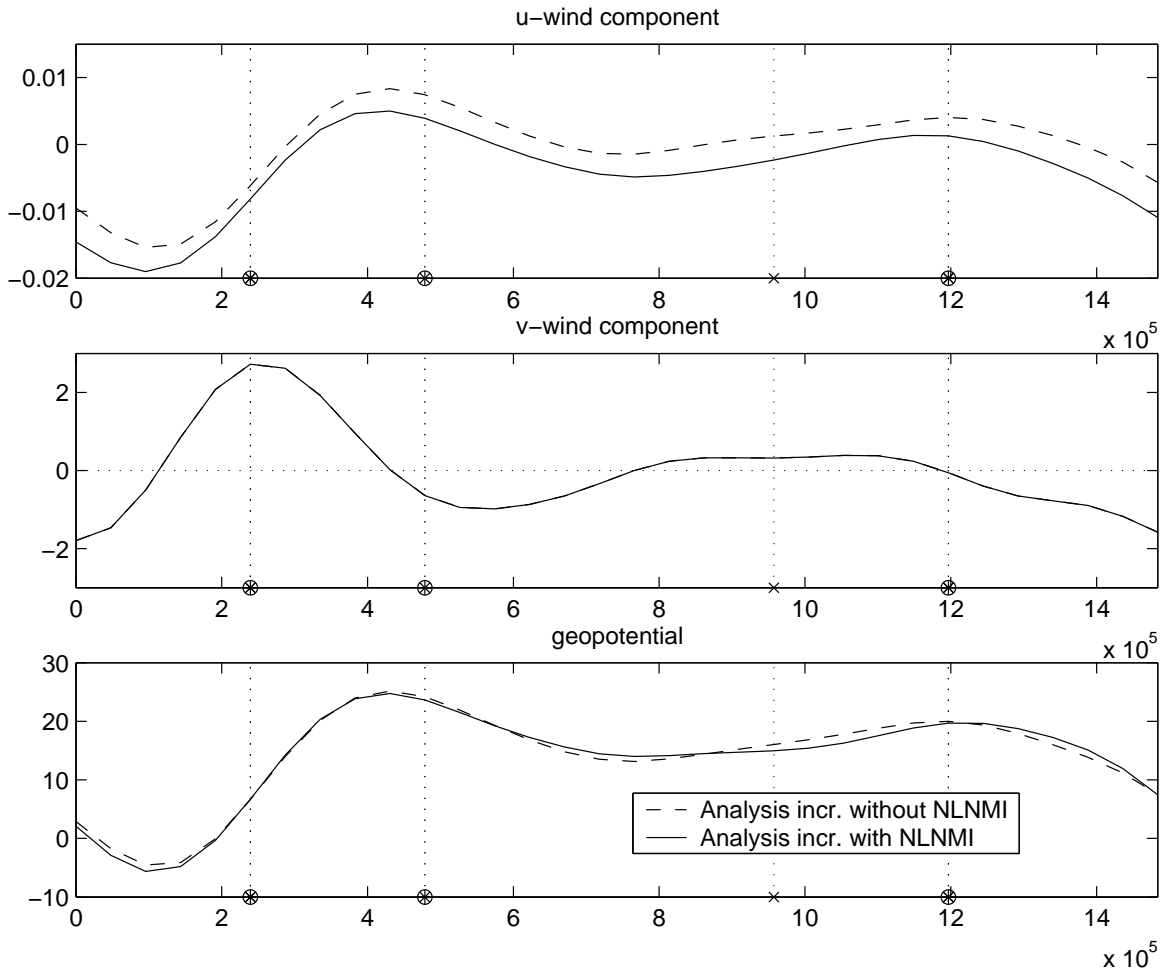


FIGURE 12. The analysis increments after assimilation of a group of 9 observations non-linearly related to the model state variable. Assimilation was performed by the bias corrected Kalman filter. Results are shown after 4 assimilation terms. The observations were simulated by the non-linear observation operator nlZ_3 and they are of "high" precision. The positions of the observations are marked on the x -axes in the same way as in Figure 10

$E[E(v_t | \mathcal{Y}_{t-1})] = 0$. $E(X_t | y_t, \mathcal{Y}_{t-1})$ is the best linear predictor of X_t , and when the observation operator is linear, this predictor is linear in y_t (or v_t). Taking (47) into account and the fact that for a linear Gaussian state space model the innovation vector v_t is independent of the history of observations \mathcal{Y}_{t-1} , we will have

$$(60) \quad \begin{aligned} E(X_t | y_t, \mathcal{Y}_{t-1}) &= E(X_t | \mathcal{Y}_{t-1}) + \text{cov}(X_t, v_t | \mathcal{Y}_{t-1}) \text{var}(v_t)^{-1} v_t \\ \text{Var}(X_t | y_t, \mathcal{Y}_{t-1}) &= \text{var}(X_t | \mathcal{Y}_{t-1}) - \text{cov}(X_t, v_t | \mathcal{Y}_{t-1}) \text{var}(v_t)^{-1} \text{cov}(v_t, X_t | \mathcal{Y}_{t-1}). \end{aligned}$$

As it already was mentioned, the observation error terms are assumed to be mutually uncorrelated, $E(\varepsilon_{t_1}, \varepsilon_{t_2}) = 0$ if $t_1 \neq t_2$, and uncorrelated with the state variable $E(\varepsilon_t, X_j) = 0$ for $j \leq t$.

$$(61) \quad \begin{aligned} v_t &= y_t - E(y_t | \mathcal{Y}_{t-1}) \\ &= Z_t(X_t - E(X_t | \mathcal{Y}_{t-1})) + \varepsilon_t \\ &= y_t - Z_t a_t^f. \end{aligned}$$

Then

$$(62) \quad \begin{aligned} \text{var}(v_t) = F_t &= E[E(v_t v_t^T | \mathcal{Y}_{t-1})] \\ &= E[E(Z_t(X_t - E(X_t | \mathcal{Y}_{t-1})))((X_t - E(X_t | \mathcal{Y}_{t-1}))^T Z_t^T | \mathcal{Y}_{t-1})] + \text{var}(\varepsilon_t) \\ &= E[Z_t \text{var}(X_t | \mathcal{Y}_{t-1}) Z_t^T] + \text{var}(\varepsilon_t) = E[Z_t B_t^f Z_t^T] + H_t \\ &= Z_t B_t^f Z_t^T + H_t \end{aligned}$$

and

$$(63) \quad \begin{aligned} \text{cov}(X_t, v_t | \mathcal{Y}_{t-1}) &= E[E\{(X_t - E(X_t | \mathcal{Y}_{t-1}))((Z_t(X_t - E(X_t | \mathcal{Y}_{t-1})) + \varepsilon_t)^T | \mathcal{Y}_{t-1})\}] \\ &= E[\text{var}(X_t | \mathcal{Y}_{t-1}) Z_t^T] + \text{cov}(X_t, \varepsilon_t) \\ &= B_t^f Z_t^T \end{aligned}$$

Inserting equations (61)-(63) into (60) we will obtain the same system of filtering equations.

Whatever linear model we have, the recursions above give the time evolution of the best predictor of the unobservable model state with knowledge improvement based on the increasing sequence of observations available up to time t . If the linear model is Gaussian, the recursions give the complete information about the time development and the improvement of the predictive posterior distribution $p(X_t | \mathcal{Y}_t)$ as well. The recursion $a_t = T_{t-1} a_{t-1} + K_t (y_t - Z_t T_{t-1} a_{t-1})$ gives the evolution of the posterior mode and the recursion on B_t gives the evolution of the curvature around the mode for the Gaussian pdf.

3.3. The classical fixed interval smoother. A smoothing is an alternative to filtering in the conditional inference about unobservable variables of interest, based on the observed

data. Smoothing deals with the conditional pdf for $\{X_0, X_1, \dots, X_n\}$, given the whole set of observations $\mathcal{Y} = \{y_1, \dots, y_n\}$. This can be written

$$\begin{aligned}
(64) \quad p(X_0, \dots, X_n | \mathcal{Y}) &\propto p(X_0, \dots, X_n, \mathcal{Y}) \\
&= p(X_0) \prod_{t=1}^n p(X_t, y_t | X_{t-1}, \dots, X_0, y_{t-1}, \dots, y_1) \\
&= p(X_0) \prod_{t=1}^n p(y_t | X_t) p(X_t | X_{t-1})
\end{aligned}$$

The last equation holds due to the Markovian properties of the state space system. For Gaussian linear systems, all the pdfs involved in (64), are Gaussian. This mean that the pdf $p(X_0, \dots, X_n | \mathcal{Y})$ is Gaussian as well. For a Gaussian distribution the mode is equal to the posterior mean $E(X | \mathcal{Y}) = (E(X_1 | \mathcal{Y}), \dots, E(X_n | \mathcal{Y}))$, and for linear state space models it is also equal to the best mean square error estimator of the state variable, given the whole set of observations \mathcal{Y} . In particular, $E(X_0 | \mathcal{Y})$ is the best linear predictor of the initial variable X_0 , which could give rise to the observed data \mathcal{Y} .

In our study a perfect model is assumed, which means that all X_t , $t \geq 1$ are deterministic function of a random initial state X_0 . At the end of the filtering procedure (see section above), in the case of a linear model, an analytic expression for the time evolution of the posterior mode is obtained, because a posterior mode is invariant under linear transformations.

$$\begin{aligned}
(65) \quad T_{n-1} \cdots T_0 E(X_0 | \mathcal{Y}) &= E(T_{n-1} \cdots T_0 X_0 | \mathcal{Y}) = E(X_n | \mathcal{Y}) = \\
&= a_n^f + K_n(y_n - Z_n a_n^f)
\end{aligned}$$

If the matrix $T_{n-1} \cdots T_0$ would be invertible, we would immediately obtain an expression for $E(X_0 | \mathcal{Y})$ in the case of a perfect model by multiplying both sides of the equation with the matrix inverse. The tangent-linear approximation of the model dynamics is singular in the meteorological models. Singularity means that the solution develops in some subspace only, determined by the approximation of the valid physical balance, for example. In other words, there exists a subspace where the solution will never appear. With the singular matrix $T_{n-1} \cdots T_0$, we cannot obtain a unique solution to equation (65) by means of matrix inversion, but we can construct a pseudo-inverse by means of backtracking. Certainly, it is possible to express $E(X_0 | \mathcal{Y})$ as a weighted average of the prior mean and the observations, but, like in case of the Kalman filter derivation, it is much simpler to use recursive formulas to obtain $E(X_0 | \mathcal{Y})$.

Let us denote $\hat{\alpha}_t = E(X_t | \mathcal{Y})$ and $V_t = \text{var}(X_t | \mathcal{Y})$. Then, obviously,

$$\begin{aligned}
(66) \quad \hat{\alpha}_n &= a_n = E(X_n | \mathcal{Y}), \\
V_n &= B_n = \text{var}(X_n | \mathcal{Y}), \\
\hat{\alpha}_t &= T_{t-1} \hat{\alpha}_{t-1}, \\
V_t &= T_{t-1} V_{t-1} T_{t-1}^T, \quad 1 \leq t \leq n
\end{aligned}$$

It is straightforward to obtain analytical expressions for $\hat{\alpha}_{n-1}, V_{n-1}$, using the Kalman filter forecasting formulas (59) with $Q_t \equiv 0$, $t \geq 0$ and $B_n^f = T_{n-1} B_{n-1} T_{n-1}^T$

$$\begin{aligned}
\hat{\alpha}_n &= a_n = a_n^f + B_n^f Z_n^T F_n^{-1} v_n \\
&= T_{n-1} a_{n-1} + T_{n-1} B_{n-1} T_{n-1}^T Z_n^T F_n^{-1} v_n \\
&= T_{n-1} (a_{n-1} + B_{n-1} (Z_n T_{n-1})^T F_n^{-1} v_n) = T_{n-1} \hat{\alpha}_{n-1}, \\
V_n &= B_n = B_n^f - B_n^f Z_n^T F_n^{-1} Z_n B_n^f \\
&= T_{n-1} B_{n-1} T_{n-1}^T - T_{n-1} B_{n-1} T_{n-1}^T Z_n^T F_n^{-1} Z_n T_{n-1} B_{n-1} T_{n-1}^T \\
&= T_{n-1} (B_{n-1} - B_{n-1} (Z_n T_{n-1})^T F_n^{-1} (Z_n * T_{n-1}) B_{n-1}) T_{n-1}^T = T_{n-1} V_{n-1} T_{n-1}^T
\end{aligned}$$

Let us denote $r_n = (Z_n T_{n-1})^T F_n^{-1} v_n$ and $N_n = (Z_n T_{n-1})^T F_n^{-1} (Z_n T_{n-1})$. Then

$$\begin{aligned}
(67) \quad \hat{\alpha}_{n-1} &= a_{n-1} + B_{n-1} r_n, \\
V_{n-1} &= B_{n-1} - B_{n-1} N_n B_{n-1}
\end{aligned}$$

In fact for all $\hat{\alpha}_t, V_t, 0 \leq t \leq n-1$, similar expressions hold.

To obtain the result it is convenient to use the following backwards recursive formulas valid for the filtering covariance matrices. First,

$$\begin{aligned}
(68) \quad B_t &= B_t^f - B_t^f Z_t^T F_t^{-1} Z_t B_t^f \\
&= T_{t-1} B_{t-1} T_{t-1}^T - T_{t-1} B_{t-1} T_{t-1}^T Z_t^T F_t^{-1} Z_t T_{t-1} B_{t-1} T_{t-1}^T \\
&= T_{t-1} (B_{t-1} - B_{t-1} (Z_t T_{t-1})^T F_t^{-1} (Z_t T_{t-1}) B_{t-1}) T_{t-1}^T
\end{aligned}$$

Secondly,

$$\begin{aligned}
(69) \quad B_t &= B_t^f - B_t^f Z_t^T F_t^{-1} Z_t B_t^f \\
&= B_t^f (I - Z_t^T K_t^T) = T_{t-1} B_{t-1} T_{t-1}^T (I - (K_t Z_t)^T) \\
&= T_{t-1} B_{t-1} ((I - (K_t Z_t)^T)^T T_{t-1})^T \\
&= T_{t-1} B_{t-1} (T_{t-1} - T_{t-1} K_t Z_t)^T = \\
&= T_{t-1} B_{t-1} L_t^T
\end{aligned}$$

with the notation $L_t = T_{t-1} - K_t Z_t T_{t-1}$.

Inserting (68) and (69) in the recursive Kalman filter formulas (59), it is easy to obtain an analytic expression for $\hat{\alpha}_{n-2}$

$$\begin{aligned}
\hat{\alpha}_{n-1} &= a_{n-1} + B_{n-1} r_n = a_{n-1}^f + B_{n-1}^f Z_{n-1}^T F_{n-1}^{-1} v_{n-1} + B_{n-1} r_n \\
&= T_{n-2} (a_{n-2} + B_{n-2} ((Z_{n-1} T_{n-2})^T F_{n-1}^{-1} v_{n-1} + L_{n-1}^T r_n)) = T_{n-2} \hat{\alpha}_{n-2}.
\end{aligned}$$

Thus, we can express $\hat{\alpha}_{n-2}$ as

$$(70) \quad \hat{\alpha}_{n-2} = a_{n-2} + B_{n-2} r_{n-1}$$

where $r_{n-1} = (Z_{n-1} T_{n-2})^T F_{n-1}^{-1} v_{n-1} + L_{n-1}^T r_n$.

It is easy to see that for all $0 \leq t \leq n-1$

$$(71) \quad \hat{\alpha}_t = a_t + B_t r_{t+1}$$

where r_t is obtained through backwards recursion

$$r_t = (Z_t T_{t-1})^T F_t^{-1} v_t + L_t^T r_{t+1}$$

with $r_n = (Z_n T_{n-1})^T F_n^{-1} v_n$

By inserting the recursive expression of B_{n-1} (68) and (69) into (67), we obtain a recursive expression for V_{n-2}

$$\begin{aligned} V_{n-1} &= B_{n-1} - B_{n-1} N_n B_{n-1} \\ &= T_{n-2} [B_{n-2} - B_{n-2} ((Z_{n-1} T_{n-2})^T F_{n-1}^{-1} (Z_{n-1} T_{n-2}) + L_{n-1}^T N_n L_{n-1}) B_{n-2}] T_{n-2}^T \\ &= T_{n-2} V_{n-2} T_{n-2}^T \end{aligned}$$

Thus, we can express V_{n-2} as

$$(72) \quad V_{n-2} = B_{n-2} - B_{n-2} N_{n-1} B_{n-2}$$

where

$$N_{n-1} = (Z_{n-1} T_{n-2})^T F_{n-1}^{-1} (Z_{n-1} T_{n-2}) + L_{n-1}^T N_n L_{n-1}$$

with $N_n = (Z_n T_{n-1})^T F_n^{-1} (Z_n T_{n-1})$.

In fact, for all V_t , $0 \leq t \leq n-1$ a similar expression holds, namely

$$(73) \quad V_t = B_t - B_t N_{t+1} B_t,$$

where a backwards recursion for N_t , $1 \leq t \leq n-1$ is defined as follows

$$N_t = (Z_t T_{t-1})^T F_t^{-1} (Z_t T_{t-1}) + L_t^T N_{t+1} L_t$$

We may summarise the results in the following backwards recursion formulas.

$$(74) \quad \begin{aligned} r_t &= (Z_t T_{t-1})^T F_t^{-1} v_t + L_t^T r_{t+1} \\ N_t &= (Z_t T_{t-1})^T F_t^{-1} (Z_t T_{t-1}) + L_t^T N_{t+1} L_t \end{aligned}$$

with

$$\begin{aligned} L_t &= T_{t-1} - T_{t-1} K_t Z_t, \quad t = 1, \dots, n-1, \\ r_n &= (Z_n T_{n-1})^T F_n^{-1} v_n, \\ N_n &= (Z_n T_{n-1})^T F_n^{-1} (Z_n T_{n-1}) \end{aligned}$$

This formulation provides possibility to calculate the best predictor of the initial state $E(X_0 | \mathcal{Y})$ given the whole sequence of observations.

$$E(X_0 | \mathcal{Y}) = \hat{\alpha}_0 = a_0 + B_0 r_1$$

$$var(X_0 | \mathcal{Y}) = V_0 = B_0 - B_0 N_1 B_0$$

where a_0, B_0 are the prior mean and the prior variance of the initial state X_0 .

From the same recursion we can obtain the time evolution of the best predictor as well

$$E(X_t | \mathcal{Y}) = \hat{\alpha}_t = a_t + B_t r_{t+1}, \quad t = 1, \dots, n-1$$

$$var(X_t | \mathcal{Y}) = V_t = B_t - B_t N_{t+1} B_t, \quad t = 1, \dots, n-1$$

with $\hat{\alpha}_n = a_n, V_n = B_n$.

Certainly, in the case with a perfect model assumption, we can obtain the time evolution of the best predictor simply by integrating the predictor over time as well

$$E(X_t | \mathcal{Y}) = T_{t-1} \cdots T_0 \hat{\alpha}_0$$

$$var(X_t | \mathcal{Y}) = T_{t-1} \cdots T_0 V_0 (T_{t-1} \cdots T_0)^T, \quad t = 1, \dots, n$$

Because the posterior distribution is Gaussian, the smoother gives not only the time evolution of the best predictor of the initial state, which coincides in this case with the evolution of the posterior predictive mode, but completely defines the evolution over time of the whole posterior distribution.

We would like to stress that this derivation of the posterior mode and the posterior variance evolution is valid only under a perfect model assumption, even if very similar results can be obtained under a general formulation, which assumes extra variability in the dynamical development of the model state. The general classical fixed interval smoother was presented by Anderson and Moore (1979).

4. THE APPLICATION OF THE KALMAN FILTER AND THE CLASSICAL FIXED INTERVAL SMOOTHER IN THE CASE OF NON-LINEAR DYNAMICS

In section 2.5 we have formulated the data assimilation problem in the form of a state space model. The numerical approximation of the time evolution of the atmospheric state results in series of unobservable $p \times 1$ - dimensional vectors $\hat{X}(t_0), \hat{X}(t_1), \dots, \hat{X}(t_{N_{ass}})$, the inference about which must be obtained from a series of observable $q \times 1$ dimensional quantities $y_1, \dots, y_{N_{ass}}$. The relationship in time between the unobservable vectors $\hat{X}(t_{i-1})$ and $\hat{X}(t_i)$ is determined through the composite model state propagator F^{i-1} , presented in section 2.5 (equation (15)), approximating the dynamical evolution of the system over the observation time window $(t_{i-1}, t_i), 1 \leq i \leq N_{ass}$

$$(75) \quad \hat{X}(t_i) = F^{i-1}(\hat{X}(t_{i-1})), \quad 1 \leq i \leq N_{ass}$$

with all uncertainty concentrated in the initial state construction $\hat{X}_{t_0} = \hat{X}_0 \sim \mathcal{N}(a_0, B_0)$. The relationship between the $\hat{X}(t_i)$'s and y_i 's is determined as well and is called the observation operator Z .

$$(76) \quad y_i = Z(\hat{X}(t_i)) + \varepsilon_i, \quad 1 \leq i \leq N_{ass}$$

The numerical propagator $F^{i-1}(\cdot)$, approximating the dynamical equations governing the atmospheric development, is non-linear and the observation operator is usually non-linear as well. Even in the case of a linear observation operator, the initially Gaussian pdf will develop to a non-Gaussian one, and will not be defined by the mean and the variance only. As it was already mentioned in the introduction, the numerical integration of the non-linear differential equations determining the time evolution of the pdf is not feasible. There is no possibility to calculate the exact dynamical time evolution of the moments involved in the Kalman filter derivation. Thus, from a theoretical point of view the Kalman filter and the fixed interval smoother cannot be used. However, different approximations can be applied. The analysis, of course, will not be optimal in this case. We will try to implement four different approximations to the standard Kalman filter, each of them utilises different optimality features of the Kalman filter. We will compare them by the quality of "the analysed state" itself and by the quality of the forecast constructed from the analysed state. In the rest of this section we will give descriptions of these different approaches and we will emphasize the optimal features of the Kalman filter and the smoother that they will utilise.

In fact the numerical propagator $F^{i-1}(\cdot)$ is able to describe only the time evolution of nearly balanced model states. We have discussed valid physical balances in section 2.7, i.e. how realistic atmospheric fields should look like. When new observations are assimilated, unrealistically large disturbances destroying the balance are created due to the imperfections of the observations. The differential equations, used in the shallow water model, are not able to provide a realistic dynamical evolution from such unbalanced initial states. Every time new observations are introduced, we therefore use the normal mode initialisation procedure, which helps to obtain a balanced state that can be governed by the propagator. The complete propagator used in the assimilation scheme is $\bar{F}^{i-1}(\cdot) = F^{i-1} \cdot f_{nmi} = (O \quad I)F \cdot F \cdot \dots \cdot FF^* \cdot f_{nmi}(\cdot)$, where $f_{nmi}(\cdot)$ denotes the iterative non-linear normal mode initialisation procedure. For the "true" model state \bar{X} (the projection of the atmospheric state on the discrete model space, in general, and the one which was used to simulate observations, in our case) the results obtained with and without the normal mode initialisation procedure will be very similar, because the normal mode initialisation procedure will only marginally influence an already "balanced" state. The tangent-linear normal mode initialisation operator is a projection operator which has eigenvalues being equal to 1's and 0's. The application of the initialisation operator is one of the reasons why the dynamical propagator is singular for the one dimensional shallow water model.

If a propagator is non-linear, it is impossible to obtain the true deterministic evolution of moments. But the evolution of the moments can be approximated, using a linearisation of the dynamics. Certainly, the degree of approximation will depend on the chosen linearisation.

Let $f(\cdot)$ denote a non-linear function. With the first-order of linearisation

$$(77) \quad \hat{X}(t) = f(\hat{X}(t_0)) \approx f(\hat{a}) + \frac{\partial f}{\partial \hat{X}}(\hat{a})(\hat{X}(t_0) - \hat{a})$$

where \hat{a} is some chosen point on the definition interval of the function. The functional $\frac{\partial f}{\partial \hat{X}}(\hat{a})$ is called a tangent linear operator at point \hat{a} . Then, with the first-order of linearisation

$$E(\hat{X}(t)) \approx f(\hat{a}) + \frac{\partial f}{\partial \hat{X}}(\hat{a})(E(\hat{X}(t_0)) - \hat{a})$$

$$Var(\hat{X}(t)) = E(\hat{X}(t) - E(\hat{X}(t)))^2 \approx \frac{\partial f}{\partial \hat{X}}(\hat{a})var(\hat{X}(t_0))\left(\frac{\partial f}{\partial \hat{X}}(\hat{a})\right)^T$$

If we choose $a = E(\hat{X}(t_0))$, the formula for evolution of the mean simplifies to $E(\hat{X}(t)) \approx f(\hat{a}) = f(E(\hat{X}(t_0)))$. For the variance, the formula of the approximate evolution remains essentially the same, with the tangent linear operator evaluated at a particular point.

In the remaining part of this subsection we will discuss the tangent linear operators that we will use, namely the tangent linear operator of the dynamical propagator and the tangent linear observation operator.

For the composite dynamical propagator

$$\bar{F}^{i-1}(\cdot) = F^{i-1} \cdot f_{nmi} = (O \quad I) \cdot F \cdot F \cdot \dots \cdot F \cdot F^* \cdot f_{nmi}(\cdot)$$

the tangent linear operator consists of $s = t_i - t_{i-1} + 1$ matrix multiplications

$$\bar{T}^{i-1}(\hat{a}) = (O \quad I) \cdot T(\hat{a}_{s-1}) \cdot \dots \cdot T(\hat{a}_1) \cdot T^*(\hat{a}_0) \cdot T_{nmi}(\hat{a}),$$

where $\hat{a}_0 = f_{nmi}(\hat{a})$, $\hat{a}_1 = (O \quad I)F^*(\hat{a}_0)$, $\hat{a}_2 = (O \quad I)F(\hat{a}_1)$, \dots , $\hat{a}_{s-1} = (O \quad I)F(\hat{a}_{s-2})$ is a trajectory of the model state evolution by the non-linear operator $\bar{F}^{i-1}(\cdot)$.

For a non-linear operator $f(\hat{X}) = C\hat{X} + B(\hat{X})$, the corresponding tangent linear operator evaluated at point \hat{a} is given by

$$T(\hat{a}) = C + \frac{\partial B}{\partial \hat{X}}(\hat{a})$$

The non-linear operators $F(\cdot)$, $F^*(\cdot)$, $f_{nmi}(\cdot)$ contain the non-linear parts in form of a linear function of the non-linear vector $B(\hat{a})$

(78)

$$B(\hat{X}) = \begin{pmatrix} B_k^u, & -M \leq k \leq M \\ B_k^v, & -M \leq k \leq M \\ B_k^\phi, & -M \leq k \leq M \end{pmatrix} = \begin{pmatrix} -\mathcal{F}_k(\mathcal{F}^{-1}(\hat{u})\mathcal{F}^{-1}(i\vec{l}\hat{u})), & -M \leq k \leq M \\ -\mathcal{F}_k(\mathcal{F}^{-1}(\hat{u})\mathcal{F}^{-1}(i\vec{l}\hat{v})), & -M \leq k \leq M \\ -i\vec{k}\mathcal{F}_k(\mathcal{F}^{-1}(\hat{u})\mathcal{F}^{-1}(\hat{\phi})), & -M \leq k \leq M \end{pmatrix} =$$

$$\begin{pmatrix} -\frac{1}{N} \sum_{j=1}^N (\sum_{l=-M}^M \hat{u}_l e^{ilx_j} \sum_{m=-M}^M i\hat{m}\hat{u}_m e^{imx_j}) e^{-ikx_j}, & -M \leq k \leq M \\ -\frac{1}{N} \sum_{j=1}^N (\sum_{l=-M}^M \hat{u}_l e^{ilx_j} \sum_{m=-M}^M i\hat{m}\hat{v}_m e^{imx_j}) e^{-ikx_j}, & -M \leq k \leq M \\ -\frac{1}{N} \sum_{j=1}^N (\sum_{l=-M}^M \hat{u}_l e^{ilx_j} \sum_{m=-M}^M \hat{\phi}_m e^{imx_j}) i\vec{k} e^{-ikx_j}, & -M \leq k \leq M \end{pmatrix}$$

Let the state \hat{a} be defined as a vector $(\hat{u}_k, \hat{v}_k, \hat{\phi}_k)$, $-M \leq k \leq M$. The tangent-linear operator $\frac{\partial B}{\partial \hat{X}}(\hat{a})$ is then a $3 * (2M + 1)$ -dimensional square matrix with coefficients

$$\begin{pmatrix} \frac{\partial B_k^u}{\partial u_l}(a), & 0, & 0 \\ \frac{\partial B_k^v}{\partial u_l}(a), & \frac{\partial B_k^v}{\partial v_l}(a), & 0 \\ \frac{\partial B_k^\phi}{\partial u_l}(a), & 0, & \frac{\partial B_k^\phi}{\partial \phi_l}(a) \end{pmatrix}$$

where

$$\begin{aligned} \frac{\partial B_k^u}{\partial u_l} &= -\frac{1}{N} \sum_{j=1}^N \left(\frac{\partial u}{\partial x}(x_j) + i\hat{l}u'(x_j) \right) e^{i(\hat{l}-\hat{k})x_j} \\ \frac{\partial B_k^v}{\partial u_l} &= -\frac{1}{N} \sum_{j=1}^N \left(\frac{\partial v}{\partial x}(x_j) \right) e^{i(\hat{l}-\hat{k})x_j} \\ \frac{\partial B_k^v}{\partial v_l} &= -\frac{1}{N} \sum_{j=1}^N i\hat{l}u'(x_j) e^{i(\hat{l}-\hat{k})x_j} \\ \frac{\partial B_k^\phi}{\partial u_l} &= -\frac{1}{N} \sum_{j=1}^N i\hat{k}\phi'(x_j) e^{i(\hat{l}-\hat{k})x_j} \\ \frac{\partial B_k^\phi}{\partial \phi_l} &= -\frac{1}{N} \sum_{j=1}^N i\hat{k}u'(x_j) e^{i(\hat{l}-\hat{k})x_j} \end{aligned} \quad (79)$$

$k = -M, \dots, M$ and $l = -M, \dots, M$. $x_j, j = 1, \dots, N$ are the grid point positions. $\hat{l} = \frac{2\pi l}{L}, \hat{k} = \frac{2\pi k}{L}$, $\frac{\partial u}{\partial x}(x_j) = \sum_{k=-M}^M i\hat{k}\hat{u}_k e^{i\hat{k}x_j}$ and $\frac{\partial v}{\partial x}(x_j)$ is defined in a similar way.

It is straightforward to obtain the explicit expression for the tangent-linear dynamical propagator $\bar{T}^{i-1}(\hat{a})$ from the given formulation of the non-linear propagator $\bar{F}^{i-1}(\cdot)$ and from $\frac{\partial B}{\partial \hat{X}}(\hat{a})$ defined above. We will not give it in full details to avoid too complex notations.

It is important to notice that the tangent-linear normal mode initialisation operator $T_{nmi}(\hat{a})$ is a projection operator, with eigen-values equal 1 or 0. The tangent-linear normal mode initialisation approximates a slow manifold, in which the solution of the differential equations develops in a smaller dimensional linear subspace along the trajectory of a chosen model state a . Even the non-singular covariance matrix B_0 becomes singular after the transformation. All the covariance matrices $B_t, V_t, t \geq 1$, as well as V_0 involved in Kalman filter and in the classical fixed interval smoother formulation, with exception for the initial B_0 , are singular in our model. It means that the whole cloud of the posterior and the posterior predictive distributions are located in a smaller dimensional subspace. This is probably a too restrictive requirement. The space of the non-linear model state development is just close to a singular one.

We have defined three non-linear observation operators nlZ_1, nlZ_2, nlZ_3 in section 2.5. The tangent linear operators tlZ_1, tlZ_2, tlZ_3 are $3 * 3 * 3 * (2M + 1)$ -dimensional matrices with the same structure of triples

$$\begin{pmatrix} \frac{\partial nlZ^1}{\partial u_k}, & \frac{\partial nlZ^1}{\partial v_k}, & 0 \\ \frac{\partial nlZ^2}{\partial u_k}, & \frac{\partial nlZ^2}{\partial v_k}, & 0 \\ 0, & 0, & \frac{\partial nlZ^3}{\partial \phi_k} \end{pmatrix}, \quad k = -M, \dots, M$$

For all three non-linear operators the two first functions of triples are the same, so the tangent-linear operators of two first functions in a triple are the same as well.

$$(80) \quad \begin{aligned} \frac{\partial nlZ^1}{\partial u_k} &= \frac{\bar{u} + u_j}{(\bar{u} + u_j)^2 + v_j^2} e^{i\hat{k}x_j} \\ \frac{\partial nlZ^1}{\partial v_k} &= \frac{v_j}{(\bar{u} + u_j)^2 + v_j^2} e^{i\hat{k}x_j} \\ \frac{\partial nlZ^1}{\partial \phi_k} &= 0 \end{aligned}$$

$$(81) \quad \begin{aligned} \frac{\partial nlZ^2}{\partial u_k} &= -\frac{v_j}{(\bar{u} + u_j)^2 + v_j^2} e^{i\hat{k}x_j} \\ \frac{\partial nlZ^2}{\partial v_k} &= \frac{u_j + \bar{u}}{(\bar{u} + u_j)^2 + v_j^2} e^{i\hat{k}x_j} \\ \frac{\partial nlZ^2}{\partial \phi_k} &= 0 \end{aligned}$$

The third function of a triple is different for every observation operator, with the tangent-linear operators having the following expressions

$$(82) \quad \frac{\partial nlZ_1^3}{\partial u_k} = 0, \frac{\partial nlZ_1^3}{\partial v_k} = 0, \frac{\partial nlZ_1^3}{\partial \phi_k} = \frac{1}{\frac{\bar{\phi}}{10} + \phi_j} e^{i\hat{k}x_j}$$

$$(83) \quad \frac{\partial nlZ_2^3}{\partial u_k} = 0, \frac{\partial nlZ_2^3}{\partial v_k} = 0, \frac{\partial nlZ_2^3}{\partial \phi_k} = \frac{1}{\frac{\bar{\phi}}{50} + \phi_j} e^{i\hat{k}x_j}$$

$$(84) \quad \frac{\partial nlZ_3^3}{\partial u_k} = 0, \frac{\partial nlZ_3^3}{\partial v_k} = 0, \frac{\partial nlZ_3^3}{\partial \phi_k} = \frac{1}{(1 + \frac{20}{\bar{\phi}}\phi_j)^2} e^{i\hat{k}x_j}$$

With u_j, v_j, ϕ_j we have denoted fields evaluated at a particular grid-point x_j , $j = 1, \dots, N$

The linear observation operators can be expressed in matrix form. Then the tangent linear and the linear operators are the same, with a triple having the form

$$(85) \quad Z = \begin{pmatrix} e^{i\hat{k}x_j}, & 0, & 0 \\ 0, & e^{i\hat{k}x_j}, & 0 \\ 0, & 0, & e^{i\hat{k}x_j} \end{pmatrix}$$

with a dummy index k corresponding to wave-number.

4.1. The extended Kalman filter. Let denote as a forecast a_i^f the time evolution of the "best" possible estimation of the "true" state up to time t_i , $a_i^f = \bar{F}^{i-1}(a_{i-1})$, $i = 1, \dots, N_{ass}$. If the time evolution of the forecast error $\delta\hat{X}(t) = \bar{X}(t) - a_t^f$ is close to linear, then the distribution of the forecast errors, initially assumed to be Gaussian, must stay close to a Gaussian one.

The dynamics of the forecast errors can be approximated by the linear development through the tangent linear operator $\bar{T}^{i-1}(a_{i-1})$ around the non-linear trajectory of the "best" estimate a_{i-1} obtained after the $i - 1$ assimilation terms.

$$\delta\hat{X}(t_i) = \bar{X}(t_i) - a_i^f = \bar{F}^{i-1}(\bar{X}(t_{i-1})) - \bar{F}^{i-1}(a_{i-1}) \approx \bar{T}^{i-1}(a_{i-1})\delta\hat{X}(t_{i-1})$$

In the extended Kalman filter approach, instead of using the non-linear model (75), describing the "true" state evolution, the tangent-linear model, which describes the evolution of the forecast errors approximately, is considered.

$$(86) \quad y_i = Z(a_i^f) + tlZ(a_i^f)\delta\hat{X}(t_i) + \varepsilon_i, \quad i = 1, \dots, N_{ass}$$

$$(87) \quad \delta\hat{X}(t_i) = \bar{T}^{i-1}(a_i)\delta\hat{X}(t_{i-1}),$$

Under such dynamics $\delta\hat{X}(t_i)$ has a Gaussian distribution with the zero mean and the covariance matrix B_i obtained from the recursive equations given below. The estimation of the "true" state is equal the sum of the non-linear evolution of the "best" state obtained after the previous loop of data assimilation and the influence from the innovation vector

$$E(\hat{X}(t_i) | \mathcal{Y}_{i-1}) = \bar{F}^{i-1}(a_{i-1})$$

$$E(\hat{X}(t_i) | \mathcal{Y}_i) = a_i = a_i^f + K_i v_i$$

Here we summarise the recursive equations for the extended Kalman filter

$$(88) \quad \begin{aligned} a_i &= a_i^f + K_i v_i, \\ B_i &= B_i^f - B_i^f tlZ^T K_i^T, \\ v_i &= y_i - Z(a_i^f), \\ K_i &= B_i^f tlZ^T F_i^{-1}, \\ F_i &= tlZ B_i^f tlZ^T + H, \\ a_i^f &= \bar{F}^{i-1}(a_{i-1}) \\ B_i^f &= \bar{T}^{i-1}(a_{i-1}) B_{i-1} (\bar{T}^{i-1}(a_{i-1}))^T, \quad i = 1, \dots, N_{ass} \end{aligned}$$

Due to the non-linear dynamics and possibly to non-linear observation operators, an analysed field cannot be expressed as a linear function of the assimilated observations. The extended Kalman filter construct an analysed field $E(\hat{X}(t_i) | \mathcal{Y}_i)$ at time t_i as a linear function of newly incoming observations y_i and the forecast $E(\hat{X}(t_i) | \mathcal{Y}_{i-1})$. This forecast is a non-linear function of already assimilated observations \mathcal{Y}_{i-1} and an initial forecast a_0 . In Figure 13 we will illustrate some results of a data assimilation process, where we have inserted a set of 9 observations at 8 time instants. The sequence of observations inserted at each time instant consists of the following observations $y_i = \{y(i, j), j = 1, \dots, 9\} = \{u_{1,i}, v_{1,i}, \phi_{1,i}, u_{2,i}, v_{2,i}, \phi_{2,i}, u_{3,i}, v_{3,i}, \phi_{3,i}\}$, located at positions x_{11}, x_{21}, x_{31} for the u -wind and the geopotential observations and at positions x_{12}, x_{22}, x_{32} for the v -wind components, respectively. For the sake of simplicity of representation, we will show the influence of the observations on the analysed field value for a certain grid-point x^0 (here, $x^0 = x_{16}$).

Let us decompose the Kalman gain matrix $K_{3(2M+1) \times 9}$ in three gain sub-matrices, corresponding to the influence of the 9 observed quantities on the model state spectral u -, v -wind components and geopotential, respectively :

$$K_{3(2M+1) \times 9} = (K_{(2M+1) \times 9}^u, K_{(2M+1) \times 9}^v, K_{(2M+1) \times 9}^\phi)$$

Then the analysed fields $u_i^a(x^0), v_i^a(x^0), \phi_i^a(x^0)$ at the position x^0 for the time instant t_i can be expressed as a sum

$$(89) \quad \begin{aligned} u_i^a(x^0) &= wu(a_i^f) + \sum_{j=1}^3 (w_{j1,i}^u u_{j,i} + w_{j2,i}^u v_{j,i} + w_{j3,i}^u \phi_{j,i}) \\ v_i^a(x^0) &= wv(a_i^f) + \sum_{j=1}^3 (w_{j1,i}^v u_{j,i} + w_{j2,i}^v v_{j,i} + w_{j3,i}^v \phi_{j,i}) \\ \phi_i^a(x^0) &= w\phi(a_i^f) + \sum_{j=1}^3 (w_{j1,i}^\phi u_{j,i} + w_{j2,i}^\phi v_{j,i} + w_{j3,i}^\phi \phi_{j,i}) \end{aligned}$$

(90)

The part of the sum originating from the forecast itself has the following expression

$$(91) \quad \begin{aligned} wu(a_i^f) &= \sum_{k=-M}^M u_k^f e^{ikx^0} - \sum_{k=-M}^M \left(\sum_{j=1}^9 K_{k,j}^u Z^j(a_i^f) \right) e^{ikx^0} \\ wv(a_i^f) &= \sum_{k=-M}^M v_k^f e^{ikx^0} - \sum_{k=-M}^M \left(\sum_{j=1}^9 K_{k,j}^v Z^j(a_i^f) \right) e^{ikx^0} \\ w\phi(a_i^f) &= \sum_{k=-M}^M \phi_k^f e^{ikx^0} - \sum_{k=-M}^M \left(\sum_{j=1}^9 K_{k,j}^\phi Z^j(a_i^f) \right) e^{ikx^0} \end{aligned}$$

Here we have denoted by $Z^j(a_i^f)$ the j -th, $1 \leq j \leq 9$, projection of the model state on the observation space by the observation operator.

The weights of the observations in the expression of the analysed u -wind component field at the point x_0 can be obtained by the following expressions

$$(92) \quad \begin{aligned} w_{11,i}^u &= \sum_{k=-M}^M (K_{k,1}^u) e^{ikx^0}, & w_{21,i}^u &= \sum_{k=-M}^M (K_{k,4}^u) e^{ikx^0}, & w_{31,i}^u &= \sum_{k=-M}^M (K_{k,7}^u) e^{ikx^0}, \\ w_{12,i}^u &= \sum_{k=-M}^M (K_{k,2}^u) e^{ikx^0}, & w_{22,i}^u &= \sum_{k=-M}^M (K_{k,5}^u) e^{ikx^0}, & w_{32,i}^u &= \sum_{k=-M}^M (K_{k,8}^u) e^{ikx^0}, \\ w_{13,i}^u &= \sum_{k=-M}^M (K_{k,3}^u) e^{ikx^0}, & w_{23,i}^u &= \sum_{k=-M}^M (K_{k,6}^u) e^{ikx^0}, & w_{33,i}^u &= \sum_{k=-M}^M (K_{k,9}^u) e^{ikx^0}, \end{aligned}$$

The weights for the observations in the expression for the v -wind and the geopotential analysed fields can be expressed in an analogous way by using K^v and K^ϕ , respectively, instead of K^u .

In Figure 13 we illustrate the result of a data assimilation procedure by the extended Kalman filter. The sequence of 9 observations described above was assimilated at 8 time instants. The upper pair of diagrams show the impact of the observations and the forecast itself on the analysed u -wind field and the lower pair of diagrams show the impact on the analysed v -wind field. The upper parts of the diagrams present weights of the 9 observations

$$w_{11,i}, w_{12,i}, w_{13,i}, w_{21,i}, w_{22,i}, w_{23,i}, w_{31,i}, w_{32,i}, w_{33,i}$$

every time t_i , $i = 1, \dots, 8$ observations were assimilated. The lower parts of each pair of diagrams present the impact of the forecast itself $w(a_i^f)$ and the impact of the observations, which is equal to a multiplication of an observation value with its weight.

$$w_{11,i}u_{1,i}, w_{12,i}v_{1,i}, w_{13,i}\phi_{1,i}, w_{21,i}u_{2,i}, w_{22,i}v_{2,i}, w_{23,i}\phi_{2,i}, w_{31,i}u_{3,i}, w_{32,i}v_{3,i}, w_{33,i}\phi_{3,i}$$

Initially we have assumed that the observations have a precision comparable with, and for some observations even higher than, the precision of the background field. Due to this, the weights of the observations are quite high in the beginning of data assimilation process. The observations located closer to the point of interest have higher weights than the observations located further away. The largest impact have observations of the v -wind component for the construction of the analysed fields of both wind components. As we already have discussed, for the shallow water model with the parameters that we have assumed, the two other fields adjust in a broad sense to the v -wind component. But geostrophic adjustment is always a process of mutual adjustment and all types of observations bring important information. For the construction of the analysed state of the u -wind component, the direct observations of the field are also important, even if the u -wind is a deduced quantity for the model. Every data assimilation term improves the precision of an analysed field, reducing its error variance. The dynamical propagator is not completely realistic in our model since it does not conserve total energy. The minor dissipation of energy on small scales by the time filter and by the horizontal diffusion can noticeably reduce the total energy after a long time integration. Probably, a probabilistic model state would collapse into a single solution after an infinite time integration. The model state becomes non-homogeneous in grid-point space after a time integration, and the initialisation procedure and the variance become dependent on position and time. In general, every time observations are assimilated, weights of newly incoming observations reduce. Small deviations from this pattern are caused by the non-homogeneity of the model state.

However, if we investigate the impact that different observations have on the analysed fields, we find that the largest impact comes from the geopotential observations, due to the large amount of energy contained in the geopotential field.

As we can see from Figure 14, the important information for the construction of the analysed field can be extracted from all kinds of observations. In the figure to the left, u -wind observations are assumed to have very high precision compared to the other types of observations. They are given very high weights even if the amount of a total energy contained in the field is very small. The impact of the u -wind observations on the analysed geopotential field is noticeable even after several cycles of data assimilation procedure. Again, even if the geopotential observations are erroneous, they have a large impact on the analysed field due the large amount of energy in the geopotential field. The figure

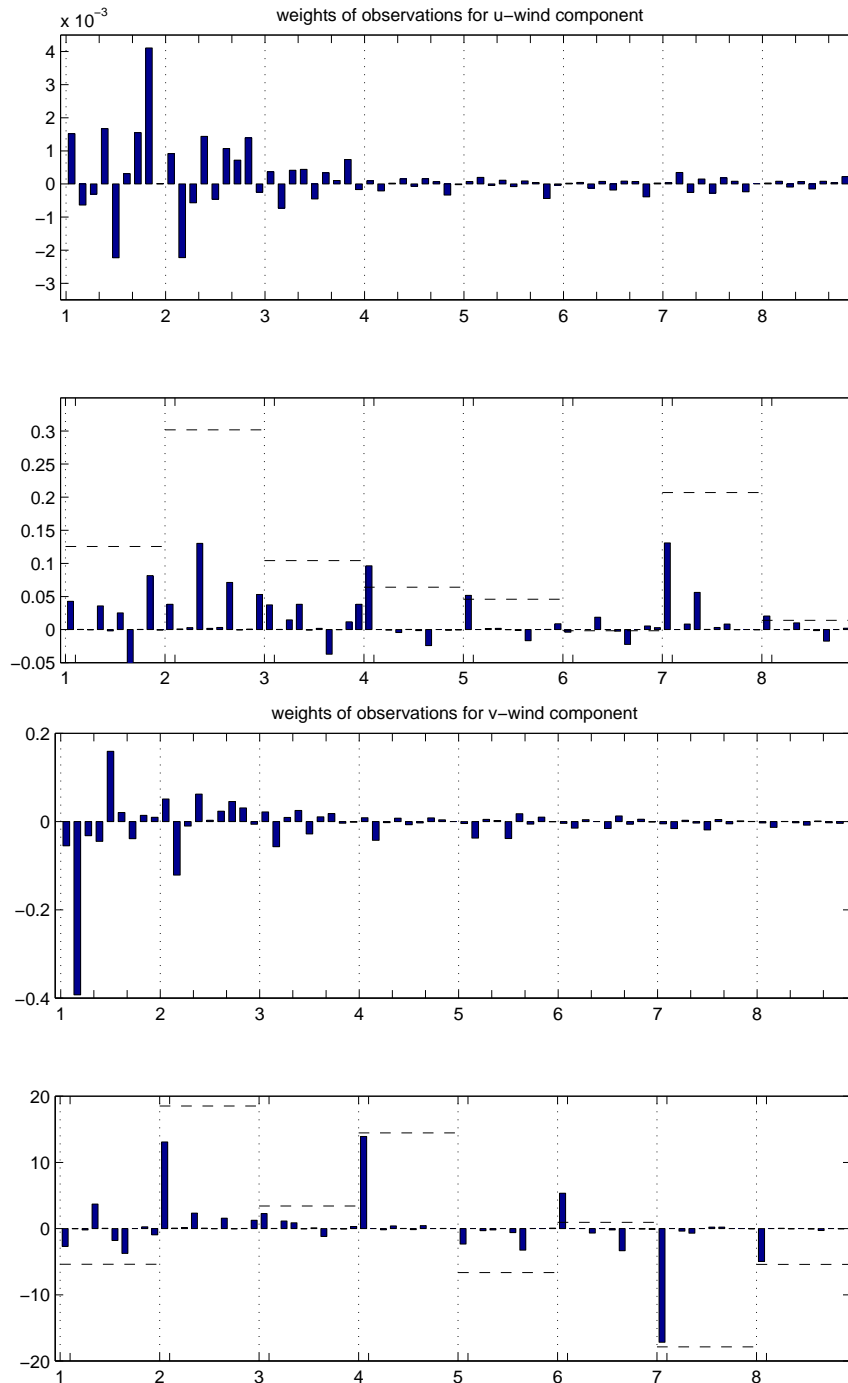


FIGURE 13. The impact of observations and the forecast itself on the analysed field for the u -wind (the upper diagrams) and the v -wind (the lower diagrams) components, obtained as a result of data assimilation with the extended Kalman filter. Observations weights (upper part of the diagrams) and observations impacts (lower part of the diagrams) are illustrated. Results are given for each assimilation term ($i = 1, \dots, 8$ on the x -axis) and for each observed quantity by a vertical bar. In the lower part of the diagrams the impact of the forecast itself is also given (the position of the vertical bars are marked on the x -axis). The values of analysed state after each assimilation term are given by dashed lines.

to the right illustrates the construction of the analysed geopotential field by assimilating

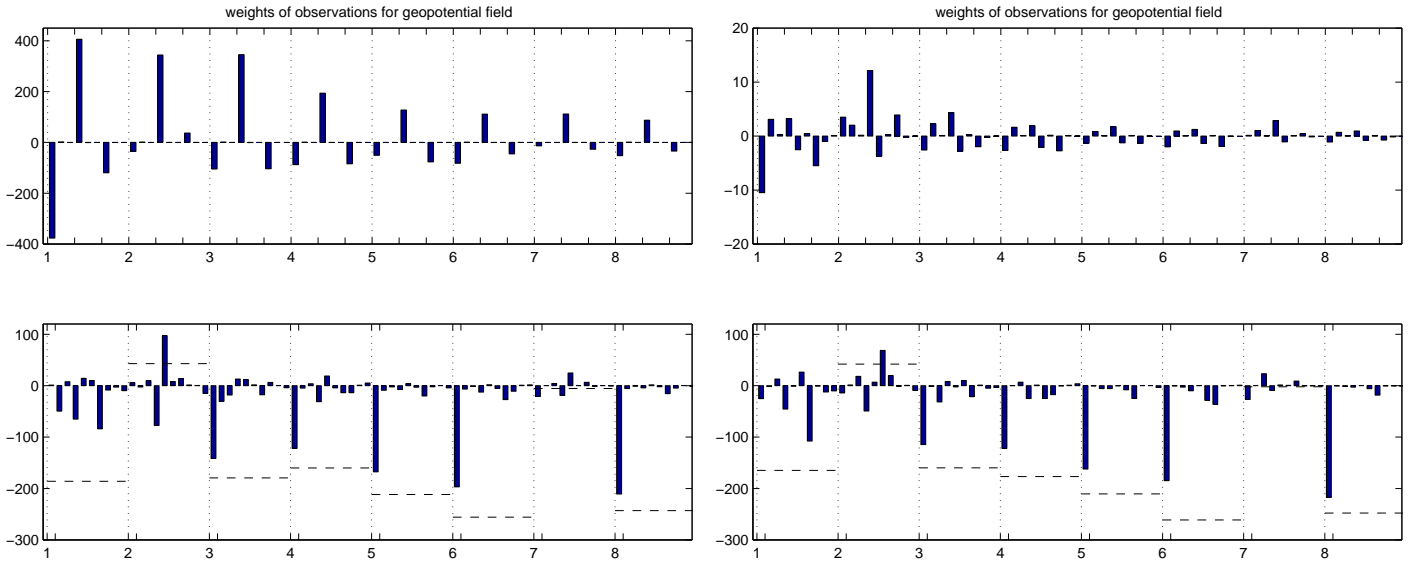


FIGURE 14. The impact of observations and the forecast itself on the analysed field for the geopotential obtained as a result of data assimilation with the extended Kalman filter. In the figure to the left, the u -wind observations have the highest precision, and in the figure to the right the v -wind components have the highest precision. For the detailed figures explanation see Figure 13 and text.

more realistic observations. Both the v -wind and the geopotential observations have quite high precision, comparable with the variance of initial background state. The results for both data assimilation procedures are quite close. In the beginning of data assimilation procedure, when the impact of observations is strong, comparable to the impact of the forecast itself, some observations seems to have contradicting influence. But, indeed, this is a positive aspect of filtering. Different observations neutralise disturbances that single observations and observation error create.

The original non-linear model is approximated by a sequence of tangent linear models. The evolution of the pdf is approximated by a sequence of Gaussian distributions. The optimality of the obtained analysed state will depend on how well the pdf is approximated by the Gaussian at every particular moment. If the distribution is skewed, the mean of the distribution can be located far away from the mode toward the heavy tail. The approximate optimality in the sense of the mean square error can be very poor. If the prior distribution is assumed to be Gaussian, quite strong evidence from the data is required to move substantially the mode of the posterior distribution. The method outlined above can give a quite good approximation of the posterior mode.

The filtering equation, summarised above, provides not only the time evolution of the moments or the time evolution of the mode, but the approximate evolution of the whole pdf.

4.2. The bias corrected Kalman filter. For any model, governed by non-linear dynamics, the time evolution of the mean of the population is not given by the propagator itself.

$$E(\hat{X}(t_i) | \mathcal{Y}_{i-1}) = E(\bar{F}^{i-1}(\hat{X}(t_{i-1})) | \mathcal{Y}_{i-1}) \neq \bar{F}^{i-1}(E(\hat{X}(t_{i-1}) | \mathcal{Y}_{i-1}))$$

A better approximation of the time evolution of the mean can be obtained by using a higher-order Taylor expansion around the mean.

With the definition of the tangent linear (77) and the Hessian (vector of matrixes)

$$(93) \quad \mathcal{H} = \mathcal{H}_{ijk} = \frac{\partial^2 \bar{F}^i(\hat{X})}{\partial \hat{X}_j \hat{X}_k} = \nabla \nabla \bar{F}^i(\hat{X})$$

the propagator can be approximated by a quadratic function in $\delta \hat{X}^m(t) = \hat{X}(t) - E(\hat{X}(t) | \mathcal{Y}_{i-1})$ for $t \geq t_{i-1}$. Denoting the non-linear one time-step propagator $F(\cdot)$, the second order Taylor expansion around the mean is

$$F(\hat{X}(t)) \approx F(a_t^m) + \frac{\partial F}{\partial \hat{X}}(a_t^m) \delta \hat{X}^m(t) + \frac{1}{2} (\delta \hat{X}^m(t))^T \mathcal{H} \delta \hat{X}^m(t)$$

where $a_t^m = E(\hat{X}(t) | \mathcal{Y}_{i-1})$. Then the bias corrected time development of the mean can be obtained by

$$(94) \quad \begin{aligned} a_{t+1}^m &= E(F(\hat{X}(t)) | \mathcal{Y}_{i-1}) = \\ &\approx F(a_t^m) + \frac{\partial F}{\partial \hat{X}}(a_t^m) E(\delta \hat{X}^m(t) | \mathcal{Y}_{i-1}) + \frac{1}{2} E((\delta \hat{X}^m(t))^T \mathcal{H} \delta \hat{X}^m(t) | \mathcal{Y}_{i-1}) \\ &\approx F(a_t^m) + 0 + \frac{1}{2} \sum_{j=-M}^M \sum_{k=-M}^M (B_{jk,t}^m \mathcal{H}_{j,k}) \end{aligned}$$

Here $B_t^m = Var(\hat{X}(t) | \mathcal{Y}_{i-1})$. The notation $B_{jk,t}^m$ denote the element of the covariance matrix B_t^m corresponding to the covariance of j th and k th spectral components of the model state variable. Up to the first-order approximation, the time evolution of the posterior variance-covariance matrix is described by the tangent-linear of the model dynamics taken around the conditional mean.

$$(95) \quad B_{t+1}^m \approx \frac{\partial F}{\partial \hat{X}}(a_t^m) B_t^m \left(\frac{\partial F}{\partial \hat{X}}(a_t^m) \right)^T$$

The shallow water model is, in fact, a quadratic function in \hat{X} , because it contains only linear and quadratic terms. The Hessian for the shallow water dynamical propagator is constant. We will not give the explicit expression for the Hessian itself, but present the whole correction term $\sum_{j=-M}^M \sum_{k=-M}^M (B_{jk,t}^m \mathcal{H}_{j,k})$, which is a linear function of B_{nlcorr}

$$B_{nlcorr} = \begin{pmatrix} B_{nlcorr,k}^u \\ B_{nlcorr,k}^v \\ B_{nlcorr,k}^\phi \end{pmatrix} = \begin{pmatrix} E(\sum_{l=-M}^M \sum_{m=-M}^M \frac{\partial^2 F^{u_k}}{\partial u_l \partial u_m} \delta \hat{u}_l^m \delta \hat{u}_m^m) \\ E(2 \sum_{l=-M}^M \sum_{m=-M}^M \frac{\partial^2 F^{v_k}}{\partial u_l \partial v_m} \delta \hat{u}_l^m \delta \hat{v}_m^m) \\ E(2 \sum_{l=-M}^M \sum_{m=-M}^M \frac{\partial^2 F^{\phi_k}}{\partial u_l \partial \phi_m} \delta \hat{u}_l^m \delta \hat{\phi}_m^m) \end{pmatrix}$$

Here

$$\begin{aligned}
(96) \quad F^{u_k} &= \frac{1}{N} \sum_{j=1}^N \left(\sum_{m_1=-M}^M \hat{u}_{m_1} e^{i\hat{m}_1 x_j} \sum_{m_2=-M}^M i\hat{m}_2 \hat{u}_{m_2} e^{i\hat{m}_2 x_j} \right) e^{-i\hat{k} x_j} \\
F^{v_k} &= \frac{1}{N} \sum_{j=1}^N \left(\sum_{m_1=-M}^M \hat{u}_{m_1} e^{i\hat{m}_1 x_j} \sum_{m_2=-M}^M i\hat{m}_2 \hat{v}_{m_2} e^{i\hat{m}_2 x_j} \right) e^{-i\hat{k} x_j} \\
F^{\phi_k} &= \frac{1}{N} \sum_{j=1}^N \left(i\hat{k} \sum_{m_1=-M}^M \hat{u}_{m_1} e^{i\hat{m}_1 x_j} \sum_{m_2=-M}^M \hat{\phi}_{m_2} e^{i\hat{m}_2 x_j} \right) e^{-i\hat{k} x_j}
\end{aligned}$$

Then, after performing partial differentiation

$$\begin{aligned}
B_{nlcorr,k}^u &= E \left(\sum_{l=-M}^M \sum_{m=-M}^M \frac{1}{N} \sum_{j=1}^N (e^{i\hat{m} x_j} i\hat{l} e^{i\hat{l} x_j} + e^{i\hat{l} x_j} i\hat{m} e^{i\hat{m} x_j}) e^{-i\hat{k} x_j} \delta \hat{u}_l^m \delta \hat{u}_m^m \right) \\
&= E \left(\sum_{l=-M}^M \sum_{m=-M}^M i(\hat{l} + \hat{m}) \frac{1}{N} \sum_{j=1}^N e^{i(\hat{l} + \hat{m} - \hat{k}) x_j} \delta \hat{u}_l^m \delta \hat{u}_m^m \right) \\
&= E \left(\sum_{l=-M}^M i\hat{k} \mathcal{I}_{\{-M \leq \hat{k} - \hat{l} \leq M\}} \delta \hat{u}_l^m \delta \hat{u}_{k-l}^m \right) = \\
&= \sum_{l=-M}^M i\hat{k} \mathcal{I}_{\{-M \leq \hat{k} - \hat{l} \leq M\}} cov(\delta \hat{u}_l \delta \hat{u}_{k-l}),
\end{aligned}$$

$$\mathcal{I}_{\{A\}} = \begin{cases} 1 & , \text{ if } A \text{ is true} \\ 0 & , \text{ if } A \text{ is false} \end{cases}$$

because for a discrete Fourier transform with period L , $x_0 \leq \dots \leq x_j \dots \leq x_N = L$

$$(97) \quad \frac{1}{N} \sum_{j=1}^N e^{i(\hat{l} + \hat{m} - \hat{k}) x_j} = \begin{cases} 1 & , \text{ if } \hat{l} + \hat{m} = \hat{k}, \\ 0 & , \text{ if } \hat{l} + \hat{m} - \hat{k} \neq 0 \end{cases}$$

In a completely analogous way we can obtain $B_{nlcorr,k}^v, B_{nlcorr,k}^\phi$.

$$\begin{aligned}
(98) \quad B_{nlcorr,k}^v &= 2E \left(\sum_{l=-M}^M \sum_{m=-M}^M \frac{1}{N} \sum_{j=1}^N (e^{i\hat{l} x_j} i\hat{m} e^{i\hat{m} x_j}) e^{-i\hat{k} x_j} \delta \hat{u}_l^m \delta \hat{v}_m^m \right) \\
&= 2E \left(\sum_{l=-M}^M \sum_{m=-M}^M i\hat{m} \frac{1}{N} \sum_{j=1}^N e^{i(\hat{l} + \hat{m} - \hat{k}) x_j} \delta \hat{u}_l^m \delta \hat{v}_m^m \right) \\
&= 2 \sum_{l=-M}^M i(\hat{k} - \hat{l}) \mathcal{I}_{\{-M \leq \hat{k} - \hat{l} \leq M\}} cov(\delta \hat{u}_l \delta \hat{v}_{k-l})
\end{aligned}$$

$$\begin{aligned}
B_{nlcorr,k}^\phi &= 2E\left(\sum_{l=-M}^M \sum_{m=-M}^M \frac{1}{N} \sum_{j=1}^N (e^{i\hat{l}x_j} i\hat{k} e^{i\hat{m}x_j}) e^{-i\hat{k}x_j} \delta\hat{u}_l^m \delta\hat{\phi}_m^m\right) \\
(99) \quad &= 2E\left(\sum_{l=-M}^M \sum_{m=-M}^M i\hat{k} \frac{1}{N} \sum_{j=1}^N e^{i(\hat{l}+\hat{m}-\hat{k})x_j} \delta\hat{u}_l^m \delta\hat{\phi}_m^m\right) \\
&= 2 \sum_{l=-M}^M i\hat{k} \mathcal{I}_{\{-M \leq \hat{k}-\hat{l} \leq M\}} cov(\delta\hat{u}_l \delta\hat{\phi}_{\hat{k}-l}^m)
\end{aligned}$$

In the case of a linear observation operator, the bias corrected Kalman filter is described by the original system of equations

$$\begin{aligned}
y_i &= Z\hat{X}(t_i) + \varepsilon_i, \quad i = 1, \dots, N_{ass} \\
\hat{X}(t_i) &= \bar{F}^{i-1}(\hat{X}(t_{i-1})), \quad \hat{X}(t_0) \sim \mathcal{N}(a_0, B_0)
\end{aligned}$$

with a second order approximation of the dynamical evolution for the mean, namely

$$\begin{aligned}
(100) \quad a^m(t) &= E(\hat{X}(t) | \mathcal{Y}_i) = F(a_{t-1}^m) + \frac{1}{2} \sum_{j=-M}^M \sum_{k=-M}^M (B_{jk}^m(t-1) \mathcal{H}_{j,k}), \\
B^m(t) &= Var(\hat{X}(t) | \mathcal{Y}_i) = T(a^m(t-1))B^m(t-1)T^T(a^m(t-1)), \quad t > t_{i-1};
\end{aligned}$$

$a_i^m = a^m(t_i)$, $B_i^m = B^m(t_i)$. where $F(\cdot)$ denotes the one step time propagator, and $T(a_{t-1}^m)$ denotes the tangent linear for $F(\cdot)$ around the mean evolution from the previous analysed state $a_{i-1} = E(\hat{X}(t_{i-1}) | \mathcal{Y}_{i-1})$, $B_{j,k,i-1} = Cov(\hat{X}_j(t_{i-1}), \hat{X}_k(t_{i-1}) | \mathcal{Y}_{i-1})$.

If the relationship between the model state and observations is linear, the analysed state can be constructed based on the principles of the second-order linear regression, which is free from any assumptions on the distribution function except for the existence of the second moment. If we would know exactly the time evolution of $E(\hat{X}(t) | \mathcal{Y}_{i-1})$ and $Var(\hat{X}(t) | \mathcal{Y}_{i-1})$, $t_{i-1} < t \leq t_i$, the obtained analysed state would be equal to the mean $E(\hat{X}(t_i) | \mathcal{Y}_i)$ and would be optimal in the sense of the mean square error. However, we do not know exactly the time development of the statistical moments, but we can only make an approximation. Thus the bias corrected Kalman filter recursion formulas summarised below provide the analysed state which is close to the optimal one.

$$\begin{aligned}
(101) \quad a_i &= a_i^m + K_i v_i^m, \\
B_i &= B_i^m - B_i^m Z^T K_i^T, \\
v_i^m &= y_i - Z a_i^m, \\
K_i &= B_i^m Z^T F_i^{-1}, \\
F_i &= Z B_i^m Z^T + H
\end{aligned}$$

with the dynamical update given in (100).

In the case of a non-linear observation operator, the relationship between the model state $\hat{X}(t_i)$ and the innovation vector

$$v_i = y_i - E(nlZ(\hat{X}(t_i)) | \mathcal{Y}_{i-1}) = nlZ(\hat{X}(t_i)) + \varepsilon_i - E(nlZ(\hat{X}(t_i)) | \mathcal{Y}_{i-1})$$

is no longer linear, but this need not prevent us from using the best linear predictor, given the history of observations \mathcal{Y}_{i-1} . For a single innovation v_i and in a sense of the least posterior squared mean, the best linear predictor is

$$(102) \quad \tilde{\hat{X}}(t_i)(\mathcal{Y}_{i-1}, v_i) = \hat{\alpha} + \hat{\beta}v_i = E(\hat{X}(t_i) | \mathcal{Y}_{i-1}) + cov(\hat{X}(t_i), v_i | \mathcal{Y}_{i-1})(var(v_i | \mathcal{Y}_{i-1}))^{-1}v_i$$

and minimises $E((\hat{X}(t_i) - \tilde{\hat{X}}(t_i))^2 | \mathcal{Y}_{i-1})$.

The regression residual θ_i is dependent of v_i . The regression residual has the following form

$$(103) \quad \theta_i = \hat{X}(t_i) - E(\hat{X}(t_i) | \mathcal{Y}_{i-1}) + cov(\hat{X}(t_i), v_i | \mathcal{Y}_{i-1})(var(v_i | \mathcal{Y}_{i-1}))^{-1}v_i$$

Regression residual θ_i , given the history of observations \mathcal{Y}_{i-1} , has zero expectation, is uncorrelated with the innovation v_i , and has a constant variance.

$$\begin{aligned} var(\theta_i | \mathcal{Y}_{i-1}) &= var(\hat{X}(t_i) | \mathcal{Y}_{i-1}) \\ &+ cov(\hat{X}(t_i), v_i | \mathcal{Y}_{i-1})(var(v_i | \mathcal{Y}_{i-1}))^{-1}var(v_i | \mathcal{Y}_{i-1})(var(v_i | \mathcal{Y}_{i-1}))^{-1}(cov(\hat{X}(t_i), v_i | \mathcal{Y}_{i-1}))^T - \\ &- 2cov(\hat{X}(t_i), v_i | \mathcal{Y}_{i-1})(var(v_i | \mathcal{Y}_{i-1}))^{-1}(cov(\hat{X}(t_i), v_i | \mathcal{Y}_{i-1}))^T \\ &= var(\hat{X}(t_i) | \mathcal{Y}_{i-1}) - cov(\hat{X}(t_i), v_i | \mathcal{Y}_{i-1})(var(v_i | \mathcal{Y}_{i-1}))^{-1}(cov(\hat{X}(t_i), v_i | \mathcal{Y}_{i-1}))^T \end{aligned}$$

In fact, the posterior mean $E(\hat{X}(t_i) | \mathcal{Y}_i)$ is not equal to the best linear predictor (102)

$$E(\hat{X}(t_i) | \mathcal{Y}_i) = E(\hat{X}(t_i) | \mathcal{Y}_{i-1}) + cov(\hat{X}(t_i), v_i | \mathcal{Y}_{i-1})(var(v_i | \mathcal{Y}_{i-1}))^{-1}v_i + E(\theta_i | \mathcal{Y}_i)$$

But if $E(\theta_i | \mathcal{Y}_i)$ is close to zero, the posterior mean recursion will hold approximately, and we will use this approximation to determine the posterior mean evolution, considering

$$(104) \quad \begin{aligned} E(\hat{X}(t_i) | \mathcal{Y}_i) &= E(\hat{X}(t_i) | \mathcal{Y}_{i-1}) + \\ &+ cov(\hat{X}(t_i), v_i | \mathcal{Y}_{i-1})(var(v_i | \mathcal{Y}_{i-1}))^{-1}v_i \end{aligned}$$

Notice that $var(\hat{X}(t_i) | \mathcal{Y}_i) = var(\theta_i | \mathcal{Y}_i)$ and

$$\begin{aligned} var(\theta_i | \mathcal{Y}_{i-1}) &= E(var(\theta_i | \mathcal{Y}_i) | \mathcal{Y}_{i-1}) + var(E(\theta_i | \mathcal{Y}_i) | \mathcal{Y}_{i-1}) \\ &\approx E(var(\theta_i | \mathcal{Y}_i) | \mathcal{Y}_{i-1}), \end{aligned}$$

if $E(\theta_i | \mathcal{Y}_i)$ is close to the zero. Then the recursive formulas for the posterior variance can be justified in the form

$$\begin{aligned} E(var(\hat{X}(t_i) | \mathcal{Y}_i) | \mathcal{Y}_{i-1}) &= var(\hat{X}(t_i) | \mathcal{Y}_{i-1}) - \\ &- cov(\hat{X}(t_i), v_i | \mathcal{Y}_{i-1})(var(v_i | \mathcal{Y}_{i-1}))^{-1}(cov(\hat{X}(t_i), v_i | \mathcal{Y}_{i-1}))^T \end{aligned}$$

However, the usual Kalman filter recursion for the posterior variances, which relates variances themselves, can hold only if $E(\text{var}(\theta_i | \mathcal{Y}_i) | \mathcal{Y}_{i-1}) \approx \text{var}(\theta_i | \mathcal{Y}_i)$, and this can occur only if θ_i is independent of v_i .

Despite of what was said, we will use the following formula to approximate the posterior variance development

$$\text{var}(\hat{X}(t_i) | \mathcal{Y}_i) = \text{var}(X_{t_i} | \mathcal{Y}_{i-1}) - \text{cov}(\hat{X}(t_i), v_i | \mathcal{Y}_{i-1}) (\text{var}(v_i | \mathcal{Y}_{i-1}))^{-1} (\text{cov}(\hat{X}(t_i), v_i | \mathcal{Y}_{i-1}))^T$$

The reason why all these simplifications can be accepted is that we have chosen a linear regression as the statistical model, and this means that we assume that the relationship between regressors and regressand to be close to a linear one.

Treating a non-linearity in the innovation vector, we will use the second order closure and expand $nlZ(\cdot)$ around the posterior predictive mean

$$\begin{aligned} nlZ(\hat{X}(t_i)) &\approx nlZ(E(\hat{X}(t_i) | \mathcal{Y}_{i-1})) + tlZ(\hat{X}(t_i) - E(\hat{X}(t_i) | \mathcal{Y}_{i-1})) + \\ &+ \frac{1}{2} \sum_{j=-M}^M \sum_{k=-M}^M ((\hat{X}_j(t_i) - E(\hat{X}_j(t_i) | \mathcal{Y}_{i-1}))(\hat{X}_{-k}(t_i) - E(\hat{X}_{-k}(t_i) | \mathcal{Y}_{i-1}))) \mathcal{H}_{jk, nlZ} \end{aligned}$$

where \mathcal{H}_{nlZ} denotes the Hessian of the non-linear observation operator and tlZ denotes the tangent linear observation operator evaluated at $E(\hat{X}(t_i) | \mathcal{Y}_{i-1})$. Then the statistical moments used in the expression (104) can be approximated by

$$\begin{aligned} (105) \quad E(nlZ(\hat{X}(t_i)) | \mathcal{Y}_{i-1}) &\approx nlZ(a_i^m) + \frac{1}{2} \sum_{j=-M}^M \sum_{k=-M}^M (B_{jk,i}^m \mathcal{H}_{jk, nlZ}), \\ \text{cov}(\hat{X}(t_i), v_i | \mathcal{Y}_{i-1}) &\approx B_i^m tlZ^T \\ \text{var}(v_i | \mathcal{Y}_{i-1}) &\approx tlZ B_i^m tlZ^T + H \end{aligned}$$

where the tangent linear observation operator is evaluated at $a_i^m = E(\hat{X}(t_i) | \mathcal{Y}_{i-1})$.

We would like to stress that a number of those limitations in the application of the bias corrected Kalman filter which occur in the case of a non-linear observation operator are common for the whole framework of Kalman filtering. First of all, as it follows from the properties of the second order regression (48), the expectation of the posterior variance $E(\text{var}(\hat{X}(t_i) | \mathcal{Y}_i))$, which takes into account all possible outcomes of observations, is estimated instead of the desirable $\text{var}(\hat{X}(t_i) | \mathcal{Y}_i)$, which depends on the particular realisation of the observation sampling only. In fact, the posterior variance is independent of the observations only in the case of a linear observation operator, which implies $E(\text{var}(\hat{X}(t_i) | \mathcal{Y}_i)) = \text{var}(\hat{X}(t_i) | \mathcal{Y}_i)$. In the case of a non-linear observation operator, the expectation of the posterior variance and the actual realisation of the posterior variance can differ substantially. The approximation of the posterior variance (105) that we are using in the Kalman filter framework estimates the expectation of the posterior variance and not the posterior variance itself, and does not give an opinion about the precision of the unobservable model state variable. The weak dependence of the estimate on the observations enters through the evaluation of the tangent linear observation operator tlZ , because the point of linearization itself depends on the observations. Secondly, the second order closure in the estimate of the posterior variance-covariance of the model state variable

can lead to an underestimation of the actual value of the posterior variance-covariance, and it can produce extra non-homogenous variance. The overestimated/underestimated posterior predictive variance results in too high/too low weights of the observations. This is why, for example, the observations taken at the two first positions from the left in Figure 12 have larger impact on the analysed field.

Here we summarise the recursion formulas that we will use in the bias-corrected Kalman filter formulation, in the case of a non-linear observation operator

$$\begin{aligned}
(106) \quad & a_i = a_i^m + K_i v_i^m, \\
& B_i = B_i^m - B_i^m t l Z^T (F_i)^{-1} t l Z B_i^m, \\
& v_i^m = y_i - n l Z(a_i^m) - \frac{1}{2} \sum_{j=-M}^M \sum_{k=-M}^M (B_{jk,i}^m \mathcal{H}_{jk,nlZ}), \\
& K_i = B_i^m t l Z^T F_i^{-1}, \\
& F_i = t l Z B_i^m t l Z^T + H
\end{aligned}$$

which relates the predictive statistical moments $a_i^m = E(\hat{X}(t_i) | \mathcal{Y}_{i-1})$, $B_i^m = \text{var}(\hat{X}(t_i) | \mathcal{Y}_{i-1})$ that are obtained in the same way as (100), with posterior moments $a_i = E(\hat{X}(t_i) | \mathcal{Y}_i)$, $B_i = \text{var}(\hat{X}(t_i) | \mathcal{Y}_i)$. The tangent-linear observation operator is evaluated at a_i^m under the i -th assimilation term.

Here we will give the explicit expressions for the second-order correction $\sum_{j=-M}^M \sum_{k=-M}^M (B_{jk,i}^m \mathcal{H}_{jk,nlZ})$ in the calculation of the innovations, depending on the type of the non-linear observation operator we use (see section 2.5). For all these observation operators, the second-order correction vector has the same structure of triples

$$\begin{pmatrix} B_{nlcorr}^{Z^1} \\ B_{nlcorr}^{Z^2} \\ B_{nlcorr}^{Z^3} \end{pmatrix} = \begin{pmatrix} \sum_{k=-M}^M \sum_{l=-M}^M \frac{\partial^2 nlZ^1}{\partial u_k \partial u_l} B_i^m(\hat{u}_k, \hat{u}_l) + \frac{\partial^2 nlZ^1}{\partial u_k \partial v_l} B_i^m(\hat{u}_k, \hat{v}_l) + \frac{\partial^2 nlZ^1}{\partial v_k \partial u_l} B_i^m(\hat{v}_k, \hat{u}_l) + \frac{\partial^2 nlZ^1}{\partial v_k \partial v_l} B_i^m(\hat{v}_k, \hat{v}_l) \\ \sum_{k=-M}^M \sum_{l=-M}^M \frac{\partial^2 nlZ^2}{\partial u_k \partial u_l} B_i^m(\hat{u}_k, \hat{u}_l) + \frac{\partial^2 nlZ^2}{\partial u_k \partial v_l} B_i^m(\hat{u}_k, \hat{v}_l) + \frac{\partial^2 nlZ^2}{\partial v_k \partial u_l} B_i^m(\hat{v}_k, \hat{u}_l) + \frac{\partial^2 nlZ^2}{\partial v_k \partial v_l} B_i^m(\hat{v}_k, \hat{v}_l) \\ \sum_{k=-M}^M \sum_{l=-M}^M \frac{\partial^2 nlZ^3}{\partial \phi_k \partial \phi_l} B_i^m(\hat{\phi}_k, \hat{\phi}_l) \end{pmatrix}$$

Here

$$\begin{aligned}
\frac{\partial^2 nlZ^1}{\partial u_k \partial u_l} &= \frac{v_j^2 - (\bar{u} + u_j)^2}{(\bar{u} + u_j)^2 + v_j^2} e^{i(\hat{k} + \hat{l})x_j}, & \frac{\partial^2 nlZ^1}{\partial v_k \partial v_l} &= \frac{(\bar{u} + u_j)^2 - v_j^2}{(\bar{u} + u_j)^2 + v_j^2} e^{i(\hat{k} + \hat{l})x_j}, & \frac{\partial^2 nlZ^1}{\partial u_k \partial v_l} &= \frac{-2v_j(\bar{u} + u_j)}{(\bar{u} + u_j)^2 + v_j^2} e^{i(\hat{k} + \hat{l})x_j}, \\
\frac{\partial^2 nlZ^2}{\partial u_k \partial u_l} &= \frac{2v_j^2(\bar{u} + u_j)}{(\bar{u} + u_j)^2 + v_j^2} e^{i(\hat{k} + \hat{l})x_j}, & \frac{\partial^2 nlZ^2}{\partial v_k \partial v_l} &= \frac{-2(\bar{u} + u_j)v_j^2}{(\bar{u} + u_j)^2 + v_j^2} e^{i(\hat{k} + \hat{l})x_j}, & \frac{\partial^2 nlZ^2}{\partial u_k \partial v_l} &= \frac{v_j^2 - (\bar{u} + u_j)^2}{(\bar{u} + u_j)^2 + v_j^2} e^{i(\hat{k} + \hat{l})x_j}
\end{aligned}$$

The two first correction vector components in a triple $B_{nlcorr}^{Z^1}, B_{nlcorr}^{Z^2}$ are the same for all three observation operators we have defined and are given by

$$B_{nlcorr}^{Z^1} = \frac{(\bar{u} + u_j)^2 - v_j^2}{(\bar{u} + u_j)^2 + v_j^2} (\text{var}(v_j | \mathcal{Y}_{i-1}) - \text{var}(u_j | \mathcal{Y}_{i-1})) - 4 \frac{v_j(\bar{u} + u_j)}{(\bar{u} + u_j)^2 + v_j^2} \text{cov}(u_j, v_j | \mathcal{Y}_{i-1})$$

$$B_{nlcorr}^{Z^2} = 2 \frac{(\bar{u} + u_j)v_j}{(\bar{u} + u_j)^2 + v_j^2} (\text{var}(u_j | \mathcal{Y}_{i-1}) - \text{var}(v_j | \mathcal{Y}_{i-1})) + 2 \frac{v_j^2 - (\bar{u} + u_j)^2}{(\bar{u} + u_j)^2 + v_j^2} \text{cov}(u_j, v_j | \mathcal{Y}_{i-1})$$

where $\text{var}(u_j)$, $\text{var}(v_j)$, $\text{cov}(u_j, v_j)$ denote the corresponding variances and covariances of the u- and v- wind components in grid-point space at the x_j positions.

For the derivation of the formula above, we have used the relationship between the covariance matrices in spectral and grid-point spaces.

$$\sum_{k=-M}^M \sum_{l=-M}^M e^{i(\hat{k}+\hat{l})x_j} \text{cov}(\hat{a}_k, \hat{b}_l) = \text{cov}(a_j, b_j)$$

The third component in a triple of the correction term is different for all three non-linear observation operators and is given by

$$(107) \quad B_{nlcorr}^{Z_1^3} = - \frac{\text{var}(\phi_j | \mathcal{Y}_{i-1})}{(\bar{\phi}/10 + \phi_j)^2}$$

$$(108) \quad B_{nlcorr}^{Z_2^3} = - \frac{\text{var}(\phi_j | \mathcal{Y}_{i-1})}{(\bar{\phi}/50 + \phi_j)^2}$$

$$(109) \quad B_{nlcorr}^{Z_3^3} = - \frac{40 \text{var}(\phi_j | \mathcal{Y}_{i-1})}{\bar{\phi} (1 + \frac{20}{\bar{\phi}} \phi_j)^3}$$

for the first, the second and the third observation operator, respectively.

The higher order closure (equation (100) for the dynamics and equation (104) for the non-linear observation operator) should improve the results of the dynamical evolution of the statistics and also provide more proper values of the innovation vectors in comparison with the extended Kalman filter, for which the non-linearities are approximated up to the first-order only. A better estimation of an innovation vector will improve the relative influence of observations in the construction of the analysed state.

The improvement achieved by the application of the bias corrected Kalman filter versus the extended Kalman filter, treating the observations non-linearly in relation to the model state variable is presented in Figure 15. The distance between the estimate of the unobservable model state and the "true" model state is measured by the spatial average squared error SE^{KF} for the extended Kalman filter (88)

$$(110) \quad SE^{KF}(i-) = \sum_{k=-M}^M (a_{k,i}^f - \bar{X}_k(t_i))(a_{-k,i}^f - \bar{X}_{-k}(t_i)) = \frac{1}{N} \sum_{j=1}^N \left(\sum_{k=-M}^M (a_{k,i}^f - \bar{X}_k(t_i)) e^{ikx_j} \right)^2$$

$$SE^{KF}(i) = \sum_{k=-M}^M (a_{k,i} - \bar{X}_k(t_i))(a_{-k,i} - \bar{X}_{-k}(t_i))$$

Here we denote by $a_{k,i}^f$ the k -th spectral component of the model state a_i^f . For the bias corrected Kalman filter $SE^{BC}(i-)$ and $SE^{BC}(i)$, $1 \leq i \leq N_{ass}$ are calculated in an analogous way replacing a_i^f by a_i^m (101). In the left part of Figure 15 are shown

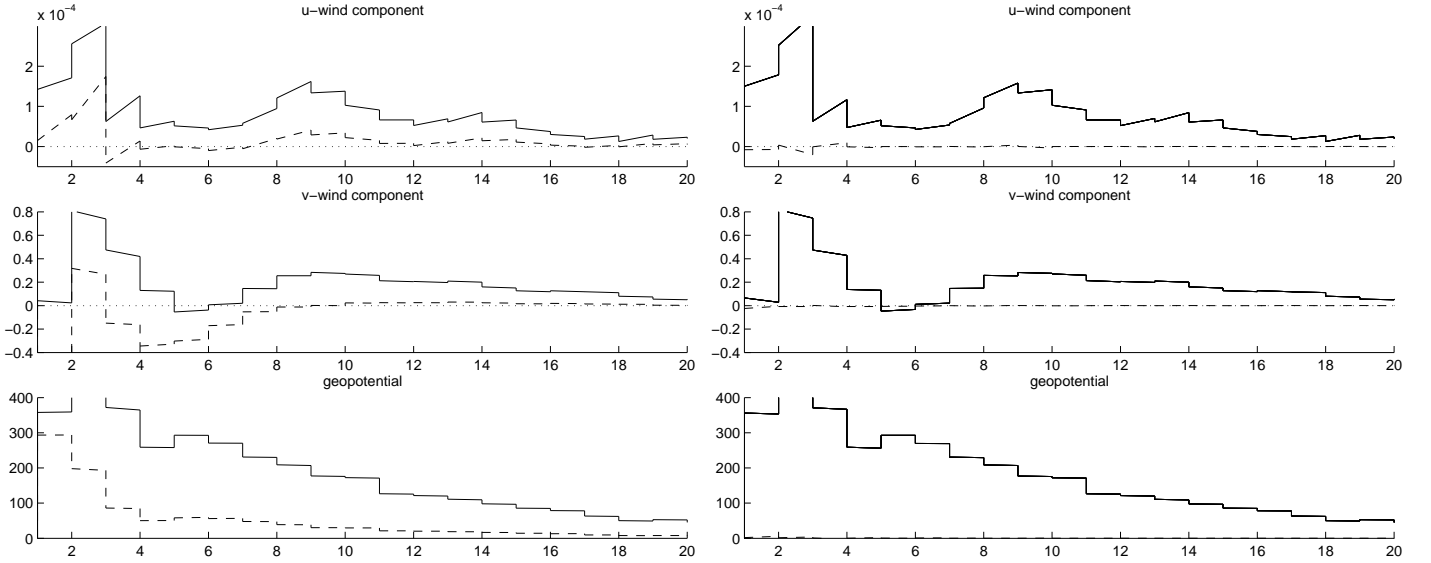


FIGURE 15. The reduction of the spatial averaged squared error of the model state variable estimate by application of the bias corrected Kalman filter. The full line represents assimilation of the "low" precision data. The dashed line on the left figure corresponds to the high precision data. The dashed line on the right figure represents improvement by implementing the bias correction for dynamical evolution of posterior mean only. The observations are simulated by the non-linear observation operator nlZ_3

$(SE^{KF}(i-, i) - SE^{BC}(i-, i))$, i.e. reduction in the spatial average squared errors by the bias corrected Kalman filter in comparison with the extended Kalman filter, obtained by assimilating data sets with different precisions. Assimilating data with "high" precision, the posterior variance of the unobservable model state decreases quickly reflecting increasing confidence in the unobservable model state variable. Assimilating "low" precision data we get the opposite effect. The bias corrections for both the dynamical evolution of the posterior predictive mean and for the expectation of the observations $E(y_i | \mathcal{Y}_{i-1})$ to be treated below are certainly functions of the posterior predictive variance-covariance matrix $var(\hat{X}(t_i) | \mathcal{Y}_{i-1})$. Therefore, the improvement in the estimate of the unobservable model state by the bias corrected Kalman filter versus the extended Kalman filter is larger for the low precision data. The improvement provided by the application of the bias corrected Kalman filter is quite small, around 5 percent on the average, and it depends strongly on the non-linearity of a observation operator. Simulating the data for the experiment above we have used the observation operator nlZ_3 , as we have defined it in section 2.5. As we can see from the right part of the Figure 15, the major part of the improvement is due to the implementation for the bias correction of the expectation of the observations. If we apply the bias correction for the dynamics and keep the approximation $E(nkZ(\hat{X}(t_i)) | \mathcal{Y}_{i-1}) \approx nlZ(E(\hat{X}(t_i) | \mathcal{Y}_{i-1}))$ used in the extended Kalman filter, the improvement of the estimate becomes very small. (See the dashed line in the right part of Figure 15). The main reason is that the non-linearity of the dynamical evolution is very weak for the one dimensional shallow water model.

The basic idea of bias corrected Kalman filter was to estimate the development of the posterior expectation and the posterior variance, putting as small as possible requirements on the statistical distribution of the population of the unobservable model states. We do not claim that the bias corrected Kalman filter has implemented the idea perfectly. It provides a refinement of the extended Kalman filter in treating non-linearities of both

the dynamics and the observation operator. On the other hand, it provides a smaller amount of information about the unobservable state than the standard Kalman filter does, because it estimates only the expected value and the expected squared distance to the mean. Another problem is that for a population varying in the non-linear subspace, it is not necessary that the mean of the population belongs to the subspace. In this chapter we have discussed those non-linear conditions that the real atmosphere must satisfy. The shallow-water model differential equations describe only the time evolution of existing states, which means states satisfying the conditions of the physical balance. If we want to use the obtained estimation of the mean as a point estimate of the unobservable state to provide a deterministic future forecast, the mean must be an existing state itself. Because the balance is close to the linear one, it is hoped that a mean, being a linear function of existing states, must be close to some existing state as well.

4.3. The time-window smoother. For the derivation of the time-window smoother, let $\mathcal{Y} = \{y_1, \dots, y_{N_{ass}}\}$ denote a subset of observations, which have fallen in the time-window $t_0 < t \leq t_{N_{ass}}$. Assuming a perfect dynamical model (75), the initial state is the only unobservable model variable, the inference about we want to obtain, based on the observed data \mathcal{Y} .

$$p(\hat{X}(t_0), \hat{X}(t_1), \dots, \hat{X}(t_{N_{ass}}) | \mathcal{Y}) = p(\hat{X}(t_0) | \mathcal{Y}) \propto p(\hat{X}(t_0), \mathcal{Y})$$

Assuming a Gaussian pdf for the initial state $p(\hat{X}(t_0)) \sim \mathcal{N}(a_0, B_0)$ and independent Gaussian observation errors, the joint distribution $p(\hat{X}(t_0), \mathcal{Y})$ will be Gaussian as well.

(111)

$$p(\hat{X}(t_0), \mathcal{Y}) = p(\hat{X}(t_0)) \prod_{j=1}^{N_{ass}} p(\varepsilon_j) \propto \exp \left(-0.5 \left[(\hat{X}(t_0) - a_0)^T B_0^{-1} (\hat{X}(t_0) - a_0) + \sum_{j=1}^{N_{ass}} \{y_j - Z(\hat{X}(t_j))\}^T H^{-1} \{y_j - Z(\hat{X}(t_j))\} \right] \right)$$

where $\hat{X}(t_j)$ are deterministically determined from $\hat{X}(t_0)$ by the model dynamics $\hat{X}(t_j) = \mathcal{F}^{t_j}(\hat{X}(t_0))$, and $Z(\cdot)$ denotes an observation operator, being a linear or a non-linear one.

The posterior mode $\hat{X}(t_0)$ is the solution of the vector equation

$$\frac{\partial \log p(\hat{X}(t_0) | \mathcal{Y})}{\partial \hat{X}(t_0)} = \frac{\partial \log p(\hat{X}(t_0), \mathcal{Y})}{\partial \hat{X}(t_0)} = 0$$

In the case of our model, the posterior mode can be determined as a solution to the following non-linear equation

(112)

$$B_0^{-1}(\hat{X}(t_0) - a_0) + \sum_{j=1}^{N_{ass}} \left(\frac{\partial \mathcal{F}^{t_j}(\hat{X}(t_0))}{\partial \hat{X}(t_0)} \right)^T \left(\frac{\partial Z(\mathcal{F}^{t_j}(\hat{X}(t_0)))}{\partial \mathcal{F}^{t_j}} \right)^T H^{-1} \{y_j - Z(\mathcal{F}^{t_j}(\hat{X}(t_0)))\} = 0$$

or the system of non-linear equations

$$(113) \quad B_0^{-1}(\hat{X}(t_0) - a_0) + \sum_{j=1}^{N_{ass}} \left(\frac{\partial \mathcal{F}^{t_j}(\hat{X}(t_0))}{\partial \hat{X}(t_0)} \right)^T \left(\frac{\partial Z(\hat{X}(t_j))}{\partial \hat{X}(t_j)} \right)^T H^{-1} \{y_j - Z\hat{X}(t_j)\} = 0$$

$$\hat{X}(t_j) = \bar{F}^{j-1}(\hat{X}(t_{j-1})), \quad j = 1, \dots, N_{ass}$$

Notice that

$$\mathcal{F}^{t_j}(\hat{X}(t_0)) = \bar{F}^{j-1}(\hat{X}(t_{j-1})) = \bar{F}^{j-1}(\bar{F}^{j-2}(\dots \bar{F}^0(\hat{X}(t_0)) \dots))$$

The tangent linear operator corresponding to the non-linear model, governing the model development over the whole time period (t_0, t_j) , is a series of multiplication with the tangent linear matrix operators $\bar{T}^{k-1}(\hat{X}(t_{k-1}))$, governing the model development over the sub-periods (t_{k-1}, t_k) , $1 \leq k \leq j$.

Then the system of non-linear equations to determine the posterior mode can be rewritten

$$(114) \quad B_0^{-1}(\hat{X}(t_0) - a_0) + \sum_{j=1}^{N_{ass}} \left(\prod_{k=1}^j \bar{T}^{k-1}(\hat{X}(t_{k-1})) \right)^T (t_l Z(\hat{X}(t_j)))^T H^{-1} \{y_j - Z(\hat{X}(t_j))\} = 0$$

$$\hat{X}(t_j) = \bar{F}^{j-1}(\hat{X}(t_{j-1})), \quad j = 1, \dots, N_{ass}$$

This non-linear system can be solved by minimisation techniques. This equation is, for example, the starting point for 4-dimensional variational data assimilation (4D-Var), which was discussed in the introduction to the report. In the incremental 4D-Var approach (Courtier et.al., 1994) the non-linear minimization problem is solved through a series of linear minimization problems, based on linearisations. We will use a different iterative procedure, discussed, for example, in Durbin and Koopman (2001).

Step 1. The original non-linear model (75) is approximated by a linear model, obtained by linearising the dynamics and the observation operators around the time evolution of a trial estimate of the posterior mode $(\alpha_{t_0}^*, \alpha_{t_1}^*, \dots, \alpha_{t_{N_{ass}}}^*)$.

$$(115) \quad y_j = Z(\alpha_{t_j}^*) + t_l Z(\alpha_{t_j}^*)(\hat{X}(t_j) - \alpha_{t_j}^*) + \varepsilon_j$$

$$(116) \quad \hat{X}(t_j) = \bar{F}^{j-1}(\alpha_{t_{j-1}}^*) + \bar{T}^{j-1}(\alpha_{t_{j-1}}^*)(\hat{X}(t_{j-1}) - \alpha_{t_{j-1}}^*)$$

Notice that under the linearization, $\hat{X}(t_j)$ is a linear function of $\hat{X}(t_0)$.

$$\begin{aligned} \hat{X}(t_j) &= \bar{F}^{j-1}(\alpha_{t_{j-1}}^*) + \bar{T}^{j-1}(\alpha_{t_{j-1}}^*)(\hat{X}(t_{j-1}) - \alpha_{t_{j-1}}^*) = \\ &= \bar{F}^{j-1}(\alpha_{t_{j-1}}^*) + \bar{T}^{j-1}(\alpha_{t_{j-1}}^*)(\bar{F}^{j-2}(\alpha_{t_{j-2}}^*) + \bar{T}^{j-2}(\alpha_{t_{j-2}}^*)(\hat{X}(t_{j-2}) - \alpha_{t_{j-2}}^*) - \alpha_{t_{j-1}}^*) = \\ &= \bar{\alpha}_j + \bar{T}^{j-1}(\alpha_{t_{j-1}}^*) \bar{T}^{j-2}(\alpha_{t_{j-2}}^*) \dots \bar{T}^0(\alpha_{t_0}^*) \hat{X}(t_0) = \\ &= \bar{\alpha}_j + \prod_{k=1}^j \bar{T}^{k-1}(\alpha_{t_{k-1}}^*) \hat{X}(t_0) \end{aligned}$$

The posterior mode for this approximate linear system $\hat{\alpha}_{t_0}$ satisfies the following linear equation

(117)

$$B_0^{-1}(\hat{X}(t_0) - a_0) + \sum_{j=1}^{N_{ass}} \left(\prod_{k=1}^j \bar{T}^{k-1}(\alpha_{t_{k-1}}^*) \right)^T (tlZ(\alpha_{t_j}^*))^T H^{-1} \{y_j - Z(\alpha_{t_j}^*) - tlZ(\alpha_{t_j}^*)(\hat{X}(t_j) - \alpha_{t_j}^*)\} = 0$$

with the following strong constraints on the dynamics

$$(118) \quad \hat{X}(t_j) = \bar{F}^{j-1}(\alpha_{t_{j-1}}^*) + \bar{T}^{j-1}(\alpha_{t_{j-1}}^*)(\hat{X}(t_{j-1}) - \alpha_{t_{j-1}}^*)$$

Notice that this linearised system of equations (117) and (118) is formally equal to the linearised sub-problems of the incremental 4D-Var.

Step 2. We obtain the posterior mode, and its dynamical evolution $(\hat{\alpha}_{t_0}, \dots, \hat{\alpha}_{t_{N_{ass}}})$ for this approximate model. The approximating model (118) is linear and Gaussian. Its posterior mode, equal to the mean of the posterior distribution $E(\hat{X}(t_0) | \mathcal{Y})$, together with the posterior variance $V_0 = var(\hat{X}(t_0) | \mathcal{Y})$ can be obtained through the standard Kalman filter and the fixed interval smoother recursions.

Step 3. This newly obtained estimate of the posterior mode and its dynamical evolution, are used as new states to linearise the dynamics and non-linear observation operators around (Step 1). The same probabilistic model, just with different strong constraints on the dynamics, is used all the time.

Step 4. We repeat the procedure until convergence $\alpha_{t_0}^* = \hat{\alpha}_{t_0}$ is achieved. The dynamical evolution of the posterior mode estimate, after convergence of this iterative procedure was achieved, is what we call the time window smoother.

It is interesting to notice that the obtained posterior mode as a result of the convergence the iterative procedure $\hat{\alpha}_{t_0}$ is the posterior mode of the original system with non-linear dynamics as well. If convergence is achieved, the strong constraints on the dynamics and on the observation operators for the approximated system become the same as for the original system

$$(119) \quad \begin{aligned} \hat{\alpha}_{t_j} &= F^{j-1}(\alpha_{t_{j-1}}^*) + T^{j-1}(\alpha_{t_{j-1}}^*)(\hat{\alpha}_{t_{j-1}} - \alpha_{t_{j-1}}^*) = \\ &= F^{j-1}(\hat{\alpha}_{t_{j-1}}) + T^{j-1}(\hat{\alpha}_{t_{j-1}})(\hat{\alpha}_{t_{j-1}} - \hat{\alpha}_{t_{j-1}}) = \\ &= F^{j-1}(\hat{\alpha}_{t_{j-1}}) \\ Z(\alpha_{t_j}^*) + tlZ(\alpha_{t_j}^*)(\hat{\alpha}_{t_j} - \alpha_{t_j}^*) &= \\ &= Z(\hat{\alpha}_{t_j}) + tlZ(\hat{\alpha}_{t_j})(\hat{\alpha}_{t_j} - \hat{\alpha}_{t_j}) = \\ &= Z(\hat{\alpha}_{t_j}), \quad 1 \leq j \leq N_{ass}. \end{aligned}$$

As soon as the posterior mode $\hat{\alpha}_{t_0}$ for the problem linearised around time evolution $(\alpha_{t_0}^*, \dots, \alpha_{t_{N_{ass}}}^*)$ satisfies the requirement $\alpha_{t_0}^* = \hat{\alpha}_{t_0}$, it is a posterior mode of the original system as well.

$$(120) \quad \begin{aligned} B_0^{-1}(\hat{\alpha}_{t_0} - a_0) + \sum_{j=1}^{N_{ass}} \left(\prod_{k=1}^j \bar{T}^{k-1}(\hat{\alpha}_{t_{k-1}}) \right)^T (nlZ(\hat{\alpha}_{t_j}))^T H^{-1} \{y_{t_j} - Z(\hat{\alpha}_{t_j})\} &= 0 \\ \hat{\alpha}_{t_j} = \bar{F}^{j-1}(\hat{\alpha}_{t_{j-1}}), \quad j = 1, \dots, N_{ass} \end{aligned}$$

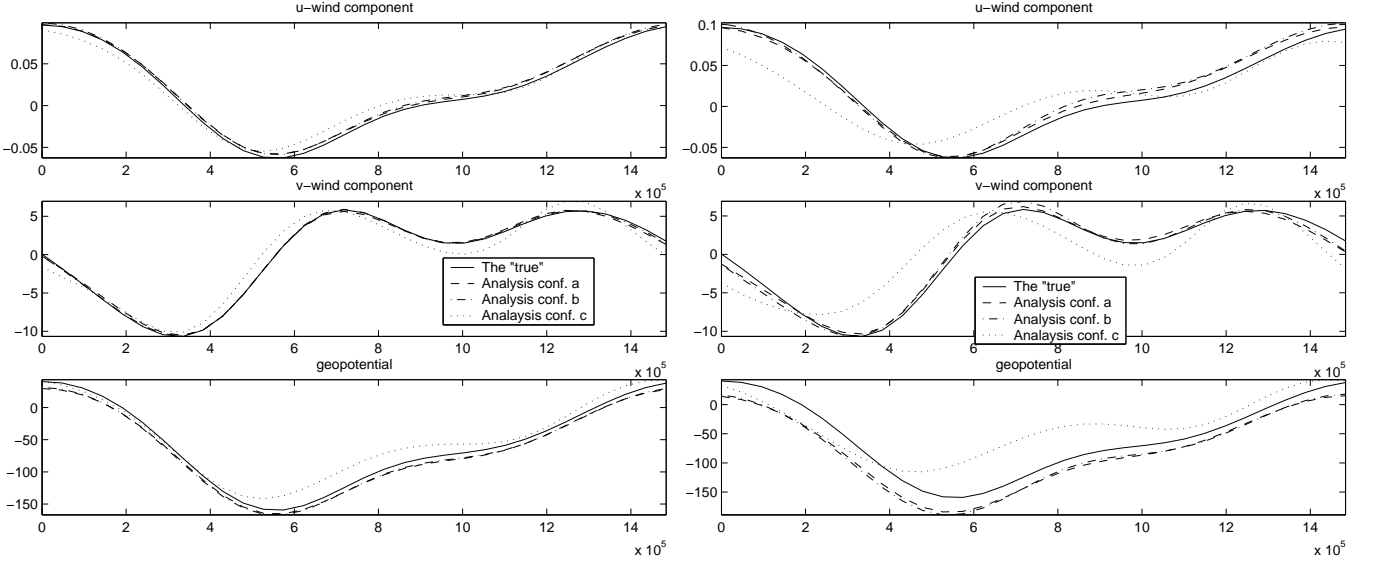


FIGURE 16. The analysed state obtained with the time smoother at the end of the fifth data assimilation cycle (the short time window) under different configurations using "high" precision data (the left picture) and ("low" precision data (the right picture)). The simulated true state is given by the full line. The analysed state obtained by the time window smoother in Configuration *a* ("long" time window) is given by dashed line. The analysed state obtained by the time window smoother in Configuration *b* ("short" time window, the initial forecast error covariance matrix is dynamically updated at the beginning of each time window) is given by the dashed-dotted line. The analysed state obtained by the time window smoother in Configuration *c* ("short" time window, the initial forecast error covariance matrix is kept unchanged at the beginning of each time window) is given by dotted line. The observations were simulated by the non-linear observation operator nlZ_3

Figure 16 shows the result of the implementation of the time-window smoother under three different configurations. For simulation of the observations we have used the non-linear observation operator nlZ_3 . Two sets of experiments were performed. In the first set (the left figure), the observations were assumed to be quite precise compared to the background state a_0 . The diagonal of the covariance matrix for the observation errors was taken as $H_i = \frac{1}{4}tlZ_3B_0(tlZ_3)^T$. Thus the variance of the observation errors was roughly set to the 25% of the variance of the corresponding background errors. In the second set (the right figure), the background field has a stronger influence on the analysed state by letting $H_i = 2tlZ_3B_0(tlZ_3)^T$.

Under Configuration *a* (the dashed line) we have used the time window smoother with one long time window. The length of the "long" time window is 40 observation windows ($N_{ass} = 40$ groups of observations y_i , with 9 observations in each group were utilised in the data assimilation). Under Configuration *b* (the dashed-dotted line) we have used the time window smoother with a "short" time window. The length of the "short" time window is 8 observation windows. The data assimilation consists of 5 cycles, when the time-window smoother is applied in a sequence. Every data assimilation cycle our knowledge about the unobservable model state variable is expressed in a form of a Gaussian prior distribution. For the first data assimilation cycle, the prior is taken to be equal $\mathcal{N}(a_0, B_0)$. In the beginning of the following data assimilation cycles, the prior is taken to be equal $\mathcal{N}(a_8, B_8)$,

where a_8, B_8 are obtained during the previous data assimilation cycle. Configuration c (dotted line) is similar to Configuration b except for the prior formulation. The initial forecast error covariance matrix B_0 is kept the same at the beginning of each assimilation cycle in Configuration c . In the beginning of the first data assimilation cycle the prior is taken to be equal $\mathcal{N}(a_0, B_0)$, in the beginning of the following data assimilation cycles, the prior is $\mathcal{N}(a_8, B_0)$, where a_8 is obtained during the previous data assimilation cycle.

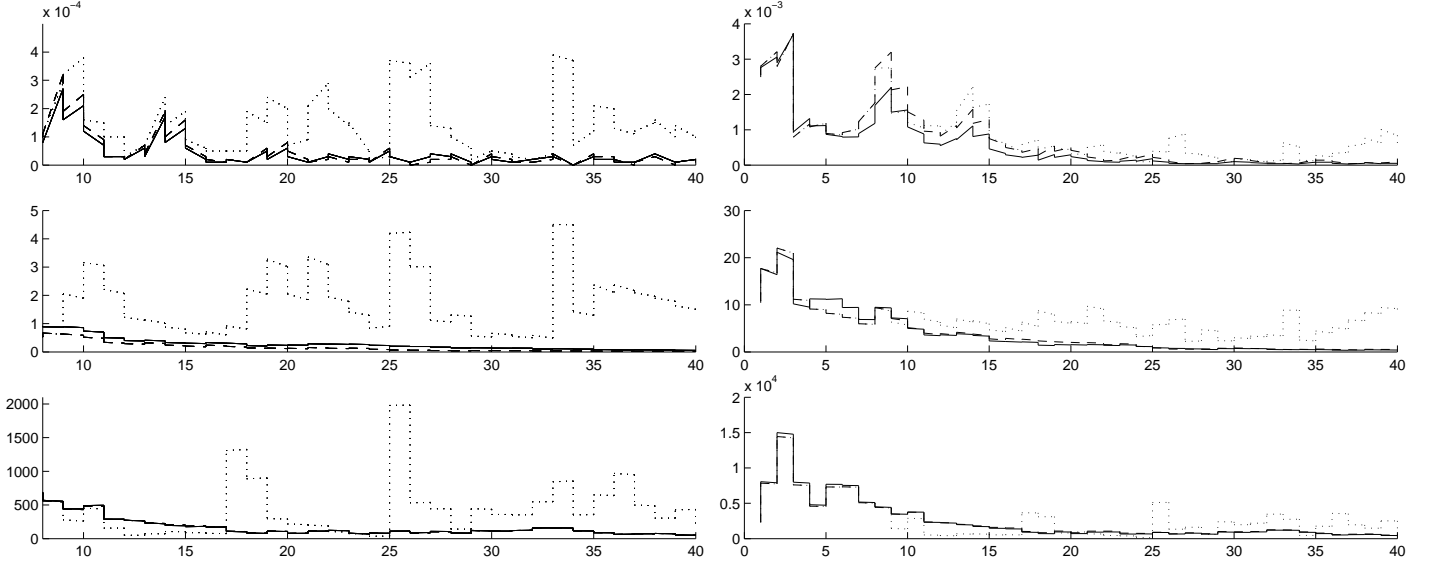


FIGURE 17. The spatial average squared error of the analysed state obtained using different configurations of the time-window smoother. The figure to the left corresponds to the case of "high" precision observations. The figure to the right corresponds to the "low" precision observations. The solid line shows the SE^{tws} corresponding to the "long" time window (Configuration a). The dashed line shows the SE^{tws} corresponding to the "short" time window (Configuration b). The dotted line shows the SE^{tws} corresponding to the short time window and the same initial forecast error covariance matrix at the beginning of each time window (Configuration c). The observations were simulated using the non-linear observation operator nlZ_3

Like we already have mentioned, every time observations are introduced, the amplitudes of the posterior covariance matrix elements decreases. This expresses our increased confidence in the knowledge about the model state variable. Even if the posterior distribution is non-Gaussian, the fact that every data assimilation cycle we formulate our opinion about the model state variable in the form of a Gaussian prior does not make much harm. Figure 17 represents the spatial average squared analysis error SE^{tws} for both sets of data assimilated under different configurations. The SE^{tws} , calculated in the same way as for the extended Kalman filter (110), obtained under Configuration a and under Configuration b are quite close. Under Configuration c we underestimate our knowledge about the model state variable. Using the same initial forecast errors covariance matrix in the formulation of the prior every data assimilation cycle, we disregard all improvement in the estimate of the unobservable model state variable we have achieved by assimilating the data during the previous data assimilation cycles. The observations have improperly high weights. The loss of information about already assimilated data destroys the mechanism of filtering observation errors. Observation errors will therefore have large impact on the construction of the analysed state. The data assimilation procedure gives

rather unsatisfactory results after five data assimilation cycles under Configuration c in comparison with the other configurations. The pattern of behaviour is similar for both sets of data (with higher precision observations and with lower precision observations). Although in the general practice of Bayesian inference, the underestimated prior is better than the overestimated prior, the prior formulation has great impact on the construction of the analysed state, in the presence of a low amount of observations in comparison with the degree of freedom of the model state variable, \cdot . The dynamical updating of the initial covariance matrix each data assimilation cycle is essential for the performance of the time-window smoother, even if the posterior predictive covariance is not estimated correctly in general.

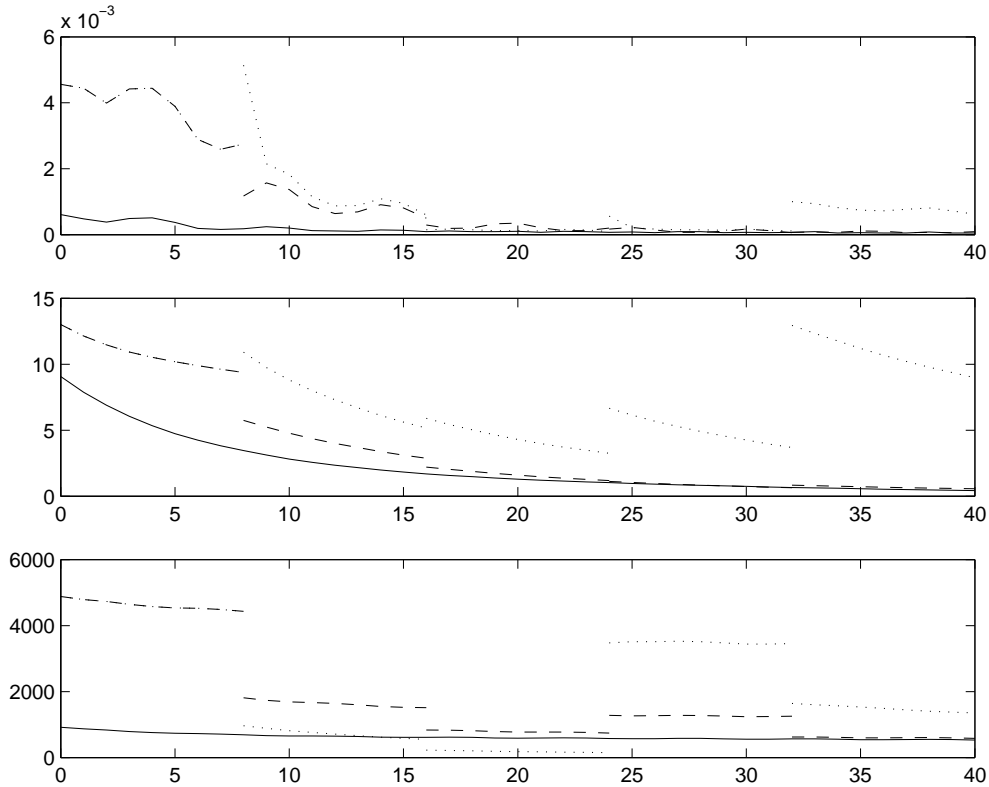


FIGURE 18. The spatial average squared error of the posterior mode of the model state variable for the u -wind component, for the v -wind component and for the geopotential, obtained using different configurations of the time-window smoother. The solid line shows the $\tilde{S}E$ corresponding to the "long" time window (Configuration a). The dashed line shows the $\tilde{S}E$ corresponding to the "short" time window (Configuration b). The dotted line shows the $\tilde{S}E$ corresponding to the "short" time window and the same initial forecast errors covariance matrix of the model state variable at the beginning of each assimilation cycles (Configuration c).

It must be considered, that in the case of a more realistic state space model, without the perfect model assumption, Configuration c will probably not provide such drastically bad results like we have shown. In the case of a stationary linear dynamical model and linear observational operator, in presence of errors of the dynamical evolution, the Kalman filter will converge to a stationary steady state solution. The growth of the uncertainty during the dynamical integration will be compensated by assimilation of new observations. However, in the case of non-linear dynamics and non-linear observation

operators, the tangent linear operator changes strongly from one data assimilation cycle to another, and an exact steady state solution will never occur.

Figure 18 shows the spatial average squared error of the posterior mode $\tilde{S}E$ obtained using different configurations of the time window smoother. The $\tilde{S}E$ is defined in the following way

$$(121) \quad \tilde{S}E(i) = \sum_{k=-M}^M (\alpha_{k,i} - \bar{X}_k(t_i))(\alpha_{-k,i} - \bar{X}_{-k}(t_i)).$$

The "low" precision data are used in the example, simulated using nlZ_3 . The results of the time smoother in Configuration c (a "short" time window and the same initial forecast error covariance matrix of the model state variable each assimilation cycle) indicate a data over-fit. Certainly, in the case of a lucky data combination when one observation does not support the observation errors of others, the result can be even better than using the "long" time filter. For example, the posterior mode of the geopotential, obtained using the configuration c , has smallest $\tilde{S}E$ during the second and the third data assimilation cycles.

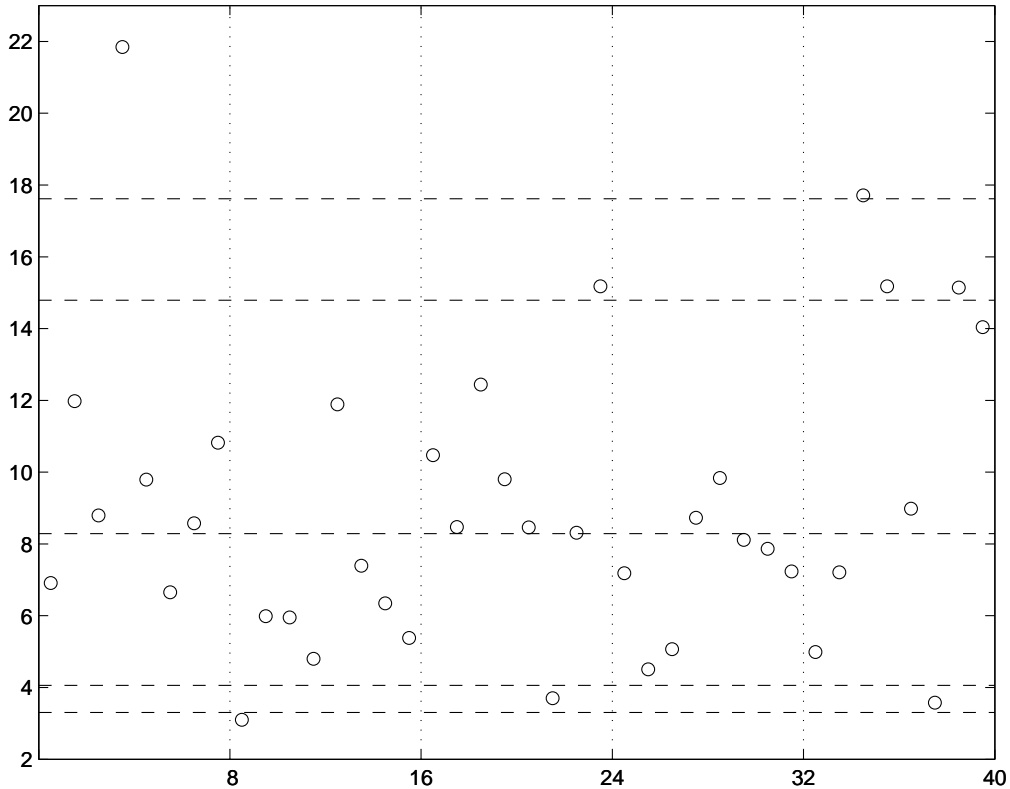


FIGURE 19. The scores of observations $sc(i)$ introduced during different assimilation cycles with the "short" time-window. The 0.05, 0.1, 0.5, 0.9 and the 0.95 quantiles of $\chi^2(9)$ are indicated by dashed lines

Figure 19 shows scores of the used observations. We define the score parameter $sc(i)$ for observation y_i

$$(122) \quad sc(i) = \{y_i - nlZ(\bar{X}(t_i))\}^T (H_i)^{-1} \{y_i - nlZ(\bar{X}(t_i))\}, \quad 1 \leq i \leq N_{ass}$$

With the definition of the observations $y_i \sim \mathcal{N}(nlZ(\bar{X}(t_i)), H)$, it is evident that the $sc(i)$ scores are $\chi^2(p)$ distributed, where $p = 9$ is the dimensionality of the vector y_i . In fact, during the first data assimilation cycle, a quite erroneous observation of the geopotential

was obtained. The assimilation of such erroneous data influences the result of the time smoother under Configuration *a* long time forward. But the more data we assimilate, the weaker is the influence of one particular "bad" observation, because the joint assimilation of a large number of observations helps to reduce the effect of an error coming from a particular "bad" one. Under Configuration *c*, the previously assimilated observation has a much smaller impact, compared with the other two configurations. The analysed state is over-fitted to the small number of newly coming observations, which are always more or less erroneous. If an unlucky data set is observed, the posterior mode, based on this small set of observations can deviate significantly from the "true" state even after a large number of performed data assimilation cycles. Whether lucky or unlucky combinations of data are observed we never now in real situations, and the data over-fit is highly undesirable.

It needs to be mentioned that in operational data assimilation schemes, applied for numerical weather prediction purposes, special quality control procedures have been introduced to handle such "particularly bad" observations. These quality control procedures are generally based on prior assumptions about the character of observation errors (also non-Gaussian ones). We have not used such quality control procedures here.

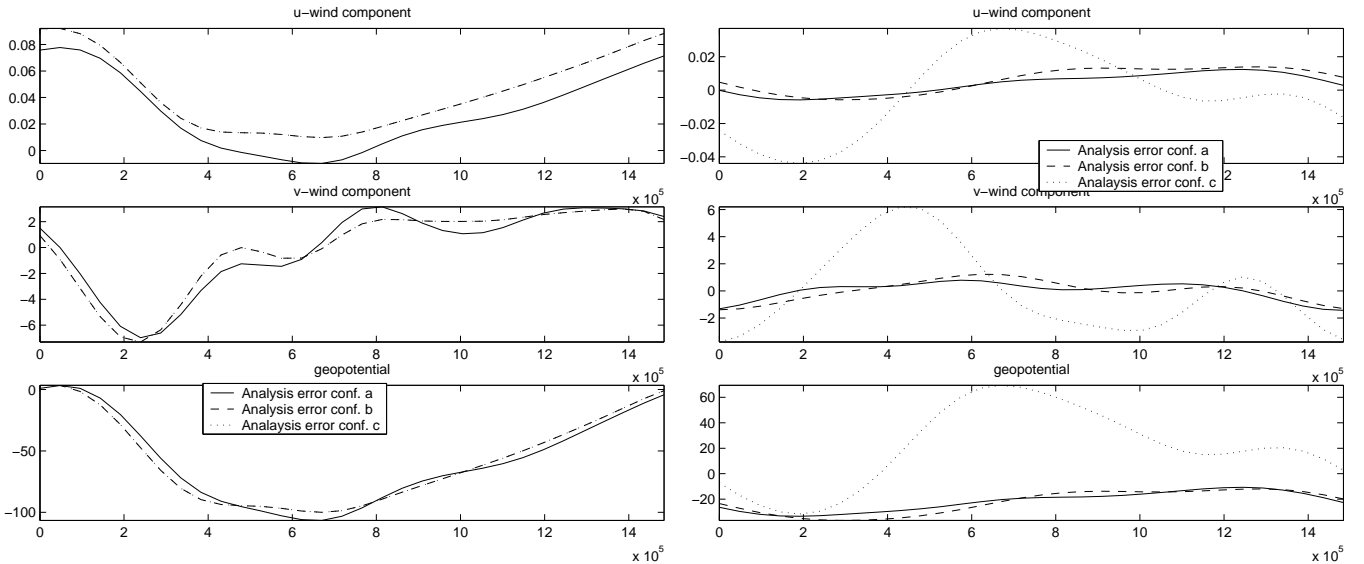


FIGURE 20. The analysis error for the "u"-wind component, for the "v"-wind component and for the geopotential, obtained at the end of the first ("short") data assimilation time window (the left figure) and those at the end of the fifth ("short") data assimilation time window with different configurations using "low" precision data. The solid line corresponds to the analysis error obtained under Configuration *a*, the dashed line corresponds to the results obtained under Configuration *b* and the dotted line corresponds to the results obtained under Configuration *c*. The observation were simulated by the non-linear observation operator nlZ_3 .

It is good to notice that the order of the amplitude of the forecast errors are in good correspondence with the estimate of the forecast error covariance matrix of the model state variable. Even if the forecast obtained under Configuration *c* after five data assimilation cycles seems to be unacceptably erroneous compared to the forecasts obtained under the other two configurations, the amplitude of the forecast error under Configuration *c* after five assimilation cycles is the same as after the first assimilation cycle (Figure 20). This is what we should expect starting each assimilation cycle with the same initial

forecast error covariance matrix. However we need always to take into account that the dynamical evolution of the covariance matrix B_i , obtained by the time-smoother, describes the dynamic evolution of the Gaussian approximation of the actual posterior distribution and B_i is not equal to the $Var(\hat{X}_{t_i} | \mathcal{Y}_i)$, but describes the evolution of the curvature of the posterior density around the mode.

The procedure to obtain the posterior mode is iterative, and like many iterative procedures it is only locally convergent. The linearization of the dynamics and the observation operators is done around an estimate of the posterior mode evolution, and this estimate must be constructed in some way. To obtain it, we have used the extended Kalman filter and the finite interval smoother with backtracking by the tangent-linear dynamics linearised around the non-linear evolution of the analysed state.

To summarise the method, we first run the extended Kalman filter forward in time, described by the recursion formulas

$$\begin{aligned}
a_i &= a_i^f + K_i v_i, \\
B_i &= B_i^f - B_i^f t l Z^T K_i^T, \\
v_i &= y_i - Z(a_i^f), \\
K_i &= B_i^f t l Z^T F_i^{-1}, \\
F_i &= t l Z B_i^f (t l Z)^T + H, \\
a_i^f &= \bar{F}^{i-1}(a_{i-1}) \\
B_i^t &= \bar{T}^{i-1} B_{i-1} (\bar{T}^{i-1})^T, \quad i = 1, \dots, N_{ass}
\end{aligned}$$

Here during i -th assimilation term, the tangent-linear observation operator $t l Z$ is evaluated at a_i^f and the tangent-linear dynamical propagator \bar{T}^{i-1} is evaluated along the time evolution of a_{i-1} .

Secondly, we run the smoother backward in time and we use the following backward recursive equations

$$\begin{aligned}
r_i &= (t l Z \bar{T}^{i-1})^T F_i^{-1} v_i + L_i^T r_{i+1} \\
N_i &= (t l Z \bar{T}^{i-1})^T F_i^{-1} (t l Z \bar{T}^{i-1}) + L_i^T N_{i+1} L_i
\end{aligned}$$

with

$$\begin{aligned}
L_i &= \bar{T}^{i-1} - \bar{T}^{i-1} K_i t l Z \quad i = 1, \dots, N_{ass} - 1, \\
r_{N_{ass}} &= (t l Z \bar{T}^{N_{ass}-1})^T F_{N_{ass}}^{-1} v_{N_{ass}}, \\
N_{N_{ass}} &= (t l Z \bar{T}^{N_{ass}-1})^T F_{N_{ass}}^{-1} (t l Z \bar{T}^{N_{ass}-1}).
\end{aligned}$$

Again, at the i -th assimilation term the tangent-linear observation operator $t l Z$ is evaluated at a_i^f and the tangent-linear dynamical propagator \bar{T}^{i-1} is evaluated along the time evolution of a_{i-1} .

Finally, we obtain the initial estimate of the posterior mode evolution

$$\begin{aligned}\alpha_i^* &= a_i + B_i r_{i+1} \\ V_i^* &= B_i - B_i N_{i+1} B_i, \quad i = 1, \dots, N_{ass} - 1\end{aligned}$$

The evolution of the posterior mode α_i^* is governed by linear dynamics obtained by linearization of the non-linear dynamics around the non-linear evolution of analysed state a_i .

The original system has the posterior mode $\hat{\alpha}_{t_0}$ and in a vicinity of that mode the posterior pdf can be well approximated by the Gaussian one $p(\hat{X}(t_0) | \mathcal{Y}) \sim \mathcal{N}(\hat{\alpha}_{t_0}, V_0)$. If we want to use the obtained posterior mode as a point estimate of an unobservable random variable, it is not only the curvature around the posterior mode V_0 that is important. The amount of mass located in the tails of the posterior distribution density is very important to know in order to conclude about the accuracy of the estimate. This information is not provided at all by the method. If the distribution is heavy tailed, the probability for the unobservable model state to be located just in the close vicinity of the posterior mode can be quite small, especially in the case of a large dimensionality. Solving the non-linear equation by the Kalman filter and smoother iteration techniques, the approximate time evolution of the posterior mode and the curvature in its vicinity are obtained as well. However, this is only an approximation of the posterior predictive mode, because the posterior mode is not parameterisation invariant in general. If we denote the dynamical evolution over the period $t_0 - t_j$ with $\hat{X}(t_j) = \mathcal{F}^{t_j}(\hat{X}(t_0))$, then from the transform theorem follows that $(\frac{\partial \mathcal{F}^{t_j}}{\partial \hat{X}(t_0)})^T p_{\mathcal{F}}(\hat{X}(t_j)) = p(\hat{X}(t_0))$. Here $p(\cdot)$ and $p_{\mathcal{F}}(\cdot)$ denote the posterior distributions for $\hat{X}(t_0)$ and $\hat{X}(t_j)$, respectively. The posterior mode $\hat{\alpha}_{t_0}$ satisfies the requirement $\frac{\partial p(\hat{X}(t_0))}{\partial \hat{X}(t_0)}(\hat{\alpha}_{t_0}) = 0$. At this point

$$(123) \quad \left(\frac{\partial \mathcal{F}^{t_j}}{\partial \hat{X}(t_0)}\right)^T \frac{\partial p_{\mathcal{F}}}{\partial \hat{X}(t_j)}(\mathcal{F}^{t_j}(\hat{\alpha}_{t_0})) \frac{\partial \mathcal{F}^{t_j}}{\partial \hat{X}(t_0)} + \left(\frac{\partial^2 \mathcal{F}^{t_j}}{\partial \hat{X}^2(t_0)}\right)^T p_{\mathcal{F}}(\mathcal{F}^{t_j}(\hat{\alpha}_{t_0})) = 0$$

Only in the case of linear dynamics $\frac{\partial^2 \mathcal{F}^{t_j}}{\partial \hat{X}^2(t_0)} \equiv 0$, the posterior distribution $p_{\mathcal{F}}$ has a mode at the point $\mathcal{F}^{t_j}(\hat{\alpha}_{t_0})$. In general, and for the shallow water model as well, these two posterior distributions have different modes. The Hessian for the dynamics of the one-dimensional shallow water model is close to zero, and we can expect that the mode of $p_{\mathcal{F}}(\cdot)$ and the time evolution of posterior mode $p(\cdot)$ must be quite close.

4.4. The ensemble Kalman filter. The ensemble Kalman filter (eKF, Evensen, 1994, 2003, Houtekamer et al., 2001) tries to preserve the optimality property only in the sense of the mean square error, and estimates the posterior mean $E(\hat{X}(t_i) | \mathcal{Y}_i)$ and posterior variance $var(\hat{X}(t_i) | \mathcal{Y}_i)$ through the construction of the best linear predictor on the last coming observations y_i given the whole history \mathcal{Y}_{i-1} each data assimilation term t_i , $i = 1, \dots, N_{ass}$. Every data assimilation term the information about the accuracy of the predictor is estimated from the ensemble of analysed fields $\{x_j^{as}(t_i)\}$, $j = 1, \dots, N_{sample}$, where N_{sample} is the ensemble size. To construct the ensemble of analysed fields, the uncertainty in the forecast valid at time t_i and the uncertainty in observations available at time t_i are utilized. The uncertainty in the forecast is sampled using the ensemble of the forecast fields $\{x_j^f(t_i)\}$, $j = 1, \dots, N_{sample}$ and the uncertainty in observations is sampled from the ensemble of randomly perturbed observations $y_{i,j}$, $j = 1, \dots, N_{sample}$. The construction of the ensemble of the forecast and the ensemble of the observations

is consistent with their error statistics. The posterior predictive statistics at a new assimilation term (say, the $i + 1$ -th) are estimated directly from an ensemble of forecast states $\{x_j^f(t_{i+1})\}$, $j = 1, \dots, N_{sample}$ valid at time t_{i+1} . This ensemble is the ensemble of analysed states $\{x_j^{as}(t_i)\}$, $j = 1, \dots, N_{sample}$ being propagated by the model non-linear dynamics over the period (t_i, t_{i+1}) .

$$(124) \quad x_j^f(t_i) = \bar{F}^{i-1}(x_j^{as}(t_{i-1})), \quad j = 1, \dots, N_{sample}, \quad i = 1, \dots, N_{ass}$$

At every moment of time t_i , $1 \leq i \leq N_{ass}$, the mean of the population, used to describe the distribution of the forecast states around the "true" state, is estimated as a sample mean

$$(125) \quad E(\hat{X}(t_i) | \mathcal{Y}_{i-1}) \approx \bar{x}^f(t_i) = \frac{1}{N_{sample}} \sum_{j=1}^{N_{sample}} x_j^f(t_i).$$

In the same way the population variance is estimated through the sample variance

$$(126) \quad var(\hat{X}(t_i) | \mathcal{Y}_{i-1}) \approx B_e^f(t_i) = \frac{1}{N_{sample} - 1} \sum_{j=1}^{N_{sample}} (x_j^f(t_i) - \bar{x}^f(t_i))(x_j^f(t_i) - \bar{x}^f(t_i))^T$$

The ensemble of forecast states is created in the following way. First, for the initial first-guess state, the best possible estimate of the true state a_0 is drawn from a population with a Gaussian distribution around the "true" state, with some known covariance matrix, describing the behaviour of the forecast errors $\mathcal{N}(\bar{X}(t_0), B_0)$. Secondly, given this "best" estimate of the "true" state a_0 , the unobservable "true" state, the inference about which we want to make, can be considered as a member of a population with a Gaussian distribution around the "best" estimate $\bar{X}(t_0) \sim \mathcal{N}(a_0, B_0)$, with the same variance. Thus to represent the uncertainty in the estimate of the "true" model state at the initial time t_0 an ensemble is drawn around the "best" estimate a_0 with the same variance B_0 , describing forecast errors $x_j^{as}(t_0) \sim \mathcal{N}(a_0, B_0)$, $j = 1, \dots, 2 * N_{sample}$. (The purpose of $2 * N_{sample}$ in the double ensemble Kalman filter will be explained below). The ensemble of the forecast state valid at the time of the first data assimilation term t_1 is obtained by dynamical forward integration of each ensemble member.

Each data assimilation term t_i , $1 \leq i \leq N_{ass}$, the ensembles of observations are created as well. As we have already mentioned, the observations are assumed to have a Gaussian distribution around the projection of the "true" model state into the space of observations by the observation operator $y_i \sim \mathcal{N}(Z(\bar{X}(t_i)), H)$ (we have denoted by Z any observation operator, a linear or a non-linear one). To represent the uncertainty in the knowledge about $Z(\bar{X}(t_i))$ coming from observation y_i , the ensemble of observations is sampled around y_i with the observation error covariance matrix $y_{i,j} \sim \mathcal{N}(y_i, H)$, $j = 1, \dots, 2 * N_{sample}$.

Figure 21 shows the result of the implementation of the double ensemble Kalman filter. We will discuss the method in details later. In short words, in the double ensemble Kalman filter, the Kalman gain matrix is estimated from one ensemble of forecast states and the analysis sample is constructed from the second ensemble of forecast states using the estimate of the Kalman gain matrix from the first ensemble. In the single (not double) ensemble Kalman filter the same ensemble of the forecast states is used to calculate the

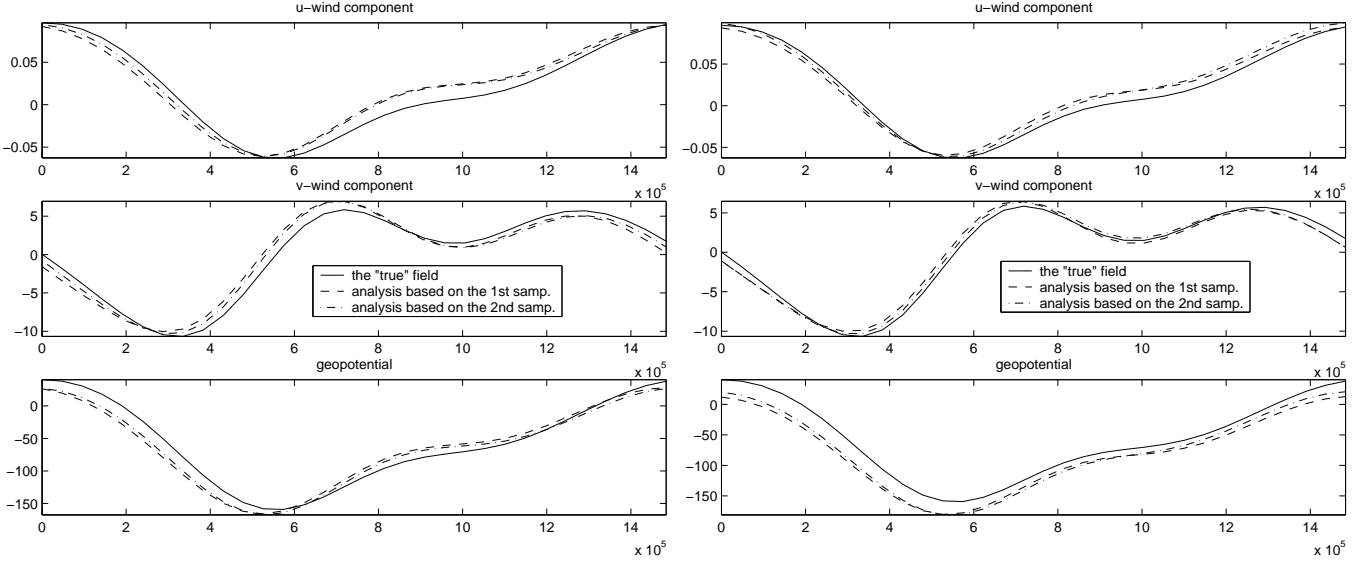


FIGURE 21. The analysed fields for the u -wind component, for the v -wind component and for the geopotential obtained after 40 assimilation terms by means of the double ensemble Kalman filter. The solid line is corresponding to the "true" model state, the dashed line is corresponding to the estimate from one sub-ensemble of the analysed states, the dashed-dotted line is corresponding to the estimate from the second sub-ensemble of analysed states. The "low" precision observations simulated by the non-linear observation operator nlZ_3 are used in the examples. The left picture shows analysis obtained from the $N_{sample} = 12$ ensemble members sample. The right picture shows analysis obtained from the $N_{sample} = 100$ ensemble members sample.

gain matrix and to construct the ensemble of the analysed states, which is used to represent the error associated with using the gain matrix. This is a duplicate use of the same information, also known as inbreeding, and it can lead to an unrealistically small spread of the ensemble of analysed states after several data assimilation terms (Houtekamer, 1998). One way to overcome the problem is to use the double ensemble Kalman filter. We can see that the idea turns out to be brilliant, because even the analysis obtained from a very small sample size on the "low" precision data looks quite reasonable. In both cases, with the small and the large sample size, both samples provide quite similar results after the two samples have stabilised (by mixing with each other and with the observations). The analysis obtained using the large size sample estimates better the wind-component fields and results in a more proper dynamical evolution.

Each data assimilation term t_i , the ensemble of analysed states $\{x_{j,k}^{as}(t_i)\}$ is created from the ensemble of forecast states $x_{j,k}^f(t_i)$ and the ensemble of observations $\{y_{i,j}\}$ by means of a linear transform. We have applied both the single ensemble Kalman filter and the double ensemble Kalman filter. Let indexes k and \bar{k} ($\{k, \bar{k}\} = \{0, 1\}$) denote the different sub-ensembles each size of N_{sample} .

In the double ensemble Kalman filter the sub-ensemble k of the analysed states is constructed from the sub-ensemble k of the forecasted states and from the sub-ensemble k of the observations

$$\begin{aligned}
(127) \quad x_{j,k}^{as}(t_i) &= x_{j,k}^f(t_i) + K_{i,\bar{k}}^e (y_{i,j,k} - Z(x_{j,k}^f(t_i))) \\
&= x_{j,k}^f(t_i) + K_{i,\bar{k}}^e v_{i,j,k}^e
\end{aligned}$$

with the Kalman gain matrix estimated from the sub-ensemble \bar{k} of the forecast states $\{x_{j,\bar{k}}^f(t_i)\}$, $j = 1, \dots, N_{sample}$

$$K_{i,\bar{k}}^e = B_{i,\bar{k}}^{f,e} Z^T (F_{i,\bar{k}}^{e,*})^{-1}$$

whis the innovation covariance matrix $F_{i,\bar{k}}^{e,*}$ is estimated by

$$(128) \quad F_{i,\bar{k}}^{e,*} = Z^T B_{i,\bar{k}}^{f,e} Z + H$$

This estimation of the innovation covariance matrix is different from the sample estimate of the innovation covariance matrix and it is assumed in order to assure invertibility of the estimate of the innovation covariance matrix.

In the single ensemble Kalman filter the sub-ensemble k of the analysed states is constructed in the similar way as in (127) but using the Kalman gain $K_{i,k}^e$, constructed from the same sub-ensemble of the forecast states k .

The ensemble of analysed states $\{x_j^{as}(t_i)\}$, $j = 1, \dots, N_{sample}$, $1 \leq i \leq N_{ass}$ is created to be used only for the purpose of estimating statistics, and does not pretend to be sampled from the true posterior distribution. Like we already have discussed in the subsection about the bias corrected Kalman filter, the posterior mean is not equal to the best linear predictor in the case of non-linear observation operators. Even in the case of a linear observation operator, after the non-linear dynamical evolution, the posterior predictive distribution is not Gaussian. It is only the posterior mean that obeys $E(\hat{X}(t_i) | \mathcal{Y}_i) \approx E(\hat{X}(t_i) | \mathcal{Y}_{i-1}) + K_i v_i$. This linear transform is not necessarily valid for a single member of the ensemble. However, in the case of our one-dimensional shallow water model, where non-linearity is very weak, in the case of a linear observation operator, the analysed ensemble state will be sampled from a distribution quite close to the posterior one. In a more realistic situation, with a non-linear observation operator, the sample does not come from the posterior distribution.

As it can be noticed from Figure 22, the double ensemble Kalman filter provides a clear advantage compared with the single ensemble Kalman filter in the case of a small sample size. In the single ensemble Kalman filter, the Kalman gain is estimated from the same ensemble of forecast states on which the analysed sample is constructed later. The small sample size represents poorly the features of the whole population and in the majority of cases the estimate of the covariance matrix constructed on the small sample size underestimate the covariance matrix of the population. Besides that, the double use of information for constructing the Kalman gain matrix and for estimating the accuracy of the analysis can lead to an unrealistically small spread of the ensemble of the analysed states after several data assimilation terms. As a result, the observations will have a very small impact and the analysed state will not approach the "true" one. In the double ensemble Kalman filter, the spread of the ensemble of the analysed states is artificially increased if the estimate of the covariance matrix from the two sub-ensembles differ significantly. This will cause the observations to be given higher weights. We can see that the solid $SE^{eKF}(i)$ verification curves on the left picture (the double ensemble Kalman filter with a small sample size) differ drastically from the dashed ones (the single ensemble

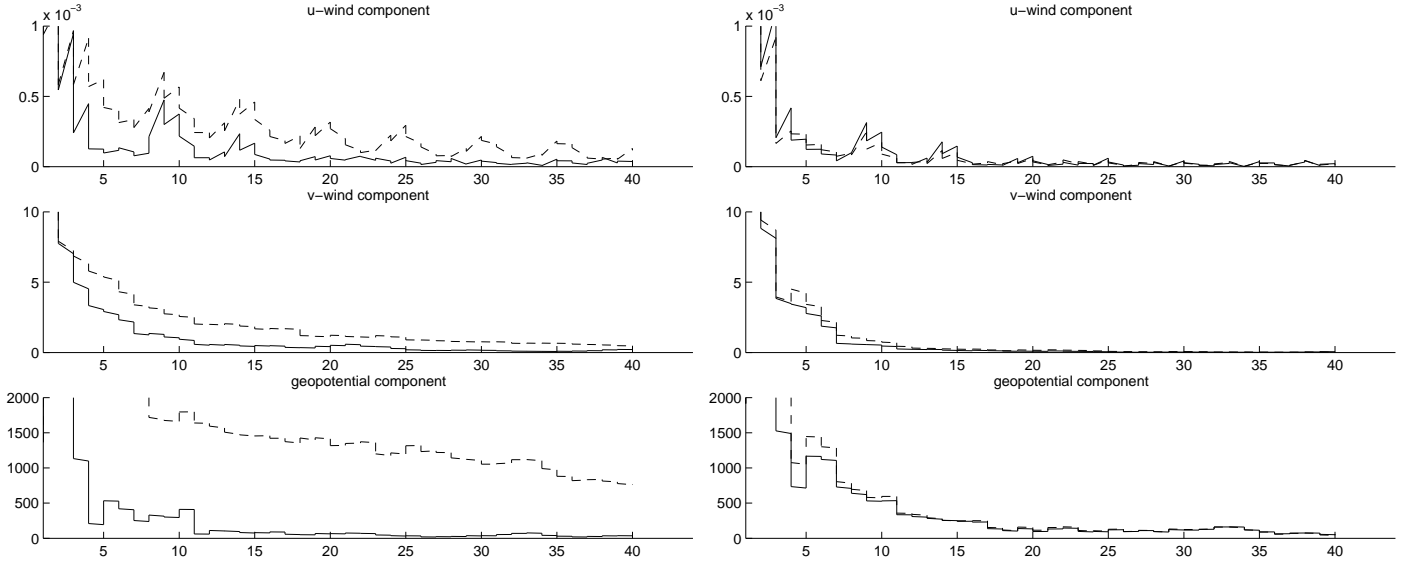


FIGURE 22. The spatial average squared error SE^{eKF} of the analysed state obtained by means of the single ensemble Kalman filter (the dashed line) and by the means of the double ensemble Kalman filter (the solid line). The left picture shows the result from using a small sample size (12 ensemble members) and the picture to the right shows the result from using a large size sample (100 ensemble members). The "high" precision data were used in these examples. The observations were simulated by the non-linear observation operator nlZ_3 . The result is corresponding to the first sub-ensemble.

Kalman filter with a small sample size). The larger values of the solid $SE^{eKF}(i)$ verification curves for winds components in the case of small sample size compared to the right picture indicates a data over-fit in the first part of the assimilation procedure due to an overestimated covariance matrix of the model state. We consider that the estimate of the forecast error covariance matrix obtained by means of the extended Kalman filter is not far away from the "true" forecast error covariance matrix of the population in the case of a one-dimensional shallow water model, and therefore we have used the behaviour of the extended Kalman filter as a reference (Figure 24, to be discussed in more details below). In the second part of the data assimilation procedure, after the two different sub-ensemble of small size have stabilised by the mixing with each other and with the observations, the overestimation of the covariance matrix values (in the double ensemble Kalman filter) decreases. In the case of a large sample size, the ensemble gives a good estimate of the covariance matrix of the whole population from the start. The double ensemble Kalman filter gives a minor improvement in the very beginning of data assimilation procedure. After a while, in the single ensemble Kalman filter, both sub-ensembles influenced by observations behave in a very similar way.

Figure 23 illustrates the analysis increments for the u -wind component, for the v -wind component and for geopotential obtained by applying the ensemble Kalman filter. The analysis state as well as the forecast state are obtained as a sample average of the corresponding sub-ensemble. The analysis state as well as the analysis increments are not well balanced, and even the spatial stationary balance between the fields does not hold. The misbalance is very light, but an additional normal mode initialisation procedure must be applied in order to use the analysed state to represent a "realistic" atmospheric state. However, for introducing the observations and for performing the dynamical propagation,

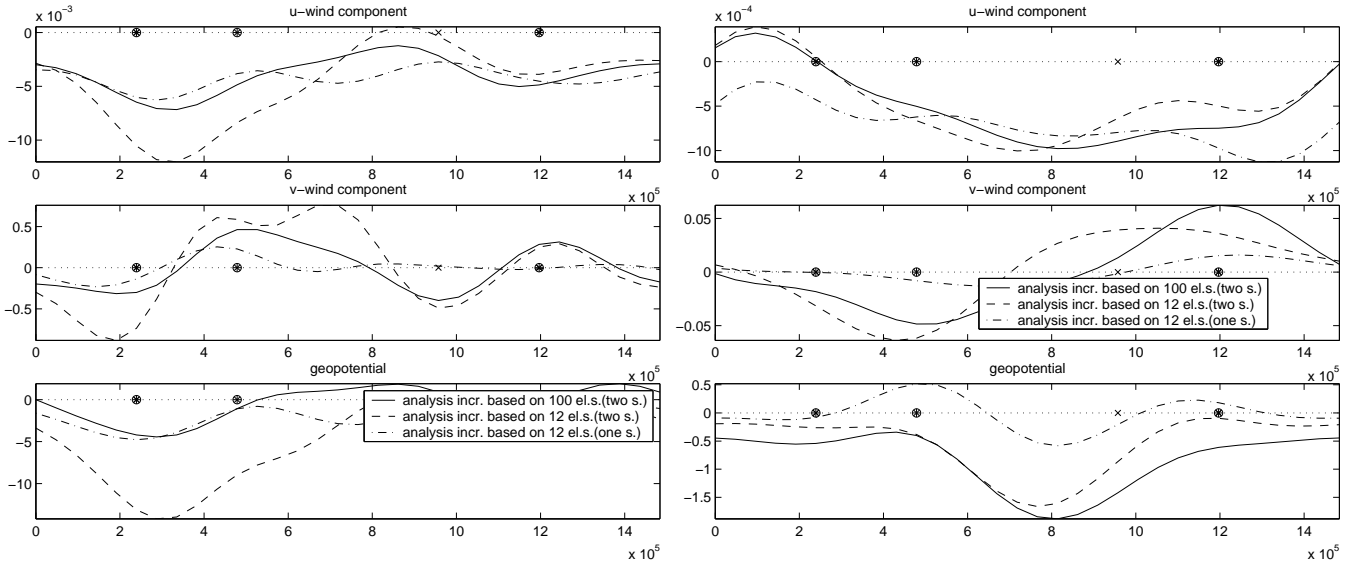


FIGURE 23. The analysis increments for the meteorological fields obtained by applying the ensemble Kalman filter. The solid line shows the analysis increment obtained by using the double ensemble Kalman filter with a large sample of size $N_{sample} = 100$, the dashed line shows the analysis increment by using the double ensemble Kalman filter with a small sample of size $N_{sample} = 12$. The dash-dot line shows the analysis increment using the single ensemble Kalman filter with a small sample of size $N_{sample} = 12$. The left picture shows the increments obtained during the 10th data assimilation term (the first part of the data assimilation procedure), the right picture shows the increments obtained during the 33rd data assimilation term (the last part of the data assimilation procedure). The shown result is corresponding to the first sub-ensemble.

the misbalance of the analysis state is unimportant, because in the ensemble Kalman filter framework all calculations are done for the individual ensemble members, which are balanced. As we can see in Figure 23, the analysis increments using the double ensemble Kalman filter with a small sample of size $N_{sample} = 12$ are much larger than the analysis increments using the double ensemble Kalman filter with a large sample of size $N_{sample} = 100$ in the beginning of data the assimilation procedure (the left figure) and that this difference decreases with time (the right picture). The analysis increments obtained by using the single ensemble Kalman filter with a small sample of size $N_{sample} = 12$ remain to be much smaller than the analysis increments obtained using the other methods, like it should be with an underestimated covariance matrix.

The large dimensional covariance matrix $B_i^{f,e}$ is never estimated directly from the ensemble. Statistics on $B_i^{f,e} Z^T$ and $Z B_i^{f,e} Z^T$ are used instead for each data assimilation term t_i , $1 \leq i \leq N_{ass}$

(129)

$$\begin{aligned}
\text{cov}(\hat{X}(t_i), Z(\hat{X}(t_i)) \mid \mathcal{Y}_{i-1}) &\approx B_i^{f,e} Z^T = \\
&= \frac{1}{N_{\text{sample}} - 1} \sum_{j=1}^{N_{\text{sample}}} (x_j^f(t_i) - \overline{x^f(t_i)})(Z(x_j^f(t_i)) - \overline{Z(x^f(t_i))})^T, \\
\text{var}(Z(\hat{X}(t_i)) \mid \mathcal{Y}_{i-1}) &\approx Z B_i^{f,e} Z^T = \\
&= \frac{1}{N_{\text{sample}} - 1} \sum_{j=1}^{N_{\text{sample}}} (Z(x_j^f(t_i)) - \overline{Z(x^f(t_i))})(Z(x_j^f(t_i)) - \overline{Z(x^f(t_i))})^T,
\end{aligned}$$

where $E(Z(\hat{X}(t_i)) \mid \mathcal{Y}_{i-1}) \approx \overline{Z(x^f(t_i))} = \frac{1}{N_{\text{sample}}} \sum_{j=1}^{N_{\text{sample}}} Z(x_j^f(t_i))$. In the case of a linear observation operator, the expression can be simplified by $\overline{Zx^f(t_i)} = \overline{Z}\overline{x^f(t_i)}$. We have omitted the indexes of the different sub-ensembles (k and \bar{k}).

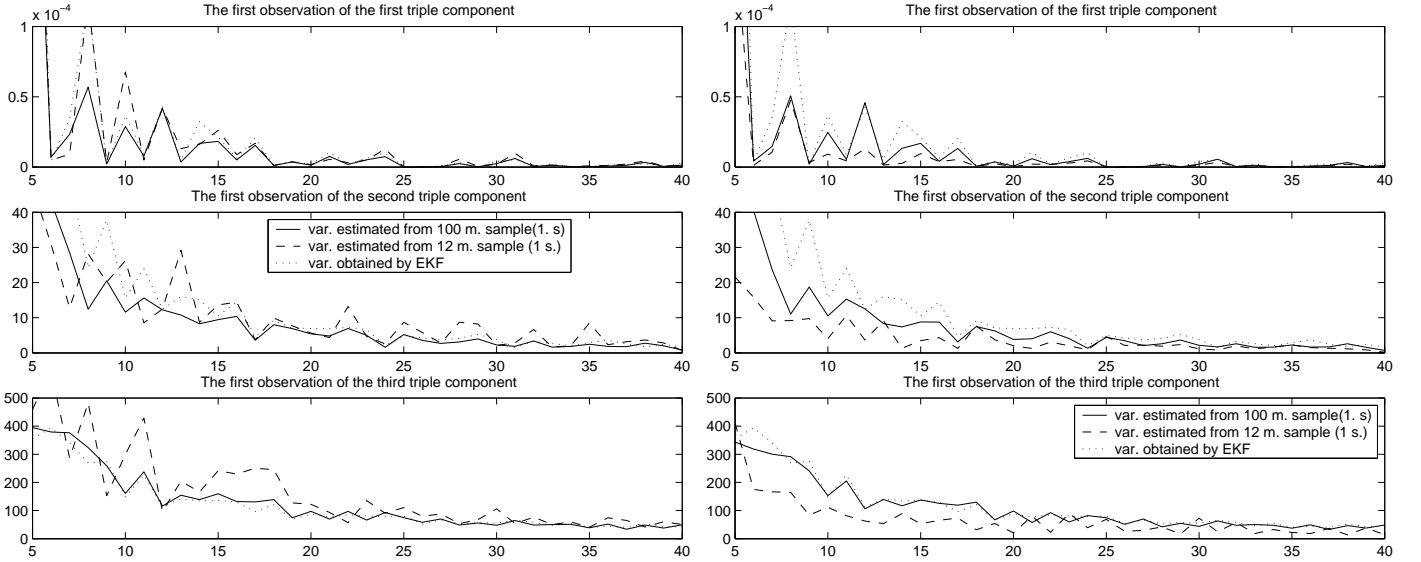


FIGURE 24. The time evolution of $\text{var}_3(t_i)$, the estimate of the forecast error covariance projected to the space of the triple of nlZ_3 (the first observation). The dotted line shows $\text{var}_3^{KF} = tlZ^3 B_i (tlZ^3)^T$ obtained by using the extended Kalman filter, the solid line shows $\text{var}_3^{e,100} = nlZ^3 B_i^{e,100} (nlZ^3)^T$ obtained by using the ensemble Kalman filter with a large sample of size $N_{\text{sample}} = 100$, the dashed line shows $\text{var}_3^{e,12} = nlZ^3 B_i^{e,12} (nlZ^3)^T$ obtained using the ensemble Kalman filter with a small sample of size $N_{\text{sample}} = 12$. The left picture shows the result implementing the double ensemble Kalman filter, the right picture shows the result implementing the single ensemble Kalman filter. The "high" precision observations simulated by the non-linear observation operator nlZ_3 are used in the example.

We show in Figure 24, we show the estimation of the forecast error covariance matrix projected on the space of the third component in triples of the non-linear observation operator nlZ_3 valid at the time moments when observations are assimilated. The results for the other observation operators look quite similar. The estimation of the projection of the forecast error covariance matrix on the space of observations is essential for a proper performance of the Kalman filtering, because, in principle, this is the quantity which in a broad sense determines the weights of the observations. We can notice a clear

overestimation of the forecast error covariance matrix values in the beginning of the data assimilation procedure for the third triple component when the double ensemble Kalman filter with a small sample of size $N_{sample} = 12$ was applied. We can also notice that the overestimation decreases with time when the sub-ensembles have stabilised due to the influence of the observations and due to the mixing with each other (the left picture). But the strong data over-fit in the beginning of the data assimilation procedure influences the quality of the data assimilation in a negative way. In any case, the result of the data assimilation procedure is much better in this case than using the single ensemble Kalman filter with a small sample of size $N_{sample} = 12$, because then the analysed state is very insensitive to the observations due to underestimated values of the quantity var_3 . Even when the single ensemble Kalman filter with a large sample of size $N_{sample} = 100$ was applied (the left picture) we can see light underestimation of $var_3^{e,100}$, although the estimation of the forecast error covariance matrix obtained by the ensemble Kalman filter with a large sample size seems to be very close to the one obtained by the extended Kalman filter var_3^{KF} . With a large sample size the ensemble Kalman filter works in an almost ideal way. The estimate of the projection of the forecast error covariance matrix on the space of the observation operator ($var_3^{e,100}$) differs for the two sub-ensembles in the beginning of the data assimilation procedure, which can be noticed from a zig-zag-shaped curves of the quantity. Later on, when the sub-ensembles have stabilised, it converges to the same estimate for both samples, and the curve becomes smooth. But using a small sample size, the zig-zag pattern remains. This indicates a poor mixing of the sub-ensembles.

Using a larger sample size when performing the data assimilation by means of the ensemble Kalman filter does not improve the estimation of the model state variable $\bar{X}(t)$. Rather an estimation of $\bar{X}(t)$ closer to the one using the extended Kalman filter is obtained. First of all, as we have mentioned above, the way in which the ensemble of the analysed state is constructed (127) does not pretend to sample from the posterior distribution of the model state variable. The larger sample size we use, the better we estimate the properties of the exact distribution of the ensemble. The ensemble of the analysed state is constructed by means of a sum of the innovation components $K_i v_i$ given the set of the previously assimilated observations \mathcal{Y}_{i-1} . From an intuitive point of view, if the amount of innovation components is large and the non-linearity of dynamics is weak, the conditional distribution of the ensemble of the analysed states $x_j^{as}(t_i)$ given \mathcal{Y}_{i-1} should come close to a Gaussian one. But the innovation components are strongly correlated and the exact convergence in distribution of the ensemble members of the analysed state to a Gaussian variable is questionable. However, the empirical observations for the model studied here support the idea.

The posterior mean and the posterior variance can be estimated from an ensemble of analysed states. To perform the filtering, we do not need to know explicitly these posterior statistics, but we can use them to obtain point estimates of the unobservable state and to judge about the precision of the estimate.

The sample estimate of the posterior mean, given \mathcal{Y}_i , omitting the indexes of the sub-ensembles k and \hat{k} , is equal

$$\begin{aligned}
 (130) \quad E(\hat{X}(t_i) | \mathcal{Y}_i) &\approx \frac{1}{N_{sample}} \sum_{j=1}^{N_{sample}} x_j^{as}(t_i) \\
 &= \bar{x}^f(t_i) + K_i^e (\bar{y}_{i,j} - \overline{Z(x^f(t_i))}) \\
 &= a_i^e \rightarrow E(\hat{X}(t_i) | \mathcal{Y}_{i-1}) + K_i (y_i - E(y_i | \mathcal{Y}_{i-1}))
 \end{aligned}$$

and this converges (as the sample size N_{sample} increases) to the standard Kalman filter analysis equation when the linear relationship between the innovation vector and the model state is assumed.

The estimate of the posterior variance has a slightly different expression, from that used in standard Kalman filtering even for the single ensemble Kalman filter. Let us denote the sample variance of the innovation $F_i^e = \frac{1}{N_{sample}-1} \sum_{j=1}^{N_{sample}} (v_{j,i}^e - \overline{v_{i,j}^e})(v_{i,j}^e - \overline{v_{i,j}^e})^T$. Then, again omitting the indexes of the sub-ensembles,

$$\begin{aligned}
var(\hat{X}(t_i) | \mathcal{Y}_i) &\approx \frac{1}{N_{sample}-1} \sum_{j=1}^{N_{sample}} \{x_j^{as}(t_i) - \overline{x_j^{as}(t_i)}\} \{x_j^{as}(t_i) - \overline{x_j^{as}(t_i)}\}^T = \\
&\frac{1}{N_{sample}-1} \sum_{j=1}^{N_{sample}} \{x_j^f(t_i) - \overline{x_j^f(t_i)}\} \{x_j^f(t_i) - \overline{x_j^f(t_i)}\}^T + \\
&\frac{1}{N_{sample}-1} \sum_{j=1}^{N_{sample}} K_i^e (v_{i,j}^e - \overline{v_{i,j}^e})(v_{i,j}^e - \overline{v_{i,j}^e})^T (K_i^e)^T + \\
&\frac{1}{N_{sample}-1} \sum_{j=1}^{N_{sample}} K_i^e (x_j^f(t_i) - \overline{x_j^f(t_i)})(y_{i,j} - \overline{y_{i,j}} - Z(x_j^f(t_i)) - \overline{Z(x^f(t_i))})^T + \\
&\frac{1}{N_{sample}-1} \sum_{j=1}^{N_{sample}} (y_{i,j} - \overline{y_{i,j}} - Z(x_j^f(t_i)) - \overline{Z(x^f(t_i))})(x_j^f(t_i) - \overline{x_j^f(t_i)})^T (K_i^e)^T \\
&= B_i^{f,e} + K_i^e F_i^e (K_i^e)^T - K_i^e (B_i^{f,e} Z^T)^T - B_i^{f,e} Z^T (K_i^e)^T
\end{aligned}$$

If we denote $B_i^e = B_i^{f,e} - B_i^{f,e} Z^T (F_i^{e,*})^{-1} Z B_i^{f,e}$, the usual form of posterior variance in Kalman filtering, we will have.

(131)

$$\begin{aligned}
var(\hat{X}(t_i) | \mathcal{Y}_i) &\approx B_i^{f,e} + K_i^e F_i^e (K_i^e)^T - K_i^e (B_i^{f,e} Z^T)^T - B_i^{f,e} Z^T (K_i^e)^T \\
&= B_i^e + K_i^e (F_i^e - F_i^{e,*}) (K_i^e)^T \\
&\approx B_i^e \rightarrow var(\hat{X}(t_i) | \mathcal{Y}_{i-1}) - cov(\hat{X}(t_i), v_i | \mathcal{Y}_{i-1}) (var(v_i))^{-1} (cov(\hat{X}(t_i), v_i | \mathcal{Y}_{i-1}))^T
\end{aligned}$$

This particular estimation of the innovation variance $F_i^{e,*}$, different from the sample estimate F_i^e , is used in the Kalman gain calculation to ensure invertibility. It is interesting that due to erroneous observations, what corresponds to a full rank matrix H , this inversion is always possible. Besides that, the use of $F_i^{e,*}$ makes the estimation of the Kalman gain more stable.

Formally, we can overcome the problem with the innovation covariance estimate $F_i^{e,*}$ being not equal to the sample estimate of the innovation covariance defining the analysed state (130) in a slightly different way. We insert y_i as the estimate of the mean of ensemble of observations $\{y(i, j), j = 1, \dots, N_{sample}\}$ instead of the $\overline{y_{i,j}}$. By this we assure as that we know the distribution of the observation errors $y_{i,j} \sim \mathcal{N}(y_i, H)$ and do not need estimate its parameter from the ensemble.

When the double ensemble Kalman filter is applied, the Kalman gain matrix $K_{i,\bar{k}}^e$, calculated from the sub-ensemble \bar{k} for the construction of the sub-ensemble k of the analysed

states, is sub-optimal for the sub-ensemble k . This means that it gives larger analysis errors for the sub-ensemble k (Lorenz, 2003), which can be calculated, if one knows a true covariance. In the similar way as when (131) was obtained, one can prove that sample estimate of the analysis error covariance matrix for the sub-ensemble k obeys the relationship

$$(132) \quad \frac{1}{N_{sample}} \sum_{j=1}^{N_{sample}} \{x_j^{as}(t_i) - \overline{x_j^{as}}(t_i)\} \{x_j^{as}(t_i) - \overline{x_j^{as}}(t_i)\}^T = \\ = B_{i,k}^e + (K_{i,k}^e - K_{i,\bar{k}}^e) F_i^e (K_{i,k}^e - K_{i,\bar{k}}^e)^T$$

disregarding the difference between the values of F_i^e and $F_i^{e,*}$.

The great advantage of the ensemble Kalman filter is that there is no need for linearization of the model dynamics, and that the method is free from any assumptions on the pdf. However, the results of data assimilation, performed in such a way, must be taken with care. One reason is that the analysed state, estimated through the analysed ensemble mean, can be optimal only in the sense of mean square error. Even this is valid only in the case of linear observation operators. If the observation operators are not linear, the conditional mean, given the recently observed data, cannot be estimated by constructing the best linear predictor on the given innovation history. Usually, the influence of observations on the analysed state will be given too small weights in such a case. Even more complicated problems arise, if the ensemble size of the forecast states is smaller than the dimension of the forecast error covariance matrix. The covariance matrix, estimated from such an ensemble, is singular. Taking the huge dimensionality of the model state variable into account, the ensemble size will always be much smaller than the dimensionality of the state variable. There exists a number of different proposals to handle the consequences of such a singularity.

4.5. The estimate of the posterior predictive mean evolution based on importance sampling. Among the four extensions of the standard Kalman that we have discussed above, three of them, the extended Kalman filter, the time-window smoother and the ensemble Kalman filter, can be used in both a deterministic and a probabilistic manner. To obtain a probabilistic representation of an unobserved model variable we can either try to estimate its posterior distribution or try to sample from the posterior distribution. In the case of the extended Kalman filter, the posterior predictive distribution is approximated by a Gaussian one. If either the dynamics of the model are strongly non-linear and/or the observation operator is non-linear, the Gaussian approximation of the posterior distribution is good only in the vicinity of the mode. As we already have mentioned, under this condition, the sample constructed by the ensemble Kalman filter tends (as the sample size increases) to be sampled from a distribution close to a Gaussian one, and the inference about the unobservable model state based on such a sample can be misleading in general. The time window smoother gives one more possibility to estimate the posterior predictive distribution, using the importance sampling technique. With the importance sampling approach, we do not obtain a sample from the distribution of interest, but we rather correct the inference from the available sample in a particular way.

Some results of the importance sampling application are presented in Figure 25 for the data simulated by the non-linear observation operator nlZ_2 . The "low" precision data are used in the experiments. The left diagrams in Figure 25 show the "true" meteorological fields (the solid line) at the end of the "long" assimilation time window (40 observation

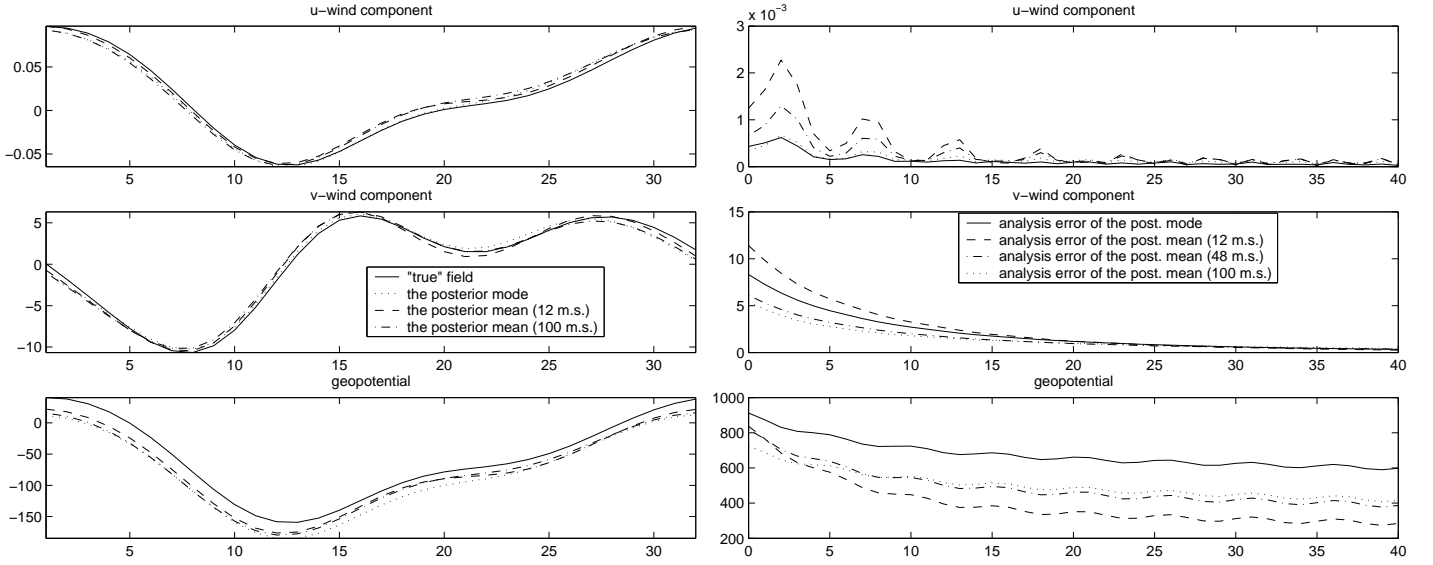


FIGURE 25. The left diagrams show the dynamically propagated posterior mode up to the end of the "long" assimilation time window, equal to 40 observation windows (dotted line), the posterior mean estimated at the end of the "long" assimilation time window from importance sampling size of $N_{sample} = 12$ (the dotted line) and the posterior mean estimated at the end of the "long" assimilation time window from importance sampling size of $N_{sample} = 100$ (the dash-dotted line). The solid line corresponds to the "true" model state at the end of the "long" assimilation time window. The right diagrams show the spatial average squared error \tilde{SE} of the posterior mode (the solid line) and the spatial average squared error of the posterior mean estimated from importance sampling size of $N_{sample} = 12$ ($\tilde{SE}^{i.s.,12}$, dash line), size of $N_{sample} = 48$ ($\tilde{SE}^{i.s.,48}$, dash-dotted line), size of $N_{sample} = 100$ ($\tilde{SE}^{i.s.,100}$, dotted line). The results are shown for the u -wind component, for the v -wind component and for the geopotential. The experiment are made with the "low" precision observations, simulated by nlZ_2

windows), the posterior mode dynamically propagated up to the same time moment (the dotted line) and the posterior predictive mean at the same time moment estimated from a sample of size $N_{sample} = 12$ (the dashed line) and from a size $N_{sample} = 100$ (the dashed-dotted line). The right diagrams show the time development of the spatial average squared errors of the different estimates. We can see that both the posterior mode, dynamically propagated up to the end of the assimilation window, and the posterior predictive mean, obtained at the same moments, come close to the "true" model state variable. A posterior mode and a posterior mean are optimal in different sense and both have certain disadvantages. The posterior mode maximizes the posterior distribution in the beginning of the time window and can significantly deviate from the posterior predictive mode at the end of the time window. This is not a serious problem in the one-dimensional shallow water model, because the dynamical propagation is very close to the linear one. In the experiments we discuss here the influence of the observations on the analysed state is strong and the posterior pdf is sharp enough for the posterior mode to come close to the "true" state. Groups of 9 observations were introduced 40 times during the experiment. The posterior predictive mean is strongly influenced by the existence of

a heavy tail. The posterior predictive mean can be significantly displaced away from the posterior predictive mode toward the heavy tail in such a case and it will therefore be inefficient as a point estimate of the "true" model state. A careful investigation of the form of the posterior predictive pdf is needed to give any preference to one type of estimator over another one, and this is impossible to perform in practice. When the assimilated data are simulated with the non-linear observation operator nlZ_2 , the posterior (as well as the posterior predictive) pdf deviates from a Gaussian one, but the posterior mean is a better estimate than the posterior mode with respect to spatial average squared error \tilde{SE} , in particular for the geopotential. This result is strongly dependent on the type of observation operator. Using the other observation operators, the results presented in Figure 25 would look different. In a majority of cases, the dynamical propagation of the posterior mode estimates the "true" model state better than the posterior predictive mean.

The estimate of the posterior mean using importance sampling is sensitive to the sample size. The sample size must be large enough to sample from the essential particularities of the posterior pdf. When new essential particularities are discovered, they can strongly influence the estimate of the posterior mean and the whole probabilistic inference based on the importance sampling.

For the derivation of the time-window smoother, we have used the analytical expression for the posterior distribution up to the normalising constant

$$p(\hat{X}(t_0) | \mathcal{Y}) \propto p(\hat{X}(t_0))p(y_1, \dots, y_{N_{ass}} | \hat{X}(t_0))$$

and we have obtained its mode $\hat{\alpha}_0$ and the curvature around the mode V_0 . Here we denote by $\mathcal{Y} = \{y_1, \dots, y_{N_{ass}}\}$ the whole sequence of observations available during the period of the assimilation time window $(t_0, t_{N_{ass}})$. The notation $p(\cdot)$ means an arbitrary probability density. The prior distribution for the assimilation window $p(\hat{X}(t_0))$ is based both on the information content of the already assimilated observations, available up to the time t_0 , and on analytically deduced and derived constraints.

As we already have discussed, the time-window smoother method allows us to find out only a mode of the posterior distribution $p(\hat{X}(t_0) | \mathcal{Y})$. For the model studied here the posterior pdf of a non-linear transform $\zeta(\hat{X}(t_0))$ (including the dynamical propagator) of the model state variable cannot be expressed analytically. Therefore we cannot use the time-window smoother to estimate the mode of the pdf for $\zeta(\hat{X}(t_0))$.

If we want to obtain an inference based on a sample, two requirements must be satisfied. First of all, the sample must be random and the sample space of the chosen data generating mechanism must include the sample space of the distribution of interest. Any random data generating mechanism with an infinite support, which is easy to sample from, could be used for this purpose. But in order to make the procedure efficient, it is better to choose a random data generating mechanism which has the main amount of mass around the mode of the distribution of interest. For example, a Gaussian distribution $g(\hat{X}(t_0) | \mathcal{Y}) = N(\hat{\alpha}_0, V_0)$ can be used as a sampling distribution.

The second requirement is that the mass of the sample must be distributed according to the distribution of interest. This requirement cannot be satisfied implicitly. However, if we can construct an estimate in form of a weighted sum of the sample members, we can choose weights such that the inference would (approximately) look like being constructed on the sample space of the distribution of interest. If we want to estimate the posterior mean

$$(133) \quad E(\zeta(\hat{X}(t_0)) | \mathcal{Y}) = \int \zeta(\hat{X}(t_0))p(\hat{X}(t_0) | \mathcal{Y})d\hat{X}(t_0)$$

of an arbitrary function $\zeta(\hat{X}(t_0))$ of $\hat{X}(t_0)$, given the whole sequence of observations \mathcal{Y} , then the estimation of the quantity $E(\zeta(\hat{X}(t_0)) | \mathcal{Y})$ can be obtained from a sample from a Gaussian distribution $g(\hat{X}(t_0) | \mathcal{Y})$, correcting the weights of the members in the estimate. In the standard sample estimate of the mean, all the members of the sample have the same weight equal to $\frac{1}{N_{sample}}$, with N_{sample} denoting sample size. If a member of the sample from a Gaussian distribution should be representative for the sample space of the distribution of interest corresponding to its heavy tail part, it must have very large weight. If we would sample from the distribution of interest, a large number of members would be placed in the sample space corresponding to the heavy tail. Due to the same reason, the weights of the large amount of sample members located around the mode of the Gaussian distribution must be decreased.

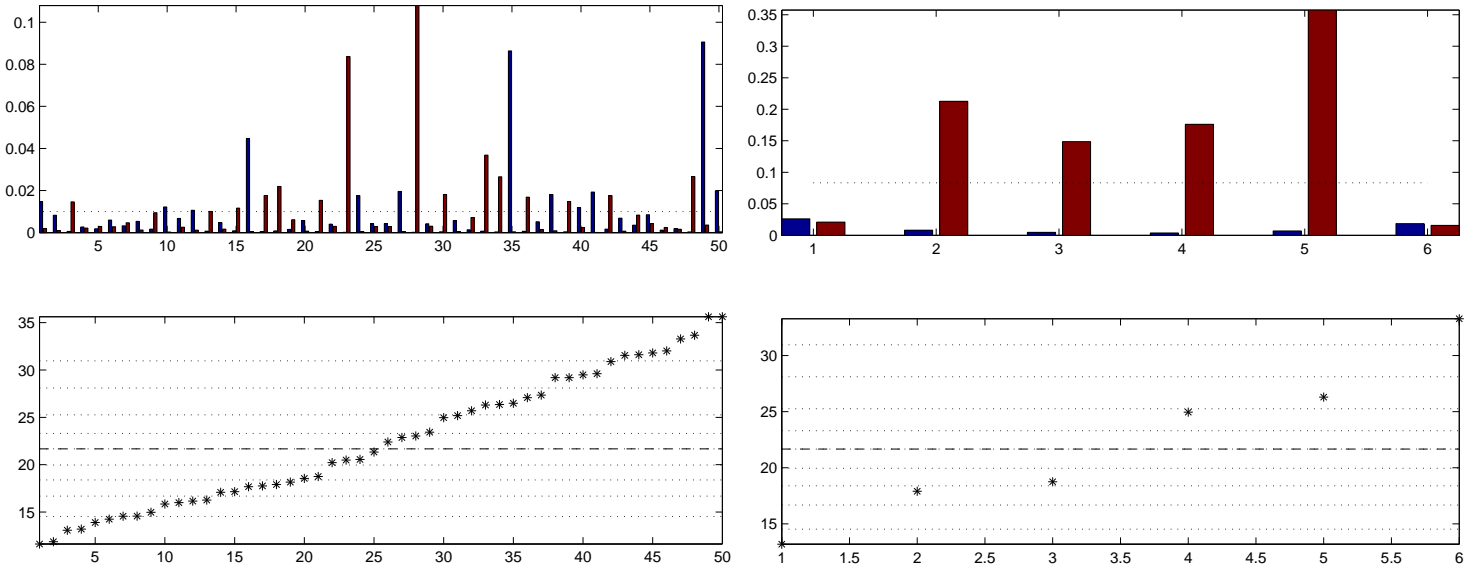


FIGURE 26. The weights of the ordered importance sample using different sample size: $N_{sample} = 100$ sample members (the left diagram), $N_{sample} = 12$ sample members (the right diagram). In the upper diagrams the weights of the realisations of the grouped antithetic variables \hat{x}^R and $\tilde{x}^R = -\hat{x}^R$, which have the same value $c = (\hat{x}^R)^T \hat{x}^R$, are shown. The dotted line indicates the "Gaussian" weight $w_G = \frac{1}{N_{sample}}$. In the lower diagrams the observed values for c for the particular realisation of the sample are shown. The dotted lines show the 0.1 : 0.1 : 0.9 quantiles of $\chi^2(p)$, $n_V = n_B = p = 22$, the dashed line denotes the median - 0.5 quantile. Experiments are made with the "low" precision data simulated by nlZ_2 .

The importance sampling weights, obtained in the experiment with the results shown in Figure 25, are presented in Figure 26. We would like to stress that in all our the experiments using importance sampling, the same set of realisations \hat{x}_i^0 of a normally distributed random p -dimensional vector $\mathcal{X}^0 \sim \mathcal{N}(0, I_p)$ is used (here $p = 22$ is the chosen number of principal components used to represent V_0) and transformed to a sample of the Gaussian approximation of the posterior pdf. The ordered values of a $\chi^2(p)$ variable $c = (\hat{\mathcal{X}}^0)^T \mathcal{X}^0$ are shown in the lower diagrams of Figure 26. Thus, a realisation which has a small value of c , happens to be drawn from the vicinity of the pdf mode, a realisation

which has a large value of the c comes from the tails of the Gaussian approximation. Every value of c corresponds to two dependent random draws, because for every $\hat{\mathcal{X}}^0$ we take $\tilde{\mathcal{X}}^0 = -\hat{\mathcal{X}}^0$. For every c_i value correspond two weights of the symmetric Gaussian draw and these weights are presented in the upper diagrams of Figure 26. We will discuss below the construction of the dependent sample in more details. The weights of the sampling allow us to look a little inside to the way the posterior pdf deviates from the Gaussian approximation. From the right diagram of Figure 26, which shows the importance weights of a small sample size (only 3 independent draws), the main pattern of the deviation can be seen. First of all, the posterior pdf is strongly asymmetric what can be seen from very different weights of most of the symmetric draws. The main disagreement in the form of the densities lies not in the tails, but more in the central parts as we can see from the big weights of the realisations having c values around the median of the $\chi^2(p)$, and the Gaussian approximation is good just in a vicinity of the posterior mode.

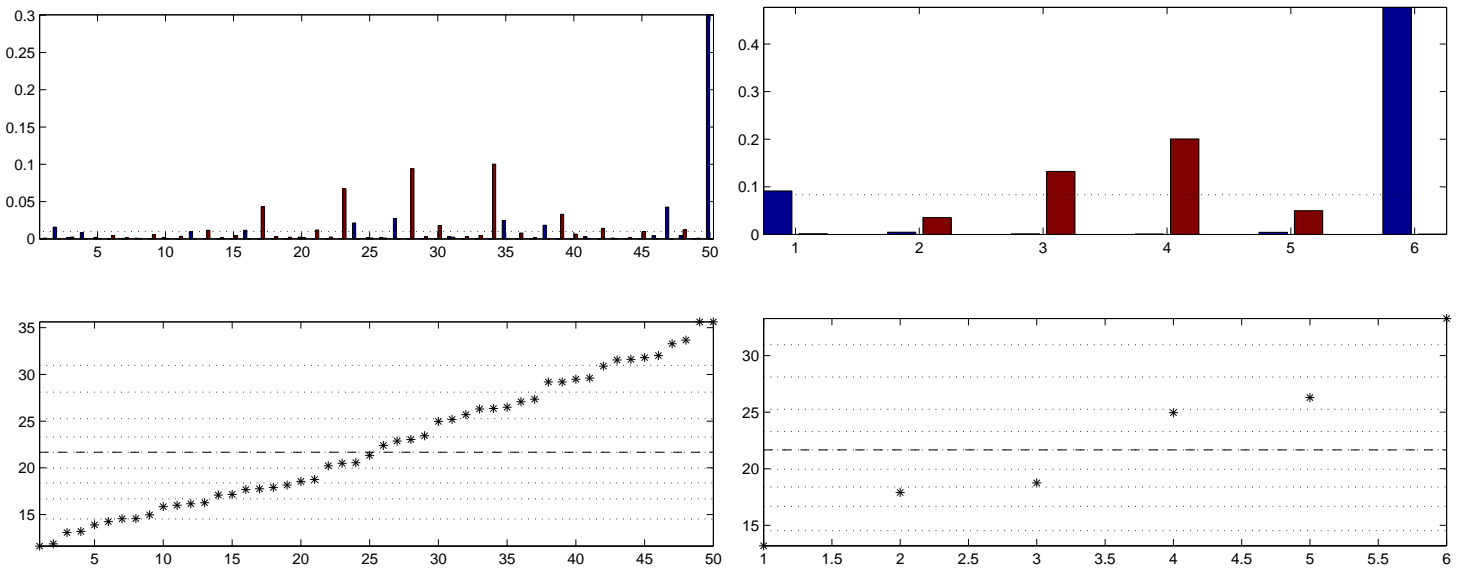


FIGURE 27. The weights of the ordered importance sample using different sample size: $N_{sample} = 100$ sample members (the left diagram), $N_{sample} = 12$ sample members (the right diagram). In the upper diagrams the weights of the realisations of the grouped antithetic variables \hat{x}^R and $\tilde{x}^R = -\hat{x}^R$, which have the same value $c = (\hat{x}^R)^T \hat{x}^R$, are shown. The dotted line indicates the "Gaussian weight" $w_G = \frac{1}{N_{sample}}$. In the lower diagrams the observed values for c for the particular realisation of the sample are shown. The dotted lines show the 0.1 : 0.1 : 0.9 quantiles of $\chi^2(p)$, $n_V = n_B = p = 22$, the dashed line denotes the median - 0.5 quantile. Experiments are made with the "low" precision data simulated by nlZ_3 .

In Figure 27 we present the weights of importance sampling obtained by assimilating data of the same "low" precision but related to the model state with another observation operator nlZ_3 . The weights of the importance sampling are different in this case. For example, even weights of the realisations drawn from a close vicinity of the mode are strongly asymmetric, and the posterior distribution has a much heavier tail than the Gaussian one. However, the patterns of weights using these two non-linear observation operators have some general similarities, as would be expected, because the observation operators differ only in the part related to the direct observations of geopotential.

In fact,

(134)

$$\begin{aligned} E(\zeta(\hat{X}(t_0)) | \mathcal{Y}) &= \int \zeta(\hat{X}(t_0)) \frac{p(\hat{X}(t_0) | \mathcal{Y})}{g(\hat{X}(t_0) | \mathcal{Y})} g(\hat{X}(t_0) | \mathcal{Y}) d\hat{X}(t_0) = \\ &= \int \zeta(\hat{X}(t_0)) \frac{1}{p(\mathcal{Y})} \frac{\mathcal{N}(a_0, B_0) \prod_{j=1}^{N_{ass}} \mathcal{N}(Z(\hat{X}(t_j)), H)}{\mathcal{N}(\hat{\alpha}_0, V_0)} g(\hat{X}(t_0) | \mathcal{Y}) d\hat{X}(t_0) \end{aligned}$$

Here the notation Z means any observation operator (both linear and non-linear ones) Let us denote

$$(135) \quad w(\hat{X}(t_0), \mathcal{Y}) = \frac{\mathcal{N}(a_0, B_0) \prod_{j=1}^{N_{ass}} \mathcal{N}(Z(\hat{X}(t_j)), H)}{\mathcal{N}(\hat{\alpha}_0, V_0)},$$

then the sample estimate of the posterior mean is equal to

$$(136) \quad \overline{\zeta(\hat{X}(t_0)) | \mathcal{Y}} = \sum_{j=1}^{N_{sample}} \zeta(\hat{x}^j(t_0)) w_j$$

where the weights are given by

$$(137) \quad w_j = \frac{w(\hat{x}^j(t_0), \mathcal{Y})}{\sum_{j=1}^{N_{sample}} w(\hat{x}^j(t_0), \mathcal{Y})}$$

Here $\hat{x}^j(t_0), j = 1, \dots, N_{sample}$ is a sample with N_{sample} members from $g(\hat{X}(t_0) | \mathcal{Y}) = \mathcal{N}(\hat{\alpha}_0, V_0)$.

To justify the expression for weights (137), one can notice that

$$\int w(\hat{X}(t_0), \mathcal{Y}) g(\hat{X}(t_0) | \mathcal{Y}) d\hat{X}(t_0) = \int \frac{p(\hat{X}(t_0), \mathcal{Y})}{g(\hat{X}(t_0) | \mathcal{Y})} g(\hat{X}(t_0) | \mathcal{Y}) d\hat{X}(t_0) = p(\mathcal{Y})$$

On the other hand,

$$\int w(\hat{X}(t_0), \mathcal{Y}) g(\hat{X}(t_0) | \mathcal{Y}) d\hat{X}(t_0) \approx \sum_{j=1}^{N_{sample}} w(\hat{x}^j(t_0), \mathcal{Y}).$$

Then, obviously, $p(\mathcal{Y}) \approx \sum_{j=1}^{N_{sample}} w(\hat{x}^j(t_0), \mathcal{Y})$. Inserting this approximation of the marginal observation density $p(\mathcal{Y})$ into eqn.(134), we get the importance sampling estimation (136) of the posterior mean $E(\zeta(\hat{X}(t_0)) | \mathcal{Y})$.

Under a perfect model assumption, which we use in our model, the whole uncertainty about the model state is concentrated in the beginning of the assimilation time window t_0 . The formula (134) for a posterior mean estimate can be used to find out, for example, the time evolution of the posterior predictive mean $E(\hat{X}(t) | \mathcal{Y}), t > t_0$, if we make a transformation $\zeta(\hat{X}(t_0))$ equal to the model dynamics governing the model evolution over period (t_0, t) . Certainly, we can obtain an estimate of the posterior predictive mean of any linear or non-linear transformation of $\hat{X}(t)$ as well. Usually, the probabilistic evolution of the huge dimensional model state variable itself is not of main interest. The most useful is to have a probabilistic representation of the evolution of a smaller

TABLE 1. The kinetic energy, valid at the end of the "long" time window at grid-point x_{16} , estimated by the double ensemble Kalman filter with a sample size of $N_{sample} = 100$ ($eKF(100 m. s.)$), by the importance sampling of size $N_{sample} = 12$ with the "long" assimilation time window smoother ($tws(12 m. s.)$) and by the importance sampling of size $N_{sample} = 100$ with the "long" assimilation time window smoother ($tws(100 m. s.)$). The results are shown for the observation simulated with the non-linear observation operator nlZ_2 and for the observations simulated with the non-linear observation operator nlZ_3 (see the first column). The estimates of 0.1, 0.5 and 0.9 quantiles of the kinetic energy ($q_{0.1}^{f_\zeta}$, $q_{0.5}^{f_\zeta}$, $q_{0.9}^{f_\zeta}$), the posterior mean of the kinetic energy ($E(f_\zeta)$), the estimate of the kinetic energy obtained from the time propagated mode, when the time-window smoother is used, ($f_\zeta(\hat{\alpha}_t)$) and the "true" value of the kinetic energy ($f_\zeta(\bar{X}(t))$) are presented.

	$q_{0.1}^{f_\zeta}$	$q_{0.5}^{f_\zeta}$	$q_{0.9}^{f_\zeta}$	$E(f_\zeta)$	$f_\zeta(\alpha_t)$	$f_\zeta(\bar{X}_t)$
$nlZ_2 : eKF(100 m. s.)$	1624.62	1632.45	1642.33	1633.21		1627.85
$nlZ_2 : tws(12 m. i.s)$	1626.52	1626.72	1635.62	1630.16	1629.42	
$nlZ_2 : tws(100 m. i.s.)$	1620.22	1633.09	1646.43	1632.44		
$nlZ_3 : eKF(100 m. s.)$	1624.66	1632.49	1642.50	1633.27		
$nlZ_3 : tws(12 m. i.s)$	1627.78	1633.84	1633.84	1633.78	1629.34	
$nlZ_3 : tws(100 m. i.s.)$	1622.14	1634.74	1649.89	1634.69		

dimensional but easily interpretable function of the model state variable, for example, the time development of the kinetic energy at a particular grid-point x_j , which is proportional to the following expression through the model state variable $f_\zeta(t) = (\bar{u} + u_j(t))^2 + (v_j(t))^2 = (\bar{u} + \sum_{k=-M}^M \hat{u}_k e^{ikx_j})^2 + (\sum_{k=-M}^M \hat{v}_k e^{ikx_j})^2$. Examples of such a probabilistic interpretation of the kinetic energy by different techniques are given in Table 1. The kinetic energy was estimated at the end of the "long" assimilation time window (40 observation windows) and valid at grid-point x_{16} .

It is interesting to notice that under the ensemble Kalman filter approach the probabilistic inference about the functional is nearly the same using the two different non-linear observation operators. The reason for this is the large amount of assimilated data. Certainly, the underlying "true" process is the same one, and if the data assimilation procedure works, the posterior mode estimate will come close to the maximum likelihood estimate for any observation operator. Besides that, both the likelihood and the posterior pdf are quite sharp in the vicinity of their modes, even if the strictly unique maximum likelihood estimate of the "true" model state is impossible within the framework of the one dimensional shallow water model. It is just the sharpness of the pdf in the vicinity of the mode that is expressed in the Gaussian approximation. Table 2 shows the largest eigenvalues of the B_0 and \hat{V}_0 matrixes obtained for the two non-linear observation operators.

The experiments which are shown here are perfectly behaving "toy" examples, since a very large amount of data comparable to the dimensionality of the model state variable can be assimilated, and the posterior mode gives an efficient estimate of the "true" model state. As we have seen, using a less computationally expensive and a practically feasible configuration of the time window smoother with the same forecast error covariance matrix at the beginning of each "short" time window, the posterior mode gives a very inefficient estimate of the "true" process. Therefore, the probabilistic inference about a smaller

TABLE 2. The 11 largest eigenvalues of the initial forecast error covariance matrix B_0 (Λ_{22}^B), of the posterior pdf "curvature" matrix around the mode \hat{V}_0 using the "high" precision observations simulated by nlZ_3 ($\Lambda_{22}^V : 3$, the second row), using the "low" precision observations simulated by nlZ_3 ($\Lambda_{22}^V : 3$, the third row), using the "high" precision observations simulated by nlZ_2 ($\Lambda_{22}^V : 2$, the fourth row), using the "low" precision observations simulated by nlZ_2 ($\Lambda_{22}^V : 2$, the fifth row)

	1	2	3	4	5	6	7	8	9	10	11
Λ_{22}^B	7815.16	663.17	663.11	167.42	167.37	35.11	35.11	7.00	7.00	1.82	1.82
$\Lambda_{22}^V : 3$	23.27	6.61	3.50	2.91	2.63	1.88	1.40	1.35	1.23	0.97	0.87
$\Lambda_{22}^V : 3$	177.97	46.91	24.83	17.70	13.40	10.69	8.84	4.81	4.60	1.65	1.63
$\Lambda_{22}^V : 2$	21.57	6.46	3.44	2.88	2.60	1.87	1.39	1.35	1.23	0.96	0.87
$\Lambda_{22}^V : 2$	202.53	48.15	25.61	17.89	13.52	10.83	8.90	4.81	4.60	1.65	1.63

dimensional transform of the model state (a model subspace) can be very useful. As we already have mentioned, the sample of analysed states created by the ensemble Kalman filter behaves (as the sample size increases and the dynamics are weakly non-linear) almost as being sampled from the Gaussian approximation of the pdf, and therefore it can not be used for the probabilistic inference about the model state variable. The posterior q -quantile q^{f_ζ} for the one dimensional functional f_ζ satisfies the following formula

$$(138) \quad \int \mathcal{I}_{\{f_\zeta(\hat{X}(t_0)) \leq q^{f_\zeta}\}} \frac{p(\hat{X}(t_0) | \mathcal{Y})}{g(\hat{X}(t_0) | \mathcal{Y})} g(\hat{X}(t_0) | \mathcal{Y}) d\hat{X}(t_0) = q$$

The posterior q -quantile is approximated by the m -th order statistics of a f_ζ transform $f_\zeta(\hat{x}^{[m]}(t_0))$, where the number m is chosen such that

$$(139) \quad \sum_{j=1}^m w_{[j]} \approx q.$$

The values w_j (137) are ordered in accordance with the order statistics of the f_ζ transform. In the equations above (139), "the j th sample member" $\hat{x}^j(t_0)$ denotes the members of the dependent sample. The construction of the dependent sample is discussed below.

Figure 28 shows the estimation of the quantiles of the functional f_ζ (kinetic energy) using the double ensemble Kalman filter with sample of size $N_{sample} = 100$ (the solid line) and the importance sampling from the "long" assimilation time window smoother with different sample sizes: size of $N_{sample} = 12$ (the dotted line), size of $N_{sample} = 48$ (the dash-dotted line), size of $N_{sample} = 100$ (the dashed line). On the horizontal axis, the symbol x denotes the position of the "true" value of the functional ($f_\zeta(\hat{X}(t))$ in Table 1) and the symbol o denotes the position of the estimation of the kinetic energy from the time propagated posterior mode ($f_\zeta(\hat{\alpha}_t)$ in Table 1). The left diagram in Figure 28 shows the result when the observations were simulated by the non-linear observation operator nlZ_3 and the right diagram shows the result when the observations were simulated by nlZ_2 . In order to estimate quantiles by the importance sampling we need to find estimate of a large dimensional integral, and the size of the sample used for the estimation of the integral is very essential for the quality of the estimate. The small size importance sampling gives very similar results for both non-linear observation operators. The estimation of the pdf seems to be strongly under-dispersed, and is in fact misleading. Some sample members can have very high absolute weight in the estimate. When the sample size increases,

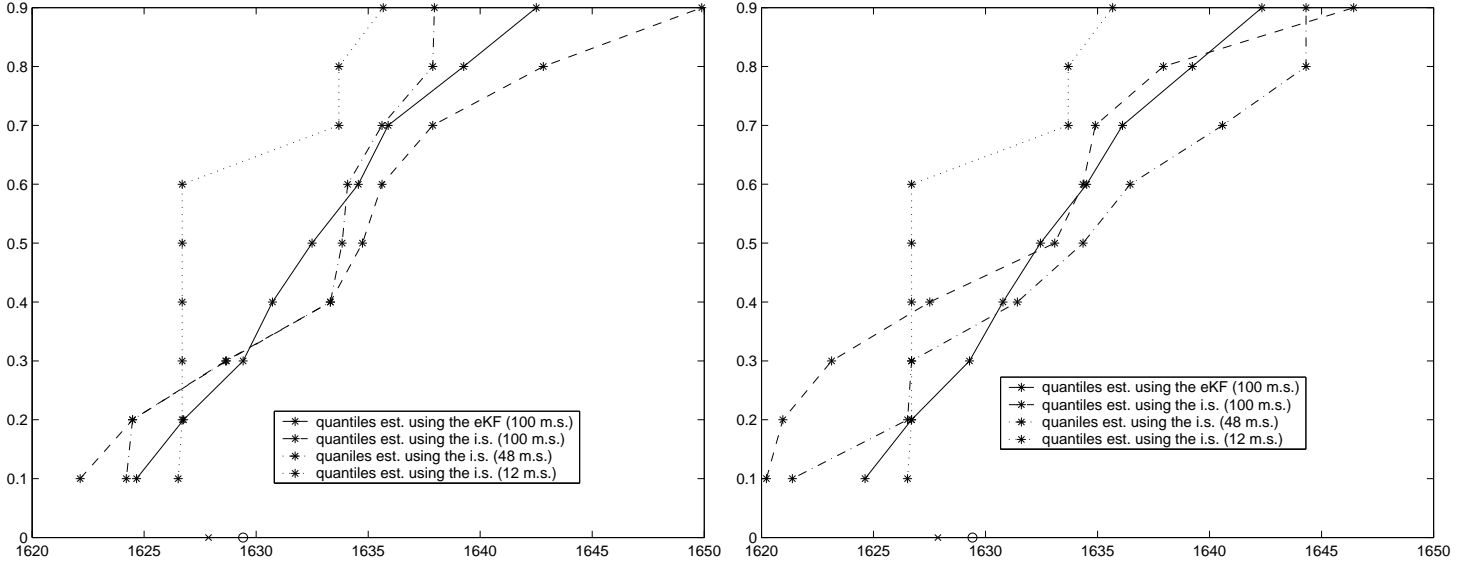


FIGURE 28. The estimation of quantiles of the functional f_ζ (kinetic energy) using the double ensemble Kalman filter with sample of size $N_{sample} = 100$ (the solid line) and the importance sampling from the "long" assimilation time window smoother with different sample sizes: size of $N_{sample} = 12$ (the dotted line), size of $N_{sample} = 48$ (the dash-dotted line), size of $N_{sample} = 100$ (the dashed line). On the horizontal axes symbol x denotes position of the "true" value of functional ($f_\zeta(\hat{X}(t))$, in Table 1) and symbol o denotes position of the estimation of the kinetic energy from the time propagated posterior mode ($f_\zeta(\hat{\alpha}_t)$, in Table 1). The left diagram in Figure 28 shows the result when the observations were simulated by the non-linear observation operator nlZ_3 and the right diagram shows the result when the observations were simulated by nlZ_2 .

the dominance of one particular sample member decreases, and this gives much better estimates of the quantiles.

The larger size importance sampling gives a real possibility to detect the particularities, which should appear due to the specific form of the posterior pdf influenced by the observation operator. The importance sampling estimate of the quantiles of the functional f_ζ with a $N_{sample} = 100$ members sample indicates bimodality of the pdf of the functional, which is not reflected at all by estimating quantiles using the ensemble Kalman filter. The pdf of the functional corresponding to observations simulated by nlZ_3 (the left diagram) seems to have a heavier tail than it could be thought if the inference would be made on the sample constructed from the Gaussian approximation of the posterior density of the model state variable. The pdf of the functional, in the case of the observation operator nlZ_2 , has the largest disagreements in the middle part around the mode with the inference made from the Gaussian approximation. In both cases, due to indication of a bimodality, the mean as a point estimate of the functional can be irrelevant, and it is better to use the transform of the posterior mode propagated in time as a point estimate.

To apply importance sampling in order to estimate a posterior mean, the expression

$$(140) \quad w(x, \mathcal{Y}) = c * e^{(x-a_0)^T B_0^{-1} (x-a_0) + \{\sum_{i=1}^{N_{ass}} (y_i - \mathcal{F}^t(x))^T H^{-1} (y_i - Z(\mathcal{F}^t(x)))\} - (x-\hat{\alpha}_0)^T V_0^{-1} (x-\hat{\alpha}_0)}$$

must be calculated explicitly up to the constant c . When the weights w_j are calculated, the constant c will cancel. We have already discussed the reasons due to which both the initial forecast error covariance matrix B_0 and the covariance matrix V_0 for the sampling

distribution are singular. The exact inverse of the matrices is impossible. We will instead apply approximate inverse matrices by decomposition into principal components. Both matrices are complex in our model. But in both cases when we perform the approximate inversion and when we sample from $g(\hat{X}(t_0) | \mathcal{Y})$ we will work with the covariance matrices B_0^R and V_0^R transformed into real value space. The model state variable $\hat{X}(t)$ has the following structure

$$\hat{X}(t) = \left[\cdots, \hat{u}_{-k}, \cdots, \hat{u}_0, \cdots, \hat{u}_k, \cdots, \hat{v}_{-k}, \cdots, \hat{v}_0, \cdots, \hat{v}_k, \cdots, \hat{\phi}_{-k}, \cdots, \hat{\phi}_0, \cdots, \hat{\phi}_k, \cdots \right]^T$$

where $k, k = 1, \dots, M$ denotes wave number. For all spectral coefficients $\hat{a}_{-k} = (\hat{a}_k)^*$. The $*$ symbol denotes complex conjugate (for any complex value $\hat{a} = \hat{a}^{Re} + i\hat{a}^{Im}$, the complex conjugate $\hat{a}^* = \hat{a}^{Re} - i\hat{a}^{Im}$). As we have already mentioned, such a particular structure of the model state variable is assumed because \hat{X}_t consists of spectral coefficients of the Fourier transform of real-valued fields.

We transform the model state variable by an orthogonal matrix $\hat{X}^R(t) = Tr \hat{X}(t)$ to the real valued vector $\hat{X}^R(t)$, with the following structure

$$\hat{X}^R(t) = \left[\hat{u}_0, \cdots, \hat{u}_k^{Re}, \cdots, \hat{u}_k^{Im}, \cdots, \hat{v}_0, \cdots, \hat{v}_k^{Re}, \cdots, \hat{v}_k^{Im}, \cdots, \hat{\phi}_0, \cdots, \hat{\phi}_k^{Re}, \cdots, \hat{\phi}_k^{Im}, \cdots \right]^T$$

The orthogonal square matrix $Tr_{3*(2M+1) \times 3(2M+1)}$ has a square-diagonal structure

$$Tr = \begin{pmatrix} Dr & \mathcal{O} & \mathcal{O} \\ \mathcal{O} & Dr & \mathcal{O} \\ \mathcal{O} & \mathcal{O} & Dr \end{pmatrix}$$

with the $(2M + 1) \times (2M + 1)$ -dimensional orthogonal matrix Dr being equal

$$(141) \quad \begin{pmatrix} 0 & \dots & 0 & 0 & 1 & 0 & 0 & \dots & 0 \\ 0 & \dots & 0 & 0.5 & 0 & 0.5 & 0 & \dots & 0 \\ 0 & \dots & 0.5 & 0 & 0 & 0 & 0.5 & \dots & 0 \\ \dots & \dots \\ 0.5 & \dots & 0 & 0 & 0 & 0 & 0 & \dots & 0.5 \\ 0 & \dots & 0 & 0.5i & 0 & -0.5i & 0 & \dots & 0 \\ 0 & \dots & 0.5i & 0 & 0 & 0 & -0.5i & \dots & 0 \\ \dots & \dots \\ 0.5i & \dots & 0 & 0 & 0 & 0 & 0 & \dots & -0.5i \end{pmatrix}$$

Thus the real valued covariance matrices defined above are $B_0^R = Cov(\hat{X}^R(t_0)) = Tr B_0 Tr^T$ and $V_0^R = Cov(\hat{X}^R(t_0) | \mathcal{Y}) = Tr V_0 Tr^T$.

In fact, for any two spectral transforms $\{\hat{a}_k, -M \leq k \leq M\}$ and $\{\hat{b}_l, -M \leq l \leq M\}$ of real valued fields $\{a_i, 1 \leq i \leq N\}$, $\{b_i, 1 \leq i \leq N\}$ the following relationships between elements of the covariance matrices $B = cov(\hat{a}, \hat{b})$ and $B^R = Tr B Tr^T$ are valid

$$\begin{aligned}
B^R(\hat{a}_0, \hat{b}_0) &= B^R(\hat{b}_0, \hat{a}_0) = B(\hat{a}_0, \hat{b}_0) \\
B^R(\hat{a}_0, \hat{b}_k^{Re}) &= B^R(\hat{b}_0^{Re}, \hat{a}_0) = Re(B(\hat{a}_0, \hat{b}_k)) \\
B^R(\hat{a}_0, \hat{b}_k^{Im}) &= B^R(\hat{b}_0^{Im}, \hat{a}_0) = Im(B(\hat{a}_0, \hat{b}_k)) \\
B^R(\hat{a}_k^{Re}, \hat{a}_k^{Re}) &= 0.5(Re(B(\hat{a}_k, \hat{a}_{-k})) + Re(B(\hat{a}_k, \hat{a}_k))) \\
B^R(\hat{a}_k^{Im}, \hat{a}_k^{Im}) &= 0.5(Re(B(\hat{a}_k, \hat{a}_{-k})) - Re(B(\hat{a}_k, \hat{a}_k))) \\
B^R(\hat{a}_k^{Re}, \hat{a}_k^{Im}) &= B^R(\hat{a}_k^{Im}, \hat{a}_k^{Re}) = 0.5Im(B(\hat{a}_k, \hat{a}_k)) \\
B^R(\hat{a}_k^{Re}, \hat{b}_l^{Re}) &= B^R(\hat{b}_l^{Re}, \hat{a}_k^{Re}) = 0.5(Re(B(\hat{a}_k, \hat{b}_{-l})) + Re(B(\hat{a}_k, \hat{b}_l))) \\
B^R(\hat{a}_k^{Im}, \hat{b}_l^{Im}) &= B^R(\hat{b}_l^{Im}, \hat{a}_k^{Im}) = 0.5(Re(B(\hat{a}_k, \hat{b}_{-l})) - Re(B(\hat{a}_k, \hat{b}_l))) \\
B^R(\hat{a}_k^{Re}, \hat{b}_l^{Im}) &= B^R(\hat{b}_l^{Im}, \hat{a}_k^{Re}) = 0.5(Im(B(\hat{a}_k, \hat{b}_l)) + Im(B(\hat{a}_{-k}, \hat{b}_l))) \\
B^R(\hat{a}_k^{Im}, \hat{b}_l^{Re}) &= B^R(\hat{b}_l^{Re}, \hat{a}_k^{Im}) = 0.5(Im(B(\hat{a}_k, \hat{b}_l)) - Im(B(\hat{a}_{-k}, \hat{b}_l)))
\end{aligned}$$

Here the element $B(\hat{a}_k, \hat{b}_l)$ of the covariance matrix B corresponds to the expectation of $B(\hat{a}_k, \hat{b}_l) = E((\hat{a}_k - E(\hat{a}_k))(\hat{b}_l - E(\hat{b}_l)))$.

The approximate inverse of a singular square matrix $B_{p \times p}$ is defined to be equal $B^{-1}(\Lambda_n) = U_n \Lambda_n^{-1} U_n^T$, $n < p$, where Λ_n is a $n \times n$ diagonal matrix containing the n largest eigenvalues of the matrix B and a $p \times n$ orthonormal matrix U_n containing the n corresponding eigenvectors of the matrix B .

The expression (140) is approximated by

$$\begin{aligned}
(142) \quad w(\hat{x}, \mathcal{Y}) &= c * e^{(Tr\hat{x} - Tra_0)^T (B_0^R)^{-1} (\Lambda_{n_B}^B) (Tr\hat{x} - Tra_0)} * \\
&* e^{\sum_{i=1}^{N_{ass}} (y_i - \mathcal{F}^i(\hat{x}))^T H^{-1} (y_i - Z(\mathcal{F}^i(\hat{x})))} * \\
&* e^{-(Tr\hat{x} - Tr\hat{\alpha}_0)^T (V_0^R)^{-1} (\Lambda_{n_V}^V) (Tr\hat{x} - Tr\hat{\alpha}_0)}
\end{aligned}$$

In the one-dimensional shallow water model the number of the largest eigenvalues is chosen to be equal for both matrices to be used in the expression (142) and is equal $n_B = n_V = 22$. The formal degrees of freedom of the model state is 63. Geostrophic balance will approximately reduce these degrees of freedom by factor 3. To compute the approximate inverse of the matrix and to sample from the Gaussian distribution all eigenvalues larger than $\lambda_\epsilon = 0.00001$ were chosen. Essentially different from each other are only the largest 13 eigenvalues. Eigenvectors corresponding to the smaller eigenvalues are nearly insensitive to the assimilated data. In Table 2 we show the 11 largest eigenvalues of the initial forecast error covariance matrix Λ_{22}^B , and the covariances of the Gaussian approximation of the posterior pdf for the non-linear observation operators nlZ_3 and nlZ_2 . For each observation operator the first line corresponds to the result of the data assimilation of "high" precision data ($H = diag(\frac{1}{4}tlZB_0(tlZ)^T)$) and the second line corresponds to results of the data assimilation of the *low* precision data ($H = diag(2tlZB_0(tlZ)^T)$). The prior pdf is Gaussian, so Λ_{22}^B gives the largest eigenvalues of the prior variance of the model state variable as well. The posterior pdf is not Gaussian, and therefore Λ_{22}^V contains the eigenvalues of the curvature of the posterior pdf around the mode, which in general can be quite different from the posterior variance.

The dependent sample $\hat{x}^j(t_0)$, $j = 1, \dots, N_{sample}$, which is represented in Figures 26 and 27, is constructed as follows. Firstly, we obtain a sample of real valued vectors $(\hat{x}^R(t_0))^j$.

$$(143) \quad (\hat{x}^R(t_0))^j = Tr \hat{\alpha}_{t_0} + U_{n_V}^V (\Lambda_{n_V}^V)^{\frac{1}{2}} \mathcal{X}_{n_V}^j$$

The random n_V -dimensional vectors $\mathcal{X}_{n_V}^j$, $j = 1, \dots, N_{sample}$ have a standard multivariate normal distribution $\mathcal{N}(0, I_{n_V \times n_V})$

Secondly, these real-valued random vectors $(\hat{x}^R(t_0))^j$ are transformed back to the complex valued model state variables $(\hat{x}(t_0))^j$ with the structure of the spectral coefficients of the discrete Fourier transform of a real valued field outlined above.

The subspace of a linear space spanned by matrix V_0^R in which the sample $(\hat{x}^R(t_0))^j$, $j = 1, \dots, N_{sample}$ varies, depends on the chosen amount of the largest eigenvalues n_V . Even if the matrix itself $V_0^R = B_0^R - Tr B_0 N_1 B_0 Tr^T$ spans the subspace spanned by B_0^R , the number of the largest eigenvalues n_B of the matrix B_0^R must be chosen so that the subspace corresponding to the matrix $U_{n_B}^B (\Lambda_{n_B}^B) (U_{n_B}^B)^T$ would include a subspace corresponding to the matrix $U_{n_V}^V (\Lambda_{n_V}^V) (U_{n_V}^V)^T$.

The efficiency of the estimate (136) depends on the sample size N_{sample} . But for every realisation of the sample, the result of the estimation will depend on the inherited randomness of the sample as well. For a moderate sample size, especially in the case of a large dimensional sampling distribution, the result of the estimation can depend significantly on how well a particular realisation of the sample represents essential properties of the sampling distribution, for example, such properties like different types of symmetry for a normal distribution. The efficiency of the estimate can be increased by constructing a dependent, often called a balanced, sample instead of the independent one described above. This improvement can be made by means of antithetic variables. An antithetic variable in the context here is a function of a random draw, it is equi-probable with the random draw and it helps to represent the particular features of a sampling distribution, when it is included in the sample together with the random draw. We will use two types of antithetic variables to balance the sample for location in a linear space and to balance the sample for scale. These antithetic variables are discussed for example in Durbin and Koopman (1997). First, for every random draw of \mathcal{X}_{n_V} we construct a variable $\tilde{\mathcal{X}}_{n_V} = -\mathcal{X}_{n_V}$, and in accordance with (143) for every $\hat{x}^R(t_0)$ we will obtain $\tilde{x}^R(t_0) = Tr \hat{\alpha}_{t_0} - U_{n_V}^V (\Lambda_{n_V}^V)^{\frac{1}{2}} \mathcal{X}_{n_V}$. The symmetry around the mean of a normal distribution density suggests this type of an antithetic variable to balance for location. The \mathcal{X}_{n_V} and $\tilde{\mathcal{X}}_{n_V}$ are equi-probable and a sample estimate of the normal mean is equal exactly to the true value. The weights for the realisation of these two antithetic variables are grouped in Figures 26 and 27.

$$(144) \quad \begin{aligned} \overline{\hat{X}^R(t_0)} &= \frac{(\hat{x}^R(t_0))^1 + (\tilde{x}^R(t_0))^1}{2} = \\ &= \frac{Tr \hat{\alpha}_{t_0} + U_{n_V}^V (\Lambda_{n_V}^V)^{\frac{1}{2}} \mathcal{X}_{n_V}^1 + Tr \hat{\alpha}_{t_0} - U_{n_V}^V (\Lambda_{n_V}^V)^{\frac{1}{2}} \mathcal{X}_{n_V}^1}{2} = \\ &= Tr \hat{\alpha}_{t_0} = \overline{E(\hat{X}^R(t_0))} \end{aligned}$$

The second type of antithetic variable was developed by Durbin and Koopman. Let $\xi = (\mathcal{X}_{n_V})^T \mathcal{X}_{n_V}$, then the variable $\xi \sim \chi_{n_V}^2$. For the particular realisation of \mathcal{X}_{n_V} let us denote q a probability $Pr(\chi_{n_V}^2 < \xi) = q$. Then a $1 - q$ -quantile of the $\chi_{n_V}^2$ distribution ξ' $Pr(\chi_{n_V}^2 \geq \xi') = q$ is equi-probable with ξ . Then a value $\mathcal{X}'_{n_V} = \sqrt{\frac{\xi'}{\xi}} \mathcal{X}_{n_V}$ is equi-probable with \mathcal{X}_{n_V} . The fact that \mathcal{X}'_{n_V} and \mathcal{X}_{n_V} have the same distribution follows because $\xi = (\mathcal{X}_{n_V})^T \mathcal{X}_{n_V}$ and $\frac{\mathcal{X}_{n_V}}{\sqrt{\xi}}$ are independently distributed (Durbin and Koopman, 1997). Such a

construction of the sample makes the sampling symmetric around a median of a certain transform (the sum of squares). If the perfect sampling could be made, it would always be symmetric around the median of any transform. Then, obviously, $X'^R(t_0) (= Tr \hat{\alpha}_{t_0} + U_{n_V}^V (\Lambda_{n_V}^V)^{\frac{1}{2}} \mathcal{X}'_{n_V}) = Tr \hat{\alpha}_{t_0} + \frac{\xi'}{\xi} U_{n_V}^V (\Lambda_{n_V}^V)^{\frac{1}{2}} \mathcal{X}_{n_V}$ and $\hat{X}_{n_V}^R$ have the same distribution and are equiprobable. Thus, for every independent draw $\mathcal{X}_{n_V}^j$, $j = \frac{N_{sample}}{4}$ we create four dependent variables $(\hat{x}^R(t_0))^j = Tr \hat{\alpha}_{t_0} + U_{n_V}^V (\Lambda_{n_V}^V)^{\frac{1}{2}} \mathcal{X}_{n_V}^j$, $(\tilde{x}^R(t_0))^j = Tr \hat{\alpha}_{t_0} - U_{n_V}^V (\Lambda_{n_V}^V)^{\frac{1}{2}} \mathcal{X}_{n_V}^j$, $(x'^R(t_0))^j = Tr \hat{\alpha}_{t_0} + \frac{\xi'}{\xi} U_{n_V}^V (\Lambda_{n_V}^V)^{\frac{1}{2}} \mathcal{X}_{n_V}^j$ and $(\tilde{x}'^R(t_0))^j = Tr \hat{\alpha}_{t_0} - \frac{\xi'}{\xi} U_{n_V}^V (\Lambda_{n_V}^V)^{\frac{1}{2}} \mathcal{X}_{n_V}^j$. Such a procedure allows us to construct a sample of a moderate size, which has some desired properties of a large dimensional independent sample from the sampling distribution. If we would like, the procedure for construction of an antithetic variable can be continued infinitely. For example, we could employ a uniform distribution of the q -quantile inverse, and instead of taking only two probability realisations q and $1 - q$ as above, we could define $q_1 = q + 0.5$ modulus 1 and take four realisations of the probability q , $1 - q$, q_1 , $1 - q_1$ and so on. In our construction of a sample from a sampling distribution, we utilize only the symmetry around a mean of the normal distribution, and a distribution of mass for the sum of n_V squares of normally distributed variables in accordance with the location of a median of a χ_{n_V} distribution density. The main goal was to estimate the posterior expectation of the model state variable $E(\hat{X}(t_0) | \mathcal{Y})$ and the posterior expectation of a usually smaller dimensional transform $E(\zeta(\hat{X}(t_0)) | \mathcal{Y})$. In fact, any function of the model state variable can be estimated in this way. Besides the importance sampling estimate of quantiles (139) we have used above, the estimate of the posterior variance of $f_\zeta(\hat{X}(t_0))$ can be useful to obtain.

$$var(f_\zeta(\hat{X}(t_0)) | \mathcal{Y}) = \int E((f_\zeta(\hat{X}(t_0)) - E(f_\zeta(\hat{X}(t_0)) | \mathcal{Y}))^2 | \mathcal{Y}) \frac{p(\hat{X}(t_0) | \mathcal{Y})}{g(\hat{X}(t_0) | \mathcal{Y})} g(\hat{X}(t_0) | \mathcal{Y}) d\hat{X}(t_0)$$

Then the importance sampling estimate of variance $var(f_\zeta(\hat{X}(t_0)) | \mathcal{Y})$ can be taken as

$$(145) \quad var(f_\zeta(\hat{X}(t_0)) | \mathcal{Y}) \approx \sum_{j=1}^{N_{sample}} (f_\zeta(\hat{x}^j(t_0)))^2 w_j - \overline{(f_\zeta(\hat{X}(t_0)) | \mathcal{Y})}^2$$

5. VALIDATION OF DATA ASSIMILATION PROVIDED BY THE DIFFERENT KALMAN FILTER EXTENSIONS

In the previous chapter we have outlined the basic properties of four different Kalman filter extensions, which we have applied to data assimilation with a one-dimensional shallow water model. All these four extensions are used with the same aim to reconstruct the "true" model state $\bar{X}(t)$ from a given forecast a_0 and observations \mathcal{Y} , in other words, to construct a point estimate of the unobservable model state $\hat{X}(t)$, where t denotes the desired time moment $t > 0$. The construction of a point estimate is a decision problem, and a point estimate can be optimal only with respect to the loss function it is supposed to minimize. We are only dealing with simulated observations in this study, and therefore the "true" model state $\bar{X}(t)$ is known over the desired time period. The objective comparison of the different Kalman filter extensions is possible with the purpose to determine which estimate comes closer to the "true" model state and it will be carried out. The main issues we would like to concentrate on are the following ones

- In what sense, i.e. with respect to which loss function, if any, is a particular Kalman filter extension more efficient than the others?

- How close, in some sense, is the estimate of the unobservable model state to its "true" value and do we have some information representing the distance?
- How feasible is it to perform the necessary computations to obtain the estimate in the case of a full scale problem?
- What type of approach is preferable for the meteorological data assimilation problem, the deterministic or the probabilistic one?

In all four extensions the unobservable model state is treated from a Bayesian point of view. The point estimates are constructed to minimize a Bayes risk, which is defined as the expected value of a frequentist risk with respect to a prior distribution for the model state variable $\hat{X}(t_0)$. Let us denote by δ a decision function, a function which is defined on the sample space of observations \mathcal{Y} (all possible outcomes of observation series) and specifies the action to take for any possible outcome. In our situation the decision δ is to use some particular estimator for $\bar{X}(t)$. The resulting error of estimation is quantified by some loss function $loss(\bar{X}(t), \delta(\mathcal{Y}))$. The frequentist risk is the expected value of the chosen loss function regarded as a function of the "true", unobservable, model state $\bar{X}(t)$ treated as a parameter.

$$risk_F(\bar{X}(t), \delta) = \int_{\bar{\mathcal{Y}}} loss(\bar{X}(t), \delta(\mathcal{Y}))p(\mathcal{Y}; \bar{X}(t_0))d\mathcal{Y}$$

Thus the Bayes risk is a function of the hyper parameters of a prior distribution for the unobservable model state ($\hat{X}(t_0) \sim \mathcal{N}(a_0, B_0)$):

$$\begin{aligned} risk_B(p(\hat{X}(t_0)), \delta) &= \int_{\hat{\mathcal{X}}(t_0)} \int_{\bar{\mathcal{Y}}} loss(\hat{X}(t), \delta(\mathcal{Y}))p(\mathcal{Y} | \hat{X}(t_0))p(\hat{X}(t_0))d\mathcal{Y}d\hat{X}(t_0) = \\ (146) \quad &= \int_{\bar{\mathcal{Y}}} \int_{\hat{\mathcal{X}}(t_0)} loss(\hat{X}(t), \delta(\mathcal{Y}))p(\hat{X}(t_0) | \mathcal{Y})p(\mathcal{Y})d\hat{X}(t_0)d\mathcal{Y} \end{aligned}$$

rewritten according to Bayes formula.

The function (146) can be minimized for each realisation \mathcal{Y} separately, so we may condition on the particular realisation of observations \mathcal{Y} and minimize the functional

$$(147) \quad loss_B(p(\hat{X}(t_0)), \delta(\mathcal{Y})) = \int_{\hat{\mathcal{X}}(t_0)} loss(\hat{X}(t), \delta(\mathcal{Y}))p(\hat{X}(t_0) | \mathcal{Y})d\hat{X}(t_0)$$

Dependent on the loss function we have chosen, different point estimates are defined.

The extended Kalman filter approximates the posterior mode of the unobservable model state variable at the time of the end of the data assimilation time window $\hat{X}(t_{N_{ass}})$ and the time-window smoother approximate the posterior mode of the unobservable model state variable at the beginning of the data assimilation time window $\hat{X}(t_0)$. The ensemble Kalman filter and the bias-corrected Kalman filter provide refinements, compared with the extended Kalman filter, in approximation of the posterior mode of the model state at the end of the data assimilation time window $\hat{X}(t_{N_{ass}})$. The importance sampling is to approximate the posterior mean of $\bar{X}(t_0)$ at the beginning of the assimilation time-window, but under the perfect model assumption it can be used to approximate the posterior mean of $\bar{X}(t_{N_{ass}})$ at the end of the data assimilation time window as well. A posterior mode and a posterior mean are point estimates which are optimal in different respects, in general. While applied to reconstruct the "true" model state, which gave rise to the observations, they both have advantages as well as limitations.

5.1. **Posterior mean as a point estimate.** Suppose we choose the loss function in equation (147) to be quadratic in $\hat{X}(t)$ (say, $t = t_{N_{ass}}$, or $t = t_0$)

$$(148) \quad loss(\hat{X}(t), \delta(\mathcal{Y})) = (\hat{X}(t) - \delta(\mathcal{Y}))^2$$

Then, since a second moment is smallest taken about the mean, the Bayes decision rule, which minimizes the Bayes expected loss (147) is the posterior predictive mean (or just the posterior mean if the loss function is evaluated at the beginning of a time window) $E(\hat{X}(t) | \mathcal{Y})$.

$$(149) \quad \delta(\mathcal{Y}) = E(\hat{X}(t) | \mathcal{Y}) = \int_{\hat{X}(t_0)} \hat{X}(t) p(\hat{X}(t_0) | \mathcal{Y}) d\hat{X}(t_0)$$

The optimal expected Bayes loss is equal to the expectation of the posterior predictive variance

$$\int_{\hat{X}(t_0)} (\hat{X}(t) - E(\hat{X}(t) | \mathcal{Y}))^2 p(\hat{X}(t_0) | \mathcal{Y}) d\hat{X}(t_0) = var(\hat{X}(t) | \mathcal{Y})$$

We intentionally specify the integrals in the expressions above with respect to the posterior pdf, evaluated at the beginning of the time window, and not the posterior predictive one, evaluated at the end of the data assimilation procedure. We know the posterior pdf $p(\hat{X}(t_0) | \mathcal{Y})$ up to the normalizing constant. Even if, under the perfect model assumption, $\hat{X}(t)$ is a unique function of the $\hat{X}(t_0)$, the posterior pdf $p(\hat{X}(t) | \mathcal{Y})$ can not be expressed analytically at all. As soon as the posterior variance is finite, the posterior mean will be optimal with respect to the mean squared error. The point estimate minimizing the risk is unique and this is a big advantage of the estimate. Even if the posterior covariance is infinite, the posterior mean can still exist. But in this case it will only denote an expectation of the unobservable model state variable according to the posterior distribution, and it can be difficult to relate the estimate to the particular realisation of the unobservable model state, the "true" value which gave rise to the observations. As it was already mentioned, the dynamics of our model is not completely correct, because the conservation of the total energy does not hold. The distribution cloud contracts with time (after a very long integration time). If the initial covariance matrix is finite, the posterior predictive covariance matrix will be finite as well.

The posterior mean as a point estimate of the unobservable model state variable is sensitive to the introduced observations. Even in the case when the observations are quite in-precise compared to the prior opinion about the model state, the posterior distribution is different from the prior distribution (except in the case of non-informative observations). Therefore, the posterior mean which is the average of the unobservable model state, weighted by the posterior pdf, is different from the prior mean.

Another advantage is that the distance, in a certain sense, between the posterior (or the posterior predictive) mean $E(\hat{X}(t) | \mathcal{Y})$ and the "true" value of $\hat{X}(t)$ is well represented by the posterior (or posterior predictive) variance.

The posterior mean is a point to which all possible values of a random variable have the shortest averaged squared distance, weighted with the posterior pdf. If the posterior pdf is heavy tailed, the posterior expectation can be displaced strongly toward the heavier tail, toward the subspace with a lower probability density. It is more believable that the

”true” value of the $\hat{X}(t_0)$ falls in the area with higher probability density, and therefore away from the point of the posterior mean.

Even more, if the model space $\tilde{X}(t_0)$, where the unobservable model state variable varies, forms a non-linear subspace, the posterior mean does not necessary fall into $\tilde{X}(t_0)$. The posterior mean can define a model state, which does not exist. However, the problem here does not lie in the estimate itself, but in the way in which the estimate is interpreted.

5.2. Posterior mode as a point estimate. If we choose the loss function in the expression of the Bayes risk (146) as

$$(150) \quad \text{loss}(\hat{X}(t_0), \delta(\mathcal{Y})) = \begin{cases} 0 & , \delta(\mathcal{Y}) = \hat{X}(t_0) \\ 1 & , \delta(\mathcal{Y}) \neq \hat{X}(t_0) \end{cases}$$

then we are supposed to minimize

$$(151) \quad \begin{aligned} \min_{\delta(\mathcal{Y})} \int_{\tilde{X}(t_0)} (1 - \mathcal{I}_{\delta(\mathcal{Y})=\hat{X}(t_0)}) p(\hat{X}(t_0) | \mathcal{Y}) d\hat{X}(t_0) = \\ = 1 - \max_{\delta(\mathcal{Y})} p(\delta(\mathcal{Y}) | \mathcal{Y}) \end{aligned}$$

Then the optimal decision with respect to the zero-one *loss* (150) will be the posterior mode of $p(\hat{X}(t_0) | \mathcal{Y})$. Let $\hat{\alpha}_0$ denote the posterior mode of the $p(\hat{X}(t_0) | \mathcal{Y})$.

The posterior mode determines simply a point at which the posterior pdf achieves its maximum. A pdf function is bounded from above, so it always achieves a maximum. It is not necessary that the maximum is unique, so just the existence of the posterior mode can not be considered as an optimality feature. Also, not only the maximum point is important, but even more the whole form of the posterior pdf. Accepting the mode as a point estimate of the unobservable model state variable, the curvature around the modes as well as the total amount of mass located in the tails of the posterior pdf must be taken into account. It is not easy to estimate the amount of mass located in the tails of the pdf, but a good estimate of the curvature around the mode of the pdf is the matrix V_0 , obtained during approximation of the mode in the time-window smoother. Approximating the mode of the posterior pdf by the time-window smoother, we apply the backwards smoothing to the filter based on the extended Kalman filter approach in order to obtain the first estimation of the posterior mode and its dynamical evolution. By the method outlined above we will find the mode of the posterior pdf which lies closest to the mode of the posterior pdf for the approximate linear state space problem with linearised dynamics and linearised observation operators. In our model the dynamics are well approximated by linearization, and in the case of a linear observation operator, with Gaussian observation errors, the posterior distribution is unimodal. If the observation operator is non-linear, multimodality of the posterior pdf can easily occur.

When a posterior pdf has several separately located modes, it means that there is evidence that several model state realisations could give rise to the same observations, and we do not have enough information to choose only one of them. The global mode can be chosen as a point estimate in such a situation. The iterative procedure used in the time-window smoother does not guarantee that it is the global mode that will be estimated.

One of the main advantages of the posterior mode as a point estimate is that it always determines an existing model state. A support of a posterior pdf is always a subspace of

the support of a prior pdf. The posterior pdf differs from zero only where the prior pdf does. The cloud of the prior pdf is concentrated (approximately) along a slowly evolving manifold (see discussion above on the approximation of the valid physical balances). The cloud of the posterior pdf is formed from the cloud of the prior pdf down-weighting values which are unlikely according to the observations.

A posterior pdf is proportional to a prior pdf multiplied by a likelihood. If the number of observations is large enough, the likelihood will dominate the prior, and the posterior mode will come close to the maximum likelihood estimate of the unobservable model state. But this is far away from the common situation in meteorological data assimilation. Here observations can have large errors and the number of them is small compared to the dimensionality of the model state variable. Even if the introduction of observations can change significantly the form of the pdf, there is often not enough evidence in the displacement of the location of the mode. In that case, interpreting the posterior mode as a point estimate of the unobservable model state, we always need to take into account that the position of the mode is strongly affected by our prior opinion about the model state variable and it can differ significantly from the most likely one in the light of observations.

It is well known that the maximum likelihood estimate of the unobservable model state variable is asymptotically efficient under quite mild regularity conditions. In fact, if necessary conditions are satisfied, even in the case of dependent observations the maximum likelihood estimate of the parameter, when the number of observations is large enough, is approximately Gaussian around the true value of the parameter as a mean and with the Fisher information matrix $I(\hat{X}(t_0))$ as a variance-covariance matrix, and asymptotically efficient. In the case of the model we are using, the exact asymptotic theory cannot be applied, because the space of the model state variable $\hat{X}(t_0)$ is not convex, and due to the irreversibility of the normal mode initialisation procedure, there exists a whole subspace of $\hat{X}(t_0)$, which could give rise to the same observations.

As first shown by Godambe (1960) and Durbin (1960) for the maximum likelihood estimate, and later generalized for the posterior mode by Durbin(1997), a finite sample property analogous to the asymptotic efficiency, the minimum variance unbiased estimating equation property, holds for the posterior mode.

Namely, the posterior mode $\hat{\alpha}_0$ is a solution of an unbiased estimating equation (with respect to the joint probability density $p(\hat{X}(t_0), \mathcal{Y})$) :

$$(152) \quad \mathcal{D}_{\hat{X}(t_0)}(\log p(\hat{X}(t_0) | \mathcal{Y})) = \mathcal{D}_{\hat{X}(t_0)}(\log p(\hat{X}(t_0), \mathcal{Y})) = 0,$$

which is proportional to the minimum variance unbiased estimating equation defined below.

$$(153) \quad h(\hat{X}(t_0), \mathcal{Y}) := \mathcal{D}_{\hat{X}(t_0)}(-(\mathcal{J})^{-1} \log p(\hat{X}(t_0), \mathcal{Y})) = 0,$$

The minimum variance unbiased estimating equation $h(\hat{X}(t_0), \mathcal{Y})$ has the smallest variance with respect to the joint probability density which is equal $(\mathcal{J})^{-1}$, where \mathcal{J} is an integrated Fisher information matrix

$$(154) \quad \mathcal{J} = \text{var}\left(\frac{\partial \log p(\hat{X}(t_0), \mathcal{Y})}{\partial \hat{X}(t_0)}\right) = -E\left(\frac{\partial^2 \log(p(\hat{X}(t_0), \mathcal{Y}))}{\partial \hat{X}^2(t_0)}\right) = E_{\hat{X}(t_0)}(I(\hat{X}(t_0)))$$

The integrated Fisher information matrix \mathcal{J} is the expectation of the Fisher information matrix $I(\hat{X}(t_0))$ with regard to the prior distribution of $\hat{X}(t_0)$. The importance of the result is that it formulates a finite-sample optimal property of the posterior estimate and relates it to the Fisher information matrix, namely to its average over the prior distribution of the parameter. However, in practice, when we obtain a posterior mode estimate given a particular set of observations \mathcal{Y} , it is difficult to apply and to interpret this optimality property, which is considered with respect to the joint probability density. Then all observations, not only the actually observed but all the possible ones to occur, are taken into account. The integrated expected information matrix \mathcal{V} , which indicates the "closeness", has little to deal with the actual value of the observed information at the point of the posterior mode $i(\hat{\alpha}_0, \mathcal{Y}) = -\frac{\partial^2 \log(p(\hat{X}(t_0), \mathcal{Y}))}{\partial \hat{X}^2(t_0)} | (\hat{\alpha}_0, \mathcal{Y}) = V_0$

$$\mathcal{J} = \int_{\bar{\hat{X}}(t_0)} \int_{\bar{\mathcal{Y}}} i(\hat{X}(t_0), \mathcal{Y}) p(\hat{X}(t_0), \mathcal{Y}) d\mathcal{Y} d\hat{X}(t_0)$$

The exception is the Gaussian linear model for which the observed information matrix is constant.

The conditional, given observations \mathcal{Y} , minimum variance optimality property does not hold in general. To make it true, a very special condition must be satisfied.

$$(155) \quad \int_{\bar{\hat{X}}(t_0)} \frac{\partial^2 p(\hat{X}(t_0) | \mathcal{Y})}{\partial \hat{X}^2(t_0)} d\hat{X}(t_0) = 0$$

In other words, the model must be such that the following property holds

$$(156) \quad \int_{\bar{\hat{X}}(t_0)} -\frac{\partial^2 \log(p(\hat{X}(t_0) | \mathcal{Y}))}{\partial \hat{X}^2(t_0)} p(\hat{X}(t_0) | \mathcal{Y}) d\hat{X}(t_0) = \int_{\bar{\hat{X}}(t_0)} \left(\frac{\partial \log(p(\hat{X}(t_0) | \mathcal{Y}))}{\partial \hat{X}(t_0)} \right)^2 p(\hat{X}(t_0) | \mathcal{Y}) d\hat{X}(t_0)$$

5.3. The estimate of the posterior predictive mode versus the estimate of the posterior predictive mean of $\hat{X}(t)$. We would like to compare the posterior mode obtained using the time-window smoother and the posterior mean estimated from importance sampling as estimators of the unobservable model state variable at the beginning of a time-window. In the experiment we have been using "low" precision data simulated with the non-linear observation operator nlZ_1 . In Figure 29 we can see the normalized squared error for the three meteorological fields of the posterior mode $N\tilde{S}E(*)$ and of the posterior mean $N\tilde{S}E^{i.s.} (+)$ as estimators of \hat{X}_t evaluated at the end of the "short" time window (8 observation windows) for different realisations of the first-guess state a_0 , which specifies the prior $\hat{X}(t_0) \sim \mathcal{N}(a_0, B_0)$. To obtain the normalized squared errors $N\tilde{S}E$ and $N\tilde{S}E^{i.s.}$ the corresponding spatial average squared errors were divided by the initial spatial average forecast error variance of the meteorological field. The normalizing quantities are $var_u^0 = 0.004375$ for the u -wind component, $var_v^0 = 38.40$ for the v -wind component and $var_\phi^0 = 11280$ for the geopotential.

The total number of the introduced observations (8 times by 9 observations) is not very large compared to the dimensionality of the model state variable, but the impact of the observations in the specification of the posterior pdf is significant. In a majority of cases (different realisations of the initial first guess) the posterior mode is a much better estimator of the "true" model state $\bar{X}(t_0)$ than the posterior mean. Even at the end of

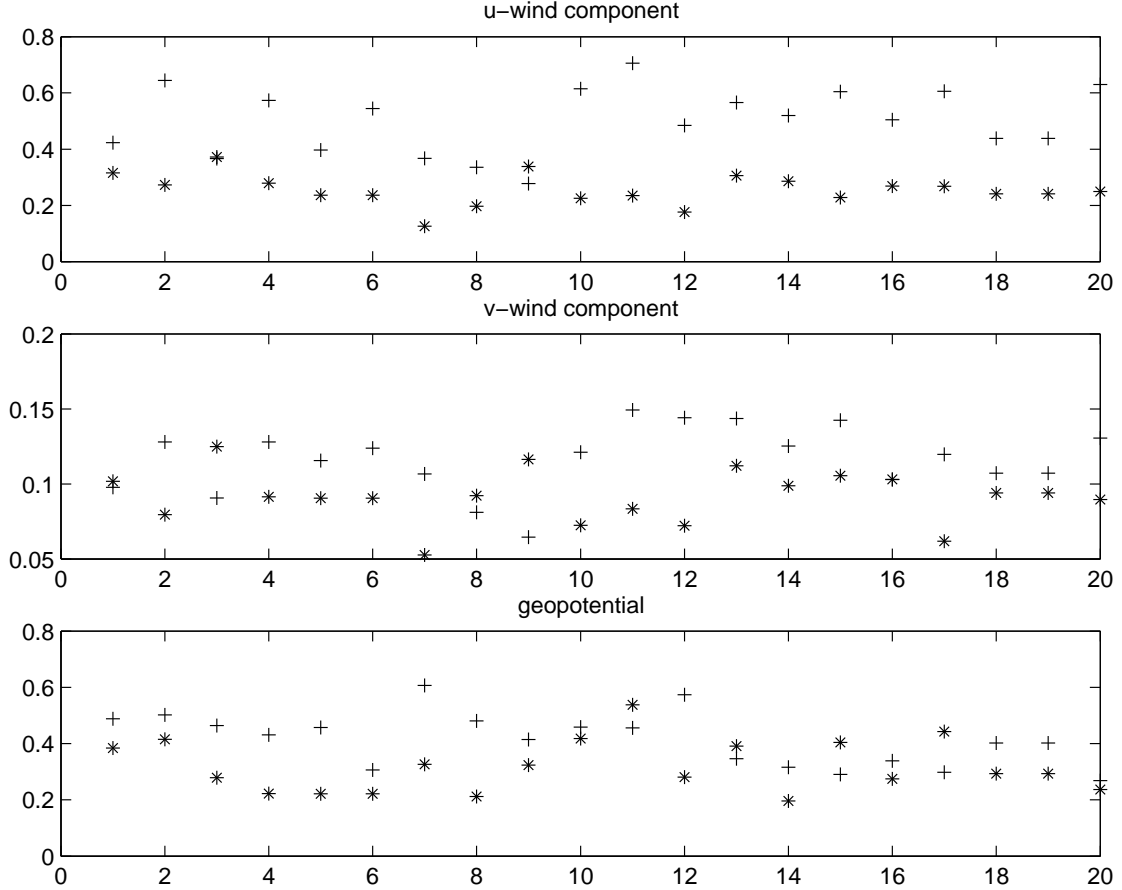


FIGURE 29. The spatial average normalised squared error for the u -wind component, for the v -wind component and for the geopotentials of the posterior mode (*) and of the posterior mean (+) as estimators of $\hat{X}(t)$, evaluated at the end of the "short" assimilation time window $t = t_{N_{ass}}$ ($N_{ass} = 8$ observation windows) for 20 different realisations of the first-guess state a_0 . The number of the realisation is indicated on the horizontal axis.

the assimilation time window the time development of the posterior mode, which is not equal to the posterior predictive mode at the time moment, estimates $\bar{X}(t)$ better than the posterior mean in a large number of cases.

Such good results are partly due to the simulation technique. The first guess states as well as the observation errors form indeed a Gaussian cloud around the "true" model state. The posterior mode is the most believable location of the "true" model state under our prior opinion and in the light of the observations. With such a "successful" specification of the prior, in accordance with the Bayesian interpretation of the probability density as a belief about the location of the "true" state, the "true" model state will appear in a vicinity of the posterior mode for the majority of the first guess realisations.

Secondly, the posterior mean as a point estimate is not so meaningful as the mean is defined in a frequentists context. The behaviour of the posterior mean as a point estimate will depend on the form of the pdf. The form of the posterior pdf will depend on the actual realisation of the first guess field, and for a large amount of realisations it is heavy tailed and non-symmetric. Therefore the location of the mean is displaced from the location of the first-guess field much toward the heavy tail. If we would repeat the "short" time window smoother several times, specifying a Gaussian prior in the beginning of every time

window as we have done it in Configuration *b* (with the dynamical update of the forecast error covariance matrix, see section 4.3), the results in Figure 29 would look differently.

We tried 5 sequential applications of the time-window smoother. During the last, the fifth, time window, the observations were considered as rather poor compared to the sharp prior, and the observations did not have enough influence to replace the mode. However, even very weak observations influence the form of the posterior pdf and move (very slightly) the posterior mean away from the first-guess state. Now the posterior mean became a better estimator of $\bar{X}(t)$, with respect to the spatial average normalised squared error. For the majority of different starting first-guess fields $N\tilde{S}E^{i.s.}$ is smaller than $N\tilde{S}E$. But we need to stress that the improvement is very small due to the sharp prior. As we have seen (Figure 17, section 4.3), in Configuration *c* (with the initial covariance matrix being the same at the beginning of every time-window) the posterior mode estimate of $\bar{X}(t_0)$ is much worse than for the other two Configurations (*a* and *b*). Because the prior in that case will never dominate the likelihood, the influence of the observations on the posterior pdf will be very strong every time window. Besides that, the prior formulation is not so "successful" in this case, because the first-guess state at the beginning of the new time-window is equal to the time development of the posterior mode up to the end of the previous time window. The cloud of the possible first-guess fields does not exactly form a Gaussian cloud, as the prior specifies. The posterior mean provides no help in the improvement of the estimation $\bar{X}(t)$, because it is often too strongly displaced towards the tail.

Under the perfect model assumption, when we have assimilated observations using the "long" assimilation time window, for almost all realisations of the starting first-guess state, the posterior mode comes so close to the "true" state $\bar{X}(t_0)$, that even at the end of the "long" assimilation time window, the time evolution of the mode is still a better forecast than the posterior predictive mean, when data were simulated with the non-linear observation operator nlZ_1 . We need to say, however, that both estimates are very close to one another. After such a large amount of data have been introduced (totally 40 times by 9 observations), the likelihood dominates over the prior and the posterior mode comes close to the maximum likelihood estimate of $\bar{X}(t_0)$. Even if a large amount of mass of the posterior pdf is concentrated around the mode, the form of the posterior pdf still deviates from the Gaussian one, and the posterior mean is displaced away from the mode toward the heavy tail. Assimilating observations simulated by other observation operators, the posterior pdf could have a lighter tail, and the result can be more in favour of the posterior predictive mean as a point estimate of the $\bar{X}(t)$ (as we can in Figure 25 when data were simulated using the non-linear observational operator nlZ_2).

For a sharp posterior pdf, the transform $f_\zeta(\alpha_t)$ of the posterior mode propagated in time is a better estimate of $f_\zeta(\bar{X}(t))$ than the mean of $f_\zeta(\hat{X}(t))$ estimated by importance sampling. If the mass of the posterior pdf is widely distributed around the posterior mode, the answer to which of these two point estimates is preferable will again depend on the form of the posterior pdf of $f_\zeta(\hat{X}(t))$. However, usually with a strongly non-linear transform the estimator, $f_\zeta(\alpha(t))$ has not much in common with $f_\zeta(\bar{X}(t))$ and the posterior predictive mean of $f_\zeta(\hat{X}(t))$ is a better estimator of $f_\zeta(\bar{X}(t))$.

We have illustrated the comparison of $f_\zeta(\alpha(t))$ and the posterior mean of $f_\zeta(\hat{X}(t))$ as estimators of $f_\zeta(\bar{X}(t))$ in Figure 30. Values of $f_\zeta(\alpha(t))$, corresponding to different realisations of the first-guess state a_0 (19 different realisations) are denoted by *, and values of the posterior mean of $f_\zeta(\hat{X}(t))$ corresponding to different realisations of a_0 are denoted by +. The dotted line defines position of the "truth", $f_\zeta(\bar{X}(t))$. To estimate the posterior mean

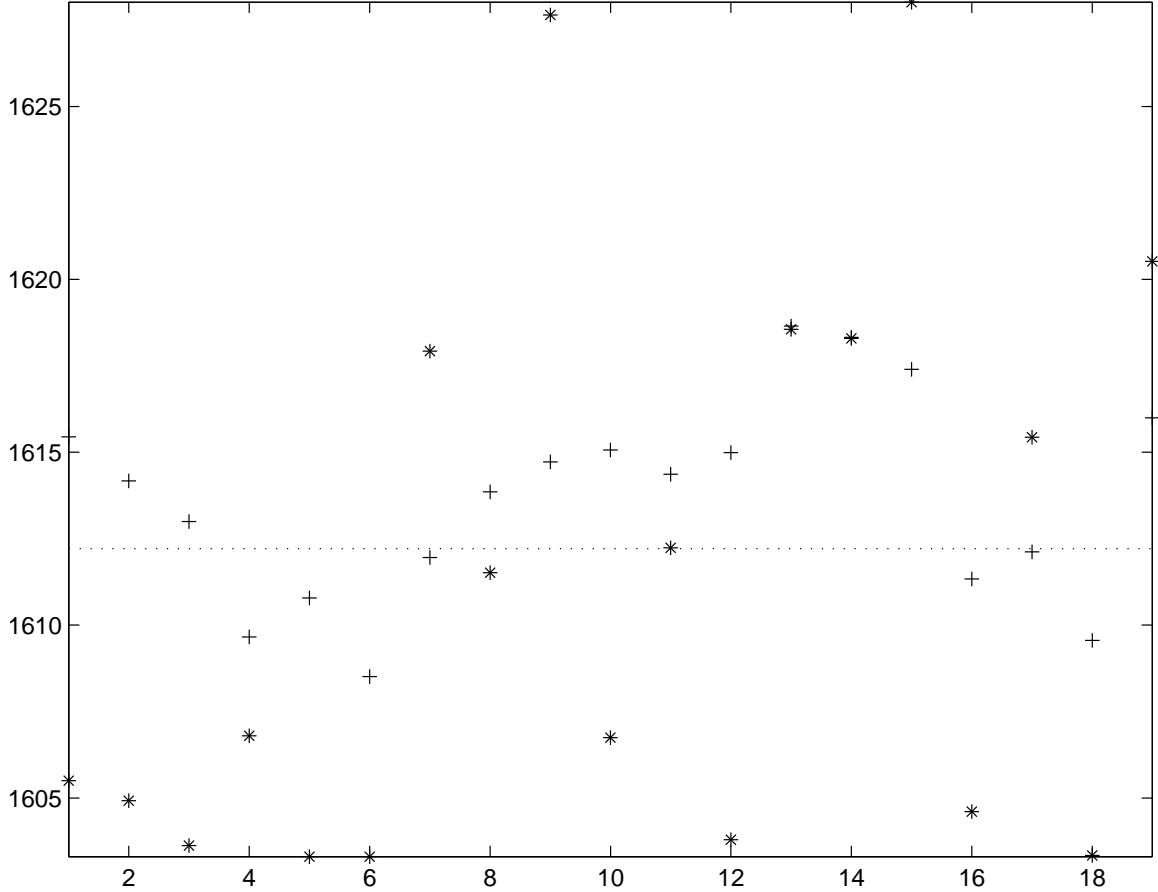


FIGURE 30. The transform $f_{\zeta}(\alpha_t)$ of the posterior mode propagated in time (*) and the posterior mean of $f_{\zeta}(\hat{X}(t))$ estimated by $N_{sample} = 100$ members importance sampling (+) as point estimators of $f_{\zeta}(\bar{X}(t))$ (the dashed line) obtained for 19 different realisations of the initial first-guess state a_0 . The number of the realisation is indicated on the horizontal axis. The comparison is made at the end of the first, "short" time window $t = t_{N_{ass}}(N_{ass} = 8)$. The assimilated data are "low" precision and are simulated using nlZ_1 .

we have used $N_{sample} = 100$ members importance sampling. The comparison is made at the end of the first, "short" time $t = t_{N_{ass}}$ - window, where assimilation for $N_{ass} = 8$ observations term have been performed. The assimilated data were simulated by the non-linear observation operator nlZ_1 . The functional f_{ζ} (kinetic energy) is a function of the u - and the v -wind components. As we have seen (Figure 29), the posterior predictive mode was a better estimate for both of these wind components compared to the posterior predictive mean. However, after the strongly non-linear transform f_{ζ} the posterior mean of $f_{\zeta}(\hat{X}(t))$ becomes a more powerful tool to estimate the true model state.

The efficiency of the posterior mean of $f_{\zeta}(\hat{X}(t))$ as an estimator of $f_{\zeta}(\bar{X}(t))$ depends on the sharpness of the posterior pdf of $\hat{X}(t_0)$, but is strongly influenced by the form of the posterior pdf of $f_{\zeta}(\hat{X}(t))$. Therefore, the possibility to judge about the posterior pdf of a non-linear transform of the model state variable, for example by estimation of its quantiles, is a stronger side of importance sampling than the possibility to estimate just the posterior mean of this non-linear transform.

TABLE 3. The spatial average squared error of the time propagated posterior mode α_t (\tilde{SE} , the first row), the posterior predictive mean estimated by the importance sampling of size $N_{sample} = 100$ ($\tilde{SE}^{i.s.,100}$, the second row) and the posterior predictive mean estimated by importance sampling of size $N_{sample} = 12$ ($\tilde{SE}^{i.s.,12}$, the third row) as estimators of the "true" model state. The time-window smoother with a "short" time window ($N_{ass} = 8$ observation windows) is used. The result is valid at the end of the assimilation window $t = t_{N_{ass}}$. The error is calculated for the u -wind component (the third column), for the v -wind component (the fourth column) and for the geopotential (the fifth column). The result is presented for the observations simulated by the three different non-linear observation operators nlZ_1 , nlZ_2 , nlZ_3 . The observations are of "low" precision.

The "short" time window; The "low" prec. dat		u -wind comp.	v -wind comp.	geopotential
nlZ_1	\tilde{SE}	0.001382	3.9086	4328.5
	$\tilde{SE}^{i.s.,100}$	0.001852	3.7524	5506.3
	$\tilde{SE}^{i.s.,12}$	0.003124	7.3060	8055.7
nlZ_2	\tilde{SE}	0.001339	3.8013	4474.5
	$\tilde{SE}^{i.s.,100}$	0.001871	3.7178	3881.8
	$\tilde{SE}^{i.s.,12}$	0.000748	2.2555	10237.5
nlZ_3	\tilde{SE}	0.001376	3.9244	4036.0
	$\tilde{SE}^{i.s.,100}$	0.001052	2.5412	3601.5
	$\tilde{SE}^{i.s.,12}$	0.002877	6.9410	6391.2

The "curvature" around the mode of the posterior pdf of $\hat{X}(t_0)$, the matrix V_0 , which is explicitly calculated by time-window smoother, can be used as a certain measure, how close the posterior mode α_0 can be located to the "true" $\bar{X}(t_0)$. In the example here, the largest eigenvalue of \hat{V}_0^R taken after the transform of V_0 to the real-valued space (141) ranges between 877 and 887. Only for two realisations of a_0 from totally 19 ones, the posterior mode of $\hat{X}(t_0)$ comes so close to its "true" value, that $f_\zeta(\alpha_t)$ is significantly closer to the $f_\zeta(\bar{X}(t))$ than the posterior mean of $f_\zeta(\hat{X}(t))$, estimated by importance sampling. The posterior variance of $f_\zeta(\hat{X}(t))$, estimated by importance sampling (145), varies very strongly for different realisations of the initial first guess state (from 46 up to 332 in the example) and is not an indicator of the distance between the estimate of the posterior mean of $f_\zeta(\hat{X}(t))$ and its "true" value $f_\zeta(\bar{X}(t))$. Dependent on the different realisations of a_0 the posterior pdf on the same set of observations can differ strongly in the form, and that is of course reflected in the posterior variance. A very large sample size is needed in order to correctly estimate the integral over the space of such a large dimensional model state variable. For the moderate sample size, the quality of the importance sampling estimate of the posterior variance is very questionable for the dependent sample. The calculation of the importance sampling weights is a computationally expensive procedure, and in practice, it is not feasible to perform it for a very large sample size.

The curvature of the posterior pdf of $\hat{X}(t_0)$ is much more sensitive to the amount of the assimilated observations than to the different realisations of the initial first guess field and/or to the different realisations of the observations. The curvature of the posterior

TABLE 4. The spatial averaged square error of the time propagated posterior mode α_t (\tilde{SE} , the first row), the posterior predictive mean estimated by the importance sampling of size $N_{sample} = 100$ ($\tilde{SE}^{i.s.,100}$, the second row) and the posterior predictive mean estimated by importance sampling of size $N_{sample} = 12$ ($\tilde{SE}^{i.s.,12}$, the third row) as estimators of the "true" model state. The time-window smoother with a "short" time window ($N_{ass} = 8$ observation windows) is used. The result is valid at the end of the assimilation window $t = t_{N_{ass}}$. The error is calculated for the u -wind component (the third column), for the v -wind component (the fourth column) and for the geopotential (the fifth column). The result is presented for the observations simulated by the three different non-linear observation operators nlZ_1 , nlZ_2 , nlZ_3 . The observations are of "high" precision.

The "short" time window; The "high" prec.data		u -wind comp.	v -wind comp.	geopotential
nlZ_1	\tilde{SE}	0.000156	0.6430	608.9
	$\tilde{SE}^{i.s.,100}$	0.000268	1.1619	617.2
nlZ_2	\tilde{SE}	0.000155	0.6641	526.6
	$\tilde{SE}^{i.s.,100}$	0.000305	1.0732	352.9
	$\tilde{SE}^{i.s.,12}$	0.000231	0.6949	535.9
nlZ_3	\tilde{SE}	0.000156	0.6631	565.8
	$\tilde{SE}^{i.s.,100}$	0.000175	0.7940	580.1
	$\tilde{SE}^{i.s.,12}$	0.000226	0.5007	573.5

pdf of $\hat{X}(t_0)$ represents well the precision of the posterior mode estimate. In the example (Figure 29, Figure 30), the total sum of the eigenvalues of \hat{V}_0^R taken for the different realisations of a_0 varies from 1214.4 to 1231.7 with a mean value 1223.0 and a variance 22.88.

The results of the comparison between the posterior mode propagated in time to the end of the data assimilation procedure $\alpha_{t_{N_{ass}}}$ and the posterior predictive mean of $\hat{X}(t_{N_{ass}})$, valid at the same time moment and estimated by importance sampling, are summarised in Table 3, Table 4 and Table 5. Table 3 presents the results of the comparison when the "short" time window smoother ($N_{ass} = 8$) was used to estimate the posterior mode by assimilating the "low" precision observations. The spatial average squared error valid at the time moment is shown for the u -wind component, the v -wind component and the geopotential and from assimilation of observations simulated with the three different non-linear observation operators nlZ_1 , nlZ_2 , nlZ_3 . To estimate the posterior predictive mean, the importance sampling of two different sizes ($N_{sample} = 12$ and $N_{sample} = 100$) were used. When a small amount of the "low" precision observations are assimilated, the posterior predictive mean and the posterior mode propagated in time are comparable in their efficiency to estimate the "true" model state. The posterior predictive mean (estimated from the "large" size sample) comes closer to the "true" model state with respect to the spatial average squared error estimating both the v -wind component and the geopotential for the case of the non-linear observation operators nlZ_2 and nlZ_3 . However, a reasonably large sample size is required. The posterior predictive mean estimated by importance sampling with $N_{sample} = 12$ gives a misleading estimate of the "true" model state for the case of all three non-linear observation operators.

Table 4 presents similar results as Table 4, but with the use of the "high" precision observations. Again, the "short" time window smoother was used to estimate the posterior mode of the model state variable. Now the observations have stronger influence on the form of the posterior pdf of the model state, and the posterior mode of the pdf comes closer to the "true" model state. The posterior pdf of the model state is much sharper now. When a small sample size for the importance sampling is used, the sample members are sampled in the close vicinity of the posterior mode of the pdf. The posterior predictive mean estimated from the "small" sample is close to the posterior mode of the pdf propagated in time. The posterior predictive mean is a slightly noisier estimate than the posterior mode propagated in time, and this is a common problem for all sampling estimates. The posterior predictive mean estimated from the "large" sample is more influenced by the information coming from the tails of the posterior pdf and it is different from the estimate of the "true" model state based on the posterior mode. The efficiency of the estimate, with respect to the spatial average squared error, of the "v"-wind component indicates the closeness of the spectral wave components of the estimate for $k > 0$ to their "true" values for the one-dimensional shallow water model. Due to this, we consider that the posterior mode propagated in time is a more efficient estimate of the "true" model state than the posterior predictive mean for the experiments presented in Table 4.

Table 5 presents the result of the comparison when the "long" time window smoother in three different configurations is used to estimate the mode of the posterior pdf of the model state for assimilation of "low" precision observations. The efficiency of the posterior predictive mode propagated to the end of the assimilation procedure (40 observation windows) is compared with the posterior predictive mean valid at the same time and estimated by importance sampling with sample size $N_{sample} = 100$ for the three different observation operators. It can easily be noticed, that the time window smoother in Configuration "c" (the same initial forecast error covariance matrix at the beginning of each "short" assimilation window) is a clear outlier. The posterior predictive mean is a more efficient estimate of the "true" model state than the posterior mode of the last assimilation cycle propagated in time, when Configuration "b" is used. For Configuration *a*, the posterior mode propagated in time is a more efficient estimate.

In summary we can say that the importance sampling estimation of the posterior mean (and the posterior predictive mean) is the only type of estimator, among those discussed in this thesis, which attempts to estimate the posterior mean in the case of non-linear observation operators. The other types of estimators, the extended Kalman filter, the bias corrected Kalman filter, the ensemble Kalman filter and the time window smoother estimate the posterior predictive mode. The results shown in the discussion at the end of this section give preference to the estimator of the posterior mode, because the repeated samples principle is not applicable here for the validation of the estimators. But in a general sense, the discussion concerns particularities of the one dimensional shallow water model, which is considered here, and it is oversimplified in many respects. The most important limitations are the nearly linear dynamics, the perfect model assumption and the simulated observations. Applying the methods of data assimilation discussed here to a more realistic model, the posterior predictive mean estimate could turn out to be more powerful. The example with the strongly non-linear transform that was applied to the model state variable (Figure 30) is an indication of this. If the model dynamics would not be perfect, the posterior mode estimate would never come very close to the maximum

TABLE 5. The spatial average squared error of the time propagated posterior mode α_t (\tilde{SE}) and the posterior predictive mean estimated by the importance sampling of size $N_{sample} = 100$ ($\tilde{SE}^{i.s.,100}$) as estimators of the "true" model state. The time-window smoother with a "long" time window ($N_{ass} = 40$ observation windows) is used in three different configurations: Configuration *a* (rows 1,2), Configuration *b* (rows 3,4), Configuration *c* (the rows 5,6). The result is valid at the end of the assimilation window $t = t_{N_{ass}}$. The error is calculated for the *u*-wind component (the fourth column), for the *v*-wind component (the fifth column) and for the geopotential (the sixth column). The result is presented for the observations simulated by the three different non-linear observation operators nlZ_1 , nlZ_2 , nlZ_3 . The observations are of "low" precision.

	The "long" time window; The "low" prec.data		<i>u</i> -wind comp.	<i>v</i> -wind comp.	geopotential
nlZ_1	Configuration <i>a</i>	\tilde{SE}	0.000023	0.3086	561.6
		$\tilde{SE}^{i.s.,100}$	0.000062	0.5582	552.2
	Configuration <i>b</i>	\tilde{SE}	0.000054	0.2923	569.3
		$\tilde{SE}^{i.s.,100}$	0.000060	0.3359	357.7
	Configuration <i>c</i>	\tilde{SE}	0.000478	7.4863	1111.4
		$\tilde{SE}^{i.s.,100}$	0.001463	11.8993	3387.3
nlZ_2	Configuration <i>a</i>	\tilde{SE}	0.000025	0.3302	598.2
		$\tilde{SE}^{i.s.,100}$	0.000044	0.4290	414.7
	Configuration <i>b</i>	\tilde{SE}	0.000054	0.3096	642.4
		$\tilde{SE}^{i.s.,100}$	0.000079	0.4657	459.4
	Configuration <i>c</i>	\tilde{SE}	0.000463	7.4265	1173.1
		$\tilde{SE}^{i.s.,100}$	0.001397	11.7583	2472.7
nlZ_3	Configuration <i>a</i>	\tilde{SE}	0.000023	0.3102	520.4
		$\tilde{SE}^{i.s.,100}$	0.000057	0.5019	591.4
	Configuration <i>b</i>	\tilde{SE}	0.000054	0.2887	545.9
		$\tilde{SE}^{i.s.,100}$	0.000075	0.4367	401.2
	Configuration <i>c</i>	\tilde{SE}	0.000472	7.4119	1152.5
		$\tilde{SE}^{i.s.,100}$	0.001218	10.0844	2189.0

likelihood estimate of model state variable, and therefore would never come close to the "true" model state, which would give rise to the real (not simulated) observations.

5.4. The estimate of the posterior predictive mode of $\hat{X}(t)$ provided by different methods as estimators of $\bar{X}(t)$. As we have already mentioned, the time-window smoother, the extended Kalman filter, the bias corrected Kalman filter and the ensemble Kalman filter, all provide different estimators of the posterior predictive mode of $\hat{X}(t)$. Therefore they can easily be compared between themselves. Applying different types of filters, the corresponding analysed states (after the tangent-linear normal mode initialisation transform) valid at the time moment t_i , $1 \leq i \leq N_{ass}$ are a_i (88) for the extended Kalman filter, a_i^m (106) for the bias-corrected Kalman filter and $x^{as}(t_i)$ (130) for the ensemble Kalman filter. They all provide the estimate of the posterior predictive mode of $\hat{X}(t_i)$, $1 \leq i \leq N_{ass}$. Applying the time-window smoother the estimate of the posterior

predictive mode of $\hat{X}(t_i)$ is given by the posterior mode estimate $\hat{\alpha}(t_i)$ propagated in time (the posterior mode $\hat{\alpha}(t_0)$ is estimated by the iterative solution of equation (117)). The corresponding spatial average squared errors of estimators for the u -wind component, the v -wind component and the geopotential SE^{KF} , SE^{bc} , SE^{eKF} and \tilde{SE} valid at the end of the "short" ($N_{ass} = 8$) and at the end of the "long" ($N_{ass} = 40$) assimilation time window are given in Table 6. We illustrate performance of the ensemble Kalman filter in three different configuration: for the double ensemble Kalman filter with a sample of size $N_{sample} = 100$ ($SE^{eKF,100}$, (2 s. m.)), for the double ensemble Kalman filter with a sample of size $N_{sample} = 12$ ($SE^{eKF,12}$ (2 s. m.)), and for the single ensemble Kalman filter with a sample of size $N_{sample} = 12$ ($SE^{eKF,12}$ (1 s. m.)). In the case of the "long" time window, besides the performance of the time-window smoother in Configuration *a* (\tilde{SE}), the performance of the time-window smoother in Configuration *b* ($\tilde{SE}(Config. b)$) and in the Configuration *c* ($\tilde{SE}(Config. c)$) are shown as well. The results shown here are for the data simulated by the non-linear observation operator nlZ_3 . The results of the comparison are nearly the same using the other non-linear observational operators. All the methods provide almost identical estimators of $\hat{X}(t_i)$ in the case of the linear observational operator due to weak non-linearity of the dynamical propagator.

Performing the comparison of the estimation of the "true" state $\bar{X}(t)$ provided by the different methods, we use the the extended Kalman filter as a reference. From what we can see in the table, when "low" precision data are assimilated, the bias corrected Kalman filter gives a very small but still an improvement in the estimation of the "true" state $\bar{X}(t)$ compared to what the extended Kalman filter provides. In the case of the "high" precision data, the spatial average squared error for the v -wind component field estimator is larger for bias-corrected Kalman filter. Performing different experiments we have noticed that the analysed state obtained by means of the bias-corrected Kalman filter comes slightly closer to the observations than the one obtained by the extended Kalman filter with respect to the measure by the spatial average squared error. The estimation of the geopotential field becomes better (or even "too good" for the "high" precision data) with the bias corrected Kalman filter, but the representation of dynamics suffers. A good representation of the dynamics in the analysed state is very important for the quality of the forecast made from the analysed state. In the one-dimensional shallow water model, the mean value of the geopotential field $\phi_0(t)$ is very weakly correlated with the other spectral components of the model state variable. To estimate the mean value of the geopotential ϕ_0 with a high precision, the direct observations of it are required, and it is not possible to obtain them when the observation operator is non-linear in geopotential. The spectral components of v -wind component with wave numbers greater than 0 have a nearly linear relationship with the corresponding spectral components of the geopotential for the model. When the estimator of the "true" model state is close to its "true" value for the "v"-wind component field, it estimates well also the higher order spectral components of the geopotential. If the spatial average squared error for the geopotential is bigger at the same time, its mainly indicates the poor estimation of the mean value of the geopotential field.

Even for the assimilation of "low" precision observations, the improvement of the estimation of $\bar{X}(t)$ given by the bias-corrected Kalman filter compared to one provided by the extended Kalman filter is quite small. In any case, we are satisfied, that the refinement in the calculation of the innovations have forced the analysed state to come closer to observations in spite of all approximations and simplifications which had to be accepted in the derivation of the bias-corrected Kalman filter. Probably, if we would try the method

		u -wind comp.	v -wind comp.	geopotential
The "short" time window; The "low" prec. data	SE^{KF}	0.000884	4.3607	3943.7
	SE^{bc}	0.000764	4.1055	3734.7
	$SE^{eKF,100}(2\text{ s. m.})$	0.000957	4.0257	3985.0
	$SE^{eKF,12}(2\text{ s. m.})$	0.001392	5.2235	2182.7
	$SE^{eKF,12}(1\text{ s. m.})$	0.001385	36.8630	12105.0
	\tilde{SE}	0.001045	3.9258	4044.3
The "long" time window; The "low" prec. data	SE^{KF}	0.000064	0.3291	549.2
	SE^{bc}	0.000060	0.3241	527.1
	$SE^{eKF,100}(2\text{ s. m.})$	0.000072	0.5865	535.3
	$SE^{eKF,12}(2\text{ s. m.})$	0.000161	1.4171	244.2
	$SE^{eKF,12}(1\text{ s. m.})$	0.000560	6.1458	11040.5
	$\tilde{SE}(\text{Config. a})$	0.000023	0.3102	520.9
	$\tilde{SE}(\text{Config. b})$	0.000053	0.2886	545.9
	$\tilde{SE}(\text{Config. c})$	0.000472	7.4119	1152.5
The "short" timw window; The "high" prec. data	SE^{KF}	0.000100	0.9485	571.2
	SE^{bc}	0.000081	0.9604	532.4
	$SE^{eKF,100}(2\text{ s. m.})$	0.000099	0.5959	639.9
	$SE^{eKF,12}(2\text{ s. m.})$	0.000213	1.3582	329.1
	$SE^{eKF,12}(1\text{ s. m.})$	0.000389	3.1713	1719.1
	\tilde{SE}	0.000156	0.6632	566.0
The "long" time window; The "high" prec. data	SE^{KF}	0.000018	0.0149	63.3
	SE^{bc}	0.000017	0.0153	60.4
	$SE^{eKF,100}(2\text{ s. m.})$	0.000015	0.0490	64.4
	$SE^{eKF,12}(1\text{ s. m.})$	0.000031	0.1884	32.2
	$SE^{eKF,12}(1\text{ s. m.})$	0.000116	0.4710	762.9
	$\tilde{SE}(\text{Config. a})$	0.000016	0.0143	62.7
	$\tilde{SE}(\text{Config. b})$	0.000017	0.0144	61.6
	$\tilde{SE}(\text{Config. c})$	0.000275	1.3555	216.0

TABLE 6. The spatial average squared error of the different posterior predictive mode estimates as estimators of the "true" model state valid at the end of the "short" assimilation time window ($N_{ass} = 8$ observation windows) and at the end of the "long" assimilation time window ($N_{ass} = 40$ observation windows) for the "low" precision observations and for the "high" precision observations. Performing the data assimilation with the "short" assimilation time window the comparison is performed between the extended Kalman filter (SE^{KF}), the bias corrected Kalman filter (SE^{bc}), the double ensemble Kalman filter with an ensemble of size $N_{sample} = 100$ ($SE^{eKF,100}(2\text{ s. m.})$), the double ensemble Kalman filter with an ensemble of size $N_{sample} = 12$ ($SE^{eKF,12}(2\text{ s. m.})$), the single ensemble Kalman filter with an ensemble of size $N_{sample} = 12$ ($SE^{eKF,12}(1\text{ s. m.})$) and the time-window smoother (\tilde{SE}). Performing the data assimilation with the "long" assimilation time window, the comparison is performed between the extended Kalman filter (SE^{KF}), the bias corrected Kalman filter (SE^{bc}), the double ensemble Kalman filter with an ensemble of size $N_{sample} = 100$ ($SE^{eKF,100}(2\text{ s. m.})$), the double ensemble Kalman filter with an ensemble of size $N_{sample} = 12$ ($SE^{eKF,12}(2\text{ s. m.})$), the single ensemble Kalman filter with an ensemble of size $N_{sample} = 12$ ($SE^{eKF,12}(1\text{ s. m.})$), the time-window smoother in Configuration a ($\tilde{SE}(\text{Config. } a)$), the time-window smoother in Configuration b ($\tilde{SE}(\text{Config. } b)$) and the time-window smoother in Configuration c ($\tilde{SE}(\text{Config. } c)$). The observations were simulated by the non-linear observation operator nlZ_3 .

in a more realistic model with stronger non-linearity in the dynamical evolution, the improvement of the estimation of the "true" model state by the bias-corrected Kalman filter would be even higher compared to the extended Kalman filter.

In fact, both the extended Kalman filter and the bias-corrected Kalman filter slightly over-fit data. The analysed state provided by both two filters comes closer to the observations than the "true" model state would have done, especially in the beginning of the data assimilation procedure. As an indication of the distance of an estimator to the observations we use the quantity

$$(157) \quad d_{obs}(\hat{X}, N_{ass}) = \sum_{j=1}^{N_{ass}} (y_j - Z(\hat{X}(t_j)))^T H^{-1} (y_j - Z(\hat{X}(t_j)))$$

where N_{ass} is the number of observation windows during the time-window.

Applying the time-window smoother in Configuration *a*, the distance $d_{obs}(\hat{\alpha}, N_{ass})$ is close to the distance $d_{obs}(\bar{X}, N_{ass})$. But the time window smoother has one serious limitation. The iteratively determined posterior mode of $\hat{X}(t_0)$ is much noisier than the "true" state $\bar{X}(t_0)$, if the amount of the assimilated data (i.e. the length of the time-window) is small. The larger the amount of assimilated data, the better the noise due to observation errors is filtered out, especially if some strongly erroneous data have fallen into the time-window. In the sequential application of the time-window smoother, the dynamical updating of the initial forecast error covariance matrix at the beginning of each time window (Configuration *b*) takes care of the problem. This dynamical updating controls the distribution of the spectral energy among different wave numbers. When the initial forecast error covariance matrix was left unchanged at the beginning of each data assimilation window (Configuration *c*), a very noisy field was obtained after several sequential applications of the time-window smoother. The problem became acute for assimilation of "high" precision data. (After 5 sequential applications of the time-window smoother in Configuration *c*, the data assimilation procedure corrupted when the "high" precision observations simulated with n/Z_1 were assimilated). An additional constraint on the smoothness of the posterior mode estimate must be imposed on the time-window smoother if Configuration *c* is going to be used. The "long" time-window smoother is very expensive computationally, and it is unfeasible for a full scale model. The sequential application of the "short" time-window smoother with an updated initial forecast error covariance matrix (Configuration *b*) gives very good results and estimates $\bar{X}(t)$ almost as well as the "long" time-window smoother does. Besides that, as we have stressed in the previous section, the posterior mean at the beginning of the last time-window estimated through importance sampling provides an even better estimate of $\bar{X}(t)$ in the case Configuration *b* for the time-window smoother is used. However, as we can see from Table 6 the application of the time-window smoother does not give the significant improvement in the estimation of the "true" model state. When the assimilation was performed during the "short" time window, the time window smoother gave even worse estimation (with respect to the space averaged squared error) than the extended Kalman filter.

The ensemble Kalman filter is the cheapest and the most feasible method for a full scale problem, because the whole necessary information is stored in the ensembles themselves. The ensemble Kalman filter allows for a non-linear dynamical evolution, as the time window smoother does through the iterative adjustment to observations assimilated at different time moments, but it makes an implicit linearisation of the observation operator with the improved estimate of the innovation vector (as the bias corrected Kalman filter does). However, a large sample size is required in order to achieve a good quality of

an estimation of the "true" model state $\bar{X}(t)$ by means of the ensemble Kalman filter. For example, the estimation of $\bar{X}(t)$ provided by the double ensemble Kalman filter with a sample of size $N_{sample} = 100$ (a large value compared to the dimensionality of the model state variable) is close to the estimation of $\bar{X}(t)$ provided by the extended Kalman filter. Using the single ensemble Kalman filter with such a large sample, the result would be nearly the same. The quality of the estimation of $\bar{X}(t)$ is nearly the same as using the extended Kalman filter, which requires an explicit time propagation of the forecast error covariance matrix. From a computational point of view, an even worse situation occurs when the time-window smoother is applied. The large dimensional forecast error covariance matrix, as well as the tangent-linear propagators from one observation window to another must be stored during the assimilation time-window. Taking into account these problems, the ensemble Kalman filter becomes even more attractive. However, if the estimation of $\bar{X}(t)$ is to be based on a small sample ($N_{sample} = 12$ here), the result can be misleading. The double ensemble Kalman filter over-fits observations of geopotential, and describes dynamics poorly. The single ensemble Kalman filter with a small sample, due to the heavy underestimation of the forecast error covariance matrix, does not extract enough information from the observations, and does not provide an acceptable estimation of the "true" model state.

In conclusion, we would like to stress that the results represented in Table 6 correspond to a particular realisation of the sampling. Certainly, for some other realisations the estimation of the "true" model state can look much better for the small size ensemble Kalman filter. The results shown in Table 6, are valid given the particular realisation of the initial first-guess field a_0 . But the relative behaviour of these different "deterministic" estimators of the "true" model state does not seem to depend (or depends very weakly) on the particular realisation of a_0 .

5.5. Validation of the future forecasts of the "true" model state obtained by means of the different data assimilation approaches. In the previous subsections we have tried to validate the different data assimilation approaches (the extended Kalman filter, the bias corrected Kalman filter, the ensemble Kalman filter and the time-window smoother) from the perspective of the estimation of the "true" model state at the end of the assimilation time window, i.e. the time moment up to which observations from the "true" model state are available. The aim of the data assimilation procedure is to extract the best possible amount of information about the underlying "true" model state from the available observations, to merge the observed information with theoretical knowledge about the "true" model state and to construct an estimate of the "true" model state. To construct an accurate estimate of the unobservable model state variable is an important task by itself. In addition, this estimate is used as an initial model state for the future forecasting based on the same available observations. The performance of the forecasts constructed by the different data assimilation approaches is probably an even more important measure of how good the particular data assimilation approach is.

In Figure 31 the performance of the future forecast of the "true" model state, obtained by the different "deterministic" data assimilation approaches discussed above, is illustrated. Values of the spatial average squared error of prediction for the "u"-wind component, the "v"-wind component and the geopotential are represented by bars in the diagrams. The groups of bars correspond to the time at the end of the different prediction periods. The time is measured in the number of the observation windows falling into the prediction period, and this number is indicated on the horizontal axes. So the first groups of bars show the errors of prediction based on the different approaches evaluated at the end of the prediction period corresponding to four observation windows, the second groups of

bars are evaluated at the end of the prediction period corresponding to eight observation windows (the length of the "short" time window). Totally the evaluation of the prediction is made at the end of five different prediction periods, corresponding to the lengths of 4, 8, 20, 40, and 76 observation time windows. The diagrams to the left illustrate the performance of the forecast based on the analysed state obtained when data assimilation was performed during a period corresponding to the "long" time window, which contains 40 observation windows. The 6 bars in each group represent the space averaged squared error of the prediction in the following order: the extended Kalman filter, the bias corrected Kalman filter, the time-window smoother in Configuration *a*, the time window smoother in Configuration *b*, the double ensemble Kalman filter with $N_{sample} = 100$ ensemble members and the double ensemble Kalman filter with $N_{sample} = 12$ ensemble members. The diagrams to the right illustrate the performance of the forecasts based on the analysed state obtained when data assimilation was performed during the "short" time window, which contains only $N_{ass} = 8$ observation windows. The 5 bars in each group represent the spatial average squared error of the prediction in the following order: the extended Kalman filter, the bias corrected Kalman filter, the time-window smoother, the double ensemble Kalman filter with $N_{sample} = 100$ ensemble members and the double ensemble Kalman filter with $N_{sample} = 12$ ensemble members.

The assimilated observations were of "low" precision and were simulated using the non-linear observation operator nlZ_3 .

When the construction of the initial state for the prediction was based on the observations assimilated during the "long" time window, the best verification scores with respect to the spatial average error were obtained with the time window smoother in Configuration *a* (the third bar in each group on the left diagrams). This is the result we can expect under the perfect model assumption. When such a large amount of data is assimilated, the posterior pdf is very sharp and the posterior mode is indeed located close to the "true" model state. The behaviour of the time window smoother in Configuration *b* (the fourth bar in each group) is slightly worse compared to the time window smoother in Configuration *a*. But still during all these long periods of prediction, the time window smoother in Configuration *b* remains superior compared to the extended Kalman filter (the first bar in each group). The bias corrected Kalman filter (the second bar in each group) provides a slightly better prediction of the geopotential, with respect to the spatial average squared error, compared to the time window smoother in Configuration *b*. However, the prediction of the dynamics (the wind components) becomes worse. We consider, that a better prediction of dynamics has a higher priority than a better prediction of the geopotential for the one dimensional shallow water model. The prediction performed by the means of the ensemble Kalman filter has large errors for the dynamics of the model. For the double ensemble Kalman filter with an ensemble of size $N_{sample} = 12$ (the sixth bar in each group), the spatial average squared errors of the *u*-wind and the *v*-wind components are several times larger than for the extended Kalman filter. We could expect this due to the strong overestimation of the forecast error covariance matrix that we have noticed. The behaviour of the double ensemble Kalman filter with an ensemble of size $N_{sample} = 100$ (the fifth bar in each group) is reasonably good taking the computational cheapness of the method into account. We have not compared the quality of the prediction performed by means of the time-window smoother in Configuration *c* and the one performed by means of the single ensemble Kalman filter with a small size ensemble. Already when the validation of the estimation of the "true" model state at the end of the data assimilation window was performed, it was clear that these methods are outliers.

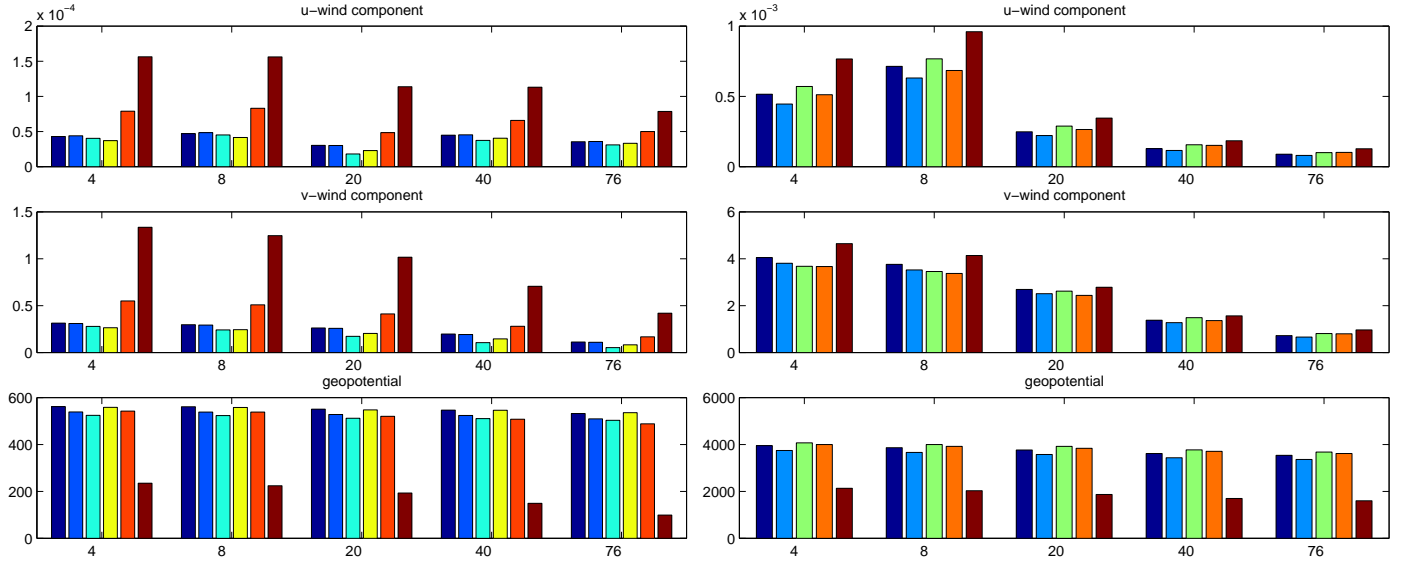


FIGURE 31. The spatial average squared error of prediction for the u -wind component, the v -wind component and the geopotential obtained by the different data assimilation approaches. The bar diagrams represent the squared errors of prediction at the end of the different prediction periods. The length of the prediction period is measured in the number of observation windows falling into the prediction period and this number is indicated on the horizontal axes. The diagrams to the left illustrate the performance of forecasts based on the analysed state obtained with data assimilation over the "long" time window. The 6 bars in each group represent the spatial average squared error of the prediction in the following order: the extended Kalman filter, the bias corrected Kalman filter, the time-window smoother in Configuration a , the time window smoother in Configuration b , the ensemble double Kalman filter with $N_{sample} = 100$ ensemble members, the double ensemble Kalman filter with $N_{sample} = 12$ ensemble members. In the diagrams to the right the initial state for the prediction is based on the data assimilated during the "short" time window. The 5 bars in each group represent the spatial average squared error of the prediction in the following order: the extended Kalman filter, the bias corrected Kalman filter, the time-window smoother, the double ensemble Kalman filter with $N_{sample} = 100$ ensemble members and the double ensemble Kalman filter with $N_{sample} = 12$ ensemble members.

When the initial state for the prediction is based on the observations assimilated during the "short" time window, containing only $N_{ass} = 8$ observation windows, the relative performance of the different approaches changes (the right diagrams). The amount of assimilated observations is not large, and even with the perfect model assumption, the mass of the posterior pdf of $\hat{X}(t_0)$ is not concentrated around a mode. As it is indicated by the large eigenvalues of the matrix of curvature around the mode of the posterior pdf, the posterior mode can be located far away from the "true" model state $\bar{X}(t_0)$. The time-window smoother (the third bar in each group) does not provide the best prediction anymore. Being quite good for the short prediction period, it becomes worse with increasing prediction length. High values of the prediction error for the u -wind component indicate that the predicted model state is noisier than the "true" model state. As we have noticed, the iterative adjustment to the observations creates a noisier estimate of the

”true” model state than the one obtained with the extended Kalman filter (the first bar in each group), if a small amount of data is assimilated. An additional constraint on the smoothness of the estimate is needed. In fact, the normal mode initialisation procedure we have used to filter out the shallow water gravity waves, is not the only one which can be used to balance the estimate of the model state. Dealing with a realistic full-scale model, a digital filter is often used. Probably, such a filter would take better care of the noise generated during the construction of the estimate of the model state. Now the best prediction with respect to the space averaged squared error is given by the bias corrected Kalman filter (the second bar in each group). Again the behaviour of the double ensemble Kalman filter with an ensemble of size $N_{sample} = 100$ (the fourth bar in each group) is very reasonable, and it is much better than of the double ensemble Kalman filter with an ensemble of size $N_{sample} = 12$ (the fifth bar in each group).

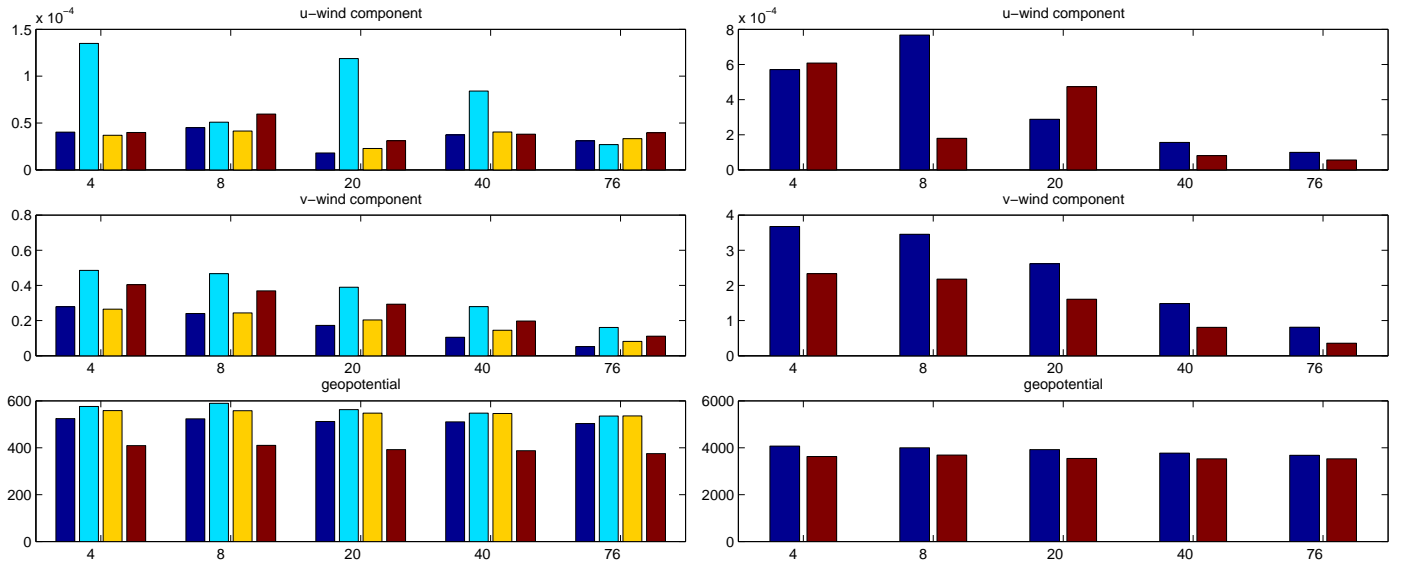


FIGURE 32. The spatial average squared error of prediction for the u -wind component, the v -wind component and the geopotential based on the posterior mode and the posterior mean estimates. The bar diagrams represent the squared errors at the end of the different prediction periods. The length of the prediction periods is measured in the number of the observation windows falling into the prediction period, and this number is indicated on the horizontal axes. The diagrams to the left illustrate the performance of forecast based on the analysed state obtained with data assimilation over the ”long” time window. The 4 bars in each group represent the spatial average squared error of the prediction in the following order: the posterior mode estimate propagated in time from the time window smoother in Configuration a , the posterior predictive mean estimate using importance sample from the time window smoother in Configuration a , the posterior mode estimate propagated in time from the time window smoother in Configuration b and the posterior predictive mean estimate using importance sample from the time window smoother in Configuration b . In the diagrams to the right the initial state for the prediction was based on data assimilation during the ”short” time window. The 2 bars in each group represent the spatial average squared error of the prediction in the following order: the posterior mode estimate propagated in time from the time window smoother and the posterior predictive mean estimate using importance sample from the time window smoother.

We would finally like to refer to Figure 32, where the prediction obtained by the posterior predictive mean estimated from the importance sampling is validated against the prediction given by the time propagation of the posterior mode of $\hat{X}(t_0)$. The structure of the diagrams in Figure 32 is the same as in Figure 31. The left diagrams illustrate the performance of the prediction for which the initial model state was based on observations assimilated during the "long" assimilation window, which contains $N_{ass} = 40$ observation windows. A bar in each group represents the spatial average squared error of the prediction. The bars in each group on the left diagrams are ordered as follows: the time propagation of the posterior mode obtained with the time window smoother in Configuration *a*, the posterior predictive mean estimated by $N_{sample} = 100$ members importance sampling using the time window smoother in Configuration *a*, the time propagation of the posterior mode obtained with the time window smoother in Configuration *b* and the posterior predictive mean estimated by $N_{sample} = 100$ members importance sampling using the time window smoother in Configuration *b*. The right diagram illustrate the performance of the prediction for which the initial model state was based on observations assimilated during the "short" assimilation window, which contains only $N_{ass} = 8$ observation windows. The bars in each group on the left diagrams are ordered as follows: the time propagation of the posterior mode obtained with the time window smoother and the posterior predictive mean estimated by $N_{sample} = 100$ members importance sampling using the time window smoother.

We can easily see that as soon as the posterior mode estimate comes close enough to the "true" model state, the construction of the posterior predictive mean estimate (the second and the fourth bars in the left diagrams) does not help to improve the prediction of the "true" model state. However, considering the possible application to more realistic models without the perfect model assumption, it is likely that the posterior pdf of $\hat{X}(t_0)$ would never be so sharp around its mode and that the mode would not come so close to the $\bar{X}(t_0)$. When the posterior mode of $\hat{X}(t_0)$ does not come close to the its "true" value, the deviation of the propagated posterior mode from the "true" model state will just increase in time.

It must be mentioned, that the reduction of height of the error bars with increased length of the prediction in the diagrams does not mean that the prediction becomes better. This simply indicates a problem with the dynamical development by the one-dimensional shallow water model, as it has been implemented for this study. The total model state energy is not conserved. The posterior predictive mean (the second bar in each group to the right), estimated by importance sampling, helps to improve the prediction as compared to the one obtained by propagation of the posterior mode. The situation is similar to the one we observed when the aspects of estimation of a strongly non-linear transform of the model state was discussed. However, accepting the posterior predictive mean as a point estimate of the model state, we need always to be aware of the problem that the estimate is not at all supposed to provide an existing model state, satisfying the physical balance requirements. The possibility to construct an estimate of a small-dimensional quantity of interest by itself is a much stronger feature of the importance sampling than the construction of the posterior predictive mean estimate of the whole model state variable.

6. CONCLUSIONS

The main aim of this thesis was to investigate possibilities and limitations of certain extensions of the Kalman filter idea for improved treatment of non-linearities with application to meteorological data assimilation. We have studied five different approaches: the

extended Kalman filter, the bias corrected Kalman filter, the time-window smoother, the ensemble Kalman filter and the importance sampling estimate of the posterior predictive mean of the model state variable. We have applied these different approaches for meteorological data assimilation within the framework of a one-dimensional shallow water model under the perfect model assumption. The observations were simulated by linear as well as non-linear observation operators. The choice of a one-dimensional shallow water model as a framework for meteorological data assimilation have had negative as well as positive influences on the study. The one-dimensional shallow water model is a very simplified atmospheric model, and does not describe many important features of the atmospheric development. It simulates, however, important characteristics of large-scale atmospheric flow, and the interpretation of results is easier than in a more complex model. Two main parts of the wave motion, the geostrophic and the ageostrophic flows, are clearly separated into the v - and u - wind components. Other limitations of the study are the perfect model assumption, the model dynamics that does not preserve total energy and the use of simulated observations only.

In the comparison between the different approaches, the extended Kalman filter was used as a reference. The bias corrected Kalman filter can be considered as a refinement of the extended Kalman filter with possibilities to handle non-linearities in the dynamics as well as in the observation operators. The second order closure is used to estimate the dynamical evolution of the posterior predictive mean of the model state variable and also to correct the bias of the innovation vector. The analysed state obtained with the bias corrected Kalman filter comes closer to the observations as compared to the analysed state obtained with the extended Kalman filter in a general sense due to bias correction of the innovation vector. This gives a positive effect for estimation of the "true" model state, when assimilated observations are of lower precision than the first-guess state projected to the space of observations. The forecast provided by the bias corrected Kalman filter is closer to the "true" state with respect to a spatial average squared prediction error compared with the forecast provided by the extended Kalman filter. It is difficult to judge about the positive effect of the second order closure applied in the estimation of the dynamical propagation of the posterior predictive mean, due to the weak non-linearity of the chosen dynamical model. We would like to stress that the bias corrected Kalman filter, as well as the extended Kalman filter and the ensemble Kalman filter, provide estimates of the posterior predictive mode of the model state variable rather than estimates of the posterior predictive mean of the model state variable. All these methods make explicit or implicit use of a linearization of the observation operator.

Among the methods considered in this study, the time-window smoother provides the best filtering of observation errors, if the amount of assimilated observations is large. The time window smoother estimates the posterior mode of the model state variable valid at the beginning of the time window as a result of an iterative adjustment to the available observations. Under the perfect model assumption, if the amount of assimilated data is large, the time development of the posterior mode of the model state estimated by the time-window smoother is the best estimate of the "true" model state with respect to the spatial average squared error. If the amount of assimilated data is small, the estimate of the posterior mode of the model state as well as its dynamical evolution appears to be too noisy. However, the reason of the problem could lie not only in the time smoother itself, but mainly in the normal mode initialisation procedure that we have used to filter out gravity waves from the analysed state. The normal mode initialisation procedure could possibly work as a noise amplifier. When the time-window smoother is applied sequentially, under the perfect model assumption and on the "short" assimilation windows, the dynamical updating of the initial forecast error covariance matrix at the

beginning of each time window seems to be very important. The dynamical updating of the initial forecast error covariance matrix at the beginning of each assimilation window improves the noise filtering.

The ensemble Kalman filter is a very attractive method because it is very cheap from a computational point of view, and it still provides a comparably good estimate of the "true" state. However, the data assimilation must be performed with a relatively large ensemble size. The sample size must be large enough to represent well the properties of the whole population. The single ensemble Kalman filter with a small size sample underestimates the posterior predictive variance of the model state and the assimilation is insensitive to the observations. The double ensemble Kalman filter with a small size sample tends to overestimate the posterior predictive variance of the model state and therefore it tends to over-fit the observations, if the estimates of the population variance provided by the two samples differ strongly. When a relatively large ensemble size is used, such that the ensemble represents well the properties of the population, both the double and the single ensemble Kalman filter provides comparably good estimates of the "true" model state. The ensemble Kalman filter constructs the analysed state with use of an implicit linearisation of the observation operator, while it preserves the non-linear dynamics. With the one-dimensional shallow water model, the dynamical development from one observation window to another one is close to the linear one. After a large number of observations have been assimilated, the ensemble Kalman filter gives very similar results to the ones obtained by using the extended Kalman filter. The ensemble members of the analysed state come close in distribution to the Gaussian approximation of the posterior predictive pdf of the model state provided by the extended Kalman filter. The members of the ensemble are not sampled from the posterior pdf exactly and therefore the ensemble Kalman filter is not good for a probabilistic inference about the model state.

The importance sampling uses the results provided by the time-window smoother (the posterior mode and the curvature around it) and gives wide possibilities for probabilistic inference about smaller dimensional non-linear transforms of the model state variable. In a certain sense the importance sampling can be used as a diagnostic tool to detect essential deviations of the posterior pdf of the model state from its Gaussian approximation provided by the time-window smoother. Again, for a good quality of the inference, a relatively large sample size is required, large enough to pick up essential particularities of the posterior pdf compared to its Gaussian approximation. The estimate of the posterior predictive mean of the model state variable appears to be a less efficient estimate of the "true" model state than the posterior mode propagated in time. One reason is that the posterior pdf of the model state, with non-linear observation operators, can appear to be non-symmetric and/or to have a heavy tail. The posterior mean can be displaced away from the posterior mode toward the heavy tail. Thus, it can be located far away from the most believable location of the "true" model state. Another reason is that the posterior mode, under the perfect model assumption, comes indeed very close to the "true" model state if a large amount of data is assimilated. However, if the amount of assimilated data is small and the posterior mode does not come very close to the "true" model state, the posterior predictive mean estimated by the importance sampling provides a more efficient forecast of the "true" model state also after a relatively long integration time compared to the posterior mode propagated in time.

The importance sampling provides one more powerful approach for the probabilistic inference about smaller dimensional quantities of interest (through smaller dimensional transforms of the model state variable), not presented in the thesis. The importance sampling weights can be used in rejection re-sampling, which provides a possibility to obtain

an over-dispersed small size sample from the posterior pdf of interest. This sample can be used later in Monte Carlo Markov Chain (MCMC) simulations, which allow generation of a large dimensional sample from the pdf. The MCMC simulations require huge computer power. For full size models, MCMC simulations are not applicable for weather forecasting at present, but they can still be useful for application in diagnostics of the atmospheric development.

My main ambition was to look inside the mechanisms of different extensions of the Kalman filter idea for assimilation of non-linear observations into a non-linear dynamical model of the atmosphere. Out of a number of questions which arose in the beginning of the study, some questions I have managed to answer, some of the questions appeared to be irrelevant, while the answers for some of them I have not yet found. But even a much larger number of new questions arose. And this seems to be a good sign. "The more I know, the more I do not know".

ACKNOWLEDGEMENTS

First of all, I would like to thank the Department of Mathematical Statistics at Stockholm University, who trusted my knowledge and who provided me with the possibility to do research in the area of my interest. The staff at the Department have created a calm and fruitful working atmosphere.

I am very grateful to my supervisor, Rolf Sundberg, for the open-minded discussions, the patience and the understanding.

Deep thanks to my family, who have accompanied me every step of my life, supporting me in my struggling with problems and being happy for my small victories. My two beautiful daughters, Margarita and Alisa, continuously help me to discover how wonderful is every day on the earth.

Most of all, I thank the Bravest Man in the World, Nils Gustafsson, for his infinite support and deepest encouragement.

REFERENCES

- Asselin, R., 1972: Frequency filter for time integrations. *Mon. Wea. Rev.*, **100**, 487-490.
- Anderson, B. D. O. and Moore, J. B., 1979: *Optimal filtering*. Englewood Cliffs: Prentice-Hall.
- Anderson, T.W., 1984: *An Introduction to Multivariate Statistical Analysis*, 2nd edition. New York: John Wiley Sons
- Bayes, T., 1763: Essay towards solving a problem in the doctrine of changes. Reproduces with a bibliographical note by Barnard, G. A., *Biometrika*, **39**, 293-315.
- Bickel, P. J., and Doksum, K. A., 1977: *Mathematical Statistics. Basic Ideas and Selected Topics*. San Francisco: Holden-Day, Inc.
- Billingsley, P., 1979: *Probability and Measure*. New York: John Wiley sons.
- Brown, P. J., 1993: *Measurement, Regression, and Calibration*. Oxford: Clarendon Press.
- Carter, C. K. and Konh, R., 1994: On Gibbs sampling for state space models. *Biometrika*, **65**, 589-601.
- Courtier, P., Thépaut, J.-N. and Hollingsworth, A., 1994: A strategy for operational implementation of 4D-Var using an incremental approach. *Q.J.Roy. Meteorol. Soc.*, **120**, 1367-1388.
- Cramer, H., 1946: *Mathematical methods in statistics*. Princeton University Press.
- de Jong, P., 1988b: The likelihood for a state space model. *Biometrika*, **75**, 165-69.
- de Jong, P., 1989: Smoothing and interpolation with the state space model. *J. American Statistical Association*, **84**, 1085-88.
- Durbin, J., 1960: Estimation of parameters in time series regression models. *J. Royal Statistical Society B*, **22**, 139-53.
- Durbin, J., 1997: Optimal estimating equations for state vectors in non-Gaussian and non-linear estimating equations. in Basawa *et al* (1997).
- Durbin, J. and Koopman, S. J., 1997: Monte Carlo maximum likelihood estimation of non-Gaussian state space model. *Biometrika*, **84**, 669-84.
- Durbin, J. and Koopman, S. J., 2000: Time series analysis of non-Gaussian observations based on state space models from both classical and Bayesian perspective. *J. Royal Statistical Society B*, **62**, 3-56.
- Durbin, J. and Koopman, S.J., 2001: *Time Series Analysis by State Space Methods*. Oxford Statistical Science Series, Oxford University Press
- Eliassen, A., 1954: Provisional report on calculation of spatial covariance and autocorrelation of the pressure field. *Inst. Weather and Climate Research, Acad. Sci., Oslo*, Report No. 5.
- Eliassen, E., Machenhauer, B. and Rasmussen, E., 1970: On a numerical method for integration of the hydrodynamical equations with a spectral representation of the horizontal fields. Report No. 2, Institut for teoretisk meteorologi, University of Copenhagen.
- Evensen, G., 1994: Sequential data assimilation with a non-linear quasi-geostrophic model using Monte-Carlo methods to forecast error statistics, *J. Geophys. Res.*, **99**, C5, 10143-10162.

- Evensen, G., 2003: The ensemble Kalman filter: Theoretical formulation and practical implementation. Submitted to *Ocean Dynamics*.
- Feller, W., 1966: *An Introduction to Probability Theory and its Applications. Volume I*. New York:John Wiley Sons
- Feller, W., 1966: *An Introduction to Probability Theory and its Applications. Volume II*. New York:John Wiley Sons
- Fisher, R. A., 1925: Theory of statistical estimation. *Proc. Camb. Phil. Soc.*, **22**, 700-725
- Fruhworth-Schnatter, S., 1994: Data augmentation and dynamical linear models. *J. Time Series Analysis*, **15**, 183-202.
- Gandin, L.S., 1963: Objective analysis of meteorological fields. *Leningrad Hydromet. Press*.
- Geweke, J., 1989: Bayesian inference in econometric models using Monte Carlo integration. *Econometrica*, **57**, 1317-39.
- Godambe, V. P., 1960: An optimal property of regular maximum likelihood estimation. *Annals of Mathematical Statistics*, **31**, 1208-12.
- Holton, J. R., 1979: *An Introduction to Dynamic Meteorology*. Second edition. New York:Academic Press, Inc.
- Houtekamer, P.L. and Mitchell, H.L., 2001: A sequential ensemble Kalman filter for atmospheric data assimilation, *Mon. Wea. Rev.*, **129**, 123-137.
- Kalman, R.E. (1960). A new approach to linear filtering and prediction problems. Trans. ASME, Ser. D, *J. Basic Eng.* **82**, 35-45.
- Kwizak, M. and Robert, A.J., 1971: A semi-implicit scheme for grid point atmospheric models of the primitive equations, *Mon. Wea. Rev.*, **99**, 32-36.
- Le Dimet, F.X. and Talagrand, O., 1986: Variational Algorithms for Analysis and Assimilation of Meteorological Observations. Theoretical Aspects. *Tellus*, **38A**, 97-110.
- Leith, C., 1980: Non-linear normal mode initialization and quasi-geostrophic theory. *J. Atmos. Sci.*, **37**, 958-968.
- Lorenc, A., 1981: A global three-dimensional multivariate statistical interpolation scheme. *Mon. Wea. Rev.*, **109**, 701-721.
- Lorenc, A., 2003: The potential of the Ensemble Kalman filter for NWP - a comparison with 4D-Var. *Met. Office Internal Report*, **5**, 27 pp.
- Machenhauer, B., 1977: On the dynamics of gravity oscillations in a shallow water model, with application to normal mode initialization. *Beitr. Phys. Atmos.*, **50**, 253-271.
- Morf, J. F. and Kailath, T. , 1975: Square root algorithms for least squares estimation. *IEEE Transaction on Automatic Control*, **20**, 487-97.
- Orszag, 1971: On the elimination of aliasing in finite-difference schemes by filtering high-wavenumber components. *J. Atmos. Sci.*, **28**, 1074.
- Parrish, D.F. and Derber, J.C., 1992: The National Meteorological Centre's spectral statistical interpolation analysis system. *Mon. Wea. Rev.*, **120**, 1747-1763.
- Rao, C. R. , 1946: Information and accuracy attained in estimation of statistical parameters. *Bull. Calcutta Math. Soc.*, **37**, 81-91.
- Ripley, B. D. , 1987: *Stochastic Simulation*, New York:Wiley.

Smith B. T., Boyle J. M., Garbow B. S., Ikebe Y., Klema V. C., Moler C. B., 1976: *Matrix Eigensystem Routines - EISPACK Guide*. Second edition. Lecture Notes in Computer Science. Springer-Verlag.

Wald, A., 1949: Note on the consistency of maximum likelihood estimate. *Ann.Math.Statist.*, **20**, 595-601.

Woodbury, 1950: Inverting modified matrices. Technical Report 42. statistical Research Group.